UNIVERSITAT POLITÈCNICA DE VALÈNCIA

EFFECT OF MULTIPLE INJECTION STRATEGIES ON THE DIESEL SPRAY FORMATION AND COMBUSTION USING OPTICAL DIAGNOSTICS

DOCTORAL THESIS

PRESENTED BY:

Alberto Viera Sotillo

SUPERVISED BY:

Dr. Raúl Payri Marín

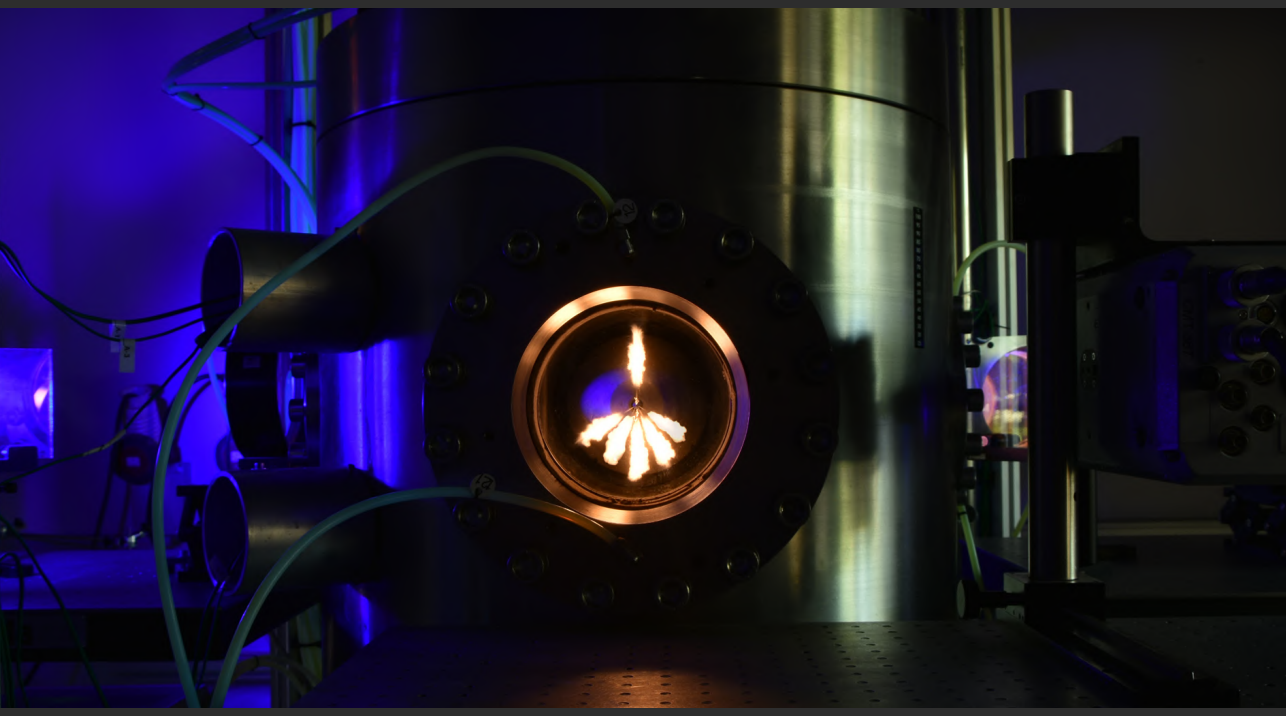

JUNE 2019

DEPARTAMENTO DE MÁQUINAS Y MOTORES TÉRMICOS

Universitat Politècnica de València
Departamento de Máquinas y Motores Térmicos

Doctoral Thesis

Effect of multiple injection strategies on the diesel spray formation and combustion using optical diagnostics

Presented by:
Alberto Viera Sotillo

Supervised by:
Dr. Raúl Payri Marín

in fulfillment of the requirements for the degree of
Doctor of Philosophy

Valencia, June 2019

Ph.D. Thesis

Effect of multiple injection strategies on the diesel spray formation and combustion using optical diagnostics

Written by: Mr. Alberto Viera Sotillo
Supervised by: Dr. Raúl Payri Marín

Examination committee:

Chairman: Dr. José Vicente Pastor
Secretary: Dr. Octavio Armas
Member: Dr. L.M.T Somers

Reviewing board:

Dr. L.M.T Somers
Dr. Jorge Martínez López
Dr. María Arántzazu Gómez Esteban

Valencia, June 2019

Abstract

Fuel injection is a very complex process due to the numerous mechanisms involved in the spray development, and its intrinsically stochastic behavior. Over the years, researchers have studied sprays thoroughly, to understand the fundamental processes as key to reduce pollutant formation, and improve the efficiency of direct injection diesel engines. In recent years, the evolution of the injection technologies has permitted not only to improve the spray mixing process but to control injection parameters accurately, adding flexibility to the systems for new strategies and an extra degree of complexity for researchers. In such sense, multiple injection strategies have proved capable of reducing fuel consumption, as well as emissions of particulate matter, carbon oxides, nitrogen oxides, soot, and unburned hydrocarbons, and has become a standard in the industry.

This thesis provides an experimental methodology to study the effects of two different multiple injection strategies (pilot-main and main-post) on spray development and combustion. Experiments were divided into four separate measurement campaigns carried out in three facilities.

In the first two campaigns, the injector was hydraulically characterized by rate of injection and spray momentum flux measurements. For a target injected mass, the fuel allocation was obtained for the different dwell times and pilot/post quantities. A new approach to evaluate the fuel distribution using the momentum flux signal was implemented. Higher shot-to-shot deviations were observed for the pilot/post pulses that are injected in an entirely transitory state. The dispersion decreased with increasing injected quantity, and also slightly with decreasing rail pressure. The repeatability of the post injections was significantly affected by the dwell time.

Then, high-speed optical diagnostics were applied to visualize the spray development in both inert and reactive atmospheres. Two novel image processing solutions were developed: one to decoupled two injection events that coexist in a single frame, and another to optically estimate the ignition delay of multiple injection pulses. On the spray development in non-reactive conditions, no influence was observed from the injected quantity of the pilot and its dwell time to the main pulse on the stabilized liquid length and spreading angle. Regarding the vapor phase, increasing the injected mass of the first pulse pushed the interaction zone past the optical limit. In general, the second pulse penetrated at a faster rate than the single injection case. Vapor phase spreading angle increased with the inclusion of a pilot injection. No clear trend was observed with either the pilot quantity nor the dwell time.

On the spray development in reactive conditions, for all test points that included multiple injections, the ignition delay of the second pulse decreased referenced to its start of injection. On average, pilot-main strategies showed reductions of 30 % to 40 %, while main-post of 40 % to 50 %. Different interaction mechanism found in the literature were used to describe the synergy between injection pulses. Regarding the stabilized lift-off length, no definite trend was observed in terms of the effects of both the dwell time and pilot quantity. The average image taken by the ICCD camera did not consider that the lift-off length can change from the inception of combustion to the established diffusion flame. Qualitative measurements of the ignition location showed that lift-off length of the main injection should start closer to the nozzle, and slowly shift towards equilibrium of the stabilized flame. Regarding soot measurements, it was generally observed that pilot-main strategies produced more soot than each of their reference case. A slight decrease in the cross-sectional optical thickness near the start of combustion was noted increasing the pilot quantity. No clear dependence of soot on the dwell time was observed. In contrast to the literature, main-post strategies depicted slightly higher (or similar) soot formation than a single injection. In combustion chambers with such large volume, the post injection behaved like a main and the actual main like a pilot. Thus, local conditions enhance the formation of soot from the post injection, instead of promoting its oxidation. Therefore, jet-wall interactions are critical for the effectiveness of the post injection on reducing soot emissions.

Resumen

La inyección de combustible es un proceso complejo, debido a que hay varios mecanismos involucrados en el desarrollo del chorro, y a su comportamiento intrínsecamente estocástico. A lo largo de los años, los investigadores han estudiado a fondo los chorros diésel, ya que es clave comprender los procesos fundamentales, para así reducir la formación de contaminantes, y mejorar la eficiencia de los motores de inyección directa. En los últimos años, la evolución de las tecnologías de inyección ha permitido no solo mejorar el proceso de mezcla, sino también controlar con precisión los parámetros de inyección, agregando flexibilidad a los sistemas para nuevas estrategias y un grado adicional de complejidad para los investigadores. Más aún, las estrategias de inyecciones múltiples han demostrado ser capaces de reducir el consumo de combustible, así como también la emisión de partículas, los óxidos de carbono, los óxidos de nitrógeno, el hollín y los hidrocarburos no quemados, convirtiéndose en un estándar en la industria.

Esta tesis presenta una metodología experimental para estudiar los efectos de dos estrategias diferentes de inyección múltiple (piloto-principal y principal-post) sobre el desarrollo fundamental y la combustión del chorro. Los experimentos se dividieron en cuatro campañas diferentes, realizadas en tres instalaciones distintas.

En las dos primeras campañas, se caracterizó hidráulicamente el inyector midiendo su tasa de inyección y flujo de cantidad de movimiento. Para una masa inyectada objetivo, se obtuvo la distribución de combustible para los diferentes tiempos de separación y las cantidades de piloto/post. Se implementó un nuevo enfoque para evaluar la distribución de combustible utilizando la señal de flujo de cantidad de movimiento. Se pudo observar que las inyecciones de piloto/post que se realizan en un estado totalmente transitorio presentan mayor desviación entre disparos. El aumento de la cantidad inyectada redujo la dispersión, con un ligero descenso al disminuir también la presión del rail. La repetibilidad de las inyecciones post se vio afectada significativamente por el tiempo de separación entre pulsos.

Luego, se aplicaron diagnósticos ópticos de alta velocidad para visualizar el desarrollo del chorro en atmósferas tanto inerte como reactiva. Se utilizaron dos nuevas soluciones de procesado de imágenes: una para desacoplar dos eventos de inyección que coexisten en un solo cuadro, y otra para estimar ópticamente el tiempo de retraso al autoencendido de múltiples pulsos de inyección. En cuanto al desarrollo del chorro en condiciones inertes evaporativas, no se observó ninguna influencia en la longitud líquida estabilizada y el ángulo del chorro, respecto a la cantidad inyectada por la piloto, ni de

su separación al pulso principal. Con respecto a la fase vapor, el aumento de la masa inyectada del primer pulso empujó la zona de transición más allá del límite óptico. En general, el segundo pulso penetró a una mayor velocidad, comparado con el caso de una inyección única. El ángulo de dispersión de la fase de vapor aumentó con la inclusión de la inyección piloto, pero no se observó una tendencia clara con respecto a la cantidad de la piloto ni a su tiempo de separación.

En cuanto al desarrollo del chorro en condiciones reactivas, para todas las medidas que incluyeron inyecciones múltiples, el tiempo de retraso al autoencendido del segundo pulso disminuyó en referencia a su inicio de inyección. En promedio, las estrategias piloto-principal vieron reducciones del 30 % al 40 %, mientras que las principal-post del 40 % al 50 %. Se utilizaron diferentes mecanismos de interacción encontrados en la literatura para describir la interacción entre los pulsos de inyección. Con respecto a la longitud de despegue estabilizada, no se observó una tendencia definida con respecto a los efectos tanto del tiempo de separación como de la cantidad de la piloto. La imagen promedio tomada por la cámara intensificada no consideró que la longitud de despegue puede cambiar desde el inicio de la combustión hasta el establecimiento de la llama de difusión. Las mediciones cualitativas de la localización del encendido mostraron que la longitud de levantamiento de la inyección principal debería comenzar más cerca de la tobera, para luego moverse lentamente hacia la zona de equilibrio en la llama de difusión estabilizada. Con respecto a las mediciones de hollín, en general se observó que las estrategias piloto-principal producen más hollín que cada uno de sus casos de referencia. Se observó una ligera disminución en el grosor óptico de la sección transversal cerca del inicio de la combustión al aumentar la masa de la piloto. No se observó una clara dependencia del hollín con respecto al tiempo de separación entre pulsos. En contraste a la literatura, las estrategias principal-post mostraron una formación de hollín ligeramente más alta (o similar) que una sola inyección. En cámaras de combustión con un volumen tan grande, la inyección posterior se comportó como una principal y la principal como una piloto. Por lo tanto, las condiciones locales favorecen a la formación de hollín para el segundo pulso, en lugar de promover su oxidación. Consecuentemente, se observó que las interacciones chorro-pared son críticas para la efectividad de las inyecciones post en la reducción de las emisiones de hollín.

Resum

La injecció de combustible és un procés complex, ja que hi ha diversos mecanismes involucrats en el desenvolupament del doll i el seu comportament és intrínsecament estocàstic. Al llarg dels anys, els investigadors han estudiat a fons els dolls dièsel, ja que cal comprendre els processos fonamentals per tal de reduir la formació de contaminants i millorar l'eficiència dels motors d'injecció directa. En els últims anys, l'evolució de les tecnologies d'injecció ha permés no només millorar el procés de mescla, sinó també controlar amb precisió els paràmetres d'injecció, afegint flexibilitat als sistemes per a noves estratègies i un grau addicional de complexitat per als investigadors. A més a més, amb les estratègies d'injeccions múltiples s'ha demostrat la possibilitat de reduir el consum de combustible, així com les partícules, els òxids de carboni, els òxids de nitrogen, el sutge i els hidrocarburs no cremats; a més, aquestes estratègies s'han convertit en un estàndard en la indústria.

Aquesta tesi estudia els efectes de dues estratègies diferents d'injecció múltiple (pilot-principal i principal-post) sobre el desenvolupament fonamental i la combustió del doll. Els experiments es van dividir en quatre campanyes diferents, realitzades en tres instal·lacions diferents.

En les dues primeres campanyes, es caracteritzar hidràulicament l'injector, mesurant la seua taxa d'injecció i flux de quantitat de moviment. Per a una massa injectada objectiu, es va obtindre la distribució de combustible per als diferents temps de separació i les quantitats de pilot/post. Es va implementar un nou enfocament per tal d'avaluar la distribució de combustible utilitzant el senyal de flux de quantitat de moviment. Es va poder observar que les injeccions de pilot/post injecció que es realitzen en un estat totalment transitori presenten major desviació entre trets. L'augment de la quantitat injectada va reduir la dispersió, observant un lleuger descens en disminuir també la pressió de rail. La repetitivitat de les injeccions post es va veure afectada significativament pel temps de separació entre polsos.

Després, es van aplicar diagnòstics òptics d'alta velocitat per a visualitzar el desenvolupament del doll en atmosferes tant inerts com reactives. Es van utilitzar dues noves solucions de processament d'imatges: una, per a desacoblar dos esdeveniments d'injecció que coexisteixen en un sol quadre, i una altra per a estimar òpticament el retard a l'encesa amb múltiples polsos d'injecció. Pel que fa al desenvolupament del doll en condicions inerts evaporatives, no es va observar cap influència en la longitud líquida estabilitzada i l'angle del doll respecte a la quantitat injectada per la pilot, ni de la seua separació al pols principal. Pel que fa a la fase de vapor, l'augment de la massa injectada del primer pols va empényer la zona de transició més enllà

del límit òptic. En general, el segon pols va penetrar a una velocitat més gran comparat amb el cas d'una injecció única. L'angle de dispersió de la fase de vapor va augmentar amb la inclusió de la injecció pilot, però no es va observar una tendència clara pel que fa a la quantitat de la pilot ni al seu temps de separació.

Pel que fa al desenvolupament del doll en condicions reactives, per a tots els mesuraments que van incloure injeccions múltiples, el retard d'encesa del segon pols va disminuir en referència a l'inici de la injecció. De mitjana, les estratègies pilot-principal van experimentar reduccions del 30 % al 40 %, mentre que les principal-post, es van veure reduides entre el 40 % i el 50 %. Es van utilitzar diferents mecanismes d'interacció trobats en la literatura per a descriure la interacció entre els pols d'injecció. Pel que fa a la longitud d'enlairament estabilitzada, no es va observar una tendència definida pel que fa als efectes tant del temps de separació com de la quantitat de la injecció pilot. La imatge mitjana presa per la càmera intensificada no va considerar que la longitud d'enlairament puga canviar des de l'inici de la combustió fins a la flama de difusió establerta. Els mesuraments qualitatius de la localització de l'encesa van mostrar que la longitud d'aixecament de la injecció principal hauria de començar més a prop de la tovera i moure's lentament cap a la zona d'equilibri en la flama de difusió estabilitzada. Pel que fa als mesuraments de sutge, en general es va observar que les estratègies pilot-principal van produir més sutge que cadascun dels seus casos de referència. Es va observar una lleugera disminució en el gruix òptic de la secció transversal prop de l'inici de la combustió en augmentar la massa de la injecció pilot. No es va observar una clara dependència del sutge amb el temps de separació entre els pols. En contrast amb la literatura, les estratègies principal-post van mostrar una formació de sutge lleugerament més alta (o similar) que una sola injecció. En cambres de combustió amb un volum tan gran, la injecció posterior es va comportar com si, fóra una principal i la principal, com si fóra una pilot. Per tant, les condicions locals afavoreixen la formació de sutge de la segona injecció en lloc de promoure la seua oxidació.

"In theory, there is no difference between theory and practice.
In practice, there is."
Yogi Berra

To my family...

It has been almost five years since I started my Ph.D. studies, and thus it is not possible to truly summarize in just a few paragraphs my gratitude towards all the people that helped me along the way. First of all, I thank Raul for being a great tutor and team leader, always willing to provide counsel, to point in the right direction, pushing us to bring the best of ourselves and promoting a great environment within the injection research group. Also, I thank Jaime, whom I find an incredibly bright and yet humble person, that for five years patiently listened to all my doubts and questions, consistently providing great advice and ideas, and from whom I learned a lot. In the same manner, I thank José María García-Oliver and José Vicente Pastor, who were always open to attend to my inquiries, and with which I had many interesting and educational discussions, even though they are in a different research group. I also thank Gaby, Javi, Joaquin, Marcos, and Pedro, who like the others provided help, support, positivity, and guidance throughout these years. In addition, I extend my gratitude towards all the personnel of the CMT Motores Térmicos, in particular, Francisco Payri, José María Desantes and Jesús Benajes, for granting me the opportunity to be part of this prestigious research group.

I want to extend my gratitude as well towards all the members of the Large Engine Competence Center. On one side, to Prof. Andreas Wimmer, Gerhard Pirker and Wibke Tritthart, for welcoming me to their research institute and helping me with all the necessary paperwork. On the other side, to Constantin, Anton, Andy, and Sebastian, as I was treated as an extra member of the team. For me, it was a great, fun, and enlightening experience, and for that, I will always be grateful.

In regards of friends and coworkers, first I would like to thank my office mates throughout the years: first, my brother Juan Pablo and Daniel, who in my newbie years guided and taught me quite a lot; later, Abian and Tomas, for the great laughs, anecdotes, and help. In addition, I'm also grateful to my other friends and colleagues in the research group: Jesús, Santiago, Armando, Cesar, Mary, Vincenzo, María, Enrique, Marco, Mario (special thanks for taking the time to review the thesis), and Lucas. I honestly believe we have an amazing group that is not bounded only to work, as we have shared beers, trips, plans, and more. I also extend my gratitude towards Michele, my bachelor thesis tutor at CMT, for teaching me the first ways of the diesel spray, and Leonardo, a good friend always available for advice and support. I also have to include the students that helped with the experimental measurements and throughout the years: Rishabh, Pablo, Miguel Ángel, Diego, Tude, John, Louise, and Alejandro. In such sense, I would like to acknowledge as well all the work done and help received by all lab technicians, but I like to give special thanks to Jose Enrique, for his experience, knowledge, and guidance

with his sometimes unique character; Omar, for his always positive attitude, sacrificing without hesitation a bunch of lunch breaks to help me with my experimental measurements; and José "Tornero", not only for all the jokes and laughs shared, but for his guidance and help in the manufacture of parts and pieces needed throughout these years with always a great mood.

Lastly, I thank my family. My wife Ilse, for being my friend and companion in life, and supporting me through the toughest times. My parents, both exemplary figures of commitment, hard work, love, and dedication. My brothers Julio Andrés, Juan Pablo and Mauricio, all excellent role-models in their own ways. And all other family members, those present and those not, that have in many ways contributed to where I am today. To all my family, I'm blessed to have you. I thank you and love you so very much.

Contents

List of Figures

List of Tables

Nomenclature

Acronyms

AHRR	Apparent Heat Release Rate.
CFD	Computational Fluid Dynamics.
CIDI	Compression-Ignition Direct-Injection.
CN	Combustion noise.
CO	Carbon monoxide.
CPF	Constant Pressure and Flow.
CV	Control volume.
DBI	Diffused back-illumination.
DP	Double-pass.
ECN	Engine Combustion Network.
ECU	Engine Control Unit.
EGR	Exhaust Gas Recirculation.
EOI	End of injection.
ICCD	Intensified Charge-Coupled Device.
ID	Ignition delay.
IRDCI	Injection Rate Discharge Curve Indicator.
LED	Light-emitting diode.
LOL	Lift-off length.
NOx	Nitrogen oxides.
OEM	Original Equipment Manufacturer.
PCR	Piezo common-rail.

PID	Proportional-Integral-Derivative.
ROD	Rate of difference.
ROI	Rate of injection.
RSD	Relative standard deviation.
SOC	Start of combustion.
SOE	Start of energizing.
SOI	Start of injection.
SpI	Spray of interest.
SP	Single-pass.
SSI	Second stage ignition.
UHC	Unburned hydrocarbon.
UV	Ultra violet.

Greek symbols

ΔP	Pressure difference throughout the nozzle.
Δp	Pressure difference (general).
Δu_f	Variation of fuel flow velocity.
ϕ	Equivalence ratio.
ρ	Chamber density.
ρ_f	Density of the fuel.
τ	Optical thickness.
θ	Spray spreading angle.
ε	Angular deflection of a ray.
ϖ	Surface of the control volume.

Latin symbols

$\dot{m}_t$	Theoretical mass flow rate.
$\dot{M}$	Momentum flux.
$\dot{m}$	Mass flow rate.
$\overline{D}_o$	Average outlet diameter.
A	Global activation energy of reactions.
a_f	Speed of sound in the fuel.
A_o	Outlet area of the nozzle.
A_t	Tube cross-sectional area.
A_{eff}	Effective area.

C_d	Discharge coefficient.
d_i	Distance for spreading angle calculations.
D_o	Nozzle outlet diameter.
D_s	Sac diameter.
DT	Dwell time.
ET	Energizing time.
F	Force (general).
I	Pixel-wise intensity distribution of the current image.
I_0	Pixel-wise intensity distribution of the reference image.
I_f	Pixel-wise intensity distribution of the flame.
Id_i	Pixel-wise intensity difference between two consecutive frames.
K	Dimensional extinction coefficient.
$k-factor$	Orifice conicity factor.
k_i	Coefficients for polynomial regressions.
k_{GD}	Gladstone-Dale coefficient.
k_{adjust}	Mass scaling factor.
KL	Optical thickness related to soot.
L	Optical path length.
L_n	Nozzle length.
L_{soot}	Path length through the soot cloud.
LL	Liquid length.
m_{int}	Mass integrated from the averaged signal.
m_{scale}	Mass measured by the scale.
n	Refractive index (general).
n_0	Refractive index of the surroundings.
$O_2\%$	Oxygen concentration.
p	Pressure (general).
p_0	Reference pressure.
P_b	Discharge pressure.
P_r	Rail pressure.
p_{cv}	Pressure in the control volume.
S	Spray penetration.
T	Chamber temperature.
t	Time (general).

T_0	Reference temperature.
T_f	Fuel temperature.
T_{cv}	Temperature in the control volume.
u	Velocity (general).
u_t	Theoretical discharge velocity.
u_{eff}	Effective velocity.

Chapter 1

Introduction

1.1 General context

In recent times, diesel engines have been subjected to public scrutiny, partly with non-objective discussions [1]. Legislations such as the Euro VI [2] have set very stringent environmental and fuel economy standards, that have pushed researchers into a continuous development of all areas, and have set the diesel engine as the most efficient alternative [3–5].

One of the main areas is the study of the diesel spray mixing, as it has been recognized as a critical factor in combustion control and the reduction of its related contaminants [6, 7]. The characteristics of fuel sprays are conditioned by many parameters, such as the injection pressure, engine load, nozzle geometry, and rate of injection, among others.

Thus, the spray development is naturally a very complex phenomenon, due to the numerous mechanisms involved and its intrinsically stochastic behavior. Over the years, researchers have studied fuel sprays thoroughly to understand the fundamental processes and establish a reliable experimental set of data that enables the validation of more detailed numerical models [8]. In such sense, computational fluid dynamics (CFD) provide unmatched advantages that coherently complement experimental measurements, as they offer detailed spatial information of complex variables with a high temporal resolution. Moreover, the predictive capabilities of validated CFD models can help to reduce testing times and production costs. However, these are limited

to high-fidelity experimental data for validation, and accurate delimitation of the problem.

The development of new optically accessible test rigs [9], as well as measurement technologies [8, 10–13], have allowed to visualize in detail the transient evolution of the whole combustion process, and quantify chemical components, along with all kind of spray parameters. In such facilities, fundamental studies of the injection event are carried out in a simplified environment, with nearly quiescent boundary conditions that can be controlled, and the large optical accesses that ease the implementation of optical diagnostics [14–16]. These studies aim at isolating and understanding single processes, for example:

- Atomization studies by injecting at ambient temperature [17, 18].
- Mixing and evaporation studies by injecting into high-temperature conditions but with an inert gas [19–22].
- Investigations of the effects of opening/closing transients on the spray development, by recording at very high speeds with a detailed spatial resolution [17, 18, 23, 24].
- The effects of different nozzles, fuels and injector technologies on the spray development [17, 20, 25–27].

In recent years, the evolution of the injection technologies has permitted not only to improve the spray mixing process, but to control injection parameters accurately, adding flexibility to the systems for new strategies [28], and an extra degree of complexity to the researchers. From what previously was a single pulse per combustion cycle, modern systems allow to inject up to 8 different times precisely [28]. To this end, multiple injection strategies have proved to be capable of reducing fuel consumption, particulate matter (soot), carbon oxides, nitrogen oxides, and unburned hydrocarbons [29–36].

1.2 Objectives and methodology

The present thesis was proposed to assess the necessity of the Injection-Combustion research group of the CMT-Motores Térmicos of developing a robust methodology to measure multiple injection events in different facilities, as these strategies become a standard in the industry. Furthermore, as a first step, reliable experimental data of multiple interacting injections was needed to improve a simple 1-D model that can accurately predict the mixing,

evaporation, and to some extend combustion processes of the diesel spray [37, 38].

On this context, this thesis follows two main objectives:

- To develop an experimental methodology to quantify the mass allocation of multiple injection strategies, as well as to measure spray variables in optically accessible test cells for different boundary conditions.
- To contribute to the current fundamental understanding of the interactions between consecutive injection pulses and their consequence in the overall diesel spray development, and provide a large database for model validation.

To this end, the technologies, optical components, and facilities available at CMT-Motores Térmicos were used to study different aspects of the injection process. The experiments carried out can be divided into three groups based on their specific goals:

- A complete hydraulic characterization of the injector for multiple injection strategies.
- A spray characterization for multiple injection strategies in inert evaporative conditions, visualizing both liquid and vapor phases for the same injection event.
- A spray characterization for multiple injection strategies in a reactive environment, considering the ignition process and soot formation.

Boundary conditions such as rail pressure, chamber density, and temperature, were selected using guidelines from the Engine Combustion Network (ECN) [39]. The fuel distribution was selected using baseline points from a 1.6 liter engine, with an injected mass per cycle of 50 mg, equipped with 100 µm - 8-orifice injector. Quantities were scale and rounded to the 90 µm - 6-orifice injector used, which resulted in an injected mass per cycle of 30 mg. The injector was fitted with a custom nozzle with an a-typical plume distribution, with a spray optically isolated from the others. This configuration allows simulating a more realistic geometry while permitting line-of-sight visualization. Two simple fuel distribution schemes were analyzed: pilot-main and main-post. For each strategy, four different dwell times and two pilot/post

quantities were tested, always comparing results with a reference single injection. Commercially available diesel was used.

The experimental campaigns of the multiple injection strategies first consisted of a complete hydraulic characterization of the injector, that is, measurements of the rate of injection and momentum flux. They included a novel approach to estimate the mass allocation in the momentum flux test rig using an upstream scale. Then, simultaneous high-speed visualization of the liquid and vapor phases of the sprays were carried out with a combined diffused back-illumination and single-pass schlieren, synchronized to capture the same injection event. Lastly, combustion diagnostics were assessed by studying the ignition performance, lift-off length, and soot formation of the reactive spray.

1.3 Thesis outline

The thesis is organized in seven chapters, starting with this brief introduction (**chapter 1**), that presented the general context and primary objectives of the work carried out.

Chapter 2 is focused on describing the fundamental concepts of diesel direct injection and serves as a brief reference for the interpretation of the results obtained. The different processes that take place during the injection of fuel into the combustion chamber are discussed, including a macroscopic description of the diesel spray, as well as some of the equations that govern the internal flow development. The section ends with a summary of the different multiple injection strategies and their impact on the global performance of the engines and their emissions.

Chapter 3 outlines the facilities, equipment and experimental methodologies used. Each test rig is described with the corresponding measurement principle and procedure. The optical techniques are detailed as well, along with the general data and image processing approach.

In **chapter 4**, the results of the hydraulic characterization for multiple injection strategies are presented. Rate of injection and momentum flux measurements are reported, both as the time-resolved signals and in terms of the estimated mass allocations. Hence, the chapter includes a new approach to quantify the distribution of the injected mass in the momentum flux test rig, verified with the rate of injection data. Results also cover a brief analysis of shot-to-shot dispersion.

Chapter 5 is centered on discussing the results from the evaporative spray development in an inert atmosphere, to analyze the effects of the interaction

between injections on the formation of the air-fuel mixture. Results are given in terms of liquid and vapor phase penetrations, and spreading angle. The chapter includes a novel image processing method that allows decoupling two injection events that coexist in the same frame.

In **chapter 6**, the results from the spray development in a reactive atmosphere are depicted to analyze the effects of the interaction between injections on the performance of the combustion. Results are given in terms of the ignition delay, lift-off length, approximate ignition location, and soot distribution maps. The chapter includes a new image processing approach to estimate the ignition delay of multiple injection pulses with the optical techniques used.

Lastly, **chapter 7** presents a review of the work carried out, as well as the main conclusions. In addition, some ideas for future directions are proposed from the knowledge and experience acquired during the development of this thesis.

References

[1] Steinparzer, F., Stütz, W., and Brüne, H.-j. "Reliable, efficient and environmentally friendly: The new BMW Diesel engines with RDE technology". In: *16th Conference The Working Process of the Internal Combustion Engine*. Ed. by H. Eichlseder and A. Wimmer. Graz: Verlag der Technischen Universität Graz, 2017, pp. 15–22.

[2] European Parliament. "Regulation (EC) No 715". In: *The Council Of The European Union - Official journal of the European Union*. Vol. L171. 2007.

[3] Johnson, T. V. "Diesel engine emissions and their control". In: *Platinum Metals Review* 52.1 (2008), pp. 23–37. DOI: 10.1595/147106708X248750.

[4] Johnson, T. V. "Diesel Emission in Review". In: *SAE Technical Paper 2011-01-0304* (2011). DOI: 10.4271/2011-01-0304.

[5] Altenschmidt, F., Banzhaf, G., Kraus, E., and Loll, S. "The SI-engine - at the end of its development?" In: *16th Conference The Working Process of the Internal Combustion Engine*. Ed. by H. Eichlseder and A. Wimmer. Graz: Verlag der Technischen Universität Graz, 2017, pp. 35–49.

[6] Musculus, M. P. B., Miles, P. C., and Pickett, L. M. "Conceptual models for partially premixed low-temperature diesel combustion". In: *Progress in Energy and Combustion Science* 39.2-3 (2013), pp. 246–283. DOI: 10.1016/j.pecs.2012.09.001.

[7] Han, S., Kim, J., and Bae, C. "Effect of air-fuel mixing quality on characteristics of conventional and low temperature diesel combustion". In: *Applied Energy* 119 (2014), pp. 454–466. DOI: 10.1016/j.apenergy.2013.12.045.

[8] Fansler, T. D. and Parrish, S. E. "Spray measurement technology: a review". In: *Measurement Science and Technology* 26.1 (2015), p. 012002. DOI: 10.1088/0957-0233/26/1/012002.

[9] Baert, R. S. G. et al. "Design and operation of a high pressure, high temperature cell for HD diesel spray diagnostics: guidelines and results". In: *SAE Technical Paper 2009-01-0649* (2009). DOI: 10.4271/2009-01-0649.

[10] Bruneaux, G. and Maligne, D. "Study of the Mixing and Combustion Processes of Consecutive Short Double Diesel Injections". In: *SAE International Journal of Engines* 2.1 (2009), pp. 2009–01–1352. DOI: 10.4271/2009-01-1352.

[11] Manin, J., Pickett, L. M., and Skeen, S. A. "Two-Color Diffused Back-Illumination Imaging as a Diagnostic for Time-Resolved Soot Measurements in Reacting Sprays". In: *SAE International Journal of Engines* 6.4 (2013), pp. 2013–01–2548. DOI: 10.4271/2013-01-2548.

[12] Westlye, F. R. et al. "Diffuse back-illumination setup for high temporally resolved extinction imaging". In: *Applied Optics* 56.17 (2017), p. 5028. DOI: 10.1364/AO.56.005028.

[13] Desantes, J. M., García-Oliver, J. M., García, A., and Xuan, T. "Optical study on characteristics of non-reacting and reacting diesel spray with different strategies of split injection". In: *International Journal of Engine Research* 301 (2018). DOI: 10.1177/1468087418773012.

[14] Viera, J. P. "Experimental study of the effect of nozzle geometry on the performance of direct-injection diesel sprays for three different fuels". PhD thesis. Universitat Politècnica de València, 2017. DOI: 10.4995/Thesis/10251/81857.

[15] Bardi, M. "Partial Needle Lift and Injection Rate Shape Effect on the Formation and Combustion of the Diesel Spray". PhD thesis. Universitat Politècnica de València, 2014. DOI: 10.4995/Thesis/10251/37374.

[16] Giraldo Valderrama, J. S. "Macroscopic and microscopic characterization of non-reacting diesel sprays at low and very high injection pressures". PhD thesis. Universitat Politècnica de València, 2018. DOI: 10.4995/Thesis/10251/113643.

[17] Payri, R., Bracho, G., Martí-Aldaraví, P., and Viera, A. "Near field visualization of diesel spray for different nozzle inclination angles in non-vaporizing conditions". In: *Atomization and Sprays* 27.3 (2017), pp. 251–267. DOI: 10.1615/AtomizSpr.2017017949.

[18] Manin, J., Bardi, M., Pickett, L. M., Dahms, R. N., and Oefelein, J. C. "Microscopic investigation of the atomization and mixing processes of diesel sprays injected into high pressure and temperature environments". In: *Fuel* 134 (2014), pp. 531–543. DOI: 10.1016/j.fuel.2014.05.060.

[19] Payri, R., Gimeno, J., Bardi, M., and Plazas, A. H. "Study liquid length penetration results obtained with a direct acting piezo electric injector". In: *Applied Energy* 106 (2013), pp. 152–162. DOI: 10.1016/j.apenergy.2013.01.027.

[20] Payri, R., Viera, J. P., Gopalakrishnan, V., and Szymkowicz, P. G. "The effect of nozzle geometry over the evaporative spray formation for three different fuels". In: *Fuel* 188 (2017), pp. 645–660. DOI: 10.1016/j.fuel.2016.06.041.

[21] Jung, Y., Manin, J., Skeen, S. A., and Pickett, L. M. "Measurement of Liquid and Vapor Penetration of Diesel Sprays with a Variation in Spreading Angle". In: *SAE Technical Paper 2015-01-0946* (2015). DOI: 10.4271/2015-01-0946.

[22] Siebers, D. L. "Liquid-Phase Fuel Penetration in Diesel Sprays". In: *SAE Technical Paper 980809* (1998). DOI: 10.4271/980809.

[23] Sechenyh, V. et al. "Quantification of diesel injector dribble using 3D reconstruction from x-ray and DBI imaging". In: *ILASS Europe 28th Conference on Liquid Atomization and Spray Systems*. Valencia, 2017, pp. 232–239. DOI: 10.4995/ILASS2017.2017.4742.

[24] Manin, J., Pickett, L. M., and Yasutomi, K. "Transient cavitation in transparent diesel injectors". In: *ICLASS 14th Triennial International Conference on Liquid Atomization and Spray Systems*. Chicago, 2018, pp. 1–9.

[25] Payri, R., Gimeno, J., Bardi, M., and Plazas, A. H. "Effect of Injection Rate Shaping Over Diesel Spray Development in Non Reacting Evaporative Conditions". In: *ASME 2012 Internal Combustion Engine Division Spring Technical Conference*. 2012, p. 347. DOI: 10.1115/ICES2012-81206.

[26] Payri, R., Gimeno, J., Viera, J. P., and Plazas, A. H. "Needle lift profile influence on the vapor phase penetration for a prototype diesel direct acting piezoelectric injector". In: *Fuel* 113 (2013), pp. 257–265. DOI: 10.1016/j.fuel.2013.05.057.

[27] Payri, R., Viera, J. P., Gopalakrishnan, V., and Szymkowicz, P. G. "The effect of nozzle geometry over ignition delay and flame lift-off of reacting direct-injection sprays for three different fuels". In: *Fuel* 199 (2017), pp. 76–90. DOI: 10.1016/j.fuel.2017.02.075.

[28] Schöppe, D., Stahl, C., Krüger, G., and Dian, V. "Servo-Driven Piezo Common Rail Diesel Injection System". In: *ATZ Autotechnology* 12.2 (2012), pp. 42–47. DOI: 10.1365/s35595-012-0107-y.

[29] Pierpont, D. A., Montgomery, D. T., and Reitz, R. D. "Reducing Particulate and NOx Using Multiple Injections and EGR in a D.I. Diesel". In: *SAE Technical Paper 950217* (1995). DOI: 10.4271/950217.

[30] Han, Z., Uludogan, A., Hampson, G. J., and Reitz, R. D. "Mechanism of Soot and NOx Emission Reduction Using Multiple-injection in a Diesel Engine". In: *SAE Technical Paper 960633* (1996). DOI: 10.4271/960633.

[31] Payri, F., Benajes, J., Pastor, J. V., and Molina, S. "Influence of the Post-Injection Pattern on Performance, Soot and NOx Emissions in a HD Diesel Engine". In: *SAE Technical Paper 2002-01-0502* (2002). DOI: 10.4271/2002-01-0502.

[32] Badami, M., Millo, F., and D'Amato, D. D. "Experimental investigation on soot and NOx formation in a DI common rail diesel engine with pilot injection". In: *SAE Technical Paper 2001-01-0657* (2001). DOI: 10.4271/2001-01-0657.

[33] Badami, M., Mallamo, F., Millo, F., and Rossi, E. E. "Influence of Multiple Injection Strategies on Emissions, Combustion Noise and BSFC of a DI Common Rail Diesel Engine". In: *SAE Technical Paper 2002-01-0503* (2002). DOI: 10.4271/2002-01-0503.

[34] Mingfa, Y., Hu, W., Zunqing, Z., and Yan, Y. "Experimental Study of Multiple Injections and Coupling Effects of Multi-Injection and EGR in a HD Diesel Engine". In: *SAE Technical Paper 2009-01-2807* (2009). DOI: 10.4271/2009-01-2807.

[35] Lee, J., Jeon, J., Park, J., and Bae, C. "Effect of Multiple Injection Strategies on Emission and Combustion Characteristics in a Single Cylinder Direct-Injection Optical Engine". In: *SAE Technical Paper 2009-01-1354* (2010). DOI: 10.4271/2009-01-1354.

[36] O'Connor, J., Musculus, M. P. B., and Pickett, L. M. "Effect of post injections on mixture preparation and unburned hydrocarbon emissions in a heavy-duty diesel engine". In: *Combustion and Flame* 170 (2016), pp. 111–123. DOI: 10.1016/j.combustflame.2016.03.031.

[37] Pastor, J. V., López, J. J., García-Oliver, J. M., and Pastor, J. M. "A 1D model for the description of mixing-controlled inert diesel sprays". In: *Fuel* 87.13-14 (2008), pp. 2871–2885. DOI: 10.1016/j.fuel.2008.04.017.

[38] Desantes, J. M., Pastor, J. V., García-Oliver, J. M., and Pastor, J. M. "A 1D model for the description of mixing-controlled reacting diesel sprays". In: *Combustion and Flame* 156.1 (2009), pp. 234–249. DOI: 10.1016/j.combustflame.2008.10.008.

[39] Engine Combustion Network. *https://ecn.sandia.gov/diesel-spray-combustion/*. Online. 2010.

Chapter 2

The diesel injection process and spray development

2.1 Introduction

Within the scope of the compression ignition engines, the fundamental understanding of the basic mechanisms of the diesel spray injection process has played a crucial role in their development. The evolution of the injection technologies has permitted not only to improve the spray mixing process, but also accurately control the injection parameters as well as adding flexibility to the systems for new injection strategies [1].

Therefore, this chapter is mainly focused on presenting the fundamental concepts of diesel direct injection. Nevertheless, this only represents a summary of decades of research and well-established results in the field [2–7].

2.2 The diesel spray

In compression-ignition direct-injection (CIDI) engines, there is a direct link between fuel delivery and combustion control. Consequently, one of the most traditional ways to depict the combustion process is by comparing the temporal evolution of the injected mass and the apparent heat release rate (AHRR), calculated from the measurement of the cylinder pressure using the first law of thermodynamics [6]. An example is presented in Figure 2.1, referenced to

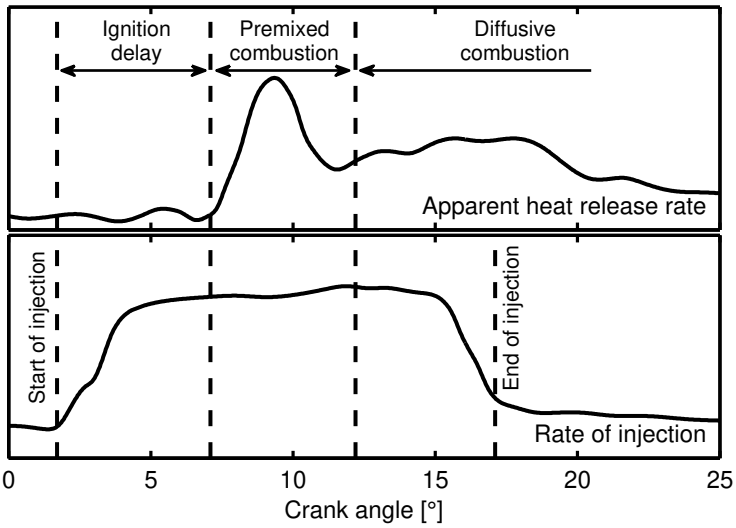

Figure 2.1: Temporal evolution of the apparent heat release rate (top) and mass flow rate (bottom) [6].

the start of energizing (SOE) of the injector. From the figure, as well as in the literature, three different phases can be distinguished [2, 3, 6–8]:

- Ignition delay: It is defined as the interval from the start of injection (SOI) up to the start of combustion (SOC). Once fuel enters the combustion chamber, there are a series of complex mechanisms that prepare the mixture for ignition, summarized in three main physical processes: atomization, air entrainment, and evaporation. Subsequently, in the presence of oxygen, low-intensity chemical pre-reactions take place, creating favorable conditions that trigger the spontaneous autoignition of the mixture. Therefore, a highly exothermic region is observed in the figure, marking the SOC, that is divided into two sequential phases. The ignition delay (ID) is highly dependent on numerous parameters such as: nozzle diameter, rail pressure, local chamber density, and temperature, among others.

- Premixed combustion: This represents the first phase of the exothermic reaction that takes place during the diesel combustion. All the fuel previously injected that is within flammability conditions, but has not yet auto-ignited, is quickly burned [9]. As a consequence, there is an abrupt liberation of heat (as observed in the figure) until all the fuel

premixed before the SOC is consumed, marking the end of the first stage of the combustion.

- Diffusion combustion: It is characterized as a mixing-controlled process since heat is released as long as fuel and air mix. Depending on the length of the injection, the flame can achieve a quasi-stationary structure, that is sustained as fuel is delivered. After the end of injection (EOI), the flame structure starts losing stability until the end of the combustion process.

2.2.1 Air-fuel mixture formation

Once the fuel is delivered into a dense atmosphere, the air-fuel mixture is driven by the momentum induced by the injection into the combustion chamber, and is described in the literature by three physical processes: atomization, air entrainment, and evaporation.

As it enters the combustion chamber, the liquid fuel column breaks up and starts disintegrating into droplets of different size, all of which sets up and favors the following processes [6]. The disintegration is a consequence of interactions that comprise surface instabilities, turbulence, surface tension, aerodynamic and inertial forces. The literature describes four different atomization regimes [10, 11]: Rayleigh, first wind-induced, second wind-induced and full atomization. Under modern diesel engine conditions with high injection pressures, the diesel spray is typically governed by full atomization [12, 13]. In such a regime, the initial perturbations cause droplets to form in the proximities of the outlet of the nozzle and are typically much smaller than the orifice diameter [12]. The intact surface length, which is the distance that an uninterrupted liquid core achieves before breaking up, trends to zero [5, 14]. García-Oliver [6] concluded that to under such conditions, full atomization is completed so promptly, and the droplets formed are so small, that there is a dynamic equilibrium between the mediums. Consequently, there is no relative velocity between the air and fuel molecules within the mixture, and it can be described by its velocity, equivalence ratio, and thermodynamic conditions.

Air entrainment is a direct consequence of the fuel atomization. Gas in the combustion chamber surrounds and starts interacting with the droplets, as they both travel downstream from the nozzle. The air entrained is linked to the momentum introduced by the fuel injection process [15–17].

As the gas possesses a higher temperature than the fuel, heat is exchanged between the liquid-gas interface, increasing the fuel vapor pressure up to evaporation. Hence, this phenomenon reduces the atomized droplet size until it

transforms all into a gaseous state downstream from the nozzle. The distance where full evaporation is fulfilled (that is, downstream there is only fuel in vapor phase) is known in the literature as the liquid length (LL) [15, 16, 18, 19]. More importantly, it is the energy provided by the air entrained that controls the evaporation, and not the heat released by the combustion [20], at least for free jets. The liquid length (LL) is dependent on numerous variables: nozzle diameter [15, 16, 21], fuel properties [15, 20, 22, 23], chamber density and temperature [15, 16, 21, 24, 25]. Contrarily, rail pressure has no apparent role in the evaporation length [15, 16, 24, 25]. Siebers [15] concluded that the process is mixed-controlled and that increasing the rail pressure increases the rate of air entrainment as well. Though, in general terms, the liquid length is achieved when enough enthalpy is provided to the fuel droplets, up to the point of its full evaporation.

A schematic diagram of these processes is presented in Figure 2.2, where only the liquid phase is delimited in the figure.

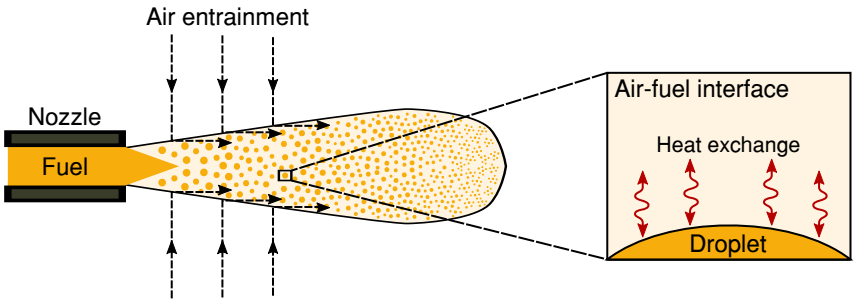

Figure 2.2: Schematic diagram of the air-fuel mixture formation. Only the liquid phase is delimited in the figure.

2.2.2 Autoignition process

The chemical reactions of the mixture start in regions with specific local conditions of air-fuel ratio and temperature that promotes autoignition. Higgins et al. [26], based on observations of their experimental data along with results presented by Westbrook et al. [27], summarized the diesel ignition in three stages:

- Physical induction: is driven by the mechanism described in the previous section. Fuel vaporization causes a decrease in temperature within the region of the spray, due to the heat absorbed by the fuel to evaporate,

temporally inhibiting any chemical reactions. As the mixture travels further downstream, its temperature increases up to flammability and first stage ignition, marking the end of the stage.

- First-stage ignition: it extends from the first noticeable chemiluminescence and rise in chamber pressure, up to when the rapid heat release begins. In general terms, conditions are fuel rich, with an average equivalence ratio between three and four. A series of chain reactions consume the premixed fuel somewhat uniformly, releasing small quantities of energy that increase chamber pressure (temperature), subsequently promoting further reactions. This stage is also known in the literature as cool flames [28], due to the low intensity of the flame chemiluminescence and heat released.

- Second-stage ignition: the temperature rises due to the heat released during the first-stage chemistry contributes to the start of the second stage ignition (SSI). It begins when hydrogen peroxide dissociation reactions dominate the chemistry due to certain temperature levels [2, 27], producing a significant heat release and triggering the premixed burn. The disassociation of the hydrogen peroxide produces the radical OH, and its transition from the excited to the ground state releases the chemiluminescence characteristic of this phase. As mentioned before, all the fuel injected that is within flammable conditions is consumed, causing a localized heat-release peak.

The high rate of pressure increase and peak temperature achieved during the premixed burn of the diesel spray are known to be one of the main sources of combustion noise and nitrogen oxides (NOx) formation. Therefore, understanding the parameters involved in diesel ignition is essential to optimize performance and pollutant emissions. To this end, different studies have characterized the ignition delay under different boundary conditions [28–35]. Authors proposed an Arrhenius equation that describes the ID as [28, 32, 33]:

$$ID \propto \exp\left(\frac{A}{T}\right) \cdot \rho^a \cdot \Delta P^b \cdot O_2^c\% \tag{2.1}$$

Where A is related to the global activation energy of reactions, T is the chamber temperature, ρ is the chamber density, ΔP is the fuel pressure drop through the nozzle, and $O_2\%$ is the oxygen concentration. From their results, the approximate coefficients for each variable calculated were: $A \approx 7500$,

$a \approx -1.3$, $b \approx -0.17$, and $c \approx -0.8$, describing the effect of each of the boundary conditions.

The evolution of the reacting mixture during the temporal discretization of the autoignition process favors the establishment of a self-sustained reaction, known as the diffusion flame.

2.2.3 The diffusion flame

Dec and Coy [36] studied the transition between the premixed combustion and the inception of the diffusion flame using spectroscopy. Their results indicated that it is established around the maximum heat release rate, near the spray head and propagates upstream to the nozzle up to a distance known in the literature as lift-off length (LOL) [32, 33, 37–40]. A flame front is formed, which is self-sustained while fuel and oxygen are supplied. The momentum provided by the injection of fuel is the backbone of the whole process, as it drives the mixing mechanisms that bolster the diffusion flame, defining the combustion as mixing-controlled.

Dec [41] established the most generally accepted diffusion flame model, presented in Figure 2.3. Flynn et al. [42] and Molina [8] described the temporal and spatial evolution the fuel as it is injected into the diffusion flame model. As observed in the figure, the flame is set at the lift-off length from the nozzle, wherein between the atomization, air entrainment and evaporation of the fuel take place, so it reaches ignition conditions. From there, the core is constituted by a rich reaction zone, partial combustion products, unburned fuel, and soot precursors. As these reach the flame front, the temperature

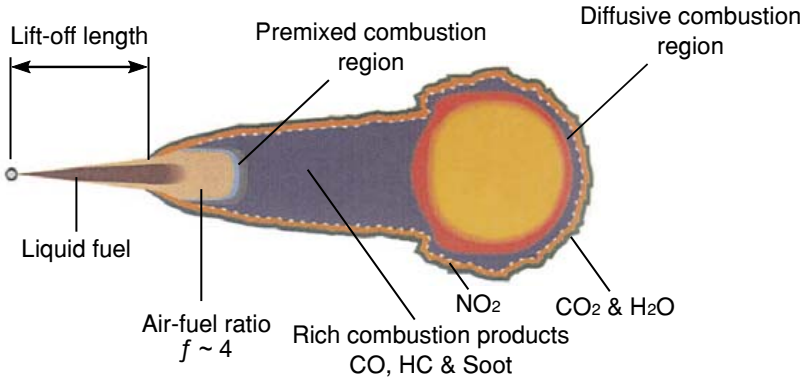

Figure 2.3: Schematic diagram of the quasi-stationary diffusion flame [41].

increases, which combined with the fuel-rich mixture, promotes the formation of small soot molecules that bind together into larger particles [43, 44]. The availability of oxygen in the flame front oxides these partial products of the combustion (including soot), providing most of the energy of the diffusion phase. Moreover, the accessibility of oxygen in the outer reactive surface of the flame promotes the formation of nitrogen oxides [45], which appear under high-temperature.

Nevertheless, depending on the conditions, fuel evaporation could be completed before the lift-off region [37, 46]. Siebers and Higgins [37] presented an alternate flame model, in which the mechanisms for fuel vaporization and combustion zones for such conditions are described. The authors concluded that the central reaction zone is more intense due to the increased air entrainment, with an overall leaner combustion, and less soot likely to be formed. Therefore, the lift-off length determines the equivalence ratio in the premixed region, and consequently, the composition of the partial products within the diffusive flame. Hence, it has been subjected to numerous studies in the literature [32, 33, 37–40]. Authors proposed an exponential equation that describes the LOL as [32, 33]:

$$LOL \propto T^a \cdot \rho^b \cdot \left(\sqrt{2 \cdot \frac{\Delta P}{\rho_f}}\right)^c \cdot O_2^d\% \tag{2.2}$$

Where ρ_f is the density of the fuel. From their results, the approximate coefficients for each variable calculated were: $a \approx -4.2$, $b \approx -1$, $c \approx 0.56$, and $d \approx -1.01$, describing the effect of each of the boundary conditions.

2.3 Fuel injection process

The diesel injection system is responsible for providing the fuel at specific conditions required by the engine. A robust system must be able to: deliver the right amount of fuel with a given mass flow rate, atomize the fuel to enhance subsequent processes, and more recently, allow for multiple injection pulses in a single combustion cycle with a very high precision [1].

2.3.1 The common-rail system

In most of the applications, the common-rail configuration [47] is the most widely used injection system in the industry [48], with a substantial increase in efficiency, reduction in the size of the engines, and consequent elimination of the pre-chamber.

Figure 2.4 presents a schematic diagram of the main components and layout of a typical common-rail system, with only one injector block shown. Fuel is filtered and sent to the pump-system from the reservoir by a low-pressure electric unit, generally placed in the tank itself. The pump-system, mechanically connected to the engine, delivers high-pressure fuel to the common-rail, with some low-pressure flow returning to the tank. The common-rail acts as an energy accumulator, storing the high-pressure fuel ready to be delivered to the injector unit that requires it. Its two main goals are to limit both the fluctuations due to the reciprocating high-pressure pump and the pressure drop that occurs during the injection process [47, 49]. A device that bleeds fuel from the rail back to the reservoir helps to control the pressure by differences of in-out flows.

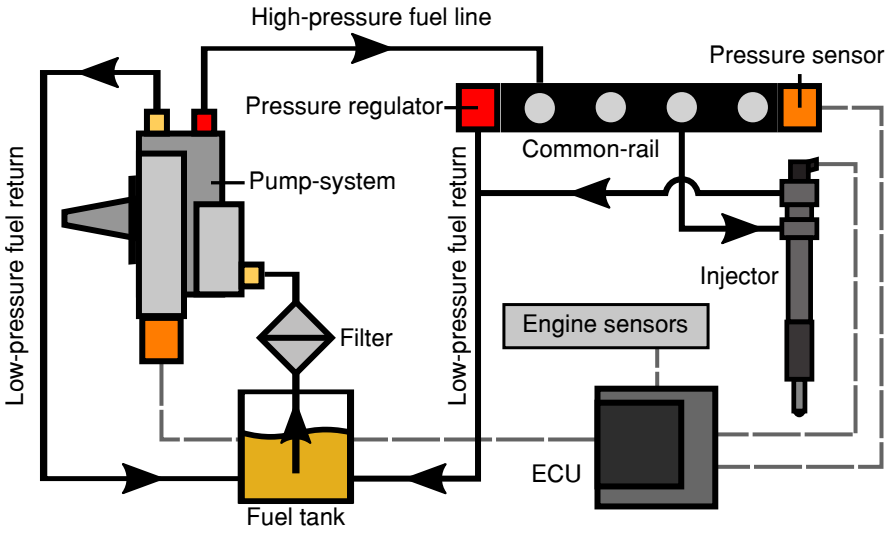

Figure 2.4: Schematic diagram of the general layout of a common rail system. Only one injector unit is shown.

Modern common-rail systems are capable of operating at a peak pressure of up to 300 MPa, considerably increasing the efficiency of the mixing and combustion process [50–53], as well as allowing to deliver the fuel in a shorter span.

2.3.2 The common-rail injector

The central and most complex elements of the common-rail system are the injectors. They can be classified into two big groups depending on the activa-

tion unit: solenoid or piezoelectric injectors. However, the working principle is somewhat similar, as both types control the rate of injection indirectly through a hydraulic mechanism. The main elements of a solenoid injector (in this case a Bosch CRI 2-25) are listed on the left side of Figure 2.5, while the basic working principle is shown on the right [17].

Fuel is fed from the common-rail through a high-pressure fitting (not shown in the figure) to the injector and is divided into two lines. One goes down towards the nozzle, whereas the other fills the control volume through a calibrated orifice. When in idle conditions (Figure 2.5.a), the resultant force due to the area difference plus the spring pushes the connecting-rod and needle downwards, preventing any injection of fuel. Once energized (Figure 2.5.b), the magnetic field induced by the solenoid pulls the ball-shaped valve upwards, opening the calibrated bleeding orifice of the control volume. Its pressure drops significantly, and the resultant force drives the rod up, initiating the injection event. After the end of the energizing signal, the valve returns to its original position (Figure 2.5.c), interrupting the return flow. Hence, the pressure in the control volume recovers progressively, until the initial conditions are attained. Then, once again, the connecting-rod and needle are pushed downwards, blocking the fuel flow through the orifices and ending the injection event.

Manufacturers have developed different solutions to enhance the accuracy and rapidity of the actuation system, but the basic working principle remains.

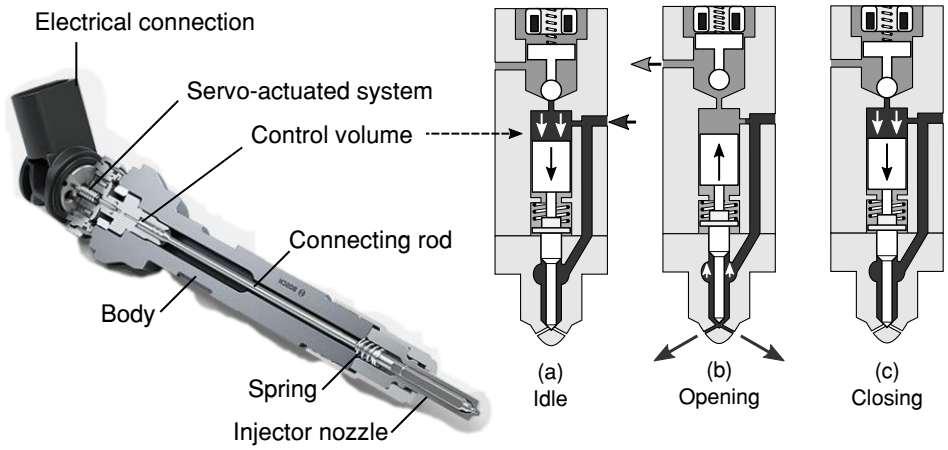

Figure 2.5: Common-rail injector with a solenoid actuator (left, Bosch CRI 2-25). Schematic diagram of the general working principle of a hydraulic injector (right) [17].

Piezoelectric driven injectors replace the solenoid elements by a piezoelectric crystal, made of layers that can either compress or expand as a function of the electric field [54]. The latest generations move the piezo-stack near the nozzle [1], ditching the connecting-rod, reducing the inertial mass, and improving its dynamic response [55, 56]. Furthermore, recent developments have permitted a direct control from the piezo stack to the rate of injection through a direct-acting mechanism [24, 57–61].

Nozzle geometry is another essential factor, as it is directly linked to the development of the spray. Some of the fundamental elements are the shape of the sac, nozzle inlet radius, nozzle length, and conicity factor (described as $k - factor$ [62]), among others. Understanding how flow develops within the injector is essential, as it defines its conditions at the outlet of the nozzle, which drives the atomization and mixing processes, that subsequently involves all of the other mechanism of the diesel combustion and pollutant emissions [46, 63–68].

2.3.3 Internal flow in the diesel nozzle

Fuel is stored in the common-rail with high hydrostatic energy due to its elevated pressure. When the injection event starts, it is forced through the internal channels of the injector and nozzle up to the chamber. As it moves, it suffers transformations mainly in pressure, velocity, and energy dissipation. This section summarizes the equations that describe in simple terms the internal flow development of the nozzle itself. However, more information is found in other works dedicated to this topic [17, 69]. The discharge coefficient is commonly used to evaluate the overall efficiency in the flow delivery of an injector. By considering a null velocity upstream in the common-rail, the Bernoulli equation can be simplified to:

$$\frac{P_r}{\rho_f} = \frac{P_b}{\rho_f} + \frac{1}{2} \cdot u_t^2 \tag{2.3}$$

Where P_r is the rail pressure, P_b is the discharge pressure, and u_t is the theoretical discharge velocity. Evaluating the equation, and defining the pressure drop along the nozzle as $\Delta P = P_r - P_b$, the theoretical velocity can be calculated as:

$$u_t = \sqrt{\frac{2 \cdot \Delta P}{\rho_f}} \tag{2.4}$$

Assuming that fuel flows throughout the entire cross-sectional outlet area of the nozzle (A_o), the theoretical mass flow ($\dot{m}_t$) is given by:

$$\dot{m}_t = A_o \cdot \rho_f \cdot u_t \tag{2.5}$$

Then, we can calculate the discharge coefficient by comparing the measured mass flow ($\dot{m}$) to the theoretical value, that is:

$$C_d = \frac{\dot{m}}{\dot{m}_t} = \frac{\dot{m}}{A_o\sqrt{2 \cdot \rho_f \cdot \Delta P}} \tag{2.6}$$

The discharge coefficient of diesel nozzle has been widely studied in the literature [59, 70–73], as it accounts for all the losses of efficiency within the injector. However, the flow structure might not be homogenous through the cross-sectional area of the nozzle. Consequently, it is useful to consider a simplified and uniform flow structure, with an effective area (A_{eff}) and velocity (u_{eff}), as represented in Figure 2.6.

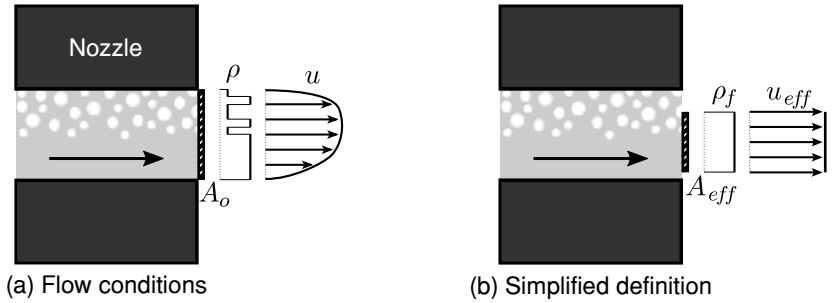

Figure 2.6: Flow conditions at the outlet of the nozzle (left) and simplified model in terms of the effective area and velocity (right) [17].

Based on the above, the mass flow rate and momentum flux ($\dot{M}$) can be defined as [17]:

$$\dot{m} = A_{eff} \cdot \rho_f \cdot u_{eff} \tag{2.7}$$

$$\dot{M} = A_{eff} \cdot \rho_f \cdot u_{eff}^2 \tag{2.8}$$

Hence, the effective area accounts for losses due to a non-uniform velocity, cavitation at the outlet of the nozzle and hydraulic flip [17, 64, 74–77]. Solving

both of the equations above, the effective area and velocity can be described in terms of the rate of injection and momentum flux:

$$u_{eff} = \frac{\dot{M}}{\dot{m}} \tag{2.9}$$

$$A_{eff} = \frac{\dot{m}^2}{\rho_f \cdot \dot{M}} \tag{2.10}$$

The expressions are dependent on variables that can be experimentally measured [64], and therefore, can be calculated and quantified. Results can be used as input for computational models [78, 79].

2.4 External flow characterization

The spray development can be generally described by studying its global interaction with the surrounding gas. Traditionally, in the literature, its characterization can be divided into two groups of variables: macroscopic and microscopic. The macroscopic characterization studies the general structure of the full spray, analyzing the temporal evolution of variables such as spray penetration (S), liquid length (LL), spreading angle (θ), and air entrainment, among others. In contrast, the microscopic characterization is focused on specific variables contained within its boundaries, such as droplet size [80–83] and velocity distribution [84–89]. Due to the scope of the present thesis, this section only describes variables related to the global spray structure, with their definition represented in Figure 2.7.

2.4.1 Spray penetration

As the spray moves further downstream, the penetration is defined as the distance from the nozzle to its furthest point. It is related to the mixing process, as it depends on the momentum exchanged with the surrounding gas, and describes how the spray would interact with either the piston or chamber walls. Through the experimental characterization of the spray penetration [5, 17, 52, 81, 90–92], authors represented its dependency to boundary conditions with the following correlation, where the coefficients were calculated by a dimensional analysis:

$$S \propto \rho^{-1/4} \cdot \dot{M}^{1/4} \cdot tan\,(\theta/2)^{-1/2} \cdot t^{1/2} \tag{2.11}$$

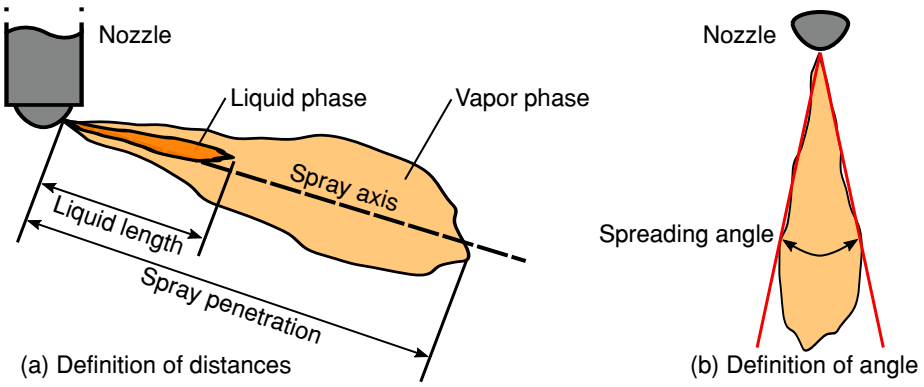

Figure 2.7: Definition of the macroscopic variables of the spray in terms of distances and angle.

Where ρ is the chamber density, and t is the time since the start of injection. The equation can also be expressed in terms of the pressure drop, and nozzle outlet diameter (D_o):

$$S \propto \rho^{-1/4} \cdot \Delta P^{1/4} \cdot tan\,(\theta/2)^{-1/2} \cdot D_o^{1/2} \cdot t^{1/2} \tag{2.12}$$

However, the development of the spray near the nozzle resembles a linear time proportionality, rather than $t^{1/2}$. As a result, some correlations were divided into a two-stage equation depending on a particular breakup time [81, 91]. Furthermore, near nozzle visualization at very high acquisition rate showed that the spray penetration is increasingly parabolic the first few millimeters, as pressure builds up in the sac of the injector [13, 93, 94].

2.4.2 Liquid length

In subsection 2.2.1, it was defined that the liquid length is the distance required by the spray to fully evaporate all fuel droplets. It is established as a distance, rather than a characteristic time, because it is dependent on the rate of air entrainment [15, 16]. Therefore, for example, increasing the rail pressure increases injection velocity that produces higher air entrainment. However, the liquid length is not affected, even though fuel droplets vaporize in a shorter span. Several studies in the literature describe the dependence of the LL on boundary conditions [15, 16, 20–25]. It can be generally be described by 1-D mixing-controlled models [78], or by empirical correlations [16, 19, 23, 95]. As an example, Equation 2.13 depicts a combination of regressions calculated by

Payri et al. [19] and Payri et al. [25] with its corresponding coefficients, where T_f represents the temperature of the fuel.

$$LL \propto D_o^{1.08} \cdot \rho_f^{0.5} \cdot \rho^{-0.61} \cdot T^{-1.7} \cdot T_f^{0.61} \cdot \Delta P^{-0.05} \tag{2.13}$$

2.4.3 Spray spreading angle

The naturally-turbulent conditions of the flow and the aerodynamic interaction between the liquid-gas interface are two of the main factors affecting the spreading angle. In general terms, it is linked to the air entrainment that subsequently affects the fuel evaporation and combustion processes, and is defined as the aperture of the spray. The spreading angle is highly transitory during the start and end of injection. However, authors have focused efforts on describing the dependence of the angle on boundary conditions during the steady state injection processes, where it reaches a somewhat stable value [13, 17, 25, 71, 81, 91, 96–98]. Empirical correlations derived from experimental measurements depict that the ratio between the chamber and fuel density is the main driving factor. Hiroyasu and Arai [81] performed a set of experimental campaigns varying the shape of the nozzle, including the sac. Based on their experimental results, they defined the spreading angle as:

$$\theta \propto \frac{L_n}{D_o}^{0.022} \cdot \frac{D_o}{D_s}^{0.15} \cdot \frac{\rho}{\rho_f}^{0.26} \tag{2.14}$$

Where L_n is the length of the nozzle, and D_s is the diameter of the sac. Other works also found similar trends [91, 97, 99], all establishing that rail pressure and fuel viscosity have negligible effects.

Payri et al. [23] studied two nozzles with different conicity factors, but the same hydro-grinding and nominal mass flow rate, concluding that cavitation [64, 67, 90] affects spreading angle fluctuations due to higher turbulence at the outlet of the nozzle, with a similar trend presented by Payri et al. [13]. Nevertheless, quantifying the spray angle is difficult, due to the complexity of the phenomenon itself. Moreover, the measurement is particularly sensitive to the experimental technique employed, light distribution, the image processing technique, and the geometrical definition of the angle, among other factors [100].

2.4.4 Temporal evolution of the macroscopic variables

The variables mentioned in this section can be temporally characterized with the proper optical diagnostics. Most of the experimental work referenced are

of measurements carried out in optically accessible test cells with high-speed imaging. Thus, for each frame, each of the variables can be extracted from the movies. Figure 2.8 depicts an example of the temporal evolution of a real spray contour of both vapor and liquid phases. From the figure, it is observed how the spray initially penetrates at a faster rate due to the high momentum, and slowly trends to a $t^{0.5}$ dependence. In contrast, the liquid phase initially penetrates equally up the vaporization length, where it then somewhat stabilizes.

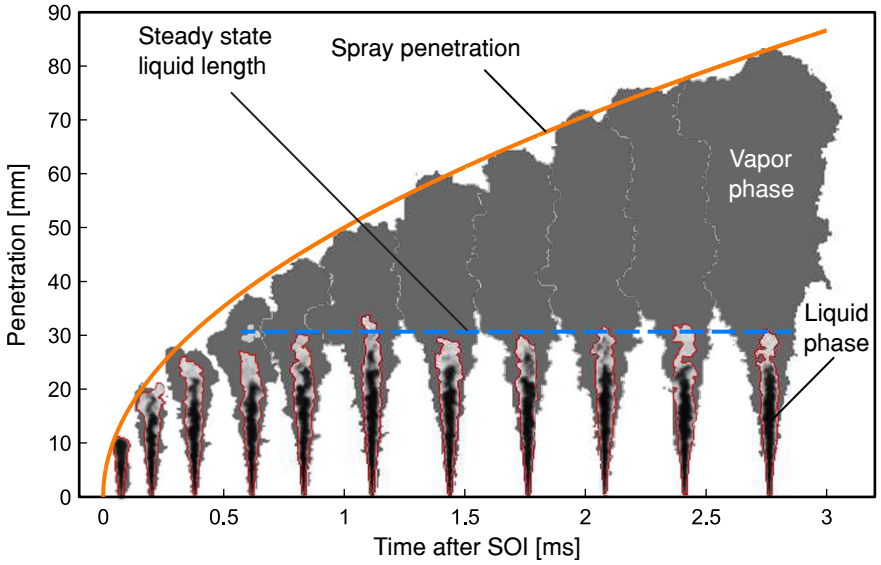

Figure 2.8: Example of the temporal evolution of the vapor and liquid phase penetration [61].

2.5 Multiple injection strategies

As stated in the previous sections, soot particles are generally formed in fuel-rich regions, and are mostly burnt off at the high-temperature near stoichiometric reaction zones within the spray boundary, due to the availability of oxygen. However, the formation of nitrogen oxides in these high-temperature regions (where soot is burnt) becomes unavoidable, establishing the widely known soot-NOx trade-off [101–103]. For example, temperatures within the combustion chamber can be lowered by either exhaust gas recirculation (EGR) or retarding the fuel injection timing, which restricts the formation of nitrogen

oxides. Nevertheless, this reduces the energy and residence time necessary to burn off soot particles, increasing its emissions as well as unburned hydrocarbons (UHC) and carbon monoxide (CO) [101].

The equivalence ratio (ϕ) vs. temperature diagram was initially proposed by Kamimoto and Bae [104] to analyze the diesel combustion [101, 102, 105, 106], as well as understand the soot-NOx trade-off. Potter and Durrett [107] used this diagram to describe the trajectory of a single fuel parcel as it travels through the combustion process. A similar representation is shown in Figure 2.9. After the initial air-fuel mixing and premixed combustion (a-b), the remnant fuel energy is released as the rich products continue to mix following the diffusion flame temperature path (b-c). The maximum temperature is obtained at stoichiometric conditions ($\phi = 1$), after which no significant chemical heat release occurs, and temperature decreases (c-d). Although the figure depicts only one path, the actual combustion processes pass through particular trajectories in this representation. It results evident from the diagram that both soot and NOx formations depend strongly on the path followed during the combustion process.

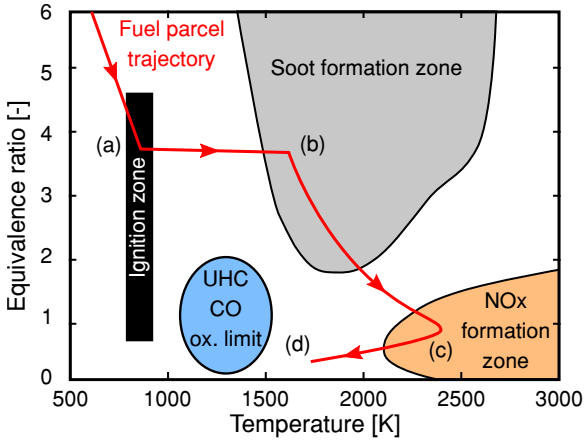

Figure 2.9: An example of the possible trajectory of a single fuel parcel through the combustion processes. Adapted from Potter and Durrett [107].

Multiple injection strategies are one of the numerous techniques/technologies implemented in modern diesel engines to reduce its emissions [103, 108–111]. A typical injection event consists of a single and continuous supply of fuel to the combustion chamber. With multiple injections, as the name suggests, the fuel is divided into many dosed quantities,

that can be either equal in mass (split strategy) or different (early-pilot-post-late strategies). First, to understand the differences in terms of fuel delivery, Figure 2.10 represents three diagrams comparing a single injection (a), split injection (b), and multiple injections with a main pulse (c). The main difference between the last two strategies is that the split injections divide the target mass uniformly across different pulses. Contrarily, in multiple injections with a main, each auxiliary pulse can be of a different quantity, trying to match the same injected target mass as a single injection event, to prevent increasing fuel consumption.

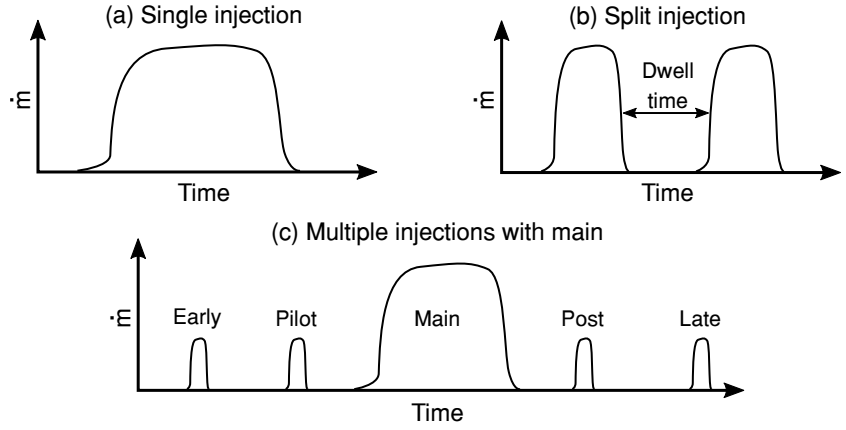

Figure 2.10: Mass delivery for the different injection strategies.

The number of pulses is limited to the capabilities of the injection system and the duration of the combustion. However, as the diesel technology evolves, newer injection systems allow to precisely inject up to 8 different times per cycle [1]. More pulses provide more flexibility and control over the heat release and air-fuel mixing process, which if tuned properly, can lead to a better engine performance [112]. Distinguishing between early/pilot and post/late is difficult to assess, as no clear definition is provided in the literature. But authors suggest that, for example, early/late injections are significantly advanced/retarded from the main pulse, in contrast to the pilot/post [113]. In general, the distance between pulses is named dwell time (DT). It is important to remark that the real dwell time is the separation between the mass flow rate pulses and not the command signal, to consider the hydraulic delay of the start and end of injection.

With an optimized configuration of the injected quantity and its dwell time, these strategies have proved capable of reducing fuel consumption, par-

ticulate matter, carbon oxides, nitrogen oxides, soot, and unburned hydrocarbons [108–110, 114–118]. This section provides a brief insight into how multiple injection strategies affect combustion mechanisms and pollutant emissions. However, the trends discussed are somewhat limited to the experimental tools and conditions used, and often works can result in slightly contradictory trends [119].

2.5.1 Injections before the main pulse

The concept of multiple injections existed since 1937 when Jafer [120] tested a pilot mass to reduce combustion noise [112]. Since then, numerous experimental works have analyzed the influence of pilot injection on the development of the combustion event.

Diesel combustion noise is associated with the maximum in-cylinder pressure rise rate [121–126], which occurs in the premixed phase. The mass of fuel burned during this step is fundamentally dependent on the air-fuel mix rate and the ignition delay [9, 26, 127]. Different authors observed a reduction in combustion noise with a pilot pulse [111, 117, 128–130]. In general terms, the ID of the main decreased, which reduced the fuel injected prior ignition and lowered the pressure rise rate [87, 109, 128, 130–132]. Badami et al. [117] carried out experimental measurements on an engine with a double pilot strategy, and noted that it effectively decreased combustion noise and fuel consumption, but with a penalty on emissions. Busch et al. [130] performed an experimental and numerical analysis of close-coupled pilot injections as a mean to reduce combustion noise, and found an optimum dwell time that notably decreased combustion noise with almost no penalty on emissions. The authors described a combination of two factors responsible for such trend: the changing phasing of the pilot heat release event relative to the main, and the suppression of the pilot AHRR by the main injection due to the energy required to heat and vaporize the fuel.

Ishida et al. [133] and Carlucci et al. [131] discussed the impact on the reduction of nitrogen oxides emissions. First, authors established that pilot injections decrease the ignition delay of the main pulse, by enhancing conditions for its combustion. As a result, the amount of fuel burned in the premixed phase is shortened, which leads to a reduction in the combustion peak temperature [111], that is determinant for the formation of NOx [108]. Han et al. [114] provided a computational analysis on the mechanism involved in the decrease of NOx, mentioning its similarity to that of a single injection with retarded timing. Hence, the authors defined that the chemistry for the formation of nitrogen oxides is sensitive not to only the peak temperature, but

also to the time that combustion products are exposed to these conditions. Badami et al. [115] performed a detailed investigation of engine-out emissions with pilot injection for increasing dwell times, concluding that NOx production increases as the mean temperature in the combustion chamber is higher, with similar trends noted by Carlucci et al. [113] when including an early pulse.

Contrarily, decreasing combustion peak temperature reduces the energy and residence time necessary to burn off soot particles [101]. Furthermore, as the ignition delay of the main shortens, more fuel is burned in the diffusion phase, which enhances soot formation [43, 44, 115, 131]. However, authors have reported that with proper tuning of the injections before the main, NOx formation can be reduced with a small penalty on soot and hydrocarbon emissions [109, 134]. To this end, Binde et al. [134] proposed a two-injector system, one to precisely control the pilot pulse, and the other for the main. With their configuration, the authors reported better oxygen utilization in the combustion chamber, enabling higher EGR rates that lowered the peak temperature but scarcely altering soot emissions.

In general terms, pilot injections increase the emissions of unburned hydrocarbons, as fuel impinge the cylinder wall and do not entirely burn [109, 113, 135]. Carlucci et al. [113] tested pilot/early strategies with different durations and timings, which resulted in higher unburned hydrocarbon emissions for all conditions compared to a single injection event.

2.5.2 Injections after the main pulse

Literature work widely refers to post injections as a tool for the reduction of soot exhaust emissions [112, 135–143]. The combustion related soot from diesel is determined by the competition between its formation and oxidation. O'Connor and Musculus [143] provided a very detailed literature review of these processes with a post injection, with multiple references of both experimental and modeling data from optical and real engines. The authors discussed several mechanisms:

- A post injection introduces momentum in the latter phase of combustion, which enhances mixing within the cylinder bowl that might increase oxidation of the soot formed by the main injection [135, 140, 142].
- Its combustion releases additional heat, which enhances the oxidation of soot formed by the main [139, 140].

- No interaction between injections avoids rich reaction zones prone to form soot [138, 141].
- The dwell time between the injections controls their interaction in the cylinder [135, 136, 138, 140, 142], and specifically the temperature and soot oxidation along the squish region [135].
- Higher swirl ratios improve soot oxidation by enhancing the targeting of the main injection residual mixture by the post injection [112, 136, 137, 142].

More mechanisms are mentioned in their work, as well as many more references from the literature than those presented in this document. Then, is it generally accepted that post injections reintroduce high-temperature reactions and increase local mixing, which promotes the oxidation of the total soot produced in the previous injection event. However, the effectiveness of the post injection on reducing soot emissions is closely linked to the confined bowl-shaped combustion chamber of the engine. Specific studies have analyzed soot formation and oxidation between a free jet and with wall interaction [144, 145]. Authors concluded that spray/wall synergy enhanced soot oxidation and reduced its production due to higher mixing with ambient air caused by wall impingement, as well as due to thermal interactions with the walls that cooled down the jet.

Although the use of EGR benefits the formation of NOx by lowering peak combustion temperature [146], it can lead to an increase in engine-out soot due to the reduction in intake oxygen [147–149]. Combining a post injection with high EGR rates improve the trade-off of soot, fuel consumption, and NOx [135, 150, 151], with numerous authors reporting no influence in the formation of nitrogen oxides [135, 138, 141]. In contrast, post injections can increase the emissions of unburned hydrocarbons [151, 152] and carbon monoxides [153, 154], as mixtures near the injector become too lean to achieve ignition in the time available, due to the lower cylinder temperatures.

Post/late injections events are also used to regenerate particle filters in the exhaust [154]. Regeneration occurs at around 900 K, where the particulate matter oxidates [155]. Hence, late injections are generally used to increase exhaust gas temperatures. Yoon et al. [154] undertook experimental measurements of the strategies for diesel particulate filter regeneration with a post injection at low and medium load. Authors found relevant to tune both the timing and number of pulses to achieve proper exhaust temperatures with an acceptable compromise in terms of unburned hydrocarbons and carbon monoxides emissions.

2.5.3 Split injections

Mendez and Thirouard [111] referred to split injections as a potential tool to divide heat released in the combustion chamber into dosed packages. The authors defined two different combustion processes depending on the ignition delay of the second injection: two premixed-type combustion phases for long dwell times, or one premixed-type followed by a diffusion combustion of the second pulse. The combustion noise can be significantly reduced, due to a slower rate of heat release [108, 111, 119].

Mohan et al. [119] provided a literature review of different studies regarding split injections. The authors suggested that the strategy depicts a potential to decrease particulate emissions significantly without a substantial compensation in NOx. However, the effectiveness and trends regarding pollutant emissions are strongly linked to the specifics of the timing and load conditions [108, 138, 141, 156, 157]. Therefore a definite pattern is hard to assess. For example, Akkurt [158] performed engine simulations using a CFD model coupled with a split injection strategy, and found that it led to a larger area of the stoichiometric mixture exposed to higher temperatures, which increased NOx formation.

Numerous authors have used split injections to analyze the interaction between two injection events [87, 132, 159–162], remarking similarities concerning pilot-main and main-post strategies. The following observations were made:

- The first injection acts as a pilot pulse to the second event. A short dwell time increases the mixing rate at the head of the second injection, due to the interaction between the velocity fields [87, 159].
- Splitting injections significantly affect the combustion structure and soot formation [87, 132, 162].
- The ignition delay of the second injection shortens due to the enhancement of local conditions by the combustion of the first pulse [87, 132, 161, 162].
- The ignition location and lift-off length of the second injection moves upstream to the nozzle [132, 162]. Consequently, soot emissions increase due to more fuel being burned in a richer diffusion combustion, although it depends on the dwell time that controls the synergy between pulses.

Even though split injections strategies were not used in the present work, many of the processes described are still valid to understand the interactions that occur in pilot-main and main-post strategies.

References

[1] Schöppe, D., Stahl, C., Krüger, G., and Dian, V. "Servo-Driven Piezo Common Rail Diesel Injection System". In: *ATZ Autotechnology* 12.2 (2012), pp. 42–47. DOI: 10.1365/s35595-012-0107-y.

[2] Heywood, J. B. *Internal Combustion Engine Fundamentals*. McGraw-Hill, 1988.

[3] Taylor, C. F. *The internal-combustion engine in theory and practice*. 2nd ed. Cambridge: MIT Press, 1989.

[4] Armas, O. "Diagnóstico experimental del proceso de combustión en motores Diesel de inyección directa". PhD thesis. Universitat Politècnica de València, 1998.

[5] Correas, D. "Estudio teórico-experimental del chorro libre Diesel isotermo". PhD thesis. Valencia: Universitat Politècnica de València, 1998.

[6] García-Oliver, J. M. "Aportaciones al estudio del proceso de combustión turbulenta de chorros en motores Diesel de inyección directa". PhD thesis. Valencia: Universitat Politècnica de València, 2004. DOI: 10.4995/Thesis/10251/55164.

[7] Payri, F. and Desantes, J. M. *Motores de combustion interna alternativos*. Editorial Universitat Politecnica de Valencia, 2011.

[8] Molina, S. *Influencia de los parámetros de inyección y la recirculación de gases de escape sobre el proceso de combustión en un motor diesel*. Ed. by F. Payri and J. M. Desantes. Barcelona, 2005.

[9] Alkidas, A. C. "On the Premixed Combustion in a Direct-Injection Diesel Engine". In: *Journal of Engineering for Gas Turbines and Power* 109.2 (1987), pp. 187–192. DOI: 10.1115/1.3240023.

[10] Reitz, R. D. "Atomisation and other breakup regimes of a liquid jet". PhD thesis. Princeton University, 1978.

[11] Reitz, R. D. and Bracco, F. V. *Mechanism of breakup of round liquid jets*. Ed. by N. Cheremisnoff. Vol. 3. Houston: Gulf Publishing, 1984, pp. 233–249.

[12] Arrègle, J. "Análisis de la estructura y dinámica interna de chorros Diesel". PhD thesis. Valencia: Universitat Politècnica de València, 1997.

[13] Payri, R., Bracho, G., Martí-Aldaraví, P., and Viera, A. "Near field visualization of diesel spray for different nozzle inclination angles in non-vaporizing conditions". In: *Atomization and Sprays* 27.3 (2017), pp. 251–267. DOI: 10.1615/AtomizSpr.2017017949.

[14] Levy, N., Amara, S., Champoussin, J. C., and Guerrassi, N. "Non-Reactive Diesel Spray Computations Supported by PDA Measurements". In: *SAE Technical Paper 970049* (1997). DOI: 10.4271/970049.

[15] Siebers, D. L. "Liquid-Phase Fuel Penetration in Diesel Sprays". In: *SAE Technical Paper 980809* (1998). DOI: 10.4271/980809.

[16] Siebers, D. L. "Scaling liquid-phase fuel penetration in diesel sprays based on mixing-limited vaporization". In: *SAE Technical Paper 1999-01-0528* (1999). DOI: 10.4271/1999-01-0528.

[17] Gimeno, J. "Desarrollo y aplicación de la medida del flujo de cantidad de movimiento de un chorro diesel". PhD thesis. Universitat Politècnica de València, 2008. DOI: 10.4995/Thesis/10251/8306.

[18] Bardi, M. et al. "Engine Combustion Network: Comparison of Spray Development, Vaporization, and Combustion in Different Combustion Vessels". In: *Atomization and Sprays* 22.10 (2012), pp. 807–842. DOI: 10.1615/AtomizSpr.2013005837.

[19] Payri, R., García-Oliver, J. M., Bardi, M., and Manin, J. "Fuel temperature influence on diesel sprays in inert and reacting conditions". In: *Applied Thermal Engineering* 35.1 (2012), pp. 185–195. DOI: 10.1016/j.applthermaleng.2011.10.027.

[20] Espey, C. and Dec, J. E. "The effect of TDC temperature and density on the liquid-phase fuel penetration in a D.I. Diesel engine". In: *SAE Technical Paper 952456* (1995). DOI: 10.4271/952456.

[21] Martínez-Martínez, S. "Desarrollo de una instalación experimental para el estudio de chorros diesel evaporados en atmósfera inerte y reactiva". PhD thesis. Universitat Politècnica de València, 2003.

[22] Higgins, B. S., Mueller, C. J., and Siebers, D. L. "Measurements of Fuel Effects on Liquid-Phase Penetration in DI Sprays". In: *SAE Technical Paper 1999-01-0519* (1999). DOI: 10.4271/1999-01-0519.

[23] Payri, R., Viera, J. P., Gopalakrishnan, V., and Szymkowicz, P. G. "The effect of nozzle geometry over the evaporative spray formation for three different fuels". In: *Fuel* 188 (2017), pp. 645–660. DOI: 10.1016/j.fuel.2016.06.041.

[24] Payri, R., Gimeno, J., Bardi, M., and Plazas, A. H. "Study liquid length penetration results obtained with a direct acting piezo electric injector". In: *Applied Energy* 106 (2013), pp. 152–162. DOI: 10.1016/j.apenergy.2013.01.027.

[25] Payri, R., Gimeno, J., Bracho, G., and Vaquerizo, D. "Study of liquid and vapor phase behavior on Diesel sprays for heavy duty engine nozzles". In: *Applied Thermal Engineering* 107 (2016), pp. 365–378. DOI: 10.1016/j.applthermaleng.2016.06.159.

[26] Higgins, B. S., Siebers, D. L., and Aradi, A. "Diesel-Spray Ignition and Premixed-Burn Behavior". In: *SAE Technical Paper 2000-01-0940* (2000). DOI: 10.4271/2000-01-0940.

[27] Westbrook, C. K. et al. "The effects of pressure, temperature, and concentration on the reactivity of alkanes: Experiments and modeling in a rapid compression machine". In: *International Symposium on Combustion* 27.1 (1998), pp. 371–378. DOI: 10.1016/S0082-0784(98)80425-6.

[28] Pickett, L. M., Siebers, D. L., and Idicheria, C. A. "Relationship Between Ignition Processes and the Lift-Off Length of Diesel Fuel Jets". In: *SAE Technical Paper 2005-01-3843* 724 (2005). DOI: 10.4271/2005-01-3843.

[29] Kobori, S., Kamimoto, T., and Aradi, A. "A study of ignition delay of diesel fuel sprays". In: *International Journal of Engine Research* 1.29 (2000), pp. 29–39. DOI: 10.1243/1468087001545245.

[30] Bruneaux, G. "Development of optical diagnostics techniques to correlate mixing and auto-ignition processes in high pressure diesel jets". In: *Oil & Gas Science and Technology* 63.4 (2008), pp. 461–477. DOI: 10.2516/ogst:2008031.

[31] Lillo, P. M., Pickett, L. M., Persson, H., Andersson, Ö., and Kook, S. "Diesel Spray Ignition Detection and Spatial/Temporal Correction". In: *SAE International Journal of Engines* 5.3 (2012), pp. 2012–01–1239. DOI: 10.4271/2012-01-1239.

[32] Benajes, J., Payri, R., Bardi, M., and Martí-Aldaraví, P. "Experimental characterization of diesel ignition and lift-off length using a single-hole ECN injector". In: *Applied Thermal Engineering* 58.1-2 (2013), pp. 554–563. DOI: 10.1016/j.applthermaleng.2013.04.044.

[33] Payri, R., Salvador, F. J., Manin, J., and Viera, A. "Diesel ignition delay and lift-off length through different methodologies using a multihole injector". In: *Applied Energy* 162 (2016), pp. 541–550. DOI: 10.1016/j.apenergy.2015.10.118.

[34] Payri, R., Viera, J. P., Pei, Y., and Som, S. "Experimental and numerical study of lift-off length and ignition delay of a two-component diesel surrogate". In: *Fuel* 158 (2015), pp. 957–967. DOI: 10.1016/j.fuel.2014.11.072.

[35] Payri, R., Viera, J. P., Gopalakrishnan, V., and Szymkowicz, P. G. "The effect of nozzle geometry over ignition delay and flame lift-off of reacting direct-injection sprays for three different fuels". In: *Fuel* 199 (2017), pp. 76–90. DOI: 10.1016/j.fuel.2017.02.075.

[36] Dec, J. E. and Coy, E. B. "OH Radical Imaging in a DI Diesel Engine and the Structure of the Early Diffusion Flame". In: *SAE Technical Paper 960831* (1996). DOI: 10.4271/960831.

[37] Siebers, D. L. and Higgins, B. S. "Flame Lift-Off on Direct-Injection Diesel Sprays Under Quiescent Conditions". In: *SAE Technical Paper 2001-01-0530* 724 (2001). DOI: 10.4271/2001-01-0530.

[38] Higgins, B. S. and Siebers, D. L. "Measurement of the Flame Lift-Off Location on DI Diesel Sprays Using OH Chemiluminescence". In: *SAE Technical Paper 2001-01-0918* (2001). DOI: 10.4271/2001-01-0918.

[39] Pickett, L. M., Kook, S., Persson, H., and Andersson, Ö. "Diesel fuel jet lift-off stabilization in the presence of laser-induced plasma ignition". In: *Proceedings of the Combustion Institute* 32 (2009), pp. 2793–2800. DOI: 10.1016/j.proci.2008.06.082.

[40] Taskiran, O. O. and Ergeneman, M. "Effect of nozzle dimensions and fuel type on flame lift-off length". In: *Fuel* 115 (2014), pp. 833–840. DOI: 10.1016/j.fuel.2013.03.005.

[41] Dec, J. E. "A Conceptual Model of DI Diesel Combustion Based on Laser-Sheet Imaging". In: *SAE Technical Paper 970873* (1997).

[42] Flynn, P. et al. "Diesel combustion: an integrated view combining laser diagnostics, chemical kinetics, and empirical validation". In: *SAE Technical Paper 1999-01-0509* 724 (1999).

[43] Lahaye, J. "Mechanisms of soot formation". In: *Polymer Degradation and Stability* 30.1 (1990), pp. 111–121. DOI: 10.1016/0141-3910(90)90121-M.

[44] Xi, J. and Zhong, B. J. "Soot in diesel combustion systems". In: *Chemical Engineering and Technology* 29.6 (2006), pp. 665–673. DOI: 10.1002/ceat.200600016.

[45] Dec, J. E. and Canaan, R. E. "PLIF Imaging of NO Formation in a DI Diesel Engine". In: *SAE Technical Paper 980147* (1998). DOI: 10.4271/980147.

[46] Payri, R., Bracho, G., Martí-Aldaraví, P., and Viera, A. "Nozzle Geometry Size Influence on Reactive Spray Development: From Spray B to Heavy Duty Applications". In: *SAE Technical Paper 2017-01-0846* (2017), p. 12. DOI: 10.4271/2017-01-0846.

[47] Boehner, W. and Hummel, K. "Common Rail Injection System for Commercial Diesel Vehicles". In: *SAE Technical Paper 970345* (1997). DOI: 10.4271/970345.

[48] Flaig, U., Polach, W., and Ziegler, G. "Common Rail System (CR-System) for Passenger Car DI Diesel Engines ; Experiences with Applications for Series Production Projects". In: *SAE Technical Paper 1999-01-0191* (1999). DOI: 10.4271/1999-01-0191.

[49] Payri, R., Tormos, B., Salvador, F. J., and Plazas, A. H. "Using one-dimensional modelling codes to analyse the influence of diesel nozzle geometry on injection rate characteristics". In: *International Journal of Vehicle Design* 38.1 (2005), pp. 58–78. DOI: 10.1504/IJVD.2005.006605.

[50] Johnson, J. E. et al. "Characteristics of 3000 bar Diesel Spray Injection under Non-Vaporizing and Vaporizing Conditions". In: *ICLASS 12th Triennial International Conference on Liquid Atomization and Spray Systems*. Heidelberg, 2012.

[51] Johnson, J. E. et al. "Correlations of Non-Vaporizing Spray Penetration for 3000 Bar Diesel Spray Injection". In: *SAE Technical Paper 2013-24-0033* (2013). DOI: 10.4271/2013-24-0033.

[52] Giraldo Valderrama, J. S. "Macroscopic and microscopic characterization of non-reacting diesel sprays at low and very high injection pressures". PhD thesis. Universitat Politècnica de València, 2018. DOI: 10.4995/Thesis/10251/113643.

[53] Boccardo, G. et al. "Experimental investigation on a 3000 bar fuel injection system for a SCR-free non-road diesel engine". In: *Fuel* 243 (2019), pp. 342–351. DOI: 10.1016/j.fuel.2019.01.122.

[54] Chaplya, P. M., Mitrovic, M., Carman, G. P., and Straub, F. K. "Durability properties of piezoelectric stack actuators under combined electromechanical loading". In: *Journal of Applied Physics* 100.12 (2006), p. 124111. DOI: 10.1063/1.2407269.

[55] Lee, J. et al. "Effect of piezo-driven and solenoid-driven needle opening of common-rail diesel injectors on internal nozzle flow and spray development". In: *International Journal of Engine Research* 7.6 (2006), pp. 489–502. DOI: 10.1243/14680874JER00806.

[56] Suh, H. K., Park, S. W., and Lee, C. S. "Effect of piezo-driven injection system on the macroscopic and microscopic atomization characteristics of diesel fuel spray". In: *Fuel* 86.17-18 (2007), pp. 2833–2845. DOI: 10.1016/j.fuel.2007.03.015.

[57] Payri, R., Gimeno, J., Viera, J. P., and Plazas, A. H. "Needle lift profile influence on the vapor phase penetration for a prototype diesel direct acting piezoelectric injector". In: *Fuel* 113 (2013), pp. 257–265. DOI: 10.1016/j.fuel.2013.05.057.

[58] Viera, J. P. et al. "Linking instantaneous rate of injection to X-ray needle lift measurements for a direct-acting piezoelectric injector". In: *Energy Conversion and Management* 112 (2016), pp. 350–358. DOI: 10.1016/j.enconman.2016.01.038.

[59] Payri, R., Gimeno, J., Mata, C., and Viera, A. "Rate of injection measurements of a direct-acting piezoelectric injector for different operating temperatures". In: *Energy Conversion and Management* 154 (2017), pp. 387–393. DOI: 10.1016/j.enconman.2017.11.029.

[60] Macian, V., Payri, R., Ruiz, S., Bardi, M., and Plazas, A. H. "Experimental study of the relationship between injection rate shape and Diesel ignition using a novel piezo-actuated direct-acting injector". In: *Applied Energy* 118 (2014), pp. 100–113. DOI: 10.1016/j.apenergy.2013.12.025.

[61] Bardi, M. "Partial Needle Lift and Injection Rate Shape Effect on the Formation and Combustion of the Diesel Spray". PhD thesis. Universitat Politècnica de València, 2014. DOI: 10.4995/Thesis/10251/37374.

[62] Payri, F., Payri, R., Salvador, F. J., and Gimeno, J. "Influence of Nozzle Geometry on Spray Characteristics in Non-Evaporative and evaporative conditions". In: *SAE Technical Paper 2007-24-0023* (2007). DOI: 10.4271/2007-24-0023.

[63] Benajes, J., Pastor, J. V., Payri, R., and Plazas, A. H. "Analysis of the influence of Diesel nozzle geometry in the Injection Rate characteristic". In: *Journal of Fluids Engineering* 126.1 (2004), pp. 63–71. DOI: 10.1115/1.1637636.

[64] Payri, R., García-Oliver, J. M., Salvador, F. J., and Gimeno, J. "Using spray momentum flux measurements to understand the influence of diesel nozzle geometry on spray characteristics". In: *Fuel* 84.5 (2005), pp. 551–561. DOI: 10.1016/j.fuel.2004.10.009.

[65] Bermúdez, V., Payri, R., Salvador, F. J., and Plazas, A. H. "Study of the influence of nozzle seat type on injection rate and spray behavior". In: *Proceedings of the Institution of Mechanical Engineers, Part D: Journal of Automobile Engineering*. Vol. 219. 5. 2005, pp. 677–689. DOI: 10.1243/095440705X28303.

[66] Kastengren, A. L. et al. "Engine Combustion Network (ECN): Measurements of Nozzle Geometry and Hydraulic Behavior". In: *Atomization and Sprays* 22.12 (2012), pp. 1011–1052. DOI: 10.1615/AtomizSpr.2013006309.

[67] Venegas, O. "Estudio del fenómeno de la cavitación en la inyección Diesel mediante la visualización del flujo interno en orificios transparentes." PhD thesis. Universitat Politècnica de València, 2014. DOI: 10.4995/Thesis/10251/37375.

[68] Viera, J. P. "Experimental study of the effect of nozzle geometry on the performance of direct-injection diesel sprays for three different fuels". PhD thesis. Universitat Politècnica de València, 2017. DOI: 10.4995/Thesis/10251/81857.

[69] Carreres, M. "Thermal effects influence on the Diesel injector performance through a combined 1D modelling and experimental approach". PhD thesis. Universitat Politècnica de València, 2016. DOI: 10.4995/Thesis/10251/73066.

[70] Fox, T. A. and Stark, J. "Discharge coefficients for miniature fuel injectors". In: *Aerospace Engineering* 203.1 (1989), pp. 75–78. DOI: 10.1243/PIME_PROC_1989_203_056_01.

[71] Payri, R., Molina, S., Salvador, F. J., and Gimeno, J. "A study of the relation between nozzle geometry, internal flow and sprays characteristics in diesel fuel injection systems". In: *KSME International Journal* 18.7 (2004), pp. 1222–1235. DOI: 10.1007/BF02983297.

[72] Salvador, F. J. "Estudio teórico experimental de la influencia de la geometría de toberas de inyección Diésel sobre las características del flujo interno y del chorro". PhD thesis. Valencia: Universitat Politècnica de València, 2003.

[73] Payri, R., Gimeno, J., Cuisano, J., and Arco, J. "Hydraulic characterization of diesel engine single-hole injectors". In: *Fuel* 180 (2016), pp. 357–366. DOI: 10.1016/j.fuel.2016.03.083.

[74] Martínez-López, J. "Estudio computacional de la influencia del levantamiento de aguja sobre el flujo interno y el fenómeno de la cavitación en toberas de inyección Diesel". PhD thesis. Valencia: Universitat Politecnica de Valencia, 2013.

[75] Salvador, F. J., Martínez-López, J., Caballer, M., and De Alfonso, C. "Study of the influence of the needle lift on the internal flow and cavitation phenomenon in diesel injector nozzles by CFD using RANS methods". In: *Energy Conversion and Management* 66 (2013), pp. 246–256. DOI: 10.1016/j.enconman.2012.10.011.

[76] Desantes, J. M., Salvador, F. J., Carreres, M., and Martínez-López, J. "Large-eddy simulation analysis of the influence of the needle lift on the cavitation in diesel injector nozzles". In: *Proceedings of the Institution of Mechanical Engineers, Part D: Journal of Automobile Engineering* 229.4 (2014), pp. 407–423. DOI: 10.1177/0954407014542627.

[77] Salvador, F. J., De la Morena, J., Crialesi-Esposito, M., and Martínez-López, J. "Comparative study of the internal flow in diesel injection nozzles at cavitating conditions at different needle lifts with steady and transient simulations approaches". In: *Proceedings of the Institution of Mechanical Engineers, Part D: Journal of Automobile Engineering* 232.8 (2018), pp. 1060–1078. DOI: 10.1177/0954407017725672.

[78] Pastor, J. V., López, J. J., García-Oliver, J. M., and Pastor, J. M. "A 1D model for the description of mixing-controlled inert diesel sprays". In: *Fuel* 87.13-14 (2008), pp. 2871–2885. DOI: 10.1016/j.fuel.2008.04.017.

[79] Desantes, J. M., Pastor, J. V., García-Oliver, J. M., and Pastor, J. M. "A 1D model for the description of mixing-controlled reacting diesel sprays". In: *Combustion and Flame* 156.1 (2009), pp. 234–249. DOI: 10.1016/j.combustflame.2008.10.008.

[80] Hiroyasu, H., Arai, M., and Tabata, M. "Empirical equations for the Sauter mean diameter of Diesel spray". In: *SAE Technical Paper 890464* (1989). DOI: 10.4271/890464.

[81] Hiroyasu, H. and Arai, M. "Structures of Fuel Sprays in Diesel Engines". In: *SAE Technical Paper 900475*. 1990. DOI: 10.4271/900475.

[82] Payri, R., Araneo, L., Shakal, J. S., and Soare, V. "Phase doppler measurements: System set-up optimization for characterization of a diesel nozzle". In: *Journal of Mechanical Science and Technology* 22.8 (2008), pp. 1620–1632. DOI: 10.1007/s12206-008-0432-7.

[83] Kastengren, A. L. et al. "Measurements of droplet size in shear-driven atomization using ultra-small angle x-ray scattering". In: *International Journal of Multiphase Flow* 92 (2017), pp. 131–139. DOI: 10.1016/j.ijmultiphaseflow.2017.03.005.

[84] Chaves, H., Kirmse, C., and Obermeier, F. "Velocity measurements of dense diesel fuel sprays in dense air". In: *Atomization and Sprays* 14.6 (2004), pp. 589–609. DOI: 10.1615/AtomizSpr.v14.i6.60.

[85] Desantes, J. M., Payri, R., Salvador, F. J., and Gil, A. "Development and validation of a theoretical model for diesel spray penetration". In: *Fuel* 85.7-8 (2006), pp. 910–917.

[86] Payri, R., Tormos, B., Salvador, F. J., and Araneo, L. "Spray droplet velocity characterization for convergent nozzles with three different diameters". In: *Fuel* 87.15-16 (2008), pp. 3176–3182. DOI: 10.1016/j.fuel.2008.05.028.

[87] Bruneaux, G. and Maligne, D. "Study of the Mixing and Combustion Processes of Consecutive Short Double Diesel Injections". In: *SAE International Journal of Engines* 2.1 (2009), pp. 2009–01–1352. DOI: 10.4271/2009-01-1352.

[88] Zama, Y., Ochiai, W., Furuhata, T., and Arai, M. "Velocity measurement inside a diesel spray by using time-resolved PIV under high ambient density condition". In: *ICLASS 12th Triennial International Conference on Liquid Atomization and Spray Systems*. Heidelberg, 2012.

[89] Payri, R., Viera, J. P., Wang, H., and Malbec, L. M. "Velocity field analysis of the high density, high pressure diesel spray". In: *International Journal of Multiphase Flow* 80 (2016), pp. 69–78. DOI: 10.1016/j.ijmultiphaseflow.2015.10.012.

[90] Payri, F., Bermúdez, V., Payri, R., and Salvador, F. J. "The influence of cavitation on the internal flow and the spray characteristics in diesel injection nozzles". In: *Fuel* 83.4-5 (2004), pp. 419–431. DOI: 10.1016/j.fuel.2003.09.010.

[91] Naber, J. D. and Siebers, D. L. "Effects of Gas Density and Vaporization on Penetration and Dispersion of Diesel Sprays". In: *SAE Technical Paper 960034* (1996). DOI: 10.4271/960034.

[92] Wan, Y. and Peters, N. "Scaling of spray penetration with evaporation". In: *Atomization and Sprays* 9.2 (1999), pp. 111–132. DOI: 10.1615/AtomizSpr.v9.i2.10.

[93] Manin, J., Bardi, M., Pickett, L. M., Dahms, R. N., and Oefelein, J. C. "Microscopic investigation of the atomization and mixing processes of diesel sprays injected into high pressure and temperature environments". In: *Fuel* 134 (2014), pp. 531–543. DOI: 10.1016/j.fuel.2014.05.060.

[94] Manin, J., Bardi, M., Pickett, L. M., and Payri, R. "Boundary condition and fuel composition effects on injection processes of high-pressure sprays at the microscopic level". In: *International Journal of Multiphase Flow* 83 (2016), pp. 267–278. DOI: 10.1016/j.ijmultiphaseflow.2015.12.001.

[95] Fujimoto, H., Arai, M., Senda, J., Suzuki, H., and Myong, K. "Vaporization Characteristics and Liquid-Phase Penetration for Multi-Component Fuels". In: *SAE Technical Paper 2004-01-0529* (2004). DOI: 10.4271/2004-01-0529.

[96] Jung, Y., Manin, J., Skeen, S. A., and Pickett, L. M. "Measurement of Liquid and Vapor Penetration of Diesel Sprays with a Variation in Spreading Angle". In: *SAE Technical Paper 2015-01-0946* (2015). DOI: 10.4271/2015-01-0946.

[97] Delacourt, E., Desmet, B., and Besson, B. "Characterisation of very high pressure Diesel sprays using digital imaging techniques". In: *Fuel* 84.7-8 (2005), pp. 859–867. DOI: 10.1016/j.fuel.2004.12.003.

[98] Wu, K. J., Su, C. C., Steinberger, R. L., Santavicca, D. A., and Bracco, F. V. "Measurements of the spray angle of atomizing jets". In: *Journal of fluids Engineering* 105.4 (1983), pp. 406–410. DOI: 10.1115/1.3241019.

[99] Desantes, J. M., Pastor, J. V., Payri, R., and Pastor, J. M. "Experimental characterization of internal nozzle flow and diesel spray behavior. Part II: Evaporative conditions". In: *Atomization and Sprays* 15.5 (2005), pp. 489–516. DOI: 10.1615/AtomizSpr.v15.i5.20.

[100] Macian, V., Payri, R., García, A., and Bardi, M. "Experimental Evaluation of the Best Approach for Diesel Spray Images Segmentation". In: *Experimental Techniques* 36.6 (2012), pp. 26–34. DOI: 10.1111/j.1747-1567.2011.00730.x.

[101] Li, T. and Ogawa, H. "Analysis of the Trade-off between Soot and Nitrogen Oxides in Diesel-Like Combustion by Chemical Kinetic Calculation". In: *SAE International Journal of Engines* (2011), pp. 2011–01–1847. DOI: 10.4271/2011-01-1847.

[102] De Lima Moradell, D. "Analysis of combustion concepts in a poppet valve two-stroke downsized compression ignition engine designed for passenger car applications". PhD thesis. Universitat Politècnica de València, 2016. DOI: 10.4995/Thesis/10251/68502.

[103] Estepa Ruiz, D. "Study of different fuel injection and air management strategies as a tool for emissions control in a compression ignition engine (Diesel engine)." PhD thesis. Universitat Politècnica de València, 2018. DOI: 10.4995/Thesis/10251/113076.

[104] Kamimoto, T. and Bae, M.-h. "High Combustion Temperature for the Reduction of Particulate in Diesel Engines". In: *SAE Technical Paper 880423* (1988). DOI: 10.4271/880423.

[105] Neely, G. D., Sasaki, S., Huang, Y., Leet, J. A., and Stewart, D. W. "New Diesel Emission Control Strategy to Meet US Tier 2 Emissions Regulations". In: *SAE Technical Paper 2005-01-1091* (2005). DOI: 10.4271/2005-01-1091.

[106] Li, T., Suzuki, M., and Ogawa, H. "Characteristics of Smokeless Low Temperature Diesel Combustion in Various Fuel-Air Mixing and Expansion of Operating Load Range". In: *SAE Technical Paper 2009-01-1449* (2009). DOI: 10.4271/2009-01-1449.

[107] Potter, M. and Durrett, R. P. "High-Efficiency Clean Combustion Design for Compression Ignition Engines". In: *Diesel Engine-Efficiency and Emissions Research*. Detroit, 2006.

[108] Pierpont, D. A., Montgomery, D. T., and Reitz, R. D. "Reducing Particulate and NOx Using Multiple Injections and EGR in a D.I. Diesel". In: *SAE Technical Paper 950217* (1995). DOI: 10.4271/950217.

[109] Mingfa, Y., Hu, W., Zunqing, Z., and Yan, Y. "Experimental Study of Multiple Injections and Coupling Effects of Multi-Injection and EGR in a HD Diesel Engine". In: *SAE Technical Paper 2009-01-2807* (2009). DOI: 10.4271/2009-01-2807.

[110] Lee, J., Jeon, J., Park, J., and Bae, C. "Effect of Multiple Injection Strategies on Emission and Combustion Characteristics in a Single Cylinder Direct-Injection Optical Engine". In: *SAE Technical Paper 2009-01-1354* (2010). DOI: 10.4271/2009-01-1354.

[111] Mendez, S. and Thirouard, B. "Using Multiple Injection Strategies in Diesel Combustion: Potential to Improve Emissions, Noise and Fuel Economy Trade-Off in Low CR Engines". In: *SAE International Journal of Fuels and Lubricants* (2010), pp. 2008–01–1329. DOI: 10.4271/2008-01-1329.

[112] Liu, Y. and Reitz, R. D. "Optimizing HSDI Diesel Combustion and Emissions Using Multiple Injection Strategies". In: *SAE Technical Paper 2005-01-0212* (2010). DOI: 10.4271/2005-01-0212.

[113] Carlucci, P., Ficarella, A., and Laforgia, D. "Effects on combustion and emissions of early and pilot fuel injections in diesel engines". In: *International Journal of Engine Research* 6.1 (2005), pp. 43–60. DOI: 10.1243/146808705X7301.

[114] Han, Z., Uludogan, A., Hampson, G. J., and Reitz, R. D. "Mechanism of Soot and NOx Emission Reduction Using Multiple-injection in a Diesel Engine". In: *SAE Technical Paper 960633* (1996). DOI: 10.4271/960633.

[115] Badami, M., Millo, F., and D'Amato, D. D. "Experimental investigation on soot and NOx formation in a DI common rail diesel engine with pilot injection". In: *SAE Technical Paper 2001-01-0657* (2001). DOI: 10.4271/2001-01-0657.

[116] Payri, F., Benajes, J., Pastor, J. V., and Molina, S. "Influence of the Post-Injection Pattern on Performance, Soot and NOx Emissions in a HD Diesel Engine". In: *SAE Technical Paper 2002-01-0502* (2002). DOI: 10.4271/2002-01-0502.

[117] Badami, M., Mallamo, F., Millo, F., and Rossi, E. E. "Influence of Multiple Injection Strategies on Emissions, Combustion Noise and BSFC of a DI Common Rail Diesel Engine". In: *SAE Technical Paper 2002-01-0503* (2002). DOI: 10.4271/2002-01-0503.

[118] O'Connor, J., Musculus, M. P. B., and Pickett, L. M. "Effect of post injections on mixture preparation and unburned hydrocarbon emissions in a heavy-duty diesel engine". In: *Combustion and Flame* 170 (2016), pp. 111–123. DOI: 10.1016/j.combustflame.2016.03.031.

[119] Mohan, B., Yang, W., and Chou, S. K. "Fuel injection strategies for performance improvement and emissions reduction in compression ignition engines: a review". In: *Renewable and Sustainable Energy Reviews* 28 (2013), pp. 664–676. DOI: 10.1016/j.rser.2013.08.051.

[120] Jafer, D. "Pilot Injection". In: *Engineering* (1937).

[121] Austen, A. E. W. and Priede, T. "Origins of diesel engine noise". In: *SAE National Diesel Engine Meeting*. SAE International, 1959. DOI: 10.4271/590127.

[122] Priede, T. "Relation between Form of Cylinder-Pressure Diagram and Noise in Diesel Engines". In: *Proceedings of the Institution of Mechanical Engineers: Automobile Division* 14.1 (1960), pp. 63–97. DOI: 10.1243/pime_auto_1960_000_012_02.

[123] Anderton, D. "Relation Between Combustion System and Engine Noise". In: *SAE Technical Paper 790270* (1979). DOI: 10.4271/790270.

[124] Pischinger, F. F., Schmillen, K. P., and Leipold, F. W. "A New Measuring Method for the Direct Determination of Diesel Engine Combustion Noise". In: *SAE Technical Paper 790267* (1979). DOI: 10.4271/790267.

[125] Payri, F., Broatch, A., Tormos, B., and Marant, V. "New methodology for in-cylinder pressure analysis in direct injection diesel engines - Application to combustion noise". In: *Measurement Science and Technology* 16.2 (2005), pp. 540–547. DOI: 10.1088/0957-0233/16/2/029.

[126] Gómez, J. "Computational assessment of combustion noise of automotive compression-ignited engines". PhD thesis. Universitat Politècnica de València, 2018. DOI: 10.4995/Thesis/10251/112726.

[127] Plee, S. L. and Ahmad, T. "Relative Roles of Premixed and Diffusion Burning in Diesel Combustion". In: *SAE Technical Paper 831733* (1983). DOI: 10.4271/831733.

[128] Dürnholz, M., Endres, H., and Frisse, P. "Preinjection A Measure to Optimize the Emission Behavior of DI-Diesel Engine". In: *SAE Technical Paper 940674* (1994). DOI: 10.4271/940674.

[129] D'Ambrosio, S. and Ferrari, A. "Potential of double pilot injection strategies optimized with the design of experiments procedure to improve diesel engine emissions and performance". In: *Applied Energy* 155 (2015), pp. 918–932. DOI: 10.1016/j.apenergy.2015.06.050.

[130] Busch, S. et al. “Experimental and Numerical Investigations of Close-Coupled Pilot Injections to Reduce Combustion Noise in a Small-Bore Diesel Engine”. In: *SAE International Journal of Engines* 8.2 (2015), pp. 2015–01–0796. DOI: 10.4271/2015-01-0796.

[131] Carlucci, P., Ficarella, A., and Laforgia, D. “Effects of pilot injection parameters on combustion for common rail diesel engines”. In: *SAE Technical Paper 2003-01-0700* (2003). DOI: 10.4271/2003-01-0700.

[132] Desantes, J. M., García-Oliver, J. M., García, A., and Xuan, T. “Optical study on characteristics of non-reacting and reacting diesel spray with different strategies of split injection”. In: *International Journal of Engine Research* 301 (2018). DOI: 10.1177/1468087418773012.

[133] Ishida, M., Chen, Z.-L., Luo, G.-F., and Ueki, H. “The Effect of Pilot Injection on Combustion in a Turbocharged D. I. Diesel Engine”. In: *SAE Technical Paper 941692* (1996). DOI: 10.4271/941692.

[134] Binde, A., Busch, S., Velji, A., and Wagner, U. “Soot and NOx Reduction by Spatially Separated Pilot Injection”. In: *SAE International Journal of Engines* Binde, A., (2012), pp. 2012–01–1159. DOI: 10.4271/2012-01-1159.

[135] Hotta, Y., Inayoshi, M., Nakakita, K., Fujiwara, K., and Sakata, I. “Achieving Lower Exhaust Emissions and Better Performance in an HSDI Diesel Engine with Multiple Injection”. In: *SAE Technical Paper 2005-01-0928* 1.724 (2005). DOI: 10.4271/2005-01-0928.

[136] Beatrice, C., Belardini, P., Bertoli, C., Lisbona, M. G., and Rossi Sebastiano, G. M. “Diesel Combustion control in common rail engines by new injection strategies”. In: *International Journal of Engine Research* 3.1 (2002), pp. 23–36. DOI: 10.1243/1468087021545513.

[137] Yun, H., Sun, Y., and Reitz, R. D. “An Experimental and Numerical Investigation on the Effect of Post Injection Strategies on Combustion and Emissions in the Low-Temperature Diesel Combustion Regime”. In: *ASME Internal Combustion Engine Division Spring Technical Conference*. 2005, pp. 25–35. DOI: 10.1115/ices2005-1043.

[138] Desantes, J. M., Arrègle, J., Lopez, J. J., and García, A. “A Comprehensive Study of Diesel Combustion and Emissions with Post-injection”. In: *SAE Technical Paper 2007-01-0915* (2007). DOI: 10.4271/2007-01-0915.

[139] Mancaruso, E., Merola, S. S., and Vaglieco, B. M. "Study of the multi-injection combustion process in a transparent direct injection common rail diesel engine by means of optical techniques". In: *International Journal of Engine Research* 9.6 (2008), pp. 483–498. DOI: 10.1243/14680874JER01308.

[140] Bobba, M., Musculus, M. P. B., and Neel, W. "Effect of Post Injections on In-Cylinder and Exhaust Soot for Low-Temperature Combustion in a Heavy-Duty Diesel Engine". In: *SAE International Journal of Engines* 3.1 (2010), pp. 2010–01–0612. DOI: 10.4271/2010-01-0612.

[141] Molina, S., Desantes, J. M., García, A., and Pastor, J. M. "A Numerical Investigation on Combustion Characteristics with the use of Post Injection in DI Diesel Engines". In: *SAE Technical Paper 2010-01-1260* (2010). DOI: 10.4271/2010-01-1260.

[142] Barro, C., Tschanz, F., Obrecht, P., and Boulouchos, K. "Influence of Post-Injection Parameters on Soot Formation and Oxidation in a Common-Rail-Diesel Engine Using Multi-Color-Pyrometry". In: *ASME Internal Combustion Engine Division Fall Technical Conference* (2012), pp. 293–302. DOI: 10.1115/icef2012-92075.

[143] O'Connor, J. and Musculus, M. P. B. "Post Injections for Soot Reduction in Diesel Engines: A Review of Current Understanding". In: *SAE International Journal of Engines* 6.1 (2013), pp. 2013–01–0917. DOI: 10.4271/2013-01-0917.

[144] Lopez, J. J. and Pickett, L. M. "Jet/wall interaction effects on soot formation in a diesel fuel jet". In: *International Symposium on Diagnostics and Modeling of Combustion in Internal Combustion Engines (COMODIA)* (2004), pp. 387–394.

[145] Pickett, L. M. and Lopez, J. J. "Jet-Wall Interaction Effects on Diesel Combustion and Soot Formation". In: *SAE Technical Paper 2005-01-0921* (2005). DOI: 10.4271/2005-01-0921.

[146] Ramos, Á., Muñoz, J., Andrés, F., and Armas, O. "NOx emissions from diesel light duty vehicle tested under NEDC and real-word driving conditions". In: *Transportation Research Part D: Transport and Environment* 63 (2018), pp. 37–48. DOI: 10.1016/j.trd.2018.04.018.

[147] Pickett, L. M. and Siebers, D. L. "Soot formation in diesel fuel jets near the lift-off length". In: *International Journal of Engine Research* 7.2 (2006), pp. 103–130. DOI: 10.1243/146808705X57793.

[148] Tree, D. R. and Svensson, K. "Soot processes in compression ignition engines". In: *Progress in Energy and Combustion Science* 33.3 (2007), pp. 272–309. DOI: 10.1016/j.pecs.2006.03.002.

[149] Armas, O., Ballesteros, R., and Gómez, A. "The effect of diesel engine operating conditions on exhaust particle size distributions". In: *Proceedings of the Institution of Mechanical Engineers, Part D: Journal of Automobile Engineering* 222.8 (2008), pp. 1513–1525. DOI: 10.1243/09544070JAUTO747.

[150] Dronniou, N., Lejeune, M., Balloul, I., and Higelin, P. "Combination of High EGR Rates and Multiple Injection Strategies to Reduce Pollutant Emissions". In: *SAE Technical Paper 2005-01-3726* (2005). DOI: 10.4271/2005-01-3726.

[151] O'Connor, J. and Musculus, M. P. B. "Effects of exhaust gas recirculation and load on soot in a heavy-duty optical diesel engine with close-coupled post injections for high-efficiency combustion phasing". In: *International Journal of Engine Research* 15.4 (2014), pp. 421–443. DOI: 10.1177/1468087413488767.

[152] Musculus, M. P. B., Lachaux, T., Pickett, L. M., and Idicheria, C. A. "End-of-Injection Over-Mixing and Unburned Hydrocarbon Emissions in Low-Temperature-Combustion Diesel Engines". In: *SAE Technical Paper 2007-01-0907* (2007). DOI: 10.4271/2007-01-0907.

[153] Han, M., Assanis, D. N., and Bohac, S. V. "Sources of hydrocarbon emissions from low-temperature premixed compression ignition combustion from a common rail direct injection diesel engine". In: *Combustion Science and Technology* 181.3 (2009), pp. 496–517. DOI: 10.1080/00102200802530066.

[154] Yoon, S., Kim, H., Kim, D., and Park, S. "Effect of Fuel Injection Strategy on DPF Regeneration in Single Cylinder Diesel Engine". In: *ASME Internal Combustion Engine Division Fall Technical Conference*. Houston, 2015. DOI: 10.1115/icef2015-1140.

[155] Singh, N., Rutland, C. J., Foster, D. E., Narayanaswamy, K., and He, Y. "Investigation into Different DPF Regeneration Strategies Based on Fuel Economy Using Integrated System Simulation". In: *SAE Technical Paper 2009-01-1275* 1 (2009). DOI: 10.4271/2009-01-1275.

[156] Yehliu, K., Boehman, A. L., and Armas, O. "Emissions from different alternative diesel fuels operating with single and split fuel injection". In: *Fuel* 89.2 (2010), pp. 423–437. DOI: 10.1016/j.fuel.2009.08.025.

[157] Herfatmanesh, M. R., Lu, P., Attar, M. A., and Zhao, H. "Experimental investigation into the effects of two-stage injection on fuel injection quantity, combustion and emissions in a high-speed optical common rail diesel engine". In: *Fuel* 109 (2013), pp. 137–147. DOI: 10.1016/j.fuel.2013.01.013.

[158] Akkurt, B. "Modelling multi-pulse diesel injection with flamelet generated manifolds". PhD thesis. Technische Universiteit Eindhoven, 2019, p. 232.

[159] Kastengren, A. L. et al. "Correlation of Split-Injection Needle Lift and Spray Structure". In: *SAE Technical Paper 2011-01-0383* (2011). DOI: 10.4271/2011-01-0383.

[160] Parrish, S. E., Zhang, G., and Zink, R. J. "Liquid and Vapor Envelopes of Sprays from a Multi-Hole Fuel Injector Operating under Closely-Spaced Double-Injection Conditions". In: *SAE International Journal of Engines* 5.2 (2012), pp. 2012–01–0462. DOI: 10.4271/2012-01-0462.

[161] Skeen, S. A., Manin, J., and Pickett, L. M. "Visualization of Ignition Processes in High-Pressure Sprays with Multiple Injections of n-Dodecane". In: *SAE International Journal of Engines* 8.2 (2015), pp. 2015–01–0799. DOI: 10.4271/2015-01-0799.

[162] Maes, N., Bakker, P. C., Dam, N., and Somers, B. "Transient Flame Development in a Constant-Volume Vessel Using a Split-Scheme Injection Strategy". In: *SAE International Journal of Fuels and Lubricants* 10.2 (2017), pp. 2017–01–0815. DOI: 10.4271/2017-01-0815.

Chapter 3

Experimental tools and methodologies

3.1 Introduction

In this chapter, all the experimental tools and analytical methodologies are described. First, the fuel delivery system is detailed, including the nozzle configuration used. The next three sections present all the experimental equipment where the measurements were carried out: the rate of injection indicator, the momentum flux rig, and an optically accessible high-temperature and high-pressure vessel. Lastly, the optical configurations and image processing strategies are explained. All measurements were carried out in the facilities of CMT-Motores Térmicos.

3.2 Injection system

Fuel needs to be delivered to the test chamber at a specific pressure. Additionally, its conditions need to be stable, to some extent, through a wide range of operating points. To this end, the injection system is composed of commercially available components adapted for laboratory use. The main elements are a fuel supply source, a high-pressure unit, a common-rail, and the injector.

3.2.1 High-pressure unit

Fuel was first purged and filtered, to remove air and particles. Then, it was pressurized by a Bosch CP3 pump powered by an electric motor. A common-rail fitted with a pressure regulator was connected to the high-pressure outlet of the pump, used as a control unit. The regulator was driven with a closed-loop proportional-integral-derivative (PID) commercial controller by Genotec. Low-pressure fuel returning from the common-rail and the pump was cooled down with a heat exchanger, and sent to the air purger along with the fuel back-flow from the injector. A flexible line transported the pressurized fuel from the control common-rail to the corresponding test rig. Figure 3.1 presents a schematic diagram of the high-pressure unit.

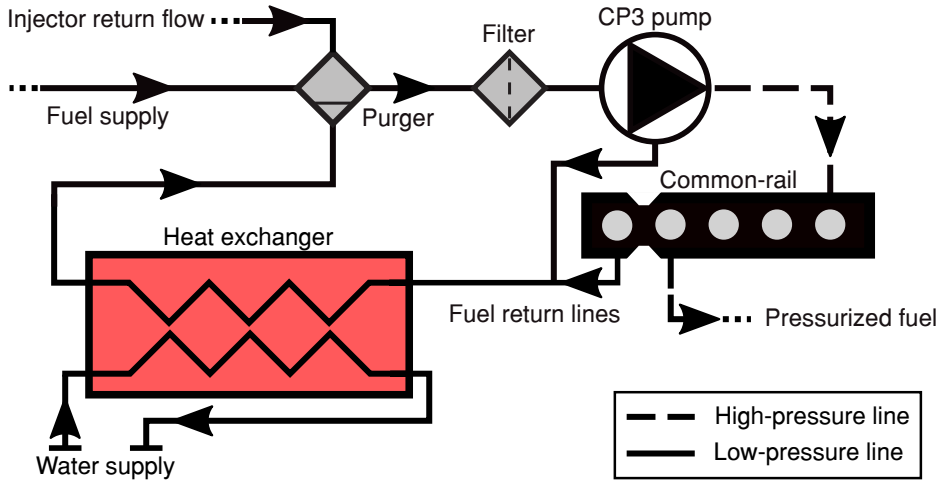

Figure 3.1: High-pressure unit schematic diagram.

3.2.2 Diesel injector

The injector used is the latest iteration of a commercially available piezo common-rail (PCR) type 5 from Continental [1]. It has a micro piezo stack actuator, which compared to the conventional ones, maximizes the internal high-pressure volume, improving its efficiency in multiple injection strategies. Besides, the piezo stack is powerful enough to handle operating injection pressures up to 250 MPa.

The injector was fitted with a custom geometry six hole nozzle distributed as shown in Figure 3.2, with a spray optically isolated from the others, labeled spray of interest (SpI) and numbered as plume 1.

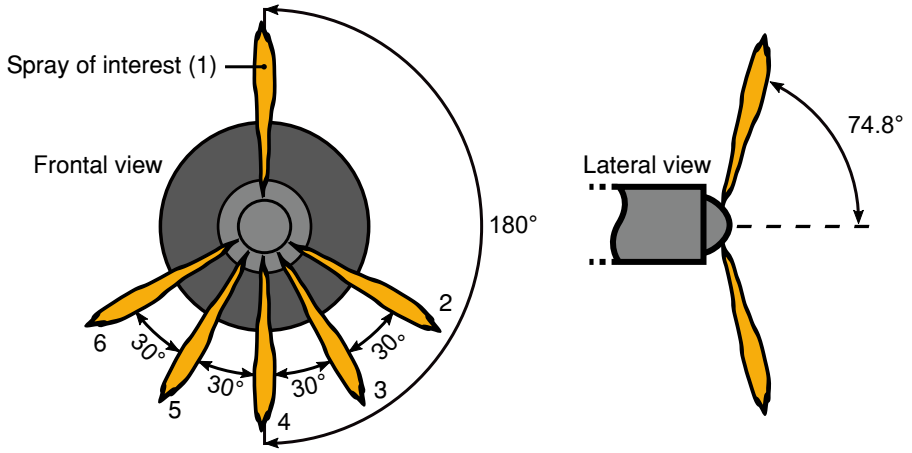

Figure 3.2: Nozzle configuration of the PCR5 injector used.

A similar distribution is present in the Spray B, a three-hole nozzle from the Engine Combustion Network [1] (ECN) [2]. The Spray B configuration is an evolution from a single-hole axially drilled nozzle (Spray A) which has been extensively used for research purposes, both experimentally [3–10] and computationally [11–15]. The ECN has found differences when comparing the performance of both nozzles: the Spray B produces a shorter liquid length [2, 9], ignition delay, and lift-off length [2, 10], and a spray with a slightly bigger spray angle [9, 16]. In general terms, the differences are due to higher turbulence at the outlet of the nozzle due to the redirection of the flow [16, 17]. So, to provide useful experimental information to modelers, with geometries that resemble more commercially available injectors, a similar 90 µm convergent nozzle was designed with the custom configuration shown. Besides, because the SpI can be visualized with line-of-sight optical configurations, the same injection event can be observed with multiple setups at once [10, 18–21], reducing experimental uncertainties and testing time. The main characteristics of the nozzle are summarized in Table 3.1.

[1] The Engine Combustion Network (ECN) is an international collaborative group that unites efforts from different institutions around the world to improve the scientific understanding of the spray combustion at engine related conditions, by establishing a library of reliable experimental data appropriate for model validation

Table 3.1: Real nozzle geometry.

Parameter	**Value**	**Units**
Number of holes	6	-
Avg. outlet diameter ($\overline{D}_o$)	90.1	µm
Outlet diameter (D_o)	91.7*	µm
Avg. *k–factor*	5.3	-
Nominal flow rate	313**	mL min^{-1}
Avg. height angle	74.8	degrees
Degree of hydro-erosion	7.7	%

* Of the spray of interest.
** At 10 MPa of injection pressure.

3.3 Rate of injection

Mass flow rate measurements were carried out using an Injection Rate Discharge Curve Indicator (IRDCI) from IAV. It measures the rate of injection (ROI) with the Bosch long-tube method [22], whose working principle is based on the theory of pressure wave propagation in a liquid column. A schematic diagram of the IRDCI is presented in Figure 3.3.

When fuel is injected into the measurement tube, a pressure wave is gen-

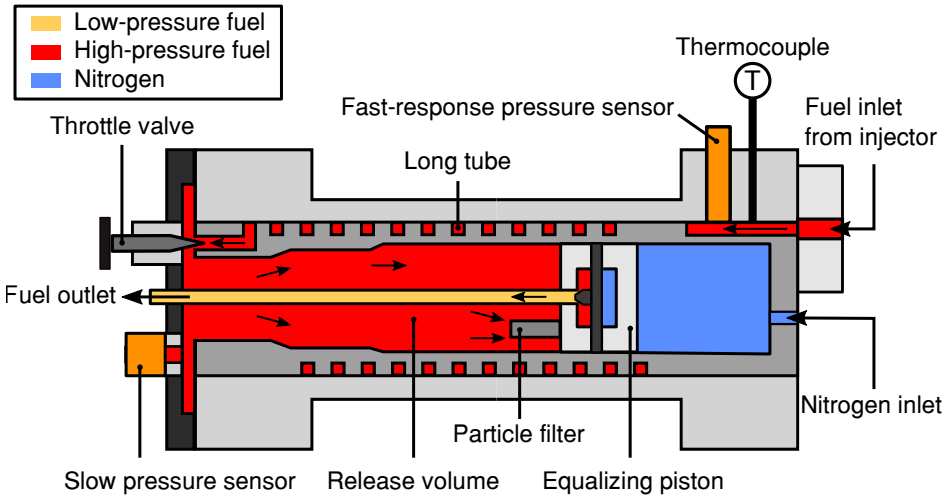

Figure 3.3: Injection Rate Discharge Curve Indicator schematic diagram.

erated. The wave travels at the speed of sound through the long tube that goes around the device, up to the release volume where it is dampened. Then, the fuel enters through a filter into the equalizing piston, which is pressurized on the other side by nitrogen set at the desired discharge pressure, sealing the outlet. Once the fuel-side sets the piston in equilibrium, any additional mass injected induces a pressure increase. In consequence, the piston moves, which unseals the exit, and lets a small amount of mass out of the IRDCI, equivalent to the mass injected.

The fast-response pressure sensor, a piezoelectric transducer, captures the pressure variation provoked by an injection event. From the signal, it is possible to calculate the instantaneous mass flow rate. Considering a cylindrical control volume of a known cross-sectional area A_t, in which the pressure wave travels, and neglecting the effect of gravity, the equation of momentum conservation results in:

$$(p_{cv} + \Delta p)\, A_t - p_{cv} \cdot A_t = \rho_f \cdot A_t \cdot a_f \cdot \Delta u_f \tag{3.1}$$

Where p_{cv} is the pressure in the control volume, Δp is the pressure difference induced by the wave, ρ_f is the density of the fuel, a_f is the speed of sound in the fuel, and Δu_f is the variation of fuel flow velocity in the section. The equation can be simplified as:

$$\Delta p = \rho_f \cdot a_f \cdot \Delta u_f \tag{3.2}$$

The piezoelectric sensor measures the pressure difference. As the wave enters the release volume, the difference in diameter induces a reflected wave that travels back through the tube and may be detected by the sensor. The IRDCI avoids the reflected wave to interfere with the main injection in two ways: the long tube to temporally divide the signals, and a throttle valve to change the cross-sectional flow area near the release volume. On the other side, both the speed of sound a_f and fuel density ρ_f were calculated with the correlations obtained by Payri et al. [23] for commercial diesel (reference fuel) used in the experimental measurements:

$$\begin{aligned}(a_f, \rho_f) = {} & k_1 + k_2\,(T_{cv} - T_0) + k_3\,(p_{cv} - p_0) \\ & + k_4\,(p_{cv} - p_0)^2 + k_5\,(T_{cv} - T_0)^2 + k_6\,(p_{cv} - p_0)\,(T_{cv} - T_0)\end{aligned} \tag{3.3}$$

With the pressure and temperature (T_{cv}) of the control volume measured by the slow pressure sensor and a thermocouple. The coefficients for the correlations are presented in Table 3.2, with $T_0 = 298\,\mathrm{K}$ and $p_0 = 0.1\,\mathrm{MPa}$.

Table 3.2: Coefficients for the correlation of the speed of sound and density for the reference fuel.

-	$a_f[\mathrm{m\,s^{-1}}]$	$\rho_f\ [\mathrm{kg\,m^{-3}}]$
$k1$	1363.05	835.698
$k2$	-3.11349	-0.6280
$k3$	4.1751	0.4914
$k4$	-0.006968	-0.000705
$k5$	0	0.000737
$k6$	0.009401	0.001036

Lastly, the continuity equation links the pressure change induced by the wave to the mass flow rate, which is expressed as:

$$\dot{m} = \rho_f \cdot A_t \cdot \Delta u_f \tag{3.4}$$

Therefore, solving for Δu_f in Equation 3.2, and combining it with Equation 3.4, mass flow rate can be calculated as:

$$\dot{m} = \frac{A_t}{a_f} \Delta p \tag{3.5}$$

3.3.1 Measurement setup

The setup used to measure the mass flow rate is presented as a schematic diagram in Figure 3.4. Fuel was supplied to the high-pressure unit by a vase mounted on an upstream scale. Then, the pressurized fuel was delivered to a second common-rail (volume = $22\,\mathrm{cm}^3$, length = 28 cm), and fed to the injector through a high-pressure rigid line (inside/outside diameter = 2.4/6 mm, length 24 cm). The rail and line configurations were selected to comply with ECN standards [2]. Fuel exited the IRDCI, and it was deposited into the downstream scale. The quantity injected was measured by both scales, accounting for the number of injections in a period of 120 s. The injector was commanded by a Genotec piezo pulse generator V2.02, which replaces the engine control unit (ECU).

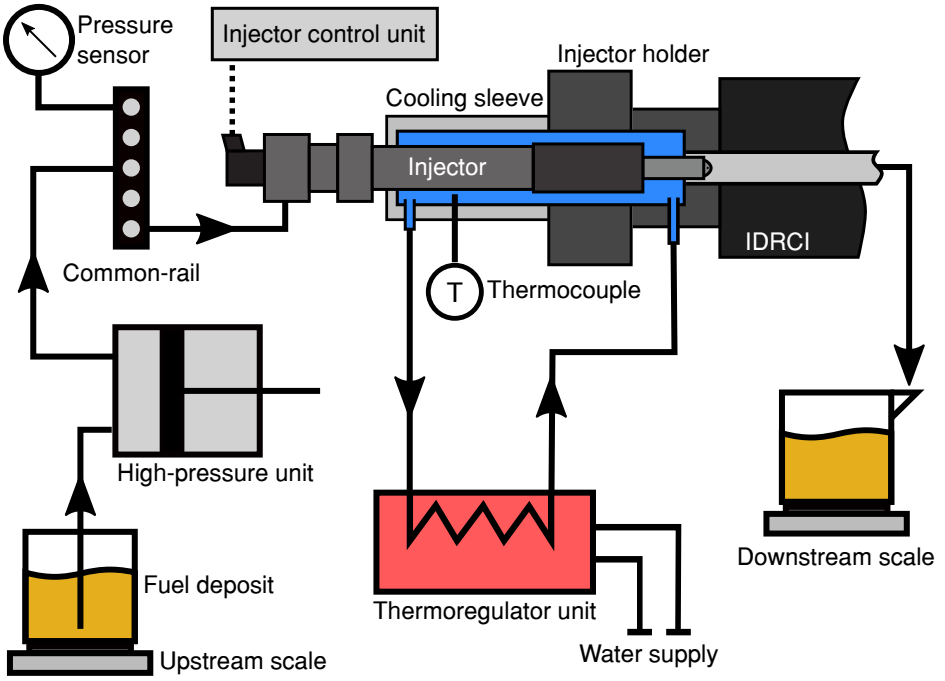

Figure 3.4: Schematic diagram of the setup used for the rate of injection measurements.

The dynamic response of the piezo stacks is very dependent on its working temperature [24], and therefore it could affect the hydraulic performance of the injector [25]. Accordingly, the injector was mounted to the IRDCI with a special holder that allows controlling its operating temperature. The holder had a cooling sleeve that extended along the body of the injector, with a thermocouple inserted in the middle to monitor the temperature. This system was driven by a thermoregulator unit that used ethylene glycol at 30 %, pumped at a rate of up to $60\,\mathrm{L\,min^{-1}}$, heated by a 6 kW unit, and cooled down by a separate water supply system.

3.3.2 Measurement procedure

A digital oscilloscope records the rate of injection, rail pressure, and driving voltage signals, for a total of 50 injections per test point at a rate of 1 injection event per second. The time reference of the measurement, that is $t = 0$, is the start of energizing (SOE) of the injector. An example of the raw data obtained is depicted in the set of plots on the left side of Figure 3.5. All the

data is averaged, and then the ROI is corrected for the signal accumulation phenomenon, with a methodology thoroughly described by Payri et al. [26]. The averaged result is shown in the right set of plots in the figure.

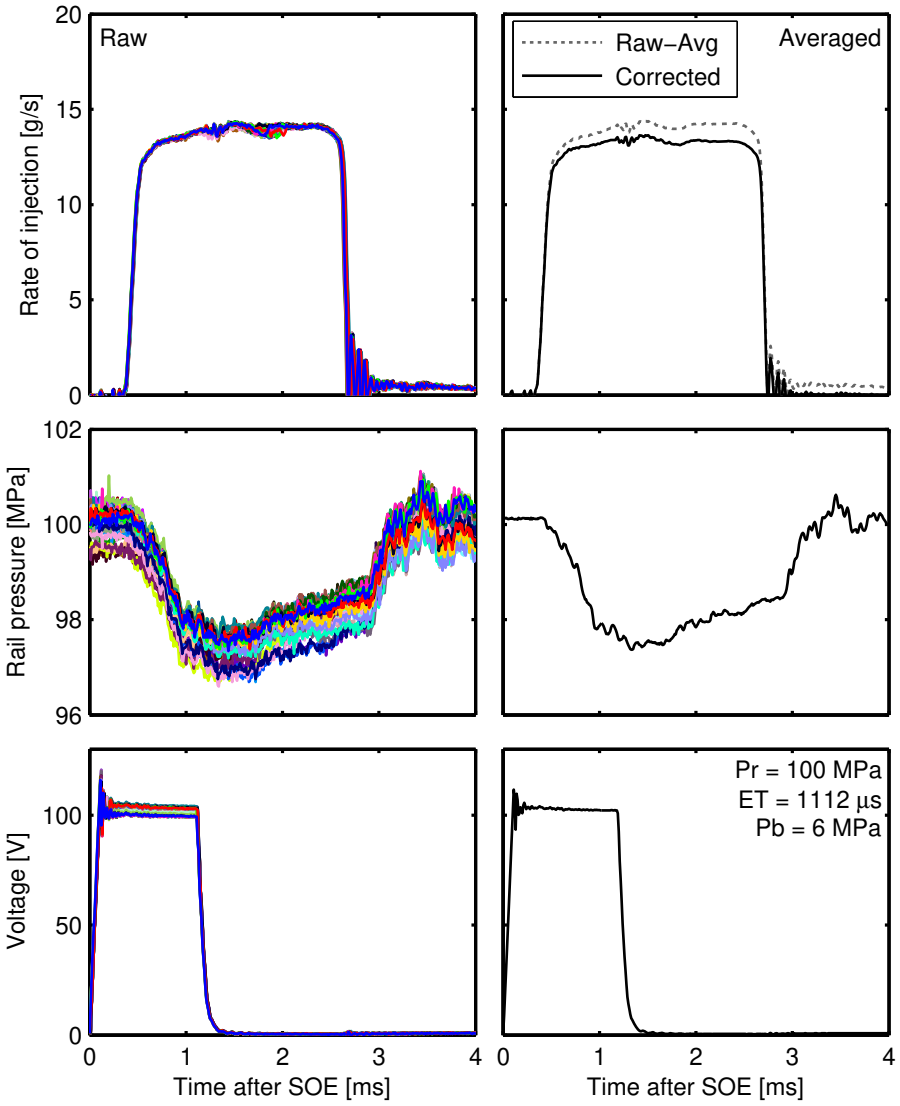

Figure 3.5: Raw (left) and averaged (right) rate of injection, rail pressure and voltage signals.

The final signal is then integrated to obtain the injected mass. Due to the uncertainties in the calculation of the speed of sound, cycle-to-cycle and

temperature variations, among others, the integral of the rate of injection signal can differ from the mass measured by the scale. Thus, to account for this difference, a standard methodology was developed in the laboratory and used in many previous publications [25–29]. A scaling factor is calculated with the ratio of the mass measured by the downstream scale divided by the integrated mass (Equation 3.6), and the latter signal is corrected. The procedure was repeated with multiple injections pulses in an injection event, but integrating each pulse separately to obtain the mass distribution, all of which is explained in more detail on chapter 4.

$$m_{int} = \frac{m_{scale}}{k_{adjust}} \tag{3.6}$$

3.4 Momentum flux

Momentum flux measurements were carried out for the SpI in a device designed at CMT-Motores Térmicos, and fully described in the work of Gimeno [27]. The measurement principle, shown in Figure 3.6, and consist of a piezoelectric sensor that measures the impact force of the spray (F in the figure). It is aligned perpendicularly to the axis of the plume and set a certain distance, so that neighbor jets do not collide with the surface of the sensor, but the impact surface captures the whole spray being measured.

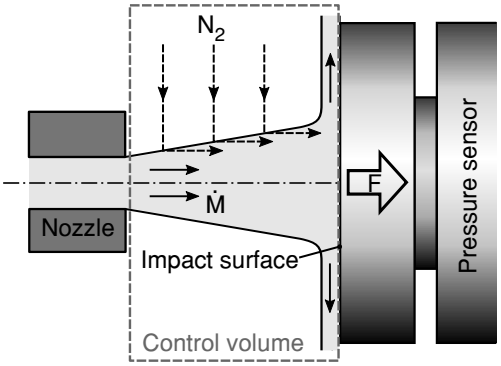

Figure 3.6: Spray momentum flux measurement principle [30].

Considering a cylindrical control volume (CV) that encloses the region between the orifice and the sensor, as depicted in the figure, the following assumptions can be made [27, 30]:

- Gravity related forces are negligible.
- Pressure within the test cell is uniform.
- The flow direction of both the nitrogen entering the control volume, and fuel exiting it after impacting the sensor, are perpendicular to the spray axis. In consequence, their axial component of momentum flux, as well as the viscous stress, are null.

Therefore, considering the law of momentum conservation, and accounting for the simplifications mentioned, the force produced by the spray in the impact surface F can be written as:

$$F = \frac{\partial}{\partial t} \int_{CV} \rho \, u \, d\varpi \, + \, \dot{M} \tag{3.7}$$

Where ρ and u are the local density and velocity of the mixture passing through the control volume, ϖ is the surface of the control volume, and $\dot{M}$ represents the momentum flux at the outlet of the orifice, considered to be parallel to the axis of the nozzle. The first term on the right side of the equation represents the variations of momentum flux within the control volume. Thus, for steady state conditions, the Equation 3.7 can be simplified as:

$$F = \dot{M} \tag{3.8}$$

Consequently, the signal of the sensor provides the momentum flux measurement directly. But this is only true if the sensor is positioned perpendicularly to the spray axis, its frontal area is larger than the impact surface, and the fuel is deflected perpendicularly as well.

3.4.1 Measurement setup

Part of the setup used to measure momentum flux is presented in Figure 3.7. The same fuel supply strategy as previously shown was used to provide the fuel to the injector, so the injected mass can be measured with the upstream scale. The injector was mounted in the test rig with the same cooling sleeve unit, to keep the operating temperature constant throughout measurements and experimental facilities. The pressure transducer was installed into a specific holder that positions the sensor perpendicularly to the SpI axis. A spacer was used to control the distance to the outlet of the nozzle. Additionally, a set of shims that act as spacers between the injector holder and the test rig can be

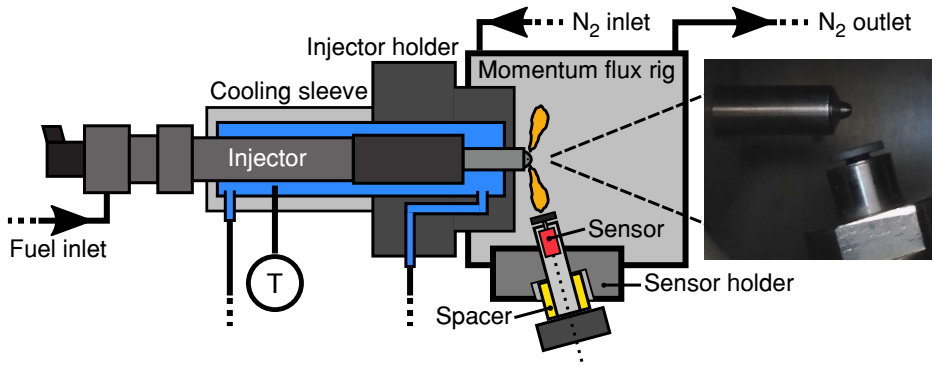

Figure 3.7: Schematic diagram of the setup used for the momentum flux measurements.

used to control the horizontal position of the injector referenced to the sensor (with the same orientation as in the figure), but it was not necessary for this configuration. Chamber pressure is controlled by a set of valves that regulate the inlet and outlet flow of nitrogen.

3.4.2 Measurement procedure

As in the rate of injection measurements, a digital oscilloscope records the momentum flux, rail pressure, and driving voltage signals, for a total of 50 injections per test point at a rate of 1 injection event per second. An example of the raw data is depicted in the left plot of Figure 3.8. Compared to the raw results from the rate of injection measurements, the signals are noticeably noisier. The source of these oscillations was discussed by Gimeno [27] with the following remarks:

- Fluctuations in the signal related to pressure waves that appear in the common-rail during the injection event. These are also visible in the rail pressure sensor, but their effect on the signal is minimal.
- Shot-to-shot deviation due to turbulence within the nozzle that affects internal flow development, as well as in the turbulent mixing process of the fuel with the gas, that disturbs spray development. Its influence can be diminished by measuring multiple injections and averaging the signal, because turbulence is a random phenomenon.
- Fluctuations in the signal due to mechanical vibrations, acoustic waves caused by the aerodynamic interaction between the spray and the gas,

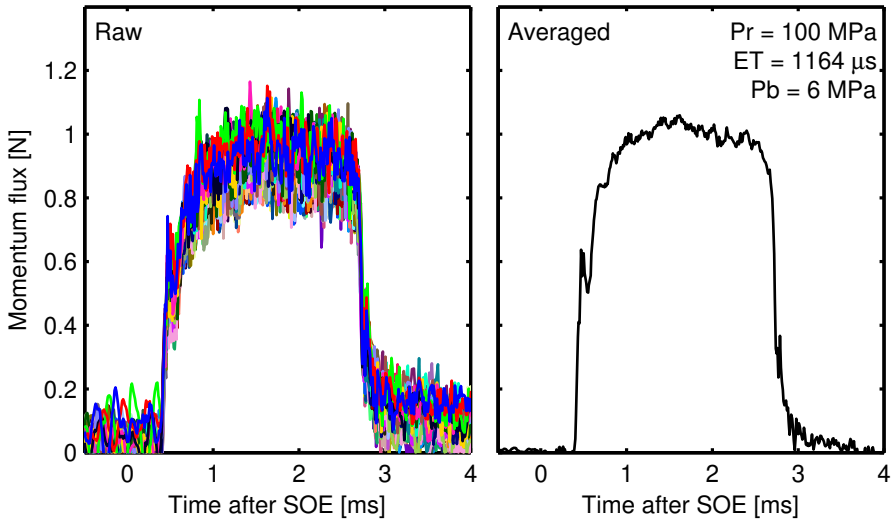

Figure 3.8: Raw and averaged momentum flux signals.

and background noise. All three comparatively smaller than the rate of momentum signal.

The average signal, shown in the right side of Figure 3.8, is corrected for the accumulation phenomenon as with rate of injection.

The injected mass is verified with the upstream scale. Nevertheless, a procedure was developed to verify that its distribution is equal to the one measured in rate of injection. If boundary conditions are comparable, by combining Equation 2.7 and Equation 2.8 and approximating the effective area to A_o, the rate of injection and rate of momentum are related as:

$$\sqrt{\dot{M}} \approx \frac{\dot{m}}{\sqrt{A_o \cdot \rho_f}} \tag{3.9}$$

Thus, the allocation of mass is approximately equal to the percentual distribution of the square root of momentum. However, for this equation is assumed that the rate of injection signal is uniformly distributed per hole. The approach was experimentally validated, and is further explained in chapter 4.

3.5 High-temperature and high-pressure test rig

For the spray visualization measurements, a new high-pressure and high-temperature facility was used, similar to those described in other experimental works [31–33]. According to the convention introduced by Baert et al. [34], the installation is equipped with an optically accessible constant pressure and flow (CPF) test chamber (also named spray box in this thesis), where engine-like conditions are reached due to a continuous flow of high-pressure and high-temperature gas. Consequently, the test chamber can achieve a nearly quiescent and steady thermodynamic environment, and thus, measurements can be performed with a much higher injection frequency, reducing testing time [6]. The facility is divided into different subsystems: gas pressurization, flow control, test chamber control, and the cooling unit.

3.5.1 Description of the facility

A schematic diagram of the facility is presented in Figure 3.9. It has two possible configurations: open-loop and closed-loop. In the first, the circuit valves are set so that air is filtered, compressed and stored in the high-pressure reservoirs. After lowering its humidity with a high-pressure industrial dryer, it enters the test chamber through a 40 kW electric heating system. Hot gases exit the vessel and, after being cooled down, are thrown into the atmosphere. A second valve, manually operated to control the gas flow, is located downstream of the test chamber. With the correct combination of the circuit valves, the closed-loop configuration is used to simulate exhaust gas recirculation (EGR), by the addition of nitrogen and continuous monitoring of the oxygen concentration. Besides, this configuration also allows using pure nitrogen, for spray measurements in a non-reactive atmosphere.

The test rig control system is in charge of regulating both chamber temperature and pressure, both signals measured in the combustion chamber. The heaters are driven by a PID governed by a temperature set-point that is fixed at the desired level. Another PID system regulates the chamber pressure with a flow control valve that feeds the high-pressure air into the test chamber. The control system also manages safety checks, for example, minimum coolant flow, maximum heater output temperature, and a minimum gas flow value to protect the heaters, among others.

The cooling system is constituted of two different circuits that run on ethylene glycol. A primary cooling unit moderates the temperature of the test chamber, o-ring seals, and the thermoregulator unit. It is composed of a pump that drives the ethylene glycol at a rate up to $20\,\mathrm{L\,min^{-1}}$ from a 300 L reservoir

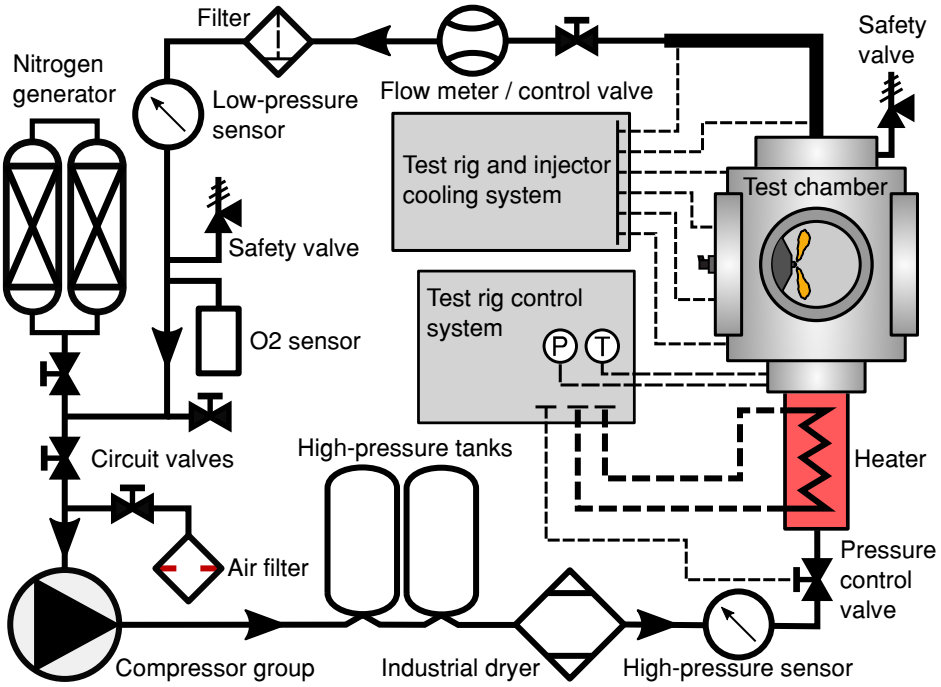

Figure 3.9: Schematic diagram of the high-temperature and high-pressure facility.

to the test chamber room. From the same reservoir, another pump sends the coolant to a 28.2 kW chiller and back to the tank. This keeps the temperature of the fluid at around 17 °C. The second circuit is, as previously shown in the rate of injection and momentum flux setups, driven by a thermoregulator unit to control the operating temperature of the injector and keep it constant throughout experiments. Due to the relatively low injection frequency, the temperature of the fuel is mainly determined by the nozzle tip temperature. Accordingly, an aluminum cap was installed, acting as a conductor between the coolant chamber around the injector and the nozzle tip, helping to control its temperature [35].

Compared to similar CPF test chamber [6, 36], this spray box features a combustion chamber that reaches temperatures up to 1100 K and 15 MPa. The test section has a cubic shape of approximately 15 liters in volume, with a double wall configuration separated by a thick insulation layer. The inner wall is for thermal control, and the outer is to withstand the structural loads. The heated gas enters the combustion chamber through a swirler-diffuser to

improve temperature distribution along the test section, but also to reduce its speed. Additionally, the gas is compelled to exit through four steel tubes that are located strategically to force its recirculation along the combustion chamber, to further improve temperature distribution [37]. The chamber is optically accessible through three windows, two of 128 mm in diameter located in a line-of-sight arrangement, and one of 181 mm in diameter perpendicular to the axis of the injector. The latter access is thought for industrial injectors, with measurable spray penetrations up to 110 mm.

3.6 Optical techniques for spray visualization

Optical diagnostics for the study of high-speed flows date backs to the 1800s [38], and are a powerful tool as they generally provide a non-intrusive way of experimentally measuring variables of interest. With the latest advancement in fast-cameras, lasers, x-ray, optics and illumination technologies, the broad range of different optical setups allow to measure numerous variables of the diesel spray development, such as: spray penetration and spreading angle at rates exceeding 120000 frames per second (fps) [16, 39], flame lift-off length [10, 20, 32], ignition delay [20, 40], soot concentration [33, 41, 42], needle movement [43, 44], droplet size [45], and projected fuel mass distribution [44, 46], among others.

The section starts with the basic principles behind the optical setups utilized, after which the two optical configurations for both spray visualization campaigns are explained.

3.6.1 Diffused back-illumination

Liquid phase penetration is often used in the literature to characterize the mixing process in diesel sprays [16, 47, 48], and it can be observed through several optical configurations that use visible-wavelength light as the source of illumination [3, 16, 35]. One example is light scattering techniques, which capture the rays elastically scattered by the droplets through a high-speed camera [3, 31, 35]. Another method, commonly used with nozzles that allow line-of-sight visualization is diffused-back illumination, in which light is extinct due to the optical depth (τ) of the spray. The extinction can be calculated for each frame using the Beer-Lambert law:

$$\frac{I - I_f}{I_0} = e^{-\tau} \tag{3.10}$$

Where I is the pixel-wise intensity distribution of the current frame that considers attenuation from the spray, I_f accounts the light emitted by the flame for the same time step, and I_0 is the reference image from the diffused source without attenuation. For non-reactive cases, the term I_f is zero. The recent introduction of fast light-emitting diodes (LED) allowed to improve the quality of the images gathered through DBI. As the duration of the light pulse can be set to very low values (nanoseconds), the amount of light available for each frame is governed by the pulse length of the LED, and not the exposure of the camera. Consequently, a DBI configuration was selected for the liquid phase visualization, as the images gathered are significantly sharper than to any other continuous light source options [3, 9, 16, 39, 49]. Moreover, the same configuration can be used for qualitative or even quantitative measurements of soot concentration [33, 50–52], as the optical thickness can also be described as:

$$\tau = K \cdot L_{soot} \tag{3.11}$$

Where K is the dimensional extinction coefficient, and L_{soot} is the path length through the soot cloud. Thus, conditions with higher soot concentrations present a higher KL_{soot} factor (renamed as KL), although it is limited to the dynamic range of the images gathered.

The DBI setup used was developed by Ghandhi and Heim [53], and was composed of a light source, diffuser, field lens, and a high-speed camera, as shown in a simplified schematic diagram in Figure 3.10. A blue LED unit (centered at 460 nm) was equipped with a parabolic reflector to reduce the light aperture angle from 120° to 25° and minimize light loss. Rays were directed

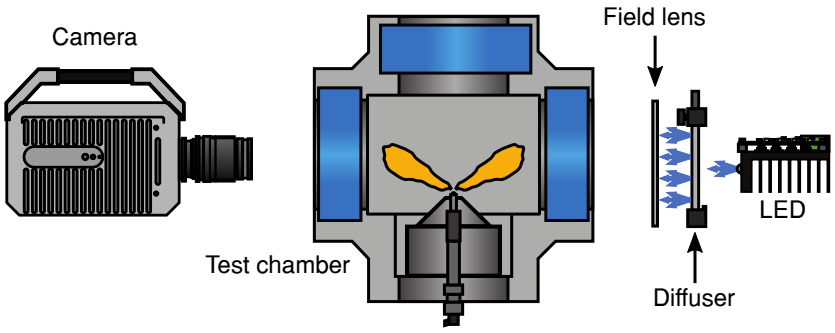

Figure 3.10: Schematic diagram of a simple diffused back-illumination setup.

to a 100 mm engineered diffuser with 20.5° of divergence angle. A Fresnel lens, with a focal length of 67 mm was located such that the diffused illumination source was reproduced near the optical plane of the spray visualized, also accounting for the lens used in the single-pass arrangement. A blue LED was chosen as the illumination source as it provides flexibility discarding light rays from other optical setups that could interfere with the measurement, as well as it allows for a higher signal-to-noise ratio in soot DBI measurements [49].

3.6.2 Single-pass schlieren

For many years, researchers have used schlieren imaging to analyze the diesel sprays evolution in both non-reactive and reactive conditions. With this technique it is possible to measure from simple macroscopic parameters, like vapor phase penetration and spreading angle [31, 54, 55], to more complex combustion variables, like ignition delay [7, 10, 18, 20, 40, 56] or even lift-off length [57]. It is not only fundamental knowledge to understand how boundary conditions affect these variables, but the experimental data is necessary to validate computational tools, such as 1-D or CFD models.

The measurement principle is simple: light rays travel uniformly through homogeneous media, but they are bent proportionally to the refractive index of the medium they enter into [58]. Gladstone and Dale [59] found that there is a linear relationship between the refractive index and gas density, presented in Equation 3.12. Where n is the refractive index, ρ is the gas density, and k_{GD} is the Gladstone-Dale coefficient.

$$n - 1 = k_{GD} \cdot \rho \tag{3.12}$$

Additionally, the angular deflection ε of a ray in the perpendicular plane $x - y$, of a light beam that is traveling in a direction z, can be obtained by the expression [58]:

$$\varepsilon_x = \frac{L}{n_0}\frac{\partial n}{\partial x} \quad , \quad \varepsilon_y = \frac{L}{n_0}\frac{\partial n}{\partial y} \tag{3.13}$$

Where L represents the optical path length, and n_0 the refractive index of the surroundings. From equations 3.12 and 3.13, there is a clear relationship between the changes in density and angular deflection of light rays, that can be visualized through schlieren or shadowgraph imaging. Although both methods are closely related, the use of a cutoff for the refracted light in schlieren systems differentiates each configuration. As explained by Settles [58], a schlieren image responds to the first spatial derivative of the refractive index, whereas the

shadowgram responds to the second spatial derivative. That is, the schlieren image captures the deflection angle of a ray (Equation 3.13), while shadowgraphy shows the ray displacement as a result of the deflection. Accordingly, the principle of the schlieren application in diesel sprays is straightforward: the density gradients between the injected fuel and the gas, along the optical path, bent the light rays passing through the test section. Subsequently, the boundary between these elements can be depicted, allowing to segment the diesel spray from the background [60].

The two most common schlieren configurations are single-pass (SP) [10, 20, 40, 54, 57, 60–68] and double-pass (DP) [31, 69–71]. Typically, the first setup is used for axially drilled single-orifice nozzles, where optical vessels with multiple access allow line of sight visualization. Contrarily, the double-pass setup is commonly applied for multi-hole nozzles, where the sprays tend to be visualized through a sole optical access. Consequently, the light crosses the test section twice, and the optical sensitivity theoretically increases by a factor of two [58]. Nevertheless, with a single optical access, a reflective surface that withstands high-temperatures mounted near the nozzle inside the test section is needed, limiting the visibility of other line-of-sight visualization setups for the same injection event. Thus, vapor phase penetration measurements were carried out with a single-pass linear dual lens system [58].

In Figure 3.11.*a*, where a basic single-pass system is presented, beams from a point light source are collimated by a lens. The trajectory i in the figure represents any of the rays deflected ε degrees by density gradients (depicted as splines) in the test section, that are blocked by a slit located at the focal distance of the second lens (or cut-off plane). On the contrary, non-deflected beams, represented as the trajectory ii in the figure, can pass through the slit and reach the screen. In theory, this produces a black and white image, because the light source is infinitesimal and located exactly at the focal distance of the first lens. Thus each point in the test section is illuminated by a single light ray. But in real practice, sources of illumination are finite. Thus the diagram of the setup is more similar to the one presented in Figure 3.11.*b*. Here, the schlieren object in the test section is illuminated by multiple infinitesimal ∂j light sources. In consequence, the image assembled by the second lens is a composition of sub-images, formed by each bundle of rays from each ∂j source [58]. More importantly, this gives the schlieren setup a continuous dynamic range, in the form of gray-scale intensities (combination of trajectories i and iii), compared to the black and white resolution from the first example.

Light from a Mercury-Xenon arc lamp, with an output power of up to 1000 W, was passed through a 1.2 mm opening, to create the point-like illumi-

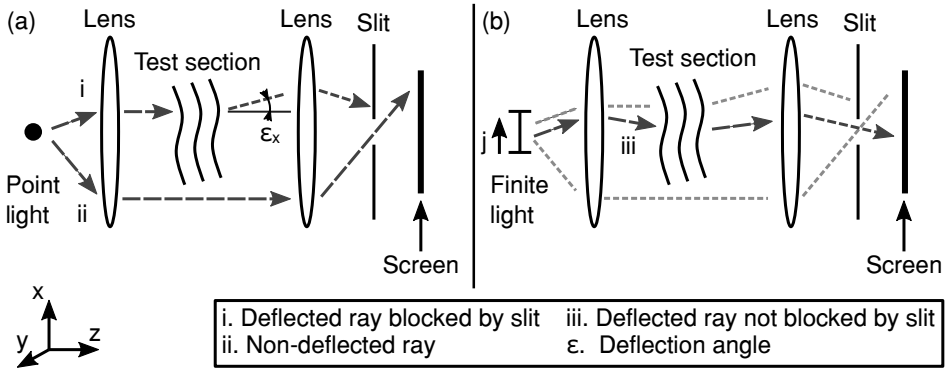

Figure 3.11: Schematic representation of the schlieren principle. Differences between a point (a) and finite (b) light sources for a single-pass setup.

nation source. To parallelize the rays, a 150 mm biconvex lens was positioned at its focal length of 450 mm. After the parallel beams pass through the test section, an equivalent biconvex lens captured the rays and converged them to its focal point, where an iris diaphragm with a 4 mm aperture was set, as the cutoff mechanism. Both apertures were set from previous experimental campaigns with similar testing conditions in the same facility [7, 10, 21, 60, 69].

3.6.3 Chemiluminescence

Chemical reactions in the combustion process produce high-energy intermediate species in an excited energy state, which then move to a lower energy level as they fragment towards their final products, emitting light in the process [72]. Thus, chemiluminescence is the phenomena in which photons are emitted from a molecule that previously reached its excited state as the result of a chemical reaction. An example of the natural light emission spectrum of a diffusion flame is presented in the left side of Figure 3.12. In this case, chemiluminescence is dominated by soot incandescence through the visible part of the spectrum. Nevertheless is not likely to appear near the lift-off region, as its formation occurs downstream of the first reaction zones [73, 74].

Contrarily, OH chemiluminescence occurs primarily under high-temperature stoichiometric combustion [77], and is present at the flame stabilization region on lifted, turbulent-diffusion flames [78]. Besides, the OH radical has the strongest emittance band at 306 nm, distant from most soot incandescence as shown in the right side of Figure 3.12. Thus, with

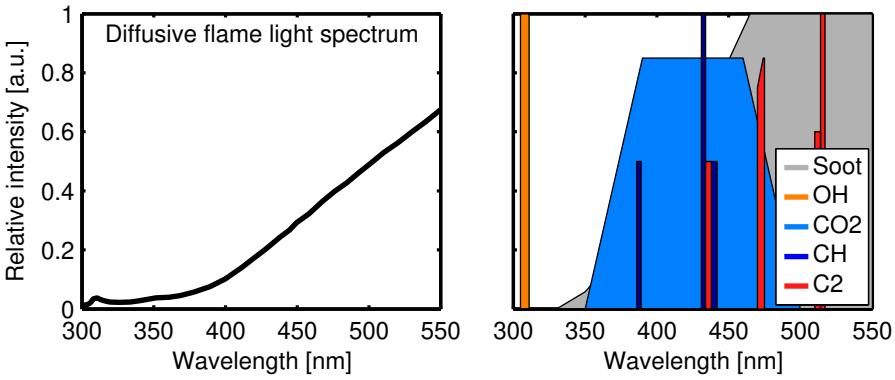

Figure 3.12: Example of the light spectrum distribution of a diffusive flame (left) [75], with peak injection pressure of 68 MPa, a chamber density of 16.6 kg m^{-3} and temperature of 900 K. Emission wavelengths and relative radiation intensities of species in different phases of ignition and combustion (right) [72, 76].

the correct optical setup, OH chemiluminescence is an excellent marker to measure lift-off length [77]. Therefore, an intensified charge-coupled device (ICCD) camera equipped with a 100 mm f/2.9 UV-capable lens was used to capture the low-intensity signal from the combustion. The chemiluminescence of the OH radical was observed through a narrow band-pass filter of 310 ± 5 nm, a configuration extensively reported in the literature [3, 7, 10, 32, 37, 56, 77].

3.6.4 Optical configuration for the non-reactive spray measurements

Both DBI and single-pass schlieren setups were used to measure liquid as well as vapor phase development in the same injection event, as shown in Figure 3.13. Two 50:50 beam splitters were needed two enable both setups to access the test section through the same optical accesses, while keeping all the optical axes aligned. The light pulse from the LED (set to 200 ns) was synchronized with the exposure cycles of the Photron SA-X2 camera. In this way, DBI illumination does not interfere with the schlieren configuration, as the exposure event of the SA5 camera occurs in a different time lapse in the frame of the video. Contrarily, the continuous light from the schlieren setup can reflect in the optical elements and be visualized in the DBI camera. Moreover, as this light source is collimated, beam steering effects are highly

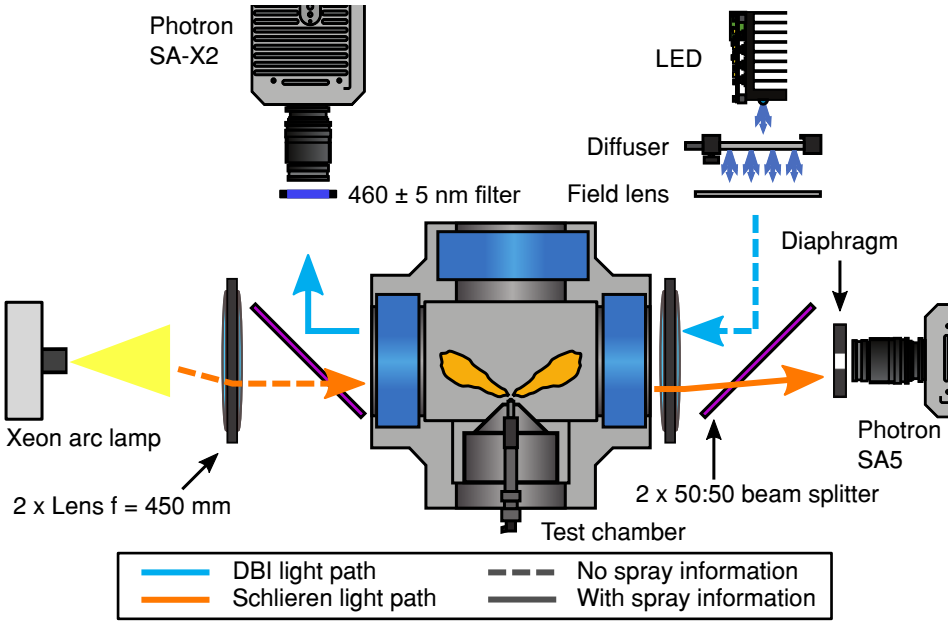

Figure 3.13: Schematic representation of the optical configuration used for the non-reactive spray diagnostics.

likely to appear in the DBI caused by these reflections. Thus a narrow bandpass filter of 460 ± 5 nm, equally centered as the blue LED, was used to minimize the interference of the schlieren light in the liquid visualization. Both cameras were set to start recording with the start of energizing of the injector.

3.6.5 Optical configuration for the reactive spray measurements

The same DBI plus single-pass schlieren configuration was used for the reacting spray diagnostics, shown in Figure 3.14. An ICCD Andor iStar camera, with the corresponding filter for OH chemiluminescence, was positioned with a slight angle to the optical axis to avoid one of the beam splitters and schlieren lens. A piezoelectric transducer was added to perform qualitative measurements of combustion noise through the acquisition of the pressure wave caused by the combustion. For soot concentration, additional repetitions were recorded with the LED light turned off to account for the broadband chemiluminescence of the flame (named bandpass chemiluminescence as it is captured with the filter). Timing for all cameras was referenced to the

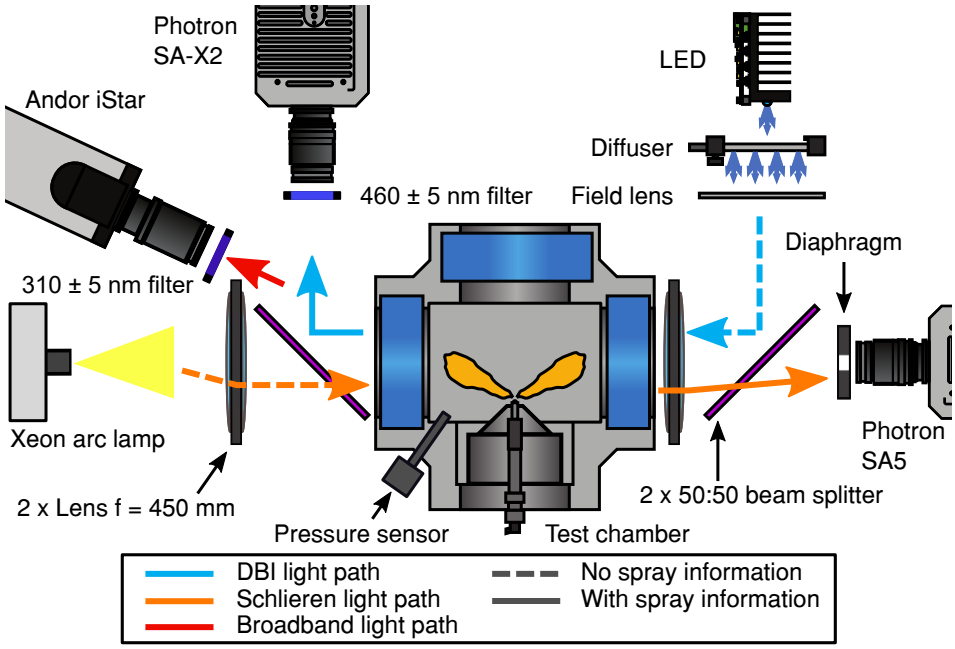

Figure 3.14: Schematic representation of the optical configuration used for the reactive spray diagnostics.

SOE of the injector. Nevertheless, the ICCD camera was set with a delay and exposure time to only record the flame in its stabilized period.

3.6.6 Camera configuration for both optical setups

The configurations of each of the cameras used for recording in both experimental campaigns are summarized in Table 3.3.

3.7 Image processing methods

The methodology for image processing depends significantly on the parameters to extract from the images measured. For most of the optical diagnostics, the primary objective is the segmentation of the spray and the background. Once segmented, a post-analysis of the contour can provide the variables of interest, for instance, spray penetration, spreading angle, or ignition delay, among others. The image processing methodology used for the time-resolved movies is composed of four main steps per frame (time-step): image masking, background subtraction, contour detection, and contour analysis. The

time-averaged OH chemiluminescence and soot concentration by light extinction images are processed differently, thus those methodologies are detailed separately. All the routines were programmed with MATLAB.

3.7.1 Image masking

Once read by the software, an image consists of a matrix where the number of rows and columns is the height and width in pixels, respectively. The value of each cell represents the normalized gray scale intensity from black to white (0 - 1). The normalization is done by dividing each pixel by the maximum possible intensity ($2^{BitDepth}$). Thus for a 12-bit image, the maximum dynamic range of a frame goes from 0 (black) to 4095 (white).

Image masking consists of providing the processing routine with a region of interest where the spray is located. Therefore, undesired elements that are present in the frame are discarded for the segmentation, such as window limits, nozzle tip, injector holder, among others, as depicted in Figure 3.15. The mask is a zero-filled-matrix with dimensions of equal size to the image. The region

Table 3.3: Summary of the configuration parameters for each of the cameras.

Parameter	**Phot. SA-X2**	**Phot. SA5**	**Andor iStar**
Camera lens	Zeiss 100 mm f/2		100 mm f/2.9 UV
Frame rate (fps)	40000		1*
Exposure (µs)	2.5	12.2	-**
Field of view (pixels)	512x360	640x280	1024x1024
Pixel-mm	9.4	11.1	13.9

* Per injection event.
** Adjusted for each injection configuration.

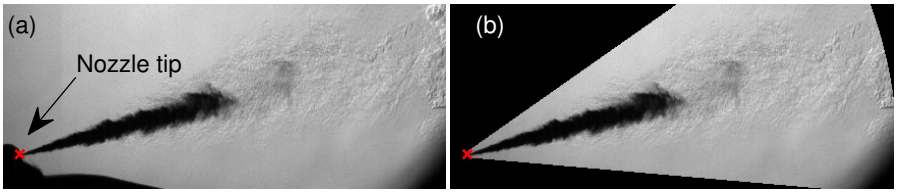

Figure 3.15: Example of the masking process. The raw and masked images are presented left and right, respectively. The frame shown is at 635 µs after SOI, for a rail pressure of 100 MPa, a chamber density of 15.2 kg m^{-3} and temperature of 800 K.

of interest is represented by cells with a value of 1. It is calculated using polar coordinates with the origin in the nozzle tip and is geometrically defined by a minimum and maximum radius, and an angle. Therefore, the masking was performed by element-to-element multiplication of the two matrices.

3.7.2 Background subtraction

With the frame masked, the next step in the image processing is the segmentation between the spray and the background. For DBI images, this was done directly with the Beer-Lambert law, previously presented in Equation 3.10, where I_o is the assembled average of the images before the injection event, and I is the frame being analyzed. As a result, the optical thickness map for each frame is obtained with the background already subtracted, as presented in Figure 3.16.

For schlieren imaging, the process is more complicated. Any density gradient that deflects the rays traveling across the test section could be visualized by the schlieren setup, depending on the sensitivity and the degree of deflection. For example, boundary layers of hot flowing gases, or subtle uneven temperature distributions in the chamber. In consequence, the images gathered with a schlieren setup have very distinctive background patterns, as they might present pixel structures of the same intensity levels as the spray, and those might move throughout the injection event.

The procedure used to depict the spray contour is a composition of two extensively used approaches, and it is thoroughly described in the work of Payri et al. [21], and shown in Figure 3.17. The core of the segmentation algorithm is based on a dynamic-background-composition subtraction [21, 31,

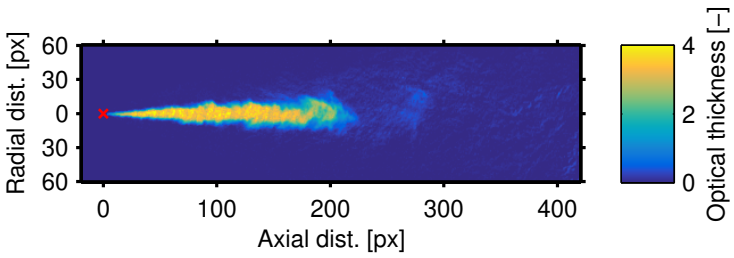

Figure 3.16: Example of the extinction map for a single frame of the DBI. The frame shown is at 635 µs after SOI, for a rail pressure of 100 MPa, a chamber density of 15.2 kg m^{-3} and temperature of 800 K.

55, 56]. But to improve its capabilities, it was combined with an image-temporal-derivative approach [3, 19, 21, 60]. Each method produces gray-scale images, which are then combined with an adjustable weighted average.

The dynamic-background method works by constantly updating the background information to be subtracted. For the frame of time step i (Figure 3.17.*a*), the background for subtraction is a composition of two areas. The first area, shown Figure 3.17.*b*, is built with the pixels from the previous frame of the time step $i-1$ that were not detected as the spray. The second, shown in Figure 3.17.*c*, is comprised of the remnant pixels which were identified as the spray in the previous image, and is filled with the original background before injection. Figure 3.17.*d* is the final background for subtraction, and is the result of mathematically adding the previous areas together. Both areas are contrasted in Figure 3.17.*e*, to illustrate the boundary between backgrounds. The result of the dynamic-background subtraction is then inverted for processing purposes and is presented in Figure 3.17.*f*.

Nevertheless, one disadvantage of this method is detecting the contour of diluted regions of the spray. As fuel mixes in the chamber, the local density

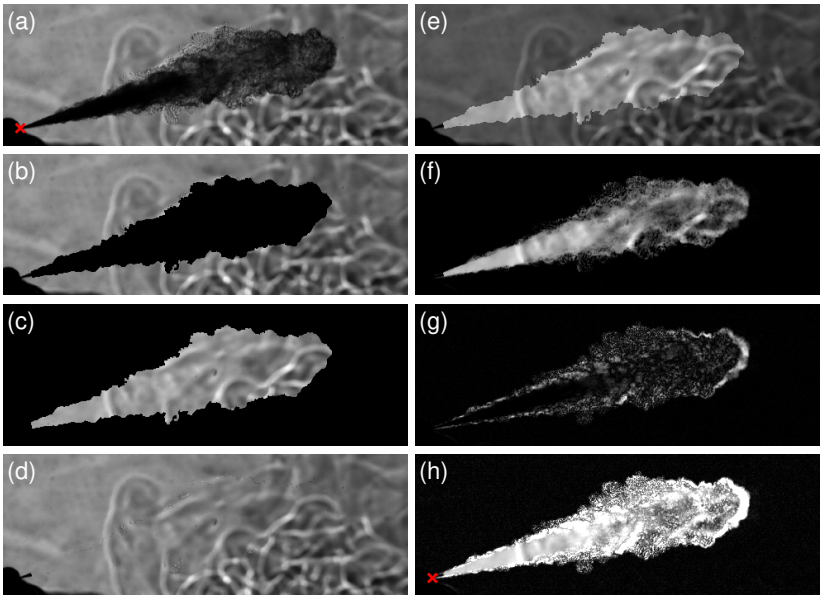

Figure 3.17: Example of the background segmentation procedure for schlieren images. The frame shown is at 560 µs after SOI, for a rail pressure of 100 MPa, a chamber density of 15.2 kg m^{-3} and temperature of 800 K.

gradients of these areas resemble their surroundings. Therefore, the deflection angle of the rays is reduced, and in consequence, the contrast between the spray and background decreases. Although lowering the threshold level (explained in the next section) in these cases would help in the segmentation of the spray, it could also implicate the detection of non-spray pixels.

The image-temporal-derivative approach works very well for capturing the contour of a spray in these diluted regions. It detects temporal changes in intensity with the pixel-wise standard deviation for three consecutive images. That is, for a time step i, the pixel-wise standard deviation was calculated between $i, i-1$ and $i-2$. An example is presented in Figure 3.17.*g*. Contrarily, this technique is not able to detect correctly the spray when the intensity levels of the pixels do not change, for example, the liquid core of the plume. Hence, both processing methodologies complement each other. The combination of both approaches provided a sharp image for contour detection, depicted in Figure 3.17.*h*.

For multi-injection, a new methodology was developed to decouple the schlieren contour of the auxiliary injections (pilot or post) from the main. In these cases, the difficulty is that the second pulse occurs in conditions where density gradients were induced already by the previous injection. To overcome this problem, the same dynamic background subtraction strategy was applied to the second injection pulse, where the non-spray pixels of the composed background (Figure 3.17.*d*) include the image with the first injections, and the remnant pixels, which were identified as the spray in the previous frame, were filled with the original background before injection. The methodology is explained in more detail in chapter 5.

3.7.3 Contour detection

With the spray mostly segmented from the background, its boundary was obtained binarizing the image with an intensity level. For DBI movies, a fixed value of optical thickness was used [49, 55]. In contrast, for schlieren images, the threshold was calculated as a fixed factor multiplied by the dynamic range of the frame being analyzed [21, 47, 54, 55]. Contour detection can be very dependent on the binarization level, and consequently, in the quality of the frames gathered. One example is DBI movies with beam-steering near the tip of the liquid phase jet [41]. Therefore, it is important for images to present sharp edges and a rapid intensity decay near the head of the spray. Figure 3.18 depicts an example of the column-wise maximum optical thickness and intensity level for the DBI and schlieren images respectively. Note that for the schlieren images (right side of the figure), intensity values can saturate

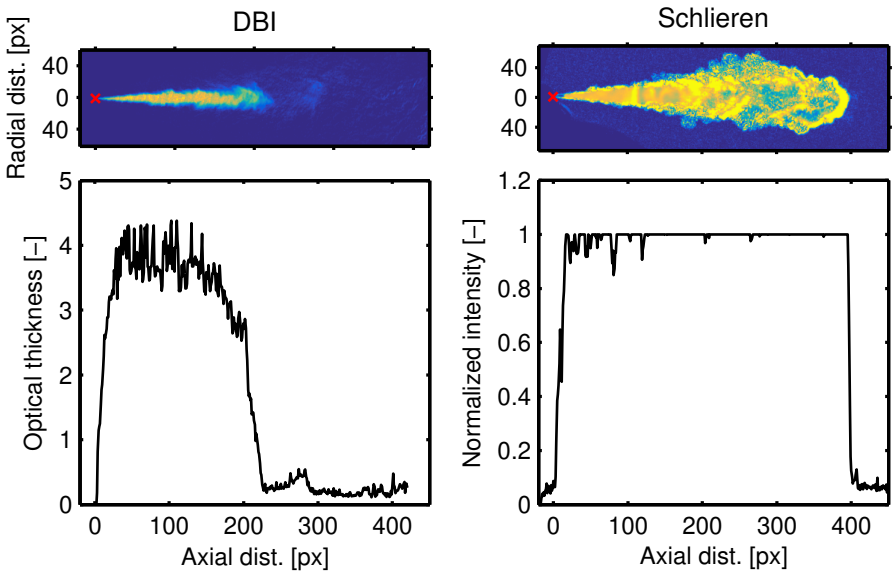

Figure 3.18: Maximum optical thickness (left, DBI) and intensity level (right, schlieren) along the spray axis. The frame shown is at 2235 µs for DBI and at 560 µs for schlieren after SOI, for a rail pressure of 100 MPa, a chamber density of 15.2 kg m^{-3} and temperature of 800 K.

in a normalized scale as pixel-wise standard deviation is not bounded to the dynamic range of the frame.

Nevertheless, the background subtraction is not perfect, and some structures could have enough intensity to be assigned as spray in the threshold binarization. Thus, these are removed through a filtering process that consists of erosion-dilation strategies, removal of small pixel areas, and pixel-connectivity criteria [21, 55, 69, 79]. Figure 3.19 presents an example of the procedure for the frame depicted in Figure 3.19.*a*, and is as follows:

- Figure 3.19.*b*: frame after the binarization. For illustration purposes, the threshold was lowered to increase background noise.
- Figure 3.19.*c*: a two-step erosion that reduced background noise, as well as spray contour dimensions.
- Figure 3.19.*d*: all the isolated pixel areas that are below a minimum pixel count are removed. The value is arbitrary and was reduced for the early stages of spray development, where its area is small too.

- Figure 3.19.*e*: a two-step dilation, to counteract the effect of the erosion on the true dimensions of the spray contour.
- Figure 3.19.*f*: pixel-connectivity criteria, to remove any remaining background in the binarized image. For early stages, the non-spray regions are filtered by selecting the contour nearest to the nozzle exit. Later in the injection event, the biggest area in terms of pixel count is selected as spray. The contour is calculated as the coordinates of the pixels in the boundary between the black and white regions.

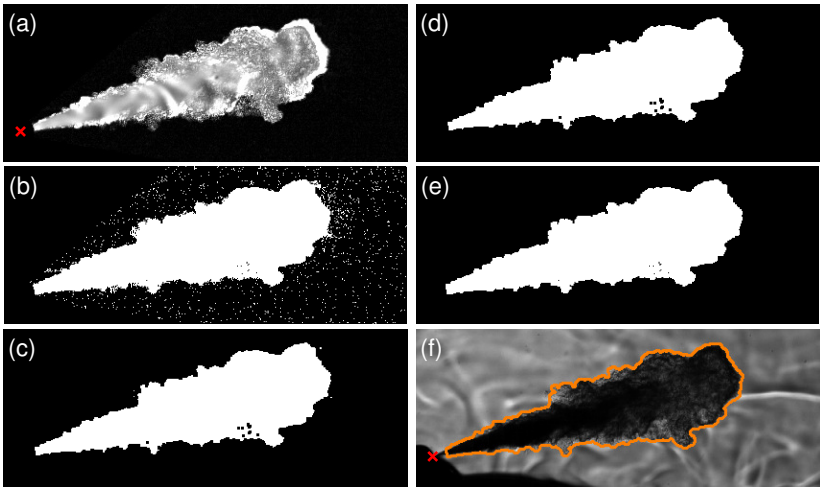

Figure 3.19: Example of the contour detection algorithm. The frame shown is at 560 µs after SOI, for a rail pressure of 100 MPa, a chamber density of 22.8 kg m^{-3} and temperature of 800 K.

3.7.4 Contour analysis

Once the boundary was obtained, macroscopic spray variables were calculated for each time step, as shown in Figure 3.20. Both liquid and vapor phase penetration were defined as the furthest pixel in the radial direction from the nozzle outlet [3, 19, 21, 47], from the DBI and schlieren images respectively. The spreading angle was measured as the angle between two linear fits, calculated in the top and bottom profiles of the spray divided through its axis [9, 16, 21, 55]. The linear fits were computed with all the contour data contained between $d_1 = 10\%$ and $d_2 = 60\%$ of the current frame spray penetration as referenced in Figure 3.20.

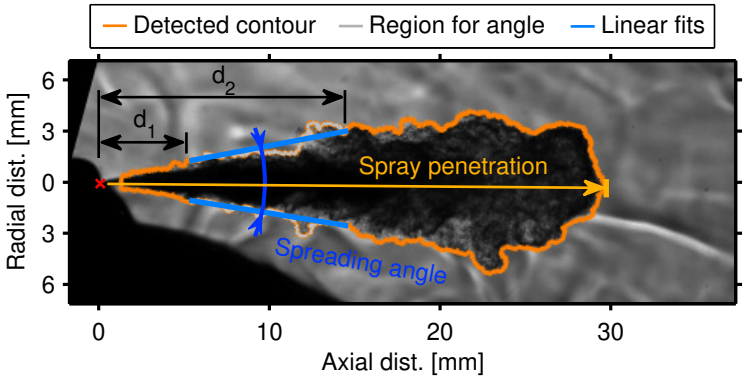

Figure 3.20: Macroscopic spray variables extracted from the contour analysis. The frame shown is at 560 µs after SOI, for a rail pressure of 100 MPa, a chamber density of 22.8 kg m^{-3} and temperature of 800 K.

As the spray mixes in the combustion chamber and reaches conditions for ignition, changes in the chemical composition and temperature in the mixture take place, and for a brief period during the first stage ignition, the refractive index near the spray head resembles that of its surrounding gas [3, 18]. Shortly after, second stage ignition unfolds and is characterized by rapid radial expansion of the spray boundary and high refractive index gradients near the spray head [7]. An example of this temporal evolution is presented in a series of frames from schlieren imaging in the top part of Figure 3.21. The plots on the bottom represent the sum of the pixel-wise intensity (left), and its 3-point-stencil (right). Thus, the SSI can be correlated with the local maximum of derivate curve [7, 10, 20, 56], as it is the point of maximum rate of radial expansion associated with the premixed combustion [63].

3.7.5 Data averaging and calculation of the start of injection

Because several repetitions were carried out per test condition, the data gathered with the image processing routine was analyzed with a moving average to assess shot-to-shot dispersion, and obtain a global value for each variable per time step [7, 21]. Thus, for a time instant t_i, the correspondent value of the variable being averaged $f(t_i)$, was computed with the linear regression $f(t) = k_1 t + k_2$. The fitting constants k_1 and k_2 were calculated by solving the regression for t and $f(t)$ consisting of all the data contained in the time interval $t_i \pm \Delta t$, with Δt =150 µs. Subsequently, the average value $\bar{f}$ was estimated by evaluating t_i in the regression previously found. This process was

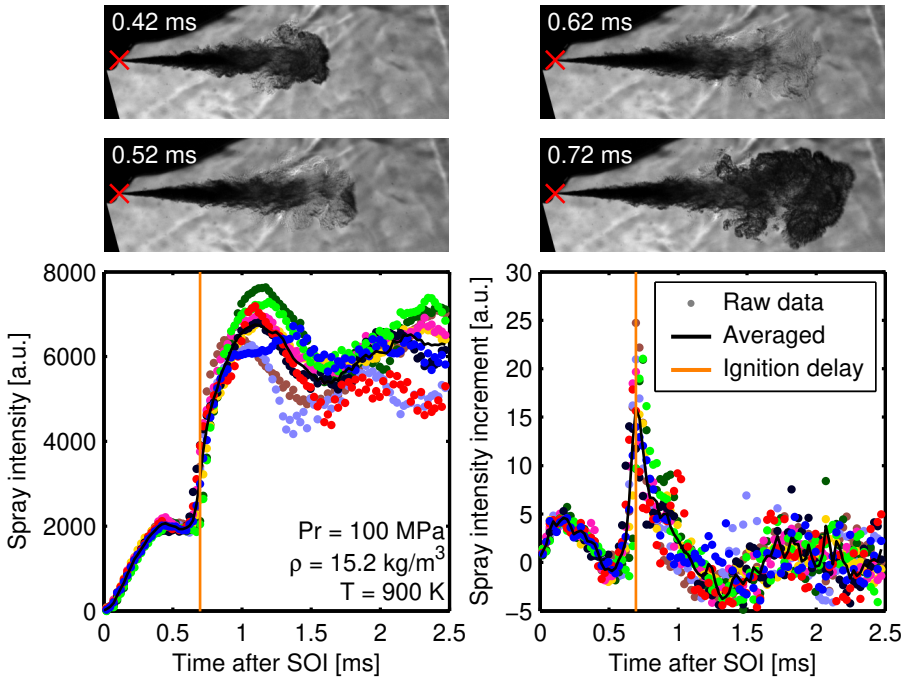

Figure 3.21: Temporal evolution of spray ignition as observed with schlieren imaging. The corresponding total spray intensity and its derivative is presented in the left and right plots, respectively.

repeated for each time-step up to the end of injection, and the result is shown in Figure 3.22.

It is necessary to determine the start-of-injection to phase the time domain of the results and adequately compare test points, decoupling the effect that boundary conditions have on the hydraulic delay of the injector [80]. The SOI was estimated by extrapolating the liquid phase penetration curve to zero, using a quadratic fit with the raw data found in the first 10 mm of penetration curves of all repetitions [16, 19, 69, 81]. An example is presented in Figure 3.22, where the value is presented as the orange vertical line. Considering that all the optical configuration always visualized the same injection event, the SOI obtained from the DBI configuration was used for all other results per test conditions.

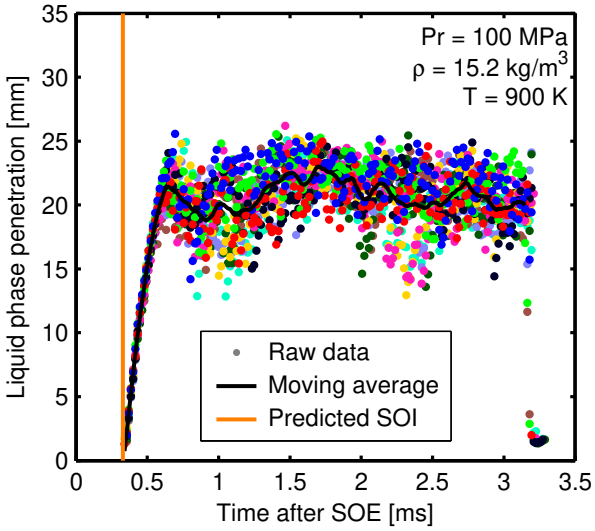

Figure 3.22: Example of the moving average of the raw data (black line). The start of injection is calculated extrapolating the liquid phase penetration curve to zero, the value is depicted as the orange vertical line.

3.7.6 OH chemiluminescence lift-off length

The steps presented in the previous sections are carried out for time-resolved movies, where each frame was processed gradually up to the end of the injection event. Because an ICCD camera was used for OH chemiluminescence, lift-off length was measured with an averaged image of the stabilized period of combustion. Thus, only one frame is analyzed per injection event, and was focused on studying how a pilot injection affects the lift-off length of the main pulse.

The ECN [2] has developed and validated a standard approach to obtained lift-off in light-duty injectors, based on the processing methodology by Siebers [47]. After filtering the image with a 3 x 3 filter, the flame is divided through its axis into a top and bottom profile, to account for different flame shapes. Then, the maximum intensity is traced for each axial position. Finally, the lift-off length is defined as the average distance between the nozzle tip and the first axial position with an intensity above 50 % of the leveling-off peak of the curve [3, 7, 10, 20, 56, 82].

However, some boundary conditions showed no leveling-off value. Therefore, lift-off length was measured with a methodology similar to the one presented by Payri et al. [32]. That is, a fixed percentual threshold above back-

ground noise. Because combustion from the other plumes affected shot-to-shot noise levels, this was calculated as the intensity between two fixed distances for each frame. The averaged image is still filtered and divided by its axis into top and bottom profiles. Then, partial lift-off length was defined as the distance between the nozzle tip and the closest point in the flame where there is at least a minimum flame width above the calculated threshold. The minimum flame width is an arbitrary value in pixels for tuning and prevents lift-off length from being defined by a single pixel above the estimated level. Finally, the global lift-off length is determined as the average between the top and bottom values for every repetition. An example of the definition is depicted in Figure 3.23.

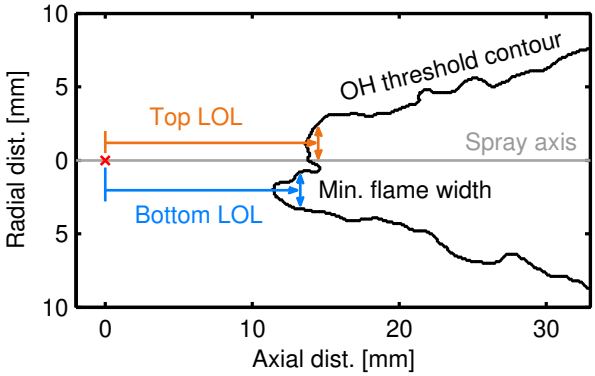

Figure 3.23: Example of the definition used for lift-off length [32], the flame contour was calculated with the set threshold.

3.7.7 Soot DBI

Even though images for the soot DBI were recorded with a high-speed camera, the processing methodology is somewhat different and therefore is described in a separate section. Two optical techniques were required: the diffused back-illumination to directly measure extinction caused by the soot cloud, and bandpass chemiluminescence to correct for the incident combustion light. Previous authors performed experiments with a single high-speed camera alternating frames between optical methods, by switching off the illumination source on every other frame [33, 42, 50, 51]. Then, for example, Payri et al. [33] interpolated alternating frames to have the same temporal reference within the same injection event. Nevertheless, in general, authors averaged all repetitions for each optical technique to reduce the impact of stochastic variations, minimizing the importance of the temporal interpolation.

Moreover, some cameras have problems with fully resetting the sensor after the readout process when recording at high speeds. Hence a weak ghost image is observed in the bandpass chemiluminescence frames, affecting the correction of the light coming from the combustion. For such reasons, soot extinction movies were recorded in separate injection events, increasing the number of repetitions carried out to improve the statistical robustness of the sample for soot concentration results, and minimize the impact of shot-to-shot variations. Likewise, averaging all repetitions helped reduce the influence of the beam-steering observed in the DBI movies on the optical thickness calculations, caused by coupling a DBI setup with a single-pass schlieren.

Therefore, the processing started by calculating the repetition-wise average of each movie for each time step. Then, the optical thickness was calculated with the Equation 3.10 previously shown, where I and I_f correspond respectively to the current frame of the DBI and bandpass chemiluminescence of the same time-step, and I_0 is the reference illumination calculated as the average of the images before the injection event. An example of the first two of these images is depicted in Figure 3.24.

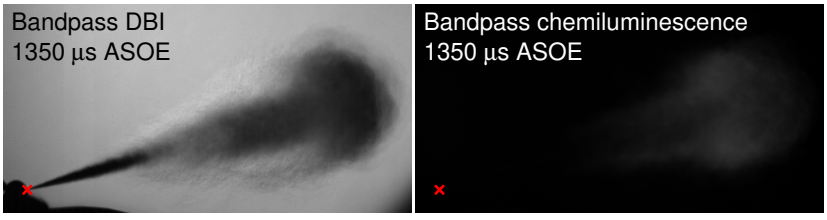

Figure 3.24: Example of the repetition-wise averaged image for the bandpass DBI (left) and chemiluminescence (right) setups. The frames shown are for a single injection event, a rail pressure of 100 MPa, a chamber density of 22.8 kg m^{-3} and temperature of 900 K.

Then the total optical thickness per axial position is calculated and traced along the spray axis, collapsing to a cross-sectional KL value per axial distance, as shown in Figure 3.25, where the liquid length is depicted with a white dashed line. In the figure, a higher cross-sectional KL value is representative of a higher presence of soot. A similar plotting structure was presented by Desantes et al. [83], where it is possible to qualitatively quantify the soot production both in terms of spray penetration and time.

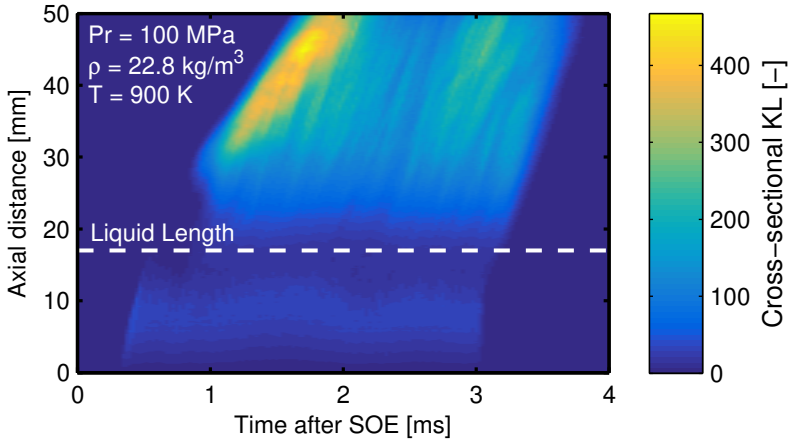

Figure 3.25: Example of a KL-map for the same conditions as before. The y-axis represents the cross-sectional KL value for a fixed axial position.

References

[1] Schöppe, D., Stahl, C., Krüger, G., and Dian, V. "Servo-Driven Piezo Common Rail Diesel Injection System". In: *ATZ Autotechnology* 12.2 (2012), pp. 42–47. DOI: 10.1365/s35595-012-0107-y.

[2] Engine Combustion Network. *https://ecn.sandia.gov/diesel-spray-combustion/*. Online. 2010.

[3] Bardi, M. et al. "Engine Combustion Network: Comparison of Spray Development, Vaporization, and Combustion in Different Combustion Vessels". In: *Atomization and Sprays* 22.10 (2012), pp. 807–842. DOI: 10.1615/AtomizSpr.2013005837.

[4] Kastengren, A. L. et al. "Engine Combustion Network (ECN): Measurements of Nozzle Geometry and Hydraulic Behavior". In: *Atomization and Sprays* 22.12 (2012), pp. 1011–1052. DOI: 10.1615/AtomizSpr.2013006309.

[5] Meijer, M., Malbec, L. M., Bruneaux, G., and Somers, B. "Engine Combustion Network: Spray A Basic Measurements and Advanced Diagnostics". In: *ICLASS 12th Triennial International Conference on Liquid Atomization and Spray Systems*. 2012.

[6] Meijer, M. et al. "Engine Combustion Network (ECN): Characterization and Comparison of Boundary Conditions for Different Combustion Vessels". In: *Atomization and Sprays* 22.9 (2012), pp. 777–806. DOI: 10.1615/AtomizSpr.2012006083.

[7] Benajes, J., Payri, R., Bardi, M., and Martí-Aldaraví, P. "Experimental characterization of diesel ignition and lift-off length using a single-hole ECN injector". In: *Applied Thermal Engineering* 58.1-2 (2013), pp. 554–563. DOI: 10.1016/j.applthermaleng.2013.04.044.

[8] Pickett, L. M., Genzale, C. L., and Manin, J. "Uncertainty quantification for liquid penetration of evaporating sprays at diesel-like conditions". In: *Atomization and Sprays* 25.5 (2015), pp. 425–452. DOI: 10.1615/AtomizSpr.2015010618.

[9] Jung, Y., Manin, J., Skeen, S. A., and Pickett, L. M. "Measurement of Liquid and Vapor Penetration of Diesel Sprays with a Variation in Spreading Angle". In: *SAE Technical Paper 2015-01-0946* (2015). DOI: 10.4271/2015-01-0946.

[10] Payri, R., Salvador, F. J., Manin, J., and Viera, A. "Diesel ignition delay and lift-off length through different methodologies using a multi-hole injector". In: *Applied Energy* 162 (2016), pp. 541–550. DOI: 10.1016/j.apenergy.2015.10.118.

[11] Xue, Q. et al. "Three-dimensional Simulations of the Transient Internal Flow in a Diesel Injector: Effects of Needle Movement". In: *ILASS Americas 25th Annual Conference on Liquid Atomization and Spray Systems*. Pittsburgh, 2013.

[12] Desantes, J. M., Payri, R., Gimeno, J., and Martí-Aldaraví, P. "Simulation of the First Millimeters of the Diesel Spray by an Eulerian Spray Atomization Model Applied on ECN Spray A Injector". In: *SAE Technical Paper 2014-01-1418*. 2014. DOI: 10.4271/2014-01-1418.

[13] Xue, Q. et al. "Eulerian CFD Modeling of Coupled Nozzle Flow and Spray with Validation Against X-Ray Radiography Data". In: *SAE International Journal of Engines* 7.2 (2014), pp. 2014–01–1425. DOI: 10.4271/2014-01-1425.

[14] Xue, Q. et al. "An Eulerian CFD model and X-ray radiography for coupled nozzle flow and spray in internal combustion engines". In: *International Journal of Multiphase Flow* 70 (2015), pp. 77–88. DOI: 10.1016/j.ijmultiphaseflow.2014.11.012.

[15] Desantes, J. M., García-Oliver, J. M., Pastor, J. M., and Pandal, A. "A Comparison of Diesel Sprays CFD Modeling Approaches: Ddm Versus E-Y Eulerian Atomization Model". In: *Atomization and Sprays* 26.7 (2016), pp. 713–737. DOI: 10.1615/AtomizSpr.2015013285.

[16] Payri, R., Bracho, G., Martí-Aldaraví, P., and Viera, A. "Near field visualization of diesel spray for different nozzle inclination angles in non-vaporizing conditions". In: *Atomization and Sprays* 27.3 (2017), pp. 251–267. DOI: 10.1615/AtomizSpr.2017017949.

[17] Arcoumanis, C., Gavaises, M., Nouri, J. M., and Abdul-Wahab, E. "Analysis of the flow in the nozzle of a vertical multi-hole Diesel engine injector". In: *SAE Technical Paper 980811* (1998). DOI: 10.4271/980811.

[18] Pickett, L. M., Kook, S., and Williams, T. C. "Visualization of Diesel Spray Penetration, Cool-Flame, Ignition, High-Temperature Combustion, and Soot Formation Using High-Speed Imaging". In: *SAE International Journal of Engines* 2.1 (2009), pp. 2009–01–0658. DOI: 10.4271/2009-01-0658.

[19] Payri, R., Viera, J. P., Gopalakrishnan, V., and Szymkowicz, P. G. "The effect of nozzle geometry over the evaporative spray formation for three different fuels". In: *Fuel* 188 (2017), pp. 645–660. DOI: 10.1016/j.fuel.2016.06.041.

[20] Payri, R., Viera, J. P., Gopalakrishnan, V., and Szymkowicz, P. G. "The effect of nozzle geometry over ignition delay and flame lift-off of reacting direct-injection sprays for three different fuels". In: *Fuel* 199 (2017), pp. 76–90. DOI: 10.1016/j.fuel.2017.02.075.

[21] Payri, R., Salvador, F. J., Bracho, G., and Viera, A. "Differences between single and double-pass schlieren imaging on diesel vapor spray characteristics". In: *Applied Thermal Engineering* 125 (2017), pp. 220–231. DOI: 10.1016/j.applthermaleng.2017.06.140.

[22] Bosch, W. "The Fuel Rate Indicator: A New Measuring Instrument For Display of the Characteristics of Individual Injection". In: *SAE Technical Paper 660749* (1966). DOI: 10.4271/660749.

[23] Payri, R., Salvador, F. J., Gimeno, J., and Bracho, G. "The effect of temperature and pressure on thermodynamic properties of diesel and biodiesel fuels". In: *Fuel* 90.3 (2011), pp. 1172–1180. DOI: 10.1016/j.fuel.2010.11.015.

[24] Altieri, L. and Tonoli, A. "Piezoelectric Injectors for Automotive Applications: Modeling and Experimental Validation of Hysteretic Behavior and Temperature Effects". In: *Journal of Dynamic Systems, Measurement, and Control* 135.1 (2012), p. 011005. DOI: 10.1115/1.4006627.

[25] Payri, R., Gimeno, J., Mata, C., and Viera, A. "Rate of injection measurements of a direct-acting piezoelectric injector for different operating temperatures". In: *Energy Conversion and Management* 154 (2017), pp. 387–393. DOI: 10.1016/j.enconman.2017.11.029.

[26] Payri, R., Salvador, F. J., Gimeno, J., and Bracho, G. "A new methodology for correcting the signal cumulative phenomenon on injection rate measurements". In: *Experimental Techniques* 32.1 (2008), pp. 46–49. DOI: 10.1111/j.1747-1567.2007.00188.x.

[27] Gimeno, J. "Desarrollo y aplicación de la medida del flujo de cantidad de movimiento de un chorro diesel". PhD thesis. Universitat Politècnica de València, 2008. DOI: 10.4995/Thesis/10251/8306.

[28] Venegas, O. "Estudio del fenómeno de la cavitación en la inyección Diesel mediante la visualización del flujo interno en orificios transparentes." PhD thesis. Universitat Politècnica de València, 2014. DOI: 10.4995/Thesis/10251/37375.

[29] Salvador, F. J., Gimeno, J., Carreres, M., and Crialesi-Esposito, M. "Fuel temperature influence on the performance of a last generation common-rail diesel ballistic injector. Part I: Experimental mass flow rate measurements and discussion". In: *Energy Conversion and Management* 114 (2016), pp. 364–375. DOI: 10.1016/j.enconman.2016.02.042.

[30] Payri, R., García-Oliver, J. M., Salvador, F. J., and Gimeno, J. "Using spray momentum flux measurements to understand the influence of diesel nozzle geometry on spray characteristics". In: *Fuel* 84.5 (2005), pp. 551–561. DOI: 10.1016/j.fuel.2004.10.009.

[31] Payri, R., Salvador, F. J., Gimeno, J., and Viera, A. "Effect of Injection Rate Shaping over Diesel Spray Development in Non-Reacting Evaporative Conditions". In: *10. Tagung Diesel- und Benzindirekteinspritzung 2016*. Ed. by H. Tschöke and R. Marohn. 1. Springer, 2017, pp. 133–152. DOI: 10.1007/978-3-658-15327-4.

[32] Payri, R., Bracho, G., Martí-Aldaraví, P., and Viera, A. "Nozzle Geometry Size Influence on Reactive Spray Development: From Spray B to Heavy Duty Applications". In: *SAE Technical Paper 2017-01-0846* (2017), p. 12. DOI: 10.4271/2017-01-0846.

[33] Payri, R., Gimeno, J., Cardona, S., and Ayyapureddi, S. "Measurement of Soot Concentration in a Prototype Multi-Hole Diesel Injector by High-Speed Color Diffused Back Illumination Technique". In: *SAE Technical Paper 2017-01-2255*. 2017. DOI: 10.4271/2017-01-2255.

[34] Baert, R. S. G. et al. "Design and operation of a high pressure, high temperature cell for HD diesel spray diagnostics: guidelines and results". In: *SAE Technical Paper 2009-01-0649* (2009). DOI: 10.4271/2009-01-0649.

[35] Payri, R., García-Oliver, J. M., Bardi, M., and Manin, J. "Fuel temperature influence on diesel sprays in inert and reacting conditions". In: *Applied Thermal Engineering* 35.1 (2012), pp. 185–195. DOI: 10.1016/j.applthermaleng.2011.10.027.

[36] Fitzgerald, R. P., Svensson, K., Martin, G., Qi, Y., and Koci, C. "Early Investigation of Ducted Fuel Injection for Reducing Soot in Mixing-Controlled Diesel Flames". In: *SAE Technical Paper 2018-01-0238* (2018), pp. 1–17. DOI: 10.4271/2018-01-0238.

[37] Bardi, M. "Partial Needle Lift and Injection Rate Shape Effect on the Formation and Combustion of the Diesel Spray". PhD thesis. Universitat Politècnica de València, 2014. DOI: 10.4995/Thesis/10251/37374.

[38] Miles, R. B. "Optical diagnostics for high-speed flows". In: *Progress in Aerospace Sciences* 72 (2015), pp. 30–36. DOI: 10.1016/j.paerosci.2014.09.007.

[39] Manin, J., Bardi, M., Pickett, L. M., Dahms, R. N., and Oefelein, J. C. "Microscopic investigation of the atomization and mixing processes of diesel sprays injected into high pressure and temperature environments". In: *Fuel* 134 (2014), pp. 531–543. DOI: 10.1016/j.fuel.2014.05.060.

[40] Lillo, P. M., Pickett, L. M., Persson, H., Andersson, Ö., and Kook, S. "Diesel Spray Ignition Detection and Spatial/Temporal Correction". In: *SAE International Journal of Engines* 5.3 (2012), pp. 2012–01–1239. DOI: 10.4271/2012-01-1239.

[41] Westlye, F. R. et al. "Diffuse back-illumination setup for high temporally resolved extinction imaging". In: *Applied Optics* 56.17 (2017), p. 5028. DOI: 10.1364/AO.56.005028.

[42] Skeen, S. A. et al. "A Progress Review on Soot Experiments and Modeling in the Engine Combustion Network (ECN)". In: *SAE International Journal of Engines* 9.2 (2016), pp. 2016–01–0734. DOI: 10.4271/2016-01-0734.

[43] Viera, J. P. et al. “Linking instantaneous rate of injection to X-ray needle lift measurements for a direct-acting piezoelectric injector”. In: *Energy Conversion and Management* 112 (2016), pp. 350–358. DOI: 10.1016/j.enconman.2016.01.038.

[44] Duke, D. J. et al. “Internal and near nozzle measurements of Engine Combustion Network Spray G gasoline direct injectors”. In: *Experimental Thermal and Fluid Science* 88 (2017), pp. 608–621. DOI: 10.1016/j.expthermflusci.2017.07.015.

[45] Kastengren, A. L. et al. “Measurements of droplet size in shear-driven atomization using ultra-small angle x-ray scattering”. In: *International Journal of Multiphase Flow* 92 (2017), pp. 131–139. DOI: 10.1016/j.ijmultiphaseflow.2017.03.005.

[46] El-hannouny, E. M. et al. “Near-Nozzle Spray Characteristics of Heavy-Duty Diesel Injectors”. In: *SAE Technical Paper 2003-01-3150* 724 (2013). DOI: 10.1016/B978-0-444-88351-3.50017-9.

[47] Siebers, D. L. “Liquid-Phase Fuel Penetration in Diesel Sprays”. In: *SAE Technical Paper 980809* (1998). DOI: 10.4271/980809.

[48] Hulkkonen, T., Sarjovaara, T., Kaario, O., Hamalainen, I., and Larmi, M. “Experimental Study of Conical Diesel Nozzle Orifice Geometry”. In: *Atomization and Sprays* 25.6 (2015), pp. 519–538. DOI: 10.1615/AtomizSpr.2015010383.

[49] Manin, J., Bardi, M., and Pickett, L. M. “Evaluation of the liquid length via diffused back-illumination imaging in vaporizing diesel sprays”. In: *The Proceedings of the International symposium on diagnostics and modeling of combustion in internal combustion engines*. Vol. 8. Fukuoka, 2012, pp. 665–673. DOI: 10.1299/jmsesdm.2012.8.665.

[50] Skeen, S. A., Manin, J., Dalen, K., and Pickett, L. M. “Extinction-based Imaging of Soot Processes over a Range of Diesel Operating Conditions”. In: *8th US National Combustion Meeting*. Utah, USA, 2013, pp. 070IC–0355. DOI: 10.1016/j.coal.2015.03.006.

[51] Manin, J., Pickett, L. M., and Skeen, S. A. “Two-Color Diffused Back-Illumination Imaging as a Diagnostic for Time-Resolved Soot Measurements in Reacting Sprays”. In: *SAE International Journal of Engines* 6.4 (2013), pp. 2013–01–2548. DOI: 10.4271/2013-01-2548.

[52] Pastor, J. V., García-Oliver, J. M., Novella, R., and Xuan, T. "Soot Quantification of Single-Hole Diesel Sprays by Means of Extinction Imaging". In: *SAE International Journal of Engines* 8.5 (2015), pp. 2068–2077. DOI: 10.4271/2015-24-2417.

[53] Ghandhi, J. B. and Heim, D. M. "An optimized optical system for backlit imaging". In: *Review of Scientific Instruments* 80.5 (2009). DOI: 10.1063/1.3128728.

[54] Naber, J. D. and Siebers, D. L. "Effects of Gas Density and Vaporization on Penetration and Dispersion of Diesel Sprays". In: *SAE Technical Paper 960034* (1996). DOI: 10.4271/960034.

[55] Payri, R., Gimeno, J., Bracho, G., and Vaquerizo, D. "Study of liquid and vapor phase behavior on Diesel sprays for heavy duty engine nozzles". In: *Applied Thermal Engineering* 107 (2016), pp. 365–378. DOI: 10.1016/j.applthermaleng.2016.06.159.

[56] Payri, R., Viera, J. P., Pei, Y., and Som, S. "Experimental and numerical study of lift-off length and ignition delay of a two-component diesel surrogate". In: *Fuel* 158 (2015), pp. 957–967. DOI: 10.1016/j.fuel.2014.11.072.

[57] Pastor, J. V., Payri, R., García-Oliver, J. M., and Briceño, F. J. "Schlieren Methodology for the Analysis of Transient Diesel Flame Evolution". In: *SAE International Journal of Engines* 6.3 (2013), pp. 2013–24–0041. DOI: 10.4271/2013-24-0041.

[58] Settles, G. S. *Shadowgraph and Schlieren Techniques*. Springer Berlin Heidelberg, 2001. DOI: 10.1007/978-3-642-56640-0.

[59] Gladstone, J. H. and Dale, T. P. "Researches on the Refraction, Dispersion, and Sensitiveness of Liquids". In: *Proceedings of the Royal Society of London* 12 (1862), pp. 448–453. DOI: 10.1098/rstl.1863.0014.

[60] Pastor, J. V., Payri, R., García-Oliver, J. M., and Nerva, J.-G. "Schlieren Measurements of the ECN-Spray A Penetration under Inert and Reacting Conditions". In: *SAE Technical Paper 2012-01-0456* (2012). DOI: 10.4271/2012-01-0456.

[61] Montanaro, A. et al. "Schlieren and Mie Scattering Visualization for Single- Hole Diesel Injector under Vaporizing Conditions with Numerical Validation". In: *SAE Technical Paper 2014-01-1406* (2014). DOI: 10.4271/2014-01-1406.

[62] Payri, R., Salvador, F. J., Martí-Aldaraví, P., and Vaquerizo, D. "ECN Spray G external spray visualization and spray collapse description through penetration and morphology analysis". In: *Applied Thermal Engineering* 112 (2017), pp. 304–316. DOI: 10.1016/j.applthermaleng.2016.10.023.

[63] Payri, R., García-Oliver, J. M., Xuan, T., and Bardi, M. "A study on diesel spray tip penetration and radial expansion under reacting conditions". In: *Applied Thermal Engineering* 90 (2015), pp. 619–629. DOI: 10.1016/j.applthermaleng.2015.07.042.

[64] Allocca, L., Lazzaro, M., Meccariello, G., and Montanaro, A. "Schlieren visualization of a GDI spray impacting on a heated wall: Non-vaporizing and vaporizing evolutions". In: *Energy* 108 (2016), pp. 93–98. DOI: 10.1016/j.energy.2015.09.107.

[65] Nerva, J.-G., Genzale, C. L., Kook, S., García-Oliver, J. M., and Pickett, L. M. "Fundamental spray and combustion measurements of soy methyl-ester biodiesel". In: *International Journal of Engine Research* 14.4 (2013), pp. 373–390. DOI: 10.1177/1468087412456688.

[66] Knox, B. and Genzale, C. L. "Effects of End-of-Injection Transients on Combustion Recession in Diesel Sprays". In: *SAE International Journal of Engines* 9.2 (2016), pp. 2016–01–0745. DOI: 10.4271/2016-01-0745.

[67] Kook, S. and Pickett, L. M. "Liquid length and vapor penetration of conventional, Fischer-Tropsch, coal-derived, and surrogate fuel sprays at high-temperature and high-pressure ambient conditions". In: *Fuel* 93 (2012), pp. 539–548. DOI: 10.1016/j.fuel.2011.10.004.

[68] Pickett, L. M. et al. "Relationship Between Diesel Fuel Spray Vapor Penetration/Dispersion and Local Fuel Mixture Fraction". In: *SAE International Journal of Engines* 4.1 (2011), pp. 2011–01–0686. DOI: 10.4271/2011-01-0686.

[69] Payri, R., Gimeno, J., Viera, J. P., and Plazas, A. H. "Needle lift profile influence on the vapor phase penetration for a prototype diesel direct acting piezoelectric injector". In: *Fuel* 113 (2013), pp. 257–265. DOI: 10.1016/j.fuel.2013.05.057.

[70] Pastor, J. V., García-Oliver, J. M., Pastor, J. M., and Zapata, L. D. "Evaporating Diesel Spray Visualization using a Double-pass Shadowgraphy/Schlieren imaging". In: *SAE Technical Paper 2007-24-0026* (2007). DOI: 10.4271/2007-24-0026.

[71] Payri, R., Salvador, F. J., García, A., and Gil, A. "Combination of visualization techniques for the analysis of evaporating diesel sprays". In: *Energy and Fuels* 26.9 (2012), pp. 5481–5490. DOI: 10.1021/ef3008823.

[72] Gaydon, A. G. *The Spectroscopy of Flames*. Springer, 1974. DOI: 10.1007/978-94-009-5720-6.

[73] Dec, J. E. and Coy, E. B. "OH Radical Imaging in a DI Diesel Engine and the Structure of the Early Diffusion Flame". In: *SAE Technical Paper 960831* (1996). DOI: 10.4271/960831.

[74] Siebers, D. L. and Higgins, B. S. "Flame Lift-Off on Direct-Injection Diesel Sprays Under Quiescent Conditions". In: *SAE Technical Paper 2001-01-0530* 724 (2001). DOI: 10.4271/2001-01-0530.

[75] Dec, J. E. and Espey, C. "Chemiluminescence Imaging of Autoignition in a DI Diesel Engine". In: *SAE Technical Paper 982685* 724 (1998). DOI: 10.4271/982685.

[76] Pittermann, R. "Spectroscopic Analysis of the Combustion in Diesel and Gas Engines". In: *MTZ worldwide* 69 (2008), pp. 66–73. DOI: doi.org/10.1007/BF03227907.

[77] Higgins, B. S. and Siebers, D. L. "Measurement of the Flame Lift-Off Location on DI Diesel Sprays Using OH Chemiluminescence". In: *SAE Technical Paper 2001-01-0918* (2001). DOI: 10.4271/2001-01-0918.

[78] Peters, N. *Turbulent Combustion*. Vol. 12. Cambridge Monographs on Mechanics 11. Cambridge University Press, 2001, pp. 2022–2022. DOI: 10.1088/0957-0233/12/11/708.

[79] Payri, R., Gimeno, J., Bardi, M., and Plazas, A. H. "Effect of Injection Rate Shaping Over Diesel Spray Development in Non Reacting Evaporative Conditions". In: *ASME 2012 Internal Combustion Engine Division Spring Technical Conference*. 2012, p. 347. DOI: 10.1115/ICES2012-81206.

[80] Manin, J., Bardi, M., Pickett, L. M., and Payri, R. "Boundary condition and fuel composition effects on injection processes of high-pressure sprays at the microscopic level". In: *International Journal of Multiphase Flow* 83 (2016), pp. 267–278. DOI: 10.1016/j.ijmultiphaseflow.2015.12.001.

[81] Payri, R., Gimeno, J., Bardi, M., and Plazas, A. H. "Study liquid length penetration results obtained with a direct acting piezo electric injector". In: *Applied Energy* 106 (2013), pp. 152–162. DOI: 10.1016/j.apenergy.2013.01.027.

[82] Westlye, F. R. et al. “Penetration and combustion characterization of cavitating and non-cavitating fuel injectors under diesel engine conditions”. In: *SAE Technical Paper 2016-01-0860* (2016), p. 15. DOI: 10.4271/2016-01-0860.

[83] Desantes, J. M., García-Oliver, J. M., García, A., and Xuan, T. “Optical study on characteristics of non-reacting and reacting diesel spray with different strategies of split injection”. In: *International Journal of Engine Research* 301 (2018). DOI: 10.1177/1468087418773012.

Chapter 4

Hydraulic performance

4.1 Introduction

In this chapter, the hydraulic characterization of the injector is described. First, the test plan with the different boundary conditions is presented. Then, the rate of injection and momentum flux results are shown, accordingly, including an analysis of the performance of the injector in multiple injection strategies. The chapter ends with a summary and conclusions.

4.2 Test plan

Conditions for the hydraulic characterization were selected to analyze the influence between two injection events: a pilot before the main injection or the main injection on a post. A test group consisted of a single injection event with fixed boundary conditions, and then two different pilot/post quantities and four hydraulic dwell times. Each group was assessed for two rail and discharge pressures, to analyze the influence of boundary conditions on the multiple injection strategies. The test plan is presented in Table 4.1.

The proposed test matrix consists of 40 test points for the hydraulic characterization, with two repetitions per condition. Rail pressures were selected considering engine-relevant conditions and ECN guidelines [1]. The discharge pressure was calculated to resemble the chamber pressure for the optical experiments. The typical injection frequency for these tests is 10 Hz, but it was lowered to 1 Hz to maintain it throughout the different experimental campaigns,

Table 4.1: Test plan for the hydraulic characterization campaign.

Parameter	**Value**	**Units**
Rail pressure (P_r)	100 - 200	MPa
Discharge pressure (P_b)	3 - 6	MPa
Injector operating temperature	363	K
Pilot/post dwell times	200 - 350 - 500 - 650	µs
Pilot/post injected quantity	1 - 3	mg
Total mass per injection	30	mg
Injection frequency	1	Hz
Cycles measured	50	-
Repetitions per condition	2	-

as the heat produced by the piezo stack can affect its dynamic response and thus, modify the injected quantity of the pilot/post pulses [2, 3]. The total injected mass was selected accounting for a nozzle with a total nominal flow area of 0.062 83 mm^2 installed in 1.6 L engine that injects 50 mg per cycle. The pilot/post mass distribution was chosen considering 5 % and 10 % of the total injected mass, although in the first case it was reduced to 1 mg to amplify the difference between injected quantities. Dwell times were selected considering a minimum hydraulic separation between injection pulses of 200 µs, increasing it by increments of 150 up to 650 µs.

The injector was driven with a two-stage voltage signal per injection pulse. The signal is comprised of a boost stage to aid needle lift, and then a hold-off stage that controls injection duration. Voltage levels and ramp-off (volts per second) were provided by the original equipment manufacturer (OEM), and they depend on the injection pressure.

4.3 Rate of injection

This section presents the results relevant to the rate of injection. First, the signal treatment for multiple injection strategies is described, followed by the rate of injection measured for all conditions, along with an analysis of shot-to-shot dispersion. The section concludes with a brief description and verification of the two scale system to corroborate the injected mass in momentum flux.

4.3.1 Averaged signal treatment for multiple injections

As the number of pulses increases in an injection event, it is necessary to decouple each process to quantify their respective injected mass. Accordingly, because the signal-to-noise ratio is high enough, the start and end of injection for each pulse were calculated with the rising and falling edge of each curve. Then the injected mass was estimated by integrating each of the pulses within these limits, and the total mass adding these values. An example of the result obtained is depicted in Figure 4.1. Note that the dwell time was measured from the end of injection of the first pulse to the start of injection of the second pulse.

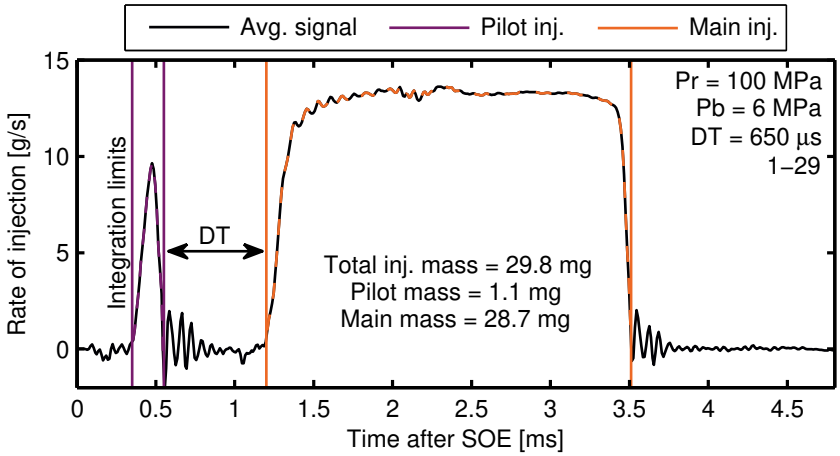

Figure 4.1: Example of the decoupling of two injection pulses and their respective injected quantities. The labeling 1-29 refers to the nominal strategy of 1 mg and 29 mg for the injected mass of pilot and main pulses respectively.

The nominal strategy is presented with a label (for example, $1-29$ in the figure) that refers to the target mass of the auxiliary and main injection, while the order of these numbers refers to either a pilot-main or a main-post case. This labeling structure is maintained throughout the document. For multiple injections, the energizing time of the first pulse was kept for fixed conditions of injected mass and different dwell times. However, because of the rail pressure drop induced by the first injection pulse, and the pressure waves that appear within the injector, the energizing time of the second pulse had to be slightly modified when the dwell time was changed, to maintain the target of a total injected mass of 30 mg per injection event.

4.3.2 Rate of injection for multiple injection strategies

Rate of injection results are presented in a set of three vertical subplots that consist of the driving signal (top), rail pressure measurement (middle), and rate of injection (bottom). All results are always compared with their baseline point, which is at the same conditions of rail and discharge pressure, and named "Single" (or with zero dwell time) as it has no multiple injections. Rail pressure signals were phased to their nominal level for comparison purposes. Nevertheless, the differences in rail pressure levels before injection between test points were less than 1 %, thanks to a robust pressure control system.

Figures 4.2 and 4.3 depict examples of the rate of injection for different pilot injection masses of 1 mg on the left side and 3 mg on the right side, at two

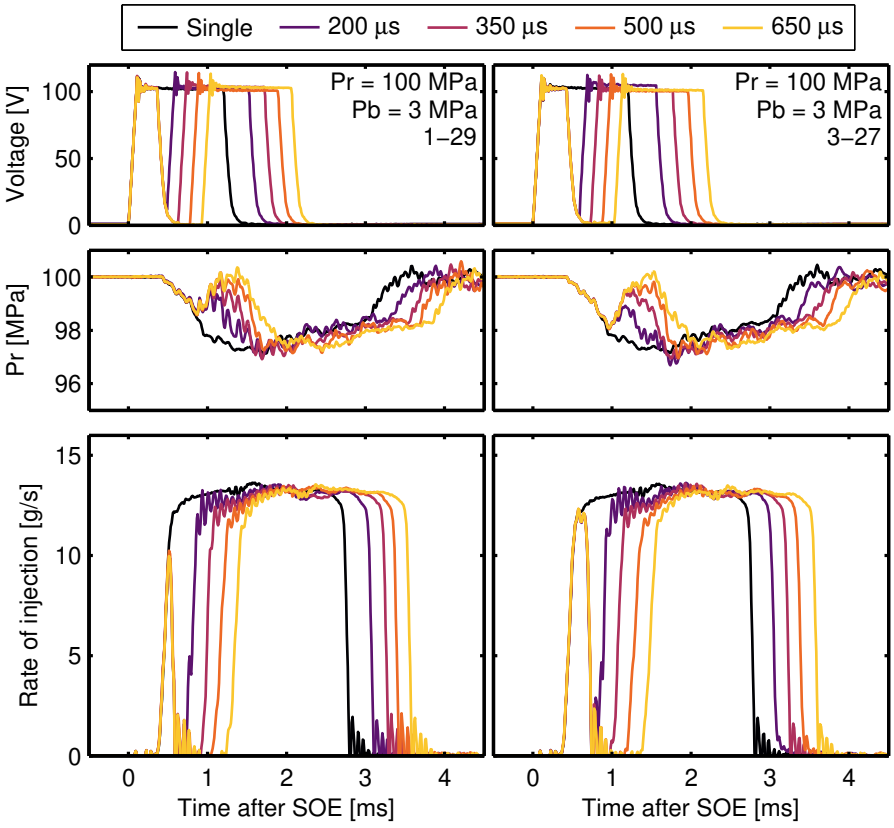

Figure 4.2: Driving signal (top), rail pressure (middle) and rate of injection (bottom) measured for pilot injection quantities of 1 mg (left) and 3 mg (right), for a rail pressure of 100 MPa.

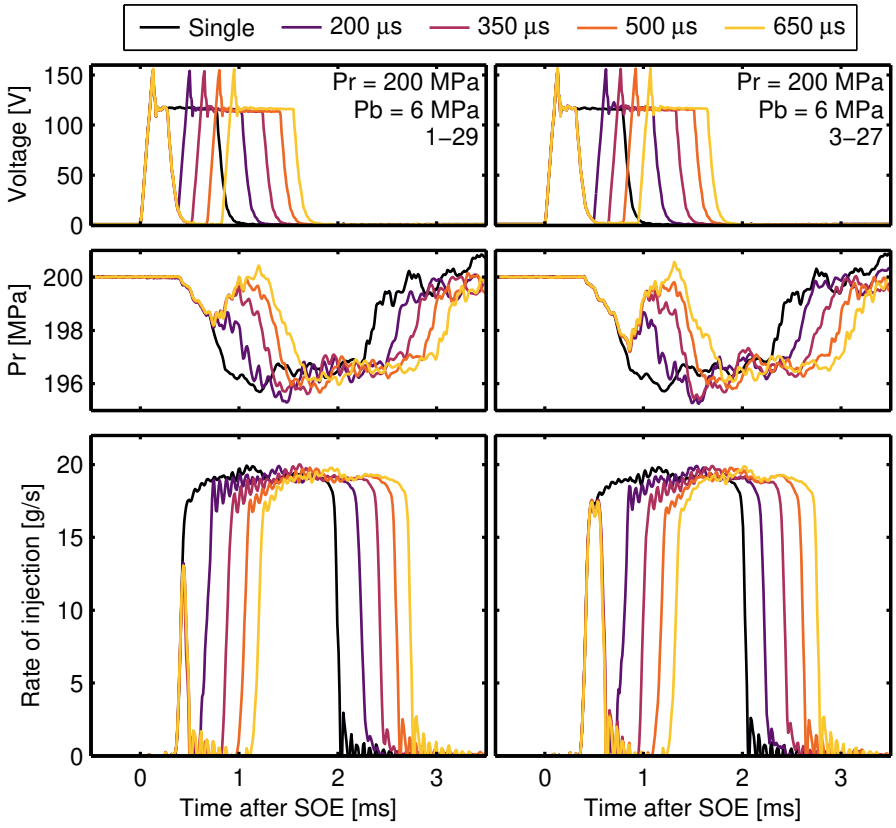

Figure 4.3: Driving signal (top), rail pressure (middle) and rate of injection (bottom) measured for pilot injection quantities of 1 mg (left) and 3 mg (right), for a rail pressure of 200 MPa.

different rail pressure levels respectively. Each color represents a hydraulic dwell time. Due to the high number of test points carried out, only one discharge pressure is depicted for each rail pressure, as it is well-known that it has little influence in the hydraulic performance of the injector [4–8].

For both rail pressures and the smallest pilot quantities, the injector did not achieve a stabilized operation and ran entirely in a transitory state through this first injection event. When the pilot quantity increased to 3 mg, stable conditions were reached but not with a fully developed flow, probably due to the sac pressure loss during the start of the injection process [9–11]. Sac pressure decreases mainly for two reasons: the volume of the displaced needle that is filled with fuel from its surroundings, plus the fuel that is injected into

the chamber. Thus, even though the needle reached lift levels where it does not have any influence on the internal flow development, fully developed flow conditions are not reached until sac pressure recovers [10].

Additionally, at lower rail pressures, closed-couple pilots produced a faster rate of the start of injection for the main event, probably due to the effect of pressure waves within the injector sac and control volume [7, 11–14]. The average start of injection speed was calculated as the maximum opening slope of the curve for the conditions presented in the previous plot, and is depicted in Figure 4.4. The impact of this pressure waves can be somewhat visualized in the ROI signal, as local oscillations are observed at the beginning of the main injection signal for the shorter dwell cases, and they get smoother when increasing the dwell time. Thus, as a general consequence, the main injection needed a shorter driving signal to achieve the same mass quantity with decreasing dwell time. However, to meet the target mass of 30 mg per cycle, the injector needed to be energized for a longer time, because of the hydraulic delay each new injection pulse carries.

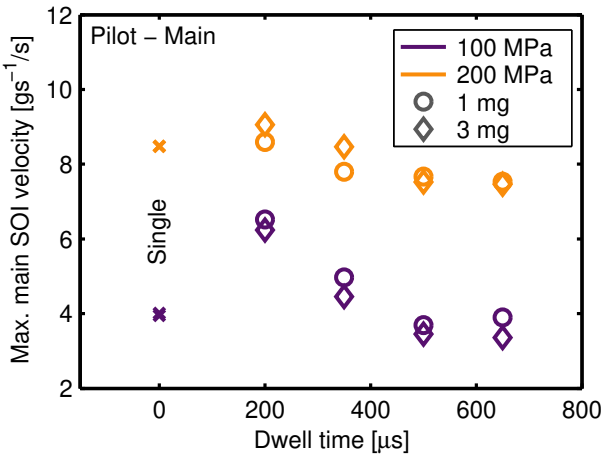

Figure 4.4: Start of injection speed of the main pulse event, calculated as its maximum opening slope, for different pilot quantities and dwell times. Data is compared to a single injection event, represented with a null dwell time.

Examples of the results regarding post injections are depicted in Figures 4.5 and 4.6. As with the pilot injections, a similar behavior was observed. For the smallest post quantities, the injector does not achieve a stabilized operation and runs entirely in a transitory state through this second injection event. Consequently, the control of the mass quantity of the smaller post

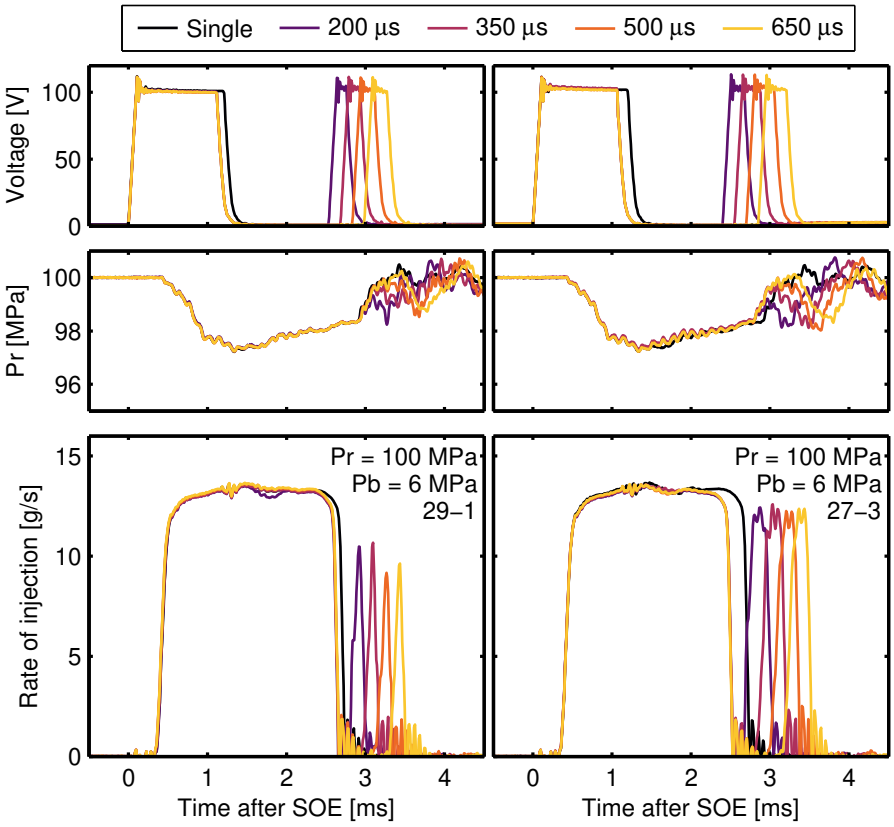

Figure 4.5: Driving signal (top), rail pressure (middle) and rate of injection (bottom) measured for post injection quantities of 1 mg (left) and 3 mg (right), for a rail pressure of 100 MPa.

injection was rather difficult, because the performance of the injector highly depends on the behavior of the pressure waves in the transient of the needle. Moreover, in pilot-main strategies, the SOI velocity of the second pulse was affected by the pilot injection, as the first pulse had no prior event affecting its hydraulic performance. Thus, the same effect is observed on main-post strategies, but much amplified as this second pulse is entirely transitory. A similar conclusion was reached in the work of Carreres [7], where the pressure within the control volume was calculated through 1-D modeling, and the effect of pressure waves in the performance of post injections was quantified. Note that when the post quantity is increased, and the injector reaches a stable operation regime, the signals depict less variability. Further analysis regarding pilot and post injections control is found in subsection 4.3.3.

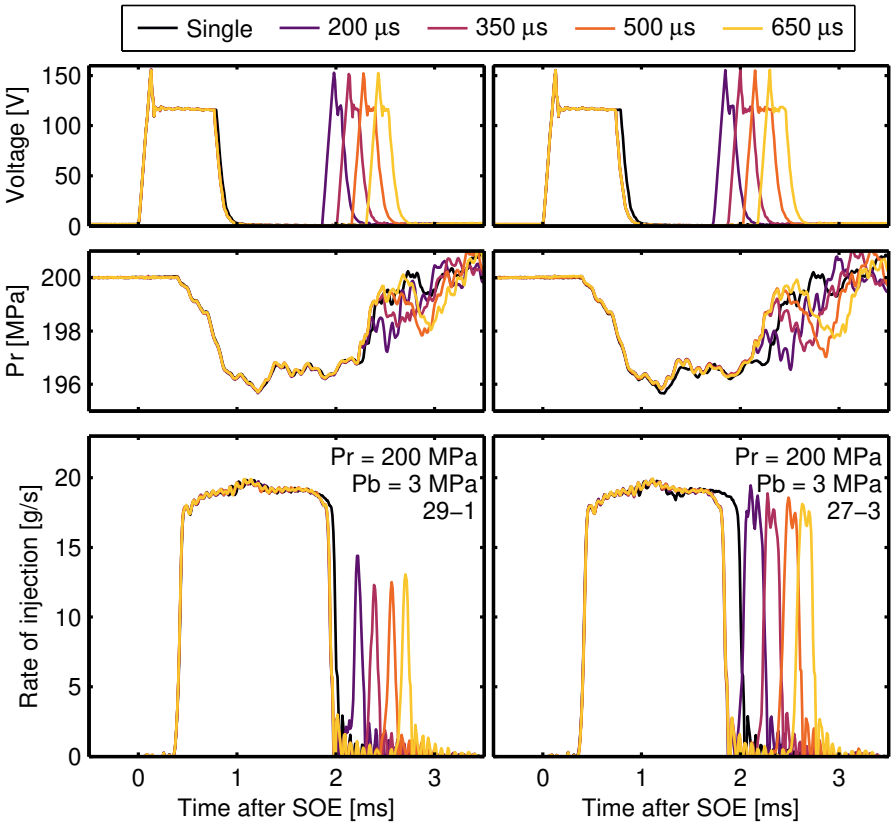

Figure 4.6: Driving signal (top), rail pressure (middle) and rate of injection (bottom) measured for post injection quantities of 1 mg (left) and 3 mg (right), for a rail pressure of 200 MPa.

Altogether, the pilot/post target mass of 1 mg were managed with a 10 % deviation, with some specific conditions measuring overshoots up to 20 %. However, this is a combination of the precision of both the injector and the measurement system. For the target mass of 3 mg, pilot/post injection quantities were attained within a reasonable deviation under 5 %, with some outliers above this value. The total target mass of 30 mg was achieved in general with deviations below 2 %. Nevertheless, an analysis of the relative standard deviation is presented in the next section. The data presented in this section could be useful to validate zero-dimensional models that calculate the rate of injection signals for numerous boundary conditions [15, 16]. Results of the injected mass and its distribution over all the test conditions are summarized in Tables 4.2 and 4.3.

Table 4.2: Summary of injected quantities measured for pilot-main strategies.

-	***Pr*** [MPa]	***Pb*** [MPa]	***DT*** [μs]	**Pilot mass [mg]**	**Main mass [mg]**	**Total mass [mg]**
30	100	3	0	0	30.1	30.1
1-29	100	3	200	1.1	29.1	30.2
1-29	100	3	350	1.2	29.1	30.3
1-29	100	3	500	1.2	28.7	29.9
1-29	100	3	650	1.1	28.6	29.7
30	100	3	0	0	30.1	30.1
3-27	100	3	200	3	27.2	30.2
3-27	100	3	350	3	27.3	30.3
3-27	100	3	500	3.1	26.8	29.9
3-27	100	3	650	3.1	27	30.1
30	100	6	0	0	29.8	29.8
1-29	100	6	200	1.1	29	30.1
1-29	100	6	350	1.1	29	30.1
1-29	100	6	500	1.2	28.9	30.1
1-29	100	6	650	1.1	28.7	29.8
30	100	6	0	0	29.8	29.8
3-27	100	6	200	3.1	27	30.1
3-27	100	6	350	2.9	27	29.9
3-27	100	6	500	3	27.1	30.1
3-27	100	6	650	3	26.9	29.9
30	200	3	0	0	30	30
1-29	200	3	200	0.9	29.1	30
1-29	200	3	350	0.9	29	29.9
1-29	200	3	500	0.9	29.1	30
1-29	200	3	650	1	29.3	30.3
30	200	3	0	0	30.3	30.3
3-27	200	3	200	3	27.1	30.1
3-27	200	3	350	2.9	26.8	29.7
3-27	200	3	500	3	27.2	30.2
3-27	200	3	650	3	27.2	30.2
30	200	6	0	0	30.1	30.1
1-29	200	6	200	1	29	30
1-29	200	6	350	0.9	29.1	30
1-29	200	6	500	1	28.9	29.9
1-29	200	6	650	1	29	30
30	200	6	0	0	30.5	30.5
3-27	200	6	200	3.2	26.4	29.6
3-27	200	6	350	3.2	26.9	30.1
3-27	200	6	500	3.1	27	30.1
3-27	200	6	650	3.1	27.1	30.2

Table 4.3: Summary of injected quantities measured for main-post strategies.

-	***Pr*** [MPa]	***Pb*** [MPa]	***DT*** [μs]	**Post mass [mg]**	**Main mass [mg]**	**Total mass [mg]**
30	100	3	0	0	29.8	29.8
29-1	100	3	200	29	1	30
29-1	100	3	350	29	1.1	30.1
29-1	100	3	500	29	1.1	30.1
29-1	100	3	650	29	1	30
30	100	3	0	0	30	30
27-3	100	3	200	26.9	3	29.9
27-3	100	3	350	27.1	3	30.1
27-3	100	3	500	27.1	3.1	30.2
27-3	100	3	650	27	3.1	30.1
30	100	6	0	0	29.4	29.4
29-1	100	6	200	28.5	1.1	29.6
29-1	100	6	350	28.8	1	29.8
29-1	100	6	500	28.9	1	29.9
29-1	100	6	650	29.1	1	30.1
30	100	6	0	0	29.2	29.2
27-3	100	6	200	26.9	3	29.9
27-3	100	6	350	27	3.1	30.1
27-3	100	6	500	27	3	30
27-3	100	6	650	27	3	30
30	200	3	0	0	29.9	29.9
29-1	200	3	200	28.9	1.1	30
29-1	200	3	350	28.9	1	29.9
29-1	200	3	500	28.9	1	29.9
29-1	200	3	650	29	1	30
30	200	3	0	0	30.1	30.1
27-3	200	3	200	26.9	3	29.9
27-3	200	3	350	27.1	2.9	30
27-3	200	3	500	27	3	30
27-3	200	3	650	27	3	30
30	200	6	0	0	29.9	29.9
29-1	200	6	200	29	1	30
29-1	200	6	350	29	1.1	30.1
29-1	200	6	500	29.1	1.1	30.2
29-1	200	6	650	29	1.1	30.1
30	200	6	0	0	30.1	30.1
27-3	200	6	200	26.9	3	29.9
27-3	200	6	350	26.9	3.1	30
27-3	200	6	500	27.1	3	30.1
27-3	200	6	650	27	3	30

4.3.3 Effect of the boundary conditions on the shot-to-shot dispersion

One of the main challenges of multiple injection strategies is the control of the auxiliary pulses, especially when quantities are small, because the injector operates only in a transitory state, as seen in the previous section. To this end, a shot-to-shot dispersion analysis was carried out to observe in which conditions the injector operates with a considerate variability.

The relative standard deviation (RSD) was calculated as the standard deviation of the integrated mass m_{int} for each pulse of the 50 cycles, divided by the value for the integrated mass of the averaged signal, that is:

$$RSD = 100\ \frac{std([m1_{int}\ m2_{int}\ m3_{int}\ \ldots\ m50_{int}])}{m_{int}} \qquad [\%] \qquad (4.1)$$

Therefore, Equation 4.1 represents the ratio of the standard deviation to the mean value in a percentual scale. Results regarding the dispersion of the pilot-main strategies are presented in Figure 4.7. Single injection cases, depicted as the data with zero dwell time, show the lowest RSD of all. The highest deviation was observed for the pilot masses of 1 mg, as expected due to its transient behavior. Moreover, the shot-to-shot dispersion was higher

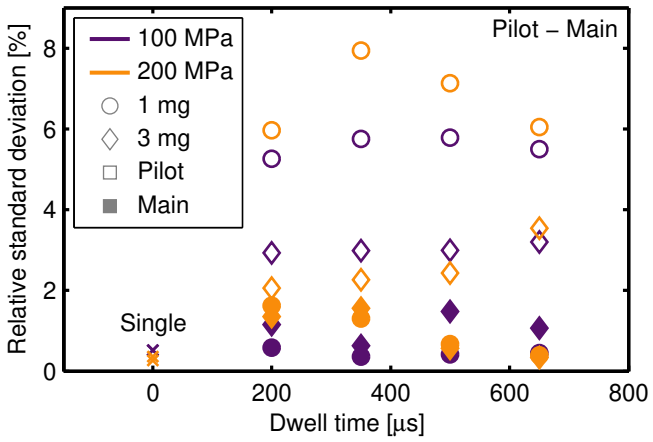

Figure 4.7: Relative standard deviation of the rate of injection results presented in the previous section for pilot-main strategies. Different symbols represent either the single injection or each of the injected quantities of the pilot pulse. Filled symbols depict the main injection associated with a pilot mass at a specific rail pressure and dwell time.

with increasing rail pressure, meaning that injection control difficulty also increases as well. Note that the deviations observed for these cases are within the reported dispersion for the measured pilot mass in the previous section. When the pilot mass is increased to 3 mg, RSD decreases significantly, but still, values calculated are higher than their respective reference case of a single injection. The trend regarding the rail pressure is reversed, probably because at 200 MPa stationary conditions are reached faster as the SOI velocity is higher (Figure 4.4). For each pilot-main case, their corresponding main injection is depicted with filled symbols. When including a pilot mass, the variability of the main injection marginally increases compared to the reference case, probably due to pressure waves within the sac of the nozzle affecting the dynamic of the needle for the second pulse [7, 11, 14, 17].

Results regarding the dispersion of the main-post strategies are presented in Figure 4.8. Once again, the lowest RSD values were obtained for the reference single injection cases, and the main pulses (filled symbols) that correspond to the main event of a post injection at a specific value of rail pressure and dwell time. These injections are non perturbed by any prior event and have the same behavior as the reference case. Overall, deviations values for the post mass were higher than those obtained for pilot-main strategies, as the pressure drop and waves generated by the main pulse have a substantial

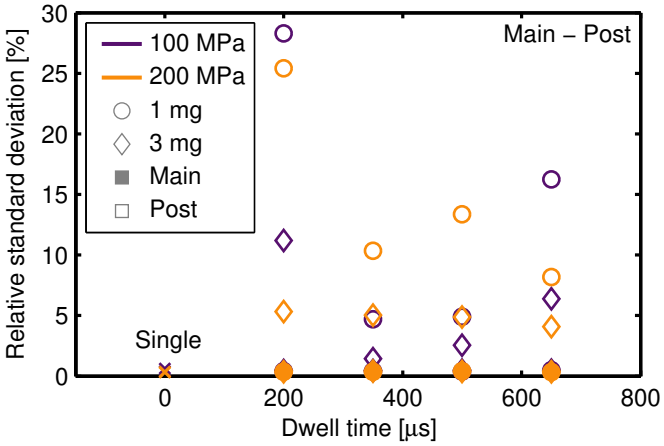

Figure 4.8: Relative standard deviation of the rate of injection results presented in the previous section for main-post strategies. Different symbols represent either the single injection or each of the injected quantities of the post pulse. Filled symbols depict the main injection associated with a post mass at a specific rail pressure and dwell time.

impact in the transients of the post injections. In addition, as observed in the previous figure, increasing the post quantity also decreases the shot-to-shot dispersion at fixed conditions of rail pressure and dwell time, probably because partially stable operations are reached. Interestingly, for a fixed dwell time, if less shot-to-shot dispersion was achieved at lower rail pressure for a 1 mg post injected mass, the same trend is observed for the 3 mg quantity, highlighting the influence of pressure waves in the injection control for post-pulses [7, 17]. The highest RSD was attained for 1 mg and 200 µs of dwell time. At these conditions, the short dwell between pulses probably does not provide enough time for the pressure within the nozzle to partially stabilize, and thus, as the injector is operating in a fully transitory state, pressure waves or transients, that might vary for each cycle, have a more significant impact on the cycle-to-cycle dispersion of the post injection. As an example, Figure 4.9 depicts all the 50 cycles measured for different dwell times of a 1 mg post injection. The

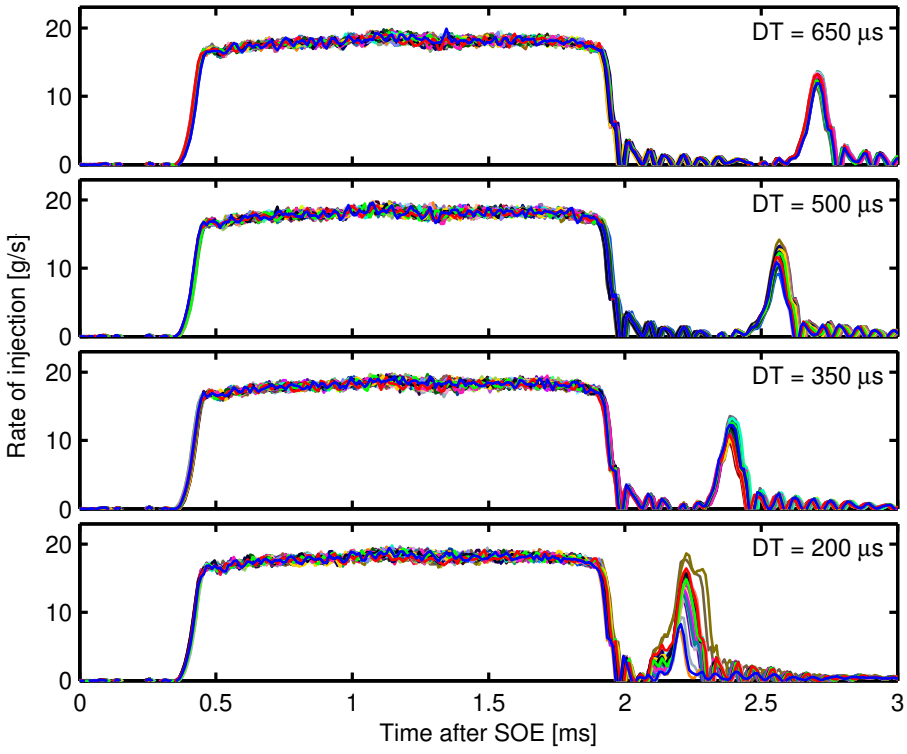

Figure 4.9: Example of the cycle-to-cycle dispersion for different dwell times obtained for a post mass of 1 mg, rail and discharge pressure of 200 MPa and 3 MPa respectively. Each color represents a different cycle.

cycle-to-cycle dispersion observed for decreasing dwell times follows the same behavior to the results presented in Figure 4.8.

4.3.4 Validation of the upstream scale

A two-scale configuration was used to also monitor the injected mass in the momentum flux test rig. The standard procedure in the laboratory for ROI measurements is to use the downstream scale to verify and correct the injected quantity of the integrated signal obtained from the IRDCI [3, 18]. A device located upstream is prone to depend on changes in fuel properties. For example, it was observed that when the fuel in the purger heats up and expands slowly, the scale can measure smaller values compared to the downstream device, in where fuel properties remain constant to some extent. Thus enough time was given for the upstream fuel to reach somewhat stable conditions. Differences between scales are depicted in Figure 4.10.

In general, the percentual error between scales was less than 5 %, with some outlying values up to 10 %. Differences between scales are probably due to the injection frequency used, as the signal-to-noise ratio is worse at lower injection frequencies.

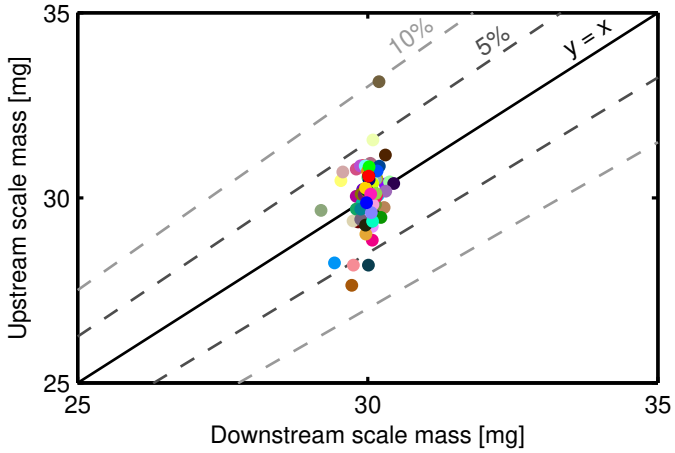

Figure 4.10: Masses measured with the downstream scale (x-axis) and the upstream scale (y-axis). The solid line represents $y = x$, and the dashed lines define a 5% and 10% deviation.

4.4 Momentum flux

Momentum flux results are presented in three parts. First, a brief analysis of plume-to-plume dispersion is depicted, to consider mass distribution among holes in the nozzle. Then, the signal treatment for multiple injection strategies is described along with the verification of the injected mass for each pulse. The last section presents the momentum flux measured for all test conditions.

4.4.1 Mass distribution per hole

The mass allocation presented in the previous section considers that all the holes of the nozzle perform equally. In the momentum flux campaign, the upstream scale quantified the total injected mass per cycle, but only the spray of interest was measured in multiple injection conditions. Thus, a hole-to-hole comparison was carried out to verify the mass distribution. The spray of interest was compared along with two of other five sprays of the nozzle (plume three and five as labeled in Figure 3.2), by rotating the injector holder and aligning each with the pressure sensor. Only single injection conditions were measured, for the same rail and discharge pressures as in the previous cases. For this verification alone, helium instead of nitrogen was used as discharge gas to reduce the spray spreading angle, and prevent plume-to-plume interaction affecting the momentum flux measurement. Due to its reduced molecular weight, the chamber density is much lower for the same discharge pressure. Results are summarized in Figure 4.11.

From the figure, the spray of interest performs at par with the other two plumes, both in the transitory and stabilized regions. Therefore, the real injected mass per hole can be approximated to the measured quantity by the upstream scale divided by the total number of holes. Nevertheless, even though only the spray of interest was measured in the momentum flux rig with multiple injection strategies, the injected quantities calculated in this section were scaled to maintain the same labeling structure throughout the document.

4.4.2 Mass quantification for multiple injection strategies

Needle dynamics can change in momentum flux test rig because the interface varies from fuel-fuel to fuel-gas [11, 19, 20], and the injection quantity and its distribution might differ slightly. Each injection pulse was decoupled with the same procedure as in the rate of injection, with the rising and falling edge of each signal. Note that because the sensor is located downstream of the nozzle outlet, so the SOI and EOI are not the same as before. The upstream scale

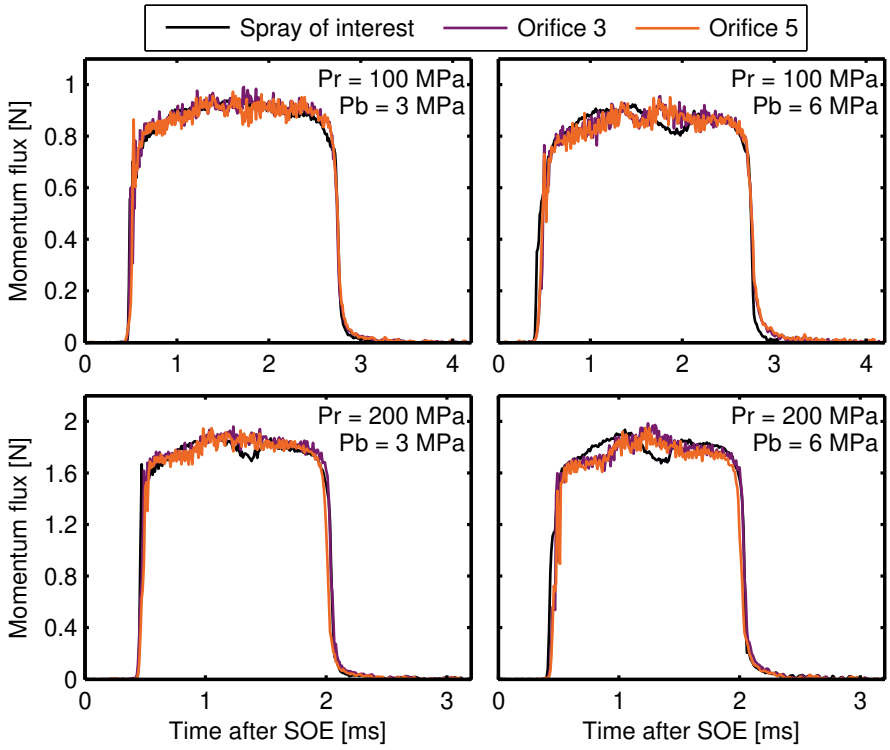

Figure 4.11: Hole-to-hole comparison for different rail and discharge pressure with a single injection.

was used to quantify the total mass injected per cycle. Nevertheless, to verify its allocation, a new procedure was implemented.

Considering that boundary conditions were kept equal along experimental vessels, Equation 3.9 provides a direct link between the ROI and momentum flux ($\sqrt{\dot{M}} \propto \dot{m}$). Therefore, the mass injected by each pulse was calculated as the area allocation, after integrating the square root of the momentum signal. An example is shown in Figure 4.12, where for a strategy of 1-29 mg, that represents a distribution of 3.3-96.7 % for a target mass of 30 mg, the area integrated from the square root of the momentum signal has to match that ratio. Then, with the total injected mass per cycle, the quantity by each pulse can be estimated (and multiplied by the number of holes as previously discussed), and the energizing times slightly corrected to achieve the target mass.

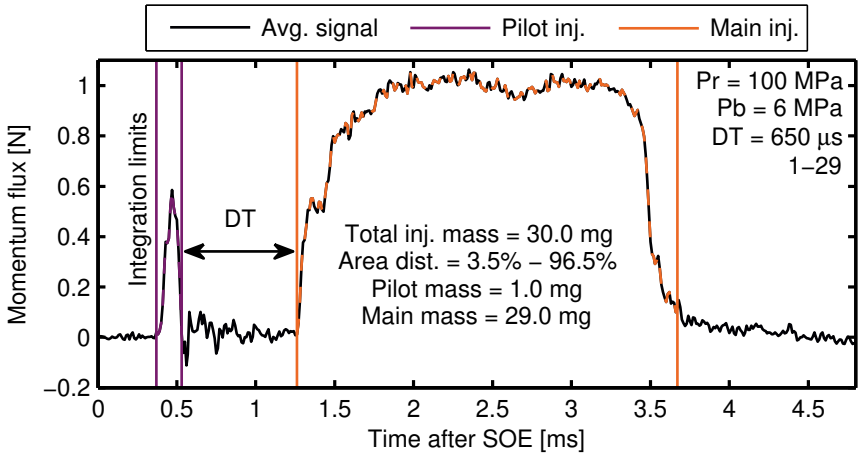

Figure 4.12: Example of the allocation of the injected mass in the momentum flux test rig. The area was calculated as the integral of the square root of the momentum flux signal for each injection pulse.

4.4.3 Momentum flux for multiple injection strategies

Momentum flux results are presented along with the rail pressure in the same plotting structure as in the previous chapter. All results are always compared with their baseline point, which is at the same conditions of rail and discharge pressure, named "Single" (or with zero dwell time) as it has no auxiliary injections. Rail pressure signals were phased to their nominal level for comparison purposes.

Figures 4.13 and 4.14 present examples of the momentum flux signals for different pilot injection masses of 1 mg on the left side and 3 mg on the right side of the plot, at two different rail pressure levels respectively. Each color represents a hydraulic dwell time. Due to the high number of test points carried out, only a discharge pressure is depicted for each rail pressure, as it is well-known that it has little influence in the hydraulic performance of the injector [4, 6–8].

In general, the results resemble trends observed in the rate of injection measurements, and total momentum is now distributed throughout the multiple pulses. The signal shows a localized step in the rising edge, characteristic of the momentum lost by the head of the spray while accelerating the stationary gas in the initial phase of mixing [4, 21–23]. Therefore the interpretation of the results has to consider that the distance from the nozzle tip to the sensor modifies the signal in such way, that it does not precisely represent the

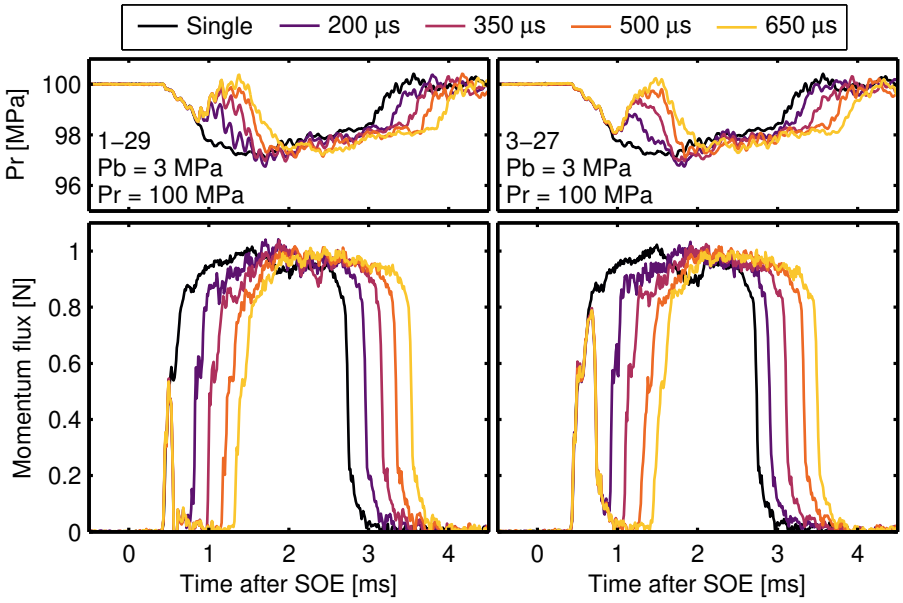

Figure 4.13: Rail pressure (top) and momentum flux (bottom) for pilot injection quantities of 1 mg (left) and 3 mg (right), and a rail pressure of 100 MPa.

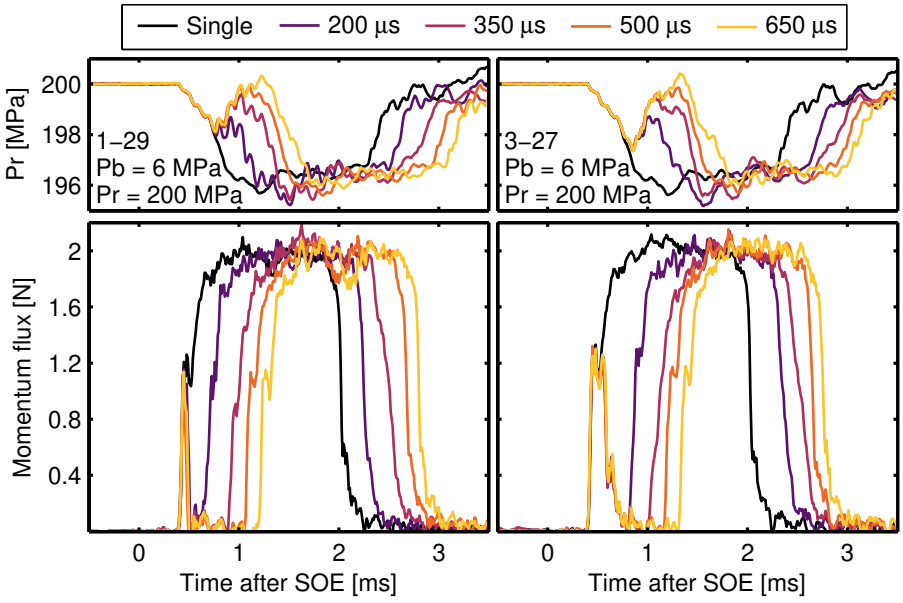

Figure 4.14: Rail pressure (top) and momentum flux (bottom) for pilot injection quantities of 1 mg (left) and 3 mg (right), and a rail pressure of 200 MPa.

momentum flux at the outlet of the nozzle. For a rail pressure of 100 MPa, the start of injection of the main pulse correlates well for each of the dwell times and pilot quantities tested. Stabilized conditions are also reached for the 3 mg pilot, but for a shorter period due to the initial momentum loss. Increasing the rail pressure induced more noise in the transient of the main signal, and the start and end of injection curves are not as smooth as in the previous case. With increasing injection pressure, both flow velocity and rate of air entrainment are higher [24]. Therefore the first injection pulse induces turbulence in the control volume that might slightly affect the signal of the main pulse.

Example of the results regarding post injections are depicted in Figures 4.15 and 4.16. As before, similar trends to ROI results were observed. For the smallest post quantities, the injector does not achieve a stabilized operation and runs entirely in a transitory state. Therefore, once again, controlling the injected mass was difficult compared to post injection with a target mass of 3 mg, where a stable operation regime was reached. As a consequence, post injection quantities of 1 mg presented the highest deviation from the target value.

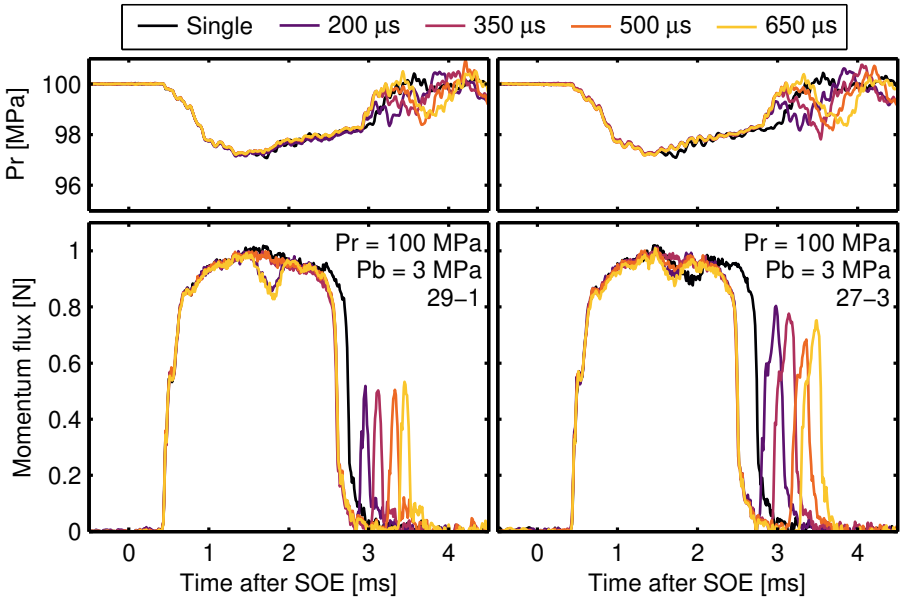

Figure 4.15: Rail pressure (top) and momentum flux (bottom) for post injection quantities of 1 mg (left) and 3 mg (right), and a rail pressure of 100 MPa.

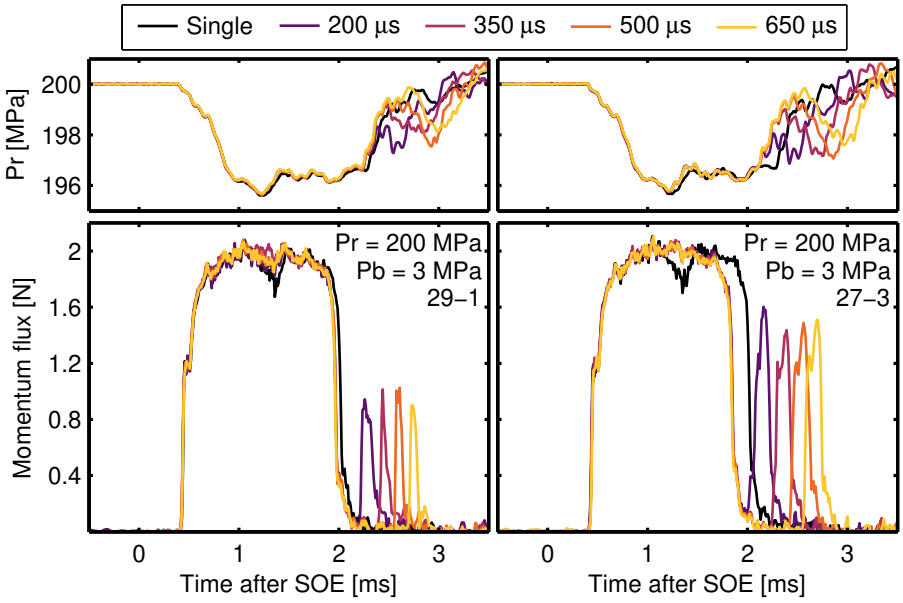

Figure 4.16: Rail pressure (top) and momentum flux (bottom) for post injection quantities of 1 mg (left) and 3 mg (right), and a rail pressure of 200 MPa.

Altogether, the pilot and post target mass of 1 mg were managed with a deviation between 10 % and 20 %, an acceptable tolerance considering that momentum flux is not measured directly at the orifice outlet. For the target mass of 3 mg, pilot and post injection quantities were attained with deviations of around 5 % to 10 %. The total mass of 30 mg was achieved overall with values within 2 % of the target. Results of the injected mass and its distribution for all the test conditions, measured with the methodology proposed in this section, are summarized in Tables 4.4 and 4.5. Note that the results presented in the tables consider the mass measured by the upstream scale, that is the injected quantity through all the holes of the nozzle.

Table 4.4: Summary of injected quantities measured with momentum flux for pilot-main strategies.

-	Pr [MPa]	Pb [MPa]	DT [μs]	Pilot mass [mg]	Main mass [mg]	Total mass [mg]
30	100	3	0	0	30	30
1-29	100	3	200	1.1	29	30.1
1-29	100	3	350	1.1	29	30.1
1-29	100	3	500	1	28.9	29.9
1-29	100	3	650	1.1	28.8	29.9
30	100	3	0	0	30	30
3-27	100	3	200	3.3	26.8	30.1
3-27	100	3	350	3.3	26.8	30.1
3-27	100	3	500	3.3	26.7	30
3-27	100	3	650	3.2	26.9	30.1
30	100	6	0	0	30	30
1-29	100	6	200	1.1	28.9	30
1-29	100	6	350	1.1	28.8	29.9
1-29	100	6	500	1.1	28.8	29.9
1-29	100	6	650	1	29	30
30	100	6	0	0	30.1	30.1
3-27	100	6	200	3.1	26.9	30
3-27	100	6	350	3.1	26.9	30
3-27	100	6	500	3.1	26.8	29.9
3-27	100	6	650	3	27	30
30	200	3	0	0	29.6	29.6
1-29	200	3	200	1.1	29	30.1
1-29	200	3	350	1	29	30
1-29	200	3	500	1.1	28.9	30
1-29	200	3	650	1.1	28.9	30
30	200	3	0	0	29.9	29.9
3-27	200	3	200	3.1	26.8	29.9
3-27	200	3	350	2.9	27.2	30.1
3-27	200	3	500	3.1	26.9	30
3-27	200	3	650	3	27.1	30.1
30	200	6	0	0	30.1	30.1
1-29	200	6	200	1.1	29	30.1
1-29	200	6	350	1	29.1	30.1
1-29	200	6	500	0.9	29.2	30.1
1-29	200	6	650	1.1	28.9	30
30	200	6	0	0	30.1	30.1
3-27	200	6	200	3	27.1	30.1
3-27	200	6	350	3	27.1	30.1
3-27	200	6	500	3.1	27	30.1
3-27	200	6	650	3.1	27.1	30.2

Table 4.5: Summary of injected quantities measured with momentum flux for main-post strategies.

-	Pr [MPa]	Pb [MPa]	DT [μs]	Post mass [mg]	Main mass [mg]	Total mass [mg]
30	100	3	0	0	29.9	29.9
29-1	100	3	200	1.1	28.8	29.9
29-1	100	3	350	1.1	29	30.1
29-1	100	3	500	1.2	28.9	30.1
29-1	100	3	650	1.2	28.9	30.1
30	100	3	0	0	30.1	30.1
27-3	100	3	200	3.1	26.8	29.9
27-3	100	3	350	3.2	26.7	29.9
27-3	100	3	500	3	27	30
27-3	100	3	650	3.1	26.9	30
30	100	6	0	0	30	30
29-1	100	6	200	1.2	28.9	30.1
29-1	100	6	350	1.1	28.9	30
29-1	100	6	500	1.1	28.9	30
29-1	100	6	650	1.1	28.9	30
30	100	6	0	0	30.1	30.1
27-3	100	6	200	3	26.9	29.9
27-3	100	6	350	3.1	27	30.1
27-3	100	6	500	3	26.9	29.9
27-3	100	6	650	3	26.9	29.9
30	200	3	0	0	30	30
29-1	200	3	200	1.2	28.8	30
29-1	200	3	350	1.1	28.9	30
29-1	200	3	500	1.1	28.9	30
29-1	200	3	650	1.1	29	30.1
30	200	3	0	0	29.8	29.8
27-3	200	3	200	3.1	26.8	29.9
27-3	200	3	350	3.1	26.8	29.9
27-3	200	3	500	3	26.9	29.9
27-3	200	3	650	3.1	26.8	29.9
30	200	6	0	0	30	30
29-1	200	6	200	1.2	28.7	29.9
29-1	200	6	350	1	28.9	29.9
29-1	200	6	500	1.1	29	30.1
29-1	200	6	650	1.1	28.8	29.9
30	200	6	0	0	30	30
27-3	200	6	200	3.1	27	30.1
27-3	200	6	350	3.2	26.9	30.1
27-3	200	6	500	3.1	27	30.1
27-3	200	6	650	3.2	26.8	30

4.5 Hydraulic analysis

Quantifying the mass in the momentum flux test rig presented challenges, because the spray impacts the pressure sensor downstream from the outlet of the nozzle, producing the initial momentum loss mentioned in the previous section. This initial loss is somewhat recovered when the inertia of the liquid fuel and the gas entrained, still in the control volume, impacts the sensor after the end of injection [4]. Therefore, the location of the end of the injection in the momentum flux signal is difficult to estimate. Thus, to verify the quantified injected mass and its allocation with the upstream scale on momentum flux test rig, results were qualitatively compared to the rate of injection curve previously depicted for each condition. An estimated momentum flux signal was calculated from the ROI data using Equation 3.9, considering the area of the spray of interest, and the density of the fuel calculated using the correlation presented by Payri et al. [25] for commercial diesel fuel, with the temperature measured by a thermocouple located in the discharge section. Additionally, for each test condition, the momentum flux was phased with the rate of injection data, to counteract the delay of the spray going through the control volume and impacting the sensor. Examples for the same pilot injections at two different rail pressures are presented in Figure 4.17 and Figure 4.18, whereas examples of both post quantities at two different rail pressures are depicted in Figure 4.19 and Figure 4.20.

In general, results from both experimental data sets showed remarkable agreement with the approximation proposed. Auxiliary injections of 1 mg that are all performed in a transitory stage resemble quite notably in shape and phasing. However, for the main-post strategy, the transition between injections was affected by the momentum recovery at the end of injection of the main pulse. But the resemblance with the rate of injection results confirms that the hydraulic dwell times were estimated correctly. For a post injected quantity of 3 mg, signals are still phased correctly in time, but the momentum curve falls short of the local maximum. This trend was observed for most of the 3 mg auxiliary injections, and is probably due to the initial momentum loss.

The excellent coherence between the data depicted in the figures proves the robustness of the methodology employed. Also, it ascertains the possibility of measuring the injected mass and its allocation (for multiple injection strategies) in the momentum flux rig, and remarks that operating conditions of the injector were correctly controlled and maintained throughout experimental vessels.

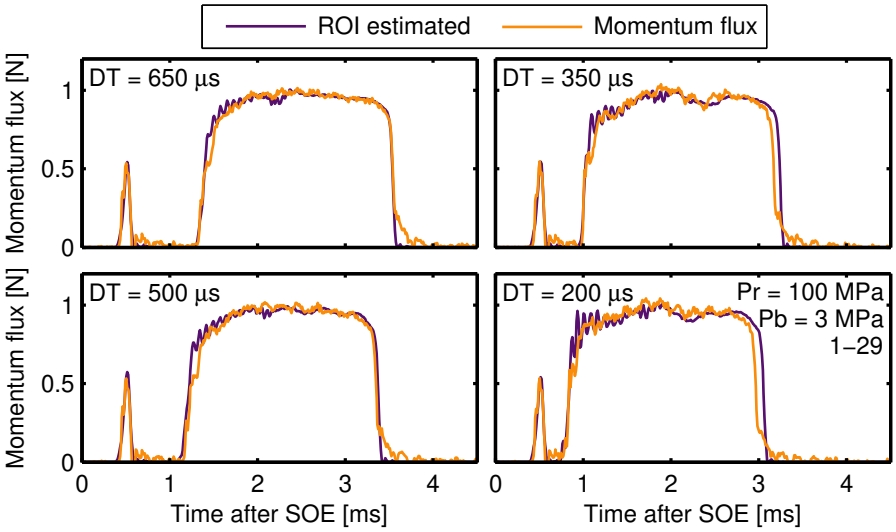

Figure 4.17: Scaled rate of injection and momentum flux signals for a pilot quantity of 1 mg, a rail pressure of 100 MPa, and a discharge pressure of 3 MPa.

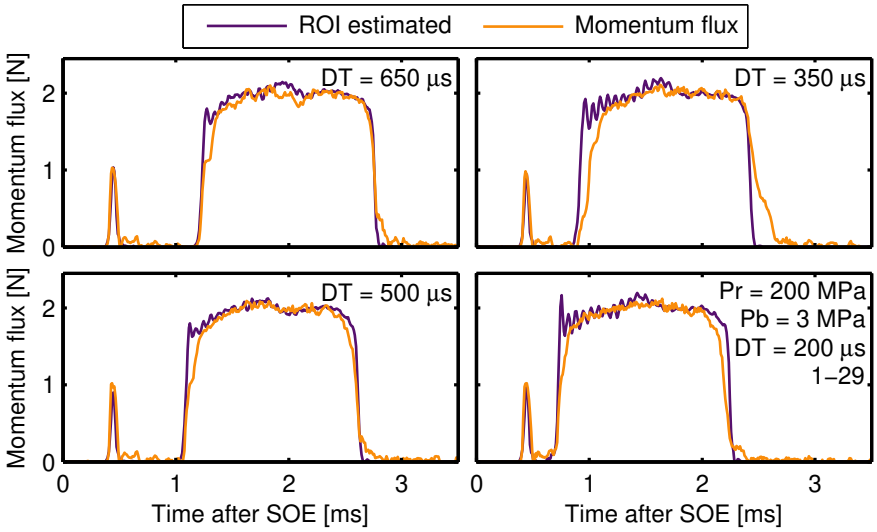

Figure 4.18: Scaled rate of injection and momentum flux signals for a pilot quantity of 1 mg, a rail pressure of 200 MPa, and a discharge pressure of 3 MPa.

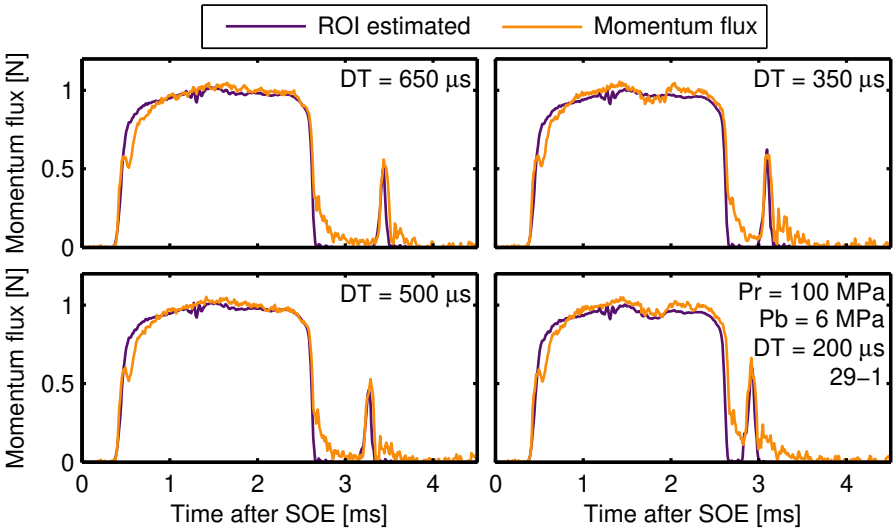

Figure 4.19: Scaled rate of injection and momentum flux signals for a post quantity of 1 mg, a rail pressure of 100 MPa, and a discharge pressure of 6 MPa.

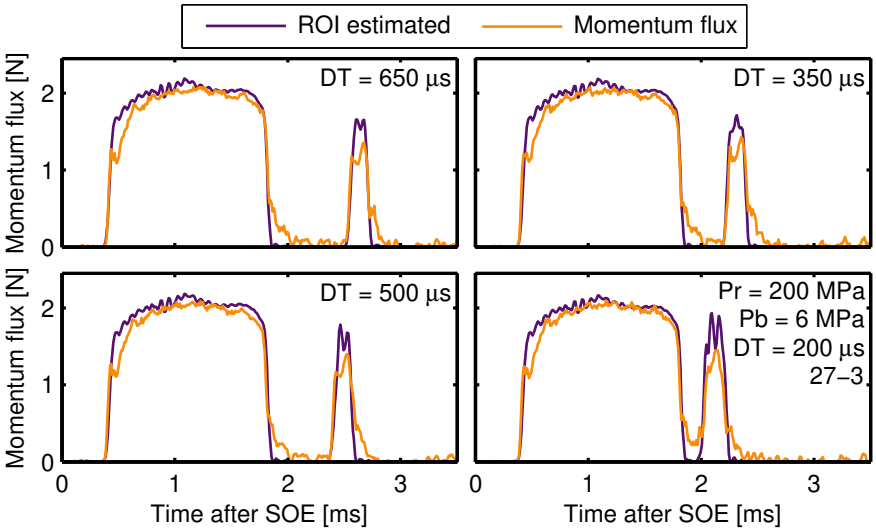

Figure 4.20: Scaled rate of injection and momentum flux signals for a post quantity of 3 mg, a rail pressure of 200 MPa, and a discharge pressure of 6 MPa.

4.6 Summary and conclusions

This chapter collects all the data describing the internal flow development for multiple injection strategies. The rate of injection measurements included a two-scale system to quantify the injected mass and its allocation between the auxiliary and main pulse, and also the differences between both scales. Additionally, a novel methodology was developed with an upstream scale to estimate the injected mass and its allocation in the momentum flux test rig for multiple injection strategies.

From the rate of injection results:

- Signals from multiple pulses were properly decoupled using the rising and falling of each injection pulse. Mass distribution was calculated as the integral of each injection.
- For an injected mass of 1 mg for both pilot-main or main-post strategies, the injector did not achieve a stabilized operation and ran entirely in a transitory state. When the auxiliary quantity was increased to 3 mg, a stable operation was achieved.
- For the lower rail pressure, decreasing the dwell time between the first and second pulses produced a faster start of injection of the second event, with a maximum value observed for 200 µs. Increasing the rail pressure reduced the dynamic influence between injections, though no significant effect was observed.
- Injection control for the pulse of 1 mg and 200 µs of dwell time in main-post strategies showed high cycle variability, because of the impact of the pressure waves produced by the first injection, especially since the second event is all transient. Increasing the injected quantity improved shot-to-shot dispersion.
- In general, both pilot and post target mass of 1 mg and 3 mg were attained with deviations between 10 % and 5 % respectively, with some specific points as outliers. The total mass was achieved with values within 2 % of the target.
- The values measured by the scale located upstream of the test rig were affected by changes in the temperature of the fuel. However, after enough time was provided for the fuel to reach steady conditions, the scale quantified the injected mass with deviations of generally less than 5 % compared to the downstream unit.

From the momentum flux results:

- Signals were properly decoupled using the rising and falling of each injection pulse. Mass allocation was calculated with the area distribution by integrating the square root of the momentum flux signal, matching the ratio of each area with the injected mass.
- Overall, results resembled the trends observed in the rate of injection measurements. The signal showed a step in the rising edge, characteristic of the momentum lost by the head of the spray while accelerating the stationary gas in the control volume. Also, it depicted a rebound on the falling edge due to the inertia of the liquid fuel and gas entrained in the control volume impacting the sensor after the end of injection.
- Auxiliary injections of 1 mg were performed fully in a transitory state for both strategies. As a consequence, injection control for the second pulse in the main-post sequence turned difficult as in ROI. Contrarily, the signal reached the stabilized region when increasing the injected mass to 3 mg.
- In general, pilot/post injections with a target mass of 1 mg were managed with variations between 10 % and 20 %, respectively. For 3 mg, deviation lowered to the range of 5 % to 10 %, respectively. The total mass was achieved with values within 2 % of the target.

Both series of results were compared to verify the quantification of the allocation of the mass in the momentum flux measurements. An estimated momentum flux trace was calculated using the rate of injection data. The momentum flux signal was phased to counteract the delay of the spray traveling through the control volume before impacting the sensor.

Overall, the results showed remarkable agreement. For the main-post strategy, the transition between pulses was slightly affected by the momentum recovery at the end of the injection of the main pulse. But the resemblance with the rate of injection results confirms that the hydraulic dwell times were estimated correctly. For most of the 3 mg auxiliary injections, signals are phased, but the momentum curve falls short of the local maximum, probably due to the initial momentum loss.

The excellent coherence between the data proves the robustness of the methodology employed. Also, it ascertains the possibility of measuring the injected mass and its allocation, especially for multiple injection strategies, in the momentum flux rig.

References

[1] Engine Combustion Network. *https://ecn.sandia.gov/diesel-spray-combustion/*. Online. 2010.

[2] Altieri, L. and Tonoli, A. "Piezoelectric Injectors for Automotive Applications: Modeling and Experimental Validation of Hysteretic Behavior and Temperature Effects". In: *Journal of Dynamic Systems, Measurement, and Control* 135.1 (2012), p. 011005. DOI: 10.1115/1.4006627.

[3] Payri, R., Gimeno, J., Mata, C., and Viera, A. "Rate of injection measurements of a direct-acting piezoelectric injector for different operating temperatures". In: *Energy Conversion and Management* 154 (2017), pp. 387–393. DOI: 10.1016/j.enconman.2017.11.029.

[4] Gimeno, J. "Desarrollo y aplicación de la medida del flujo de cantidad de movimiento de un chorro diesel". PhD thesis. Universitat Politècnica de València, 2008. DOI: 10.4995/Thesis/10251/8306.

[5] Armas, O., Mata, C., and Martínez-Martínez, S. "Effect of diesel injection parameters on instantaneous fuel delivery using a solenoid-operated injector with different fuels". In: *Revista Facultad de Ingeniería Universidad de Antioquia* 64 (2012), pp. 9–21.

[6] Venegas, O. "Estudio del fenómeno de la cavitación en la inyección Diesel mediante la visualización del flujo interno en orificios transparentes." PhD thesis. Universitat Politècnica de València, 2014. DOI: 10.4995/Thesis/10251/37375.

[7] Carreres, M. "Thermal effects influence on the Diesel injector performance through a combined 1D modelling and experimental approach". PhD thesis. Universitat Politècnica de València, 2016. DOI: 10.4995/Thesis/10251/73066.

[8] Viera, J. P. "Experimental study of the effect of nozzle geometry on the performance of direct-injection diesel sprays for three different fuels". PhD thesis. Universitat Politècnica de València, 2017. DOI: 10.4995/Thesis/10251/81857.

[9] Salvador, F. J., Gimeno, J., Carreres, M., and Crialesi-Esposito, M. "Fuel temperature influence on the performance of a last generation common-rail diesel ballistic injector. Part I: Experimental mass flow rate measurements and discussion". In: *Energy Conversion and Management* 114 (2016), pp. 364–375. DOI: 10.1016/j.enconman.2016.02.042.

[10] Payri, R., Salvador, F. J., Carreres, M., and De la Morena, J. "Fuel temperature influence on the performance of a last generation common-rail diesel ballistic injector. Part II: 1D model development, validation and analysis". In: *Energy Conversion and Management* 114 (2016), pp. 376–391. DOI: 10.1016/j.enconman.2016.02.043.

[11] Manin, J., Pickett, L. M., and Yasutomi, K. "Transient cavitation in transparent diesel injectors". In: *ICLASS 14th Triennial International Conference on Liquid Atomization and Spray Systems*. Chicago, 2018, pp. 1–9.

[12] Han, J.-S. et al. "Dynamics of Multiple-Injection Fuel Sprays in a Small-bore HSDI Diesel Engine". In: *SAE Technical Paper 2000-01-1256* (2000). DOI: 10.4271/2000-01-1256.

[13] Baratta, M., Catania, A. E., and Ferrari, A. "Hydraulic Circuit Design Rules to Remove the Dependence of the Injected Fuel Amount on Dwell Time in Multijet CR Systems". In: *Journal of Fluids Engineering* 130.12 (2008). DOI: 10.1115/1.2969443.

[14] Payri, R. et al. "One-dimensional modeling of the interaction between close-coupled injection events for a ballistic solenoid injector". In: *International Journal of Engine Research* 20.4 (2019), pp. 452–469. DOI: 10.1177/1468087418760973.

[15] Payri, R., Gimeno, J., Novella, R., and Bracho, G. "On the rate of injection modeling applied to direct injection compression ignition engines". In: *International Journal of Engine Research* 17.10 (2016), pp. 1015–1030. DOI: 10.1177/1468087416636281.

[16] Soriano, J. A., Mata, C., Armas, O., and Ávila, C. "A zero-dimensional model to simulate injection rate from first generation common rail diesel injectors under thermodynamic diagnosis". In: *Energy* 158 (2018), pp. 845–858. DOI: 10.1016/j.energy.2018.06.054.

[17] Badami, M., Mallamo, F., Millo, F., and Rossi, E. E. "Influence of Multiple Injection Strategies on Emissions, Combustion Noise and BSFC of a DI Common Rail Diesel Engine". In: *SAE Technical Paper 2002-01-0503* (2002). DOI: 10.4271/2002-01-0503.

[18] Payri, R., Salvador, F. J., Gimeno, J., and Bracho, G. "A new methodology for correcting the signal cumulative phenomenon on injection rate measurements". In: *Experimental Techniques* 32.1 (2008), pp. 46–49. DOI: 10.1111/j.1747-1567.2007.00188.x.

[19] Manin, J., Kastengren, A. L., and Payri, R. "Understanding the Acoustic Oscillations Observed in the Injection Rate of a Common-Rail Direct Injection Diesel Injector". In: *Journal of Engineering for Gas Turbines and Power* 134.12 (2012). DOI: 10.1115/1.4007276.

[20] Pickett, L. M., Manin, J., Payri, R., Bardi, M., and Gimeno, J. "Transient Rate of Injection Effects on Spray Development". In: *SAE Technical Paper 2013-24-0001* (2013). DOI: 10.4271/2013-24-0001.

[21] Payri, R., García-Oliver, J. M., Salvador, F. J., and Gimeno, J. "Using spray momentum flux measurements to understand the influence of diesel nozzle geometry on spray characteristics". In: *Fuel* 84.5 (2005), pp. 551–561. DOI: 10.1016/j.fuel.2004.10.009.

[22] Desantes, J. M., Payri, R., Salvador, F. J., and Gimeno, J. "Measurements of spray momentum for the study of cavitation in diesel injection nozzles". In: *SAE Technical Paper 2003-01-0703* (2003). DOI: 10.4271/2003-01-0703.

[23] Postrioti, L., Mariani, F., Battistoni, M., and Mariani, A. "Experimental and Numerical Evaluation of Diesel Spray Momentum Flux". In: *SAE International Journal of Engines* 4970.2 (2009). DOI: doi.org/10.4271/2009-01-2772.

[24] Siebers, D. L. "Liquid-Phase Fuel Penetration in Diesel Sprays". In: *SAE Technical Paper 980809* (1998). DOI: 10.4271/980809.

[25] Payri, R., Salvador, F. J., Gimeno, J., and Bracho, G. "The effect of temperature and pressure on thermodynamic properties of diesel and biodiesel fuels". In: *Fuel* 90.3 (2011), pp. 1172–1180. DOI: 10.1016/j.fuel.2010.11.015.

Chapter 5

Evaporative non-reactive spray development

5.1 Introduction

In this chapter, the results of the first experimental campaign in the optically accessible high-temperature and pressure vessel are presented, carried out in non-reactive evaporative conditions. First, the test plan is shown, followed by a brief description of the image processing for multiple injection strategies. Next, results are discussed in two parts: spray tip penetration and spreading angle. At the end, a summary and conclusions are presented.

5.2 Test plan

Conditions for the spray visualization were selected following ECN guidelines [1]. Boundary conditions include two rail pressures, chamber densities, and temperatures, considering the same values and injection strategies tested in the hydraulic characterization campaign. The test plan is presented in Table 5.1.

The proposed test matrix consists of 72 test points, with ten repetitions per condition. Rail pressures, chamber densities, and temperatures were selected considering engine-relevant conditions from the ECN guidelines [1]. The discharge pressure was set to achieve the target density for a given chamber temperature. The typical injection frequency for these tests is 0.25 Hz, but

Table 5.1: Test plan for the non-reactive evaporative spray visualization campaign.

Parameter	**Value**	**Units**
Rail pressure (P_r)	100 - 200	MPa
Chamber density (ρ)	15.2 - 22.8	$\mathrm{kg\,m^{-3}}$
Chamber temperature (T)	800 - 900	K
Oxygen concentration	≈ 0	%
Injector operating temperature	363	K
Pilot/post dwell times	200 - 350 - 500 - 650	µs
Pilot/post injected quantity	1 - 3	mg
Total mass per injection	30	mg
Injection frequency	1	Hz
Repetitions	10	-

it was increased to 1 Hz to maintain the same configuration throughout the different experimental campaigns. The non-reactive atmosphere was achieved using pure nitrogen as running gas in the facility, which lowered oxygen concentration to almost zero. The same high-pressure, injection control unit and driving signals as in the hydraulic characterization were used. A modification to the injector holder was done to have more or less the same cooling surface and match the operating temperature and conditions as in the hydraulic measurements.

5.3 Spray segmentation for multiple injection strategies

As mentioned in chapter 3, in multiple injection strategies, the main challenge is that the second pulse enters the combustion chambers when there still might be fuel from the first injection. In such cases, once the first injection is over droplets quickly evaporate, so this will not represent a problem for the DBI images. Nevertheless, in schlieren imaging, the density gradients induced by the first injection might still be present. Thus, a methodology was developed to decouple both injection events, with the following considerations:

- The dynamic background subtraction strategy was also applied for the second injection, as the background composed of the non-spray pixels includes information from the first pulse, so this is subtracted.

- Remnant pixels that were identified as the spray of the second pulse in the previous frame are filled with the original background before the injection.
- The image-temporal-derivative was not used for the second pulse because it is not only specific to one injection, as it calculates the overall changes between frames.
- The difficulty in segmenting the contour from the second injection increases as it mixes in the combustion chamber, or its dwell time to the previous pulse decreases. These conditions present a smaller signal-to-noise ratio, and the border between sprays is harder to depict. Thus, a higher binarization threshold was used for the second injection to minimize the probability of over-predicting its boundaries.
- Erosion-dilation strategies, removal of small pixel areas, and pixel-connectivity criteria procedures were carried out the same as with the first injection.
- To prevent poor segmentation when the contours are close to each other, both were forced to merge and treated as one injection in the image processing code when the second contour was within a fixed percentage of the first. The value is a tunable parameter, and it was set generally to 90 %.

Setting up the image processing for the schlieren movies was a time-consuming task, as fine tuning was necessary to decouple the injections for the longest interval possible. An example of the segmentation achieved is presented in Figure 5.1. The spray visualized through schlieren imaging for a given time step is shown in Figure 5.1.*a*. Next, the background subtracted for the first and second injection are depicted in Figures 5.1.*b*.1 and 5.1.*c*.1, respectively. As before, both areas are contrasted to illustrate the boundary between backgrounds. Note how in Figure 5.1.*c*.1, the spray of the first injection is accounted as background. The outcome of the subtraction and image inversion for each pulse is shown in Figures 5.1.*b*.2 and 5.1.*c*.2, respectively. Because the image-temporal-derivative was not used for the second injection, the contour depicted near its boundary is not as detailed as in the first injection. A total of three threshold levels were used for the binarization of the images. When two injections were present in a single frame, a lower threshold (higher sensitivity) allowed to detect the first pulse in its most diluted state, and as stated in the previous considerations, a higher threshold (lower sensitivity) was used to decouple the second injection pulse. Lastly, an average

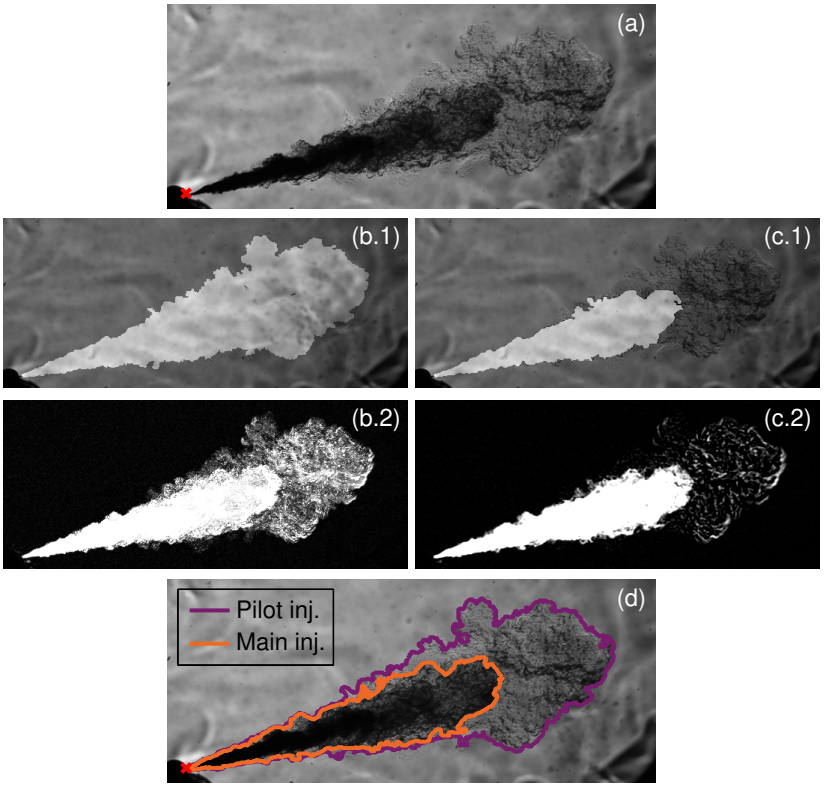

Figure 5.1: Example of the contour segmentation for multiple injection strategies. The frame shown is at 1104 µs after SOI of a 1-29 mg pilot-main event with a 350 µs of dwell time, for a rail pressure of 100 MPa, a chamber density of 15.2 kg m^{-3} and temperature of 800 K.

of the previous two values was applied to segment the first injection before the start of the second pulse. Following the detection algorithm previously described, contours for each injection pulse were extracted. An example of its application is presented in Figure 5.1.*d*. Therefore, the contrast given by the dynamic background strategy and a three threshold configuration provided enough flexibility for the spray segmentation for most of the injection pulses. Moreover, this methodology was also tested successfully for depicting spray contours for cases with more than two injection pulses.

5.3.1 Effect of the injected quantity on the spray segmentation

Increasing the injected quantity in pilot-main strategies might affect the contour detection algorithm. The first pulse could induce higher density gradients as more mass is being introduced into the test chamber, decreasing the density differences between injections that help to delimit their boundaries. Figure 5.2 presents a pilot-main strategy for a fixed dwell time and the two different pilot quantities studied. Each mass is grouped and represented by four images that individually portrait a separate time step. Overall, no apparent effect was observed between the injected mass of the first injection and the difficulty of spray segmentation of the second pulse, as shown in the figure. Increasing the pilot quantity introduced more disturbances in the test chamber, but as observed in the previous chapter, these conditions also depicted a higher momentum flux, which translated into a higher injection velocity. Consequently, the first spray penetrated a larger distance and was more diluted when met

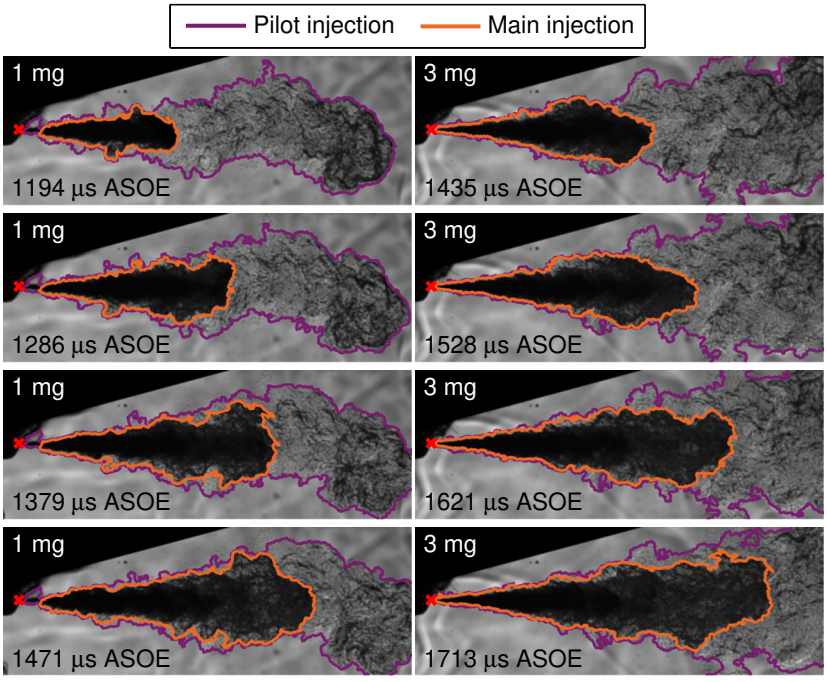

Figure 5.2: Example of the contour segmentation for different injected quantities. The frames shown are for a pilot-main event with a dwell time of 500 µs, a rail pressure of 100 MPa, a chamber density of 22.8 kg m^{-3} and temperature of 800 K.

by the second pulse. Thus, the local density difference in the limiting border between injections was approximately the same.

5.3.2 Effect of the dwell time on the spray segmentation

A critical variable that affects spray segmentation in multiple injection strategies is the dwell time between pulses. As mentioned before, the closer the injections are, the higher the difficulty is for the image processing to properly decouple each event because the local density in the limits of the sprays is similar in schlieren imaging, as well as the light attenuation in DBI.

Figure 5.3 presents an example of the segmentation achieved for the four different dwell times studied, each grouped and represented by four images that individually portraits a separate time step. It is easily recognizable that when decreasing the dwell times, the density gradient between injections pulses, or in this case the difference in pixel intensity, is much lower. Consequently, for a dwell time of 200 µs, the contour obtained is not as smooth as the one depicted for 650 µs, and the segmentation of the second injection is more likely to sometimes over-predict spray penetration values. Therefore, precise tuning was needed for these cases to get acceptable results. Nevertheless, the contours depicted for the second injection pulse were, in general, remarkably well delimited.

5.3.3 Other factors affecting the spray segmentation

As observed in the previous two sections, any parameter that affects the mixing of the first injection pulse, or that creates local conditions in which density gradients between pulses are similar, influences spray segmentation. So, for instance, increasing both chamber density or injection pressure helped the process of depicting the boundary of the second injection when it entered the frame, due to a higher contrast between sprays because of an enhancement of the mixing and evaporation of the first pulse.

However, for most of the conditions with dwell times of 200 µs for pilot-main, or 200 µs and 350 µs for main-post strategies, a clear transition between pulses did not occurred, and thus, their contours could not be decoupled. The specifics of why no visible transition was observed between injections is unclear and is very dependent on the behavior of the injector at the different conditions studied. One of the main distinctions between the test vessels is that the spray visualization campaign included a high-temperature environment. Thus, the viscosity and surface tension of the fuel that resides in the sac after the end of injection decreases, and a larger volume of liquid can flow out

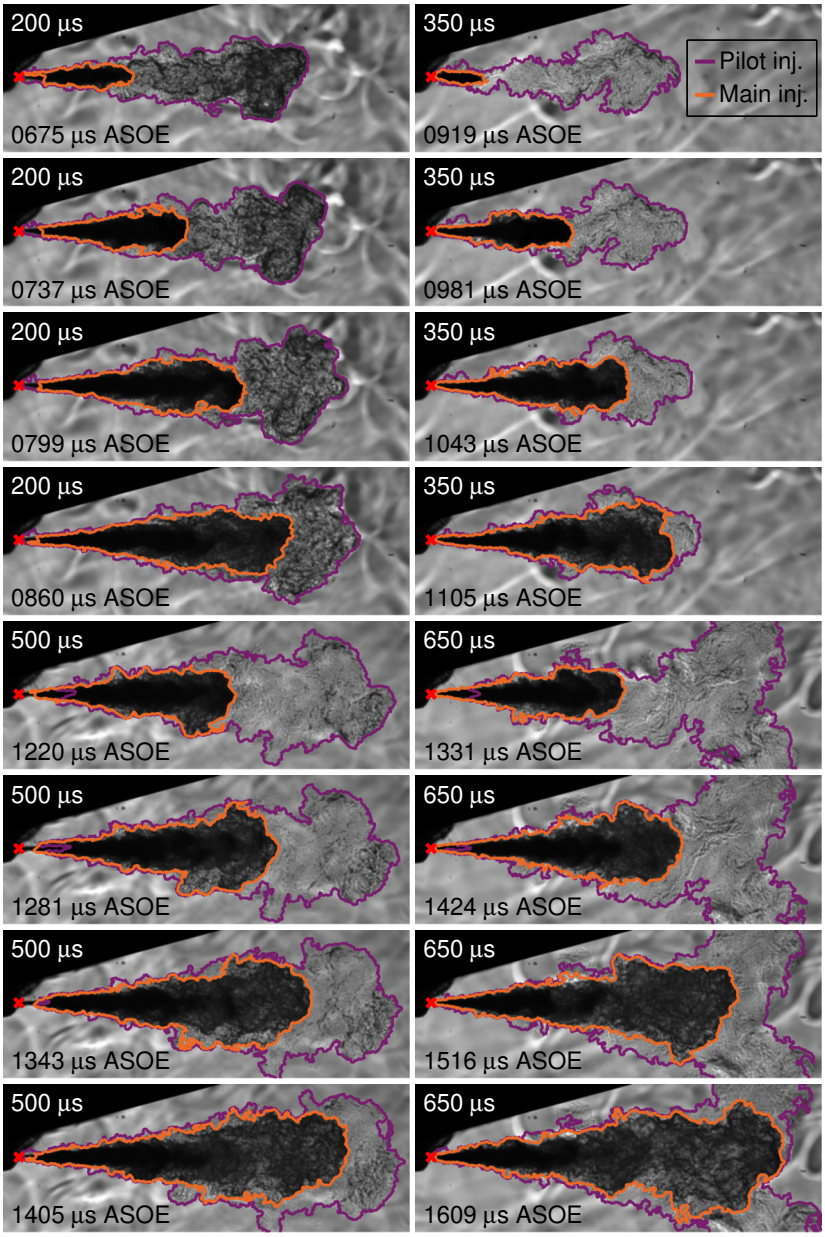

Figure 5.3: Example of the contour segmentation for different dwell times. The frames shown are for 1-29 mg pilot-main events, a rail pressure of 200 MPa, a chamber density of 22.8 kg m^{-3} and temperature of 800 K.

of the orifice [2], in a process named in the literature as dribble [2–6]. Recent studies have qualitatively and quantitatively investigated factors affecting the mechanism of EOI dribble: peak injection velocity [6], needle closing speed [6], in-cylinder pressure [6, 7], injection pressure [7], fuel mass expulsion [4], bubble ingestion at EOI [5, 8], liquid length recession at EOI [9], and different flow characteristics at EOI [3]. Additionally, at a higher temperature, evaporation of that fuel might change not its quantity but its distribution between liquid and vapor phase. Temperature also affects the propagation velocity of the pressure waves within the injector body, that can also influence the hydraulic performance of the injector [10]. All these differences can determine sac conditions and might have had an impact on the needle dynamics [8] and the transition between injection pulses.

Other factors that might explain the difference in the hydraulic performance observed with the increase in chamber temperature could be injector fouling, either as deposits within the hydraulic mechanism [11, 12] or in the nozzle [11, 13–16]. Interestingly, when the second pulse was detected, its start of injection correlated very well with that of the hydraulic measurements (presented in subsection 5.4.2), implying that fuel deposits which alter the internal operation of the injector are unlikely to be the cause. On the contrary, fuel deposits can form externally in the nozzle tip, reducing the effective area of the orifices, and thus, their discharge coefficient [15, 16]. Consequently, the stabilized ROI is lower and the injection duration for the same driving signal can increase, due to a slower mass evacuation speed when the needle is closing during the end of injection process [16]. The increase in the duration can affect the transition between pulses while having almost no impact in needle dynamics during the start of injection process, consequently changing the effective dwell time between pulses as well. Moreover, injectors with high conicity are more prone to coking [17], as cavitation helps clean fuel deposits that form near the nozzle tip, and fouling effects are more critical on the hydraulic performance of nozzles with smaller diameters [18].

To illustrate the differences in the performance of the injector, Figure 5.4 presents data of the average rail pressure measured in momentum flux (solid line) and the spray visualization campaign (symbol), for a set of conditions where both sprays were segmented for all dwell times. In contrast, Figure 5.5 shows the same plotting structure but for the dwell time of 200 µs where no visible transition between pulses was observed. Rail pressures were measured at distinct connection ports of the same common-rail, due to mounting packing in the spray box. Both figures pack a lot of information, but the main difference between them is related to the start and end of injection of the dwell time in question (purple set of data). Overall, a transition between pulses was

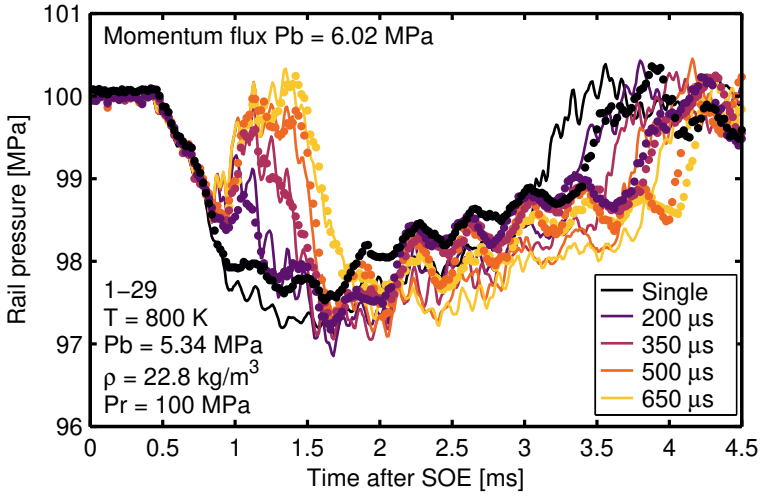

Figure 5.4: Example of the rail pressure signals in a pilot-main strategy for momentum flux (solid lines) and the spray box (symbols), in a set of boundary conditions where both spray contours were depicted for all dwell times.

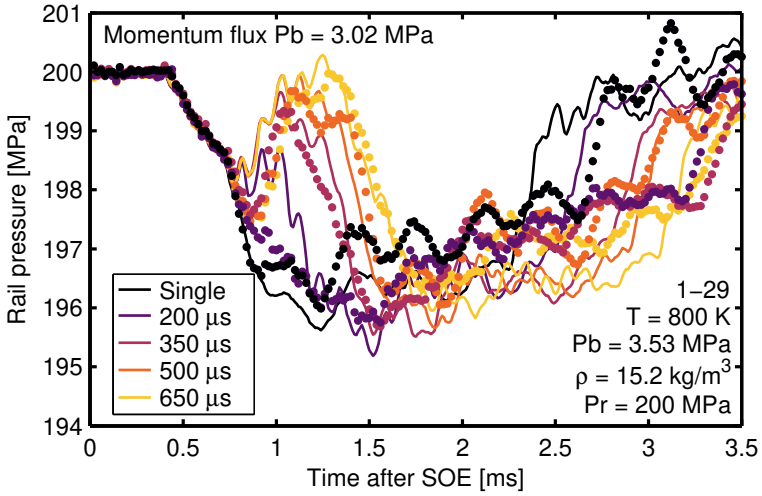

Figure 5.5: Example of the rail pressure signals in a pilot-main strategy for momentum flux (solid lines) and the spray box (symbols), in a set of boundary conditions where the transition between injections was not depicted for a dwell time of 200 µs.

observed when the rail pressure recovered at least slightly, marking the end of an injection event as in the first figure. Interestingly, for the other cases, the signal does not follow the trend of the single injection curve. Therefore flow

was being affected by the needle, but the piezo was probably energized before it reached the seat of the nozzle.

Main-posts strategies were the most affected by the differences in performance at high temperatures, as the needle lift was higher for the stabilized rate of injection of the main. As observed in the previous figures, these conditions lengthened the duration of the main pulse up to the point that it overlapped with post injections with dwell times of 200 µs and 350 µs. An example of the average rail pressure signal for these conditions is presented in Figure 5.6, where not all the dwell times were depicted for simplicity. From the figure and for the spray box measurements, tracing the drop in the rail pressure induced by main injections points to a longer injection duration, thus affecting the transition to the post injections with shorter dwell time. However, for the remaining results, the same labeling structure is used, even though the dwell times and the total injected mass are not comparable to the hydraulic measurements.

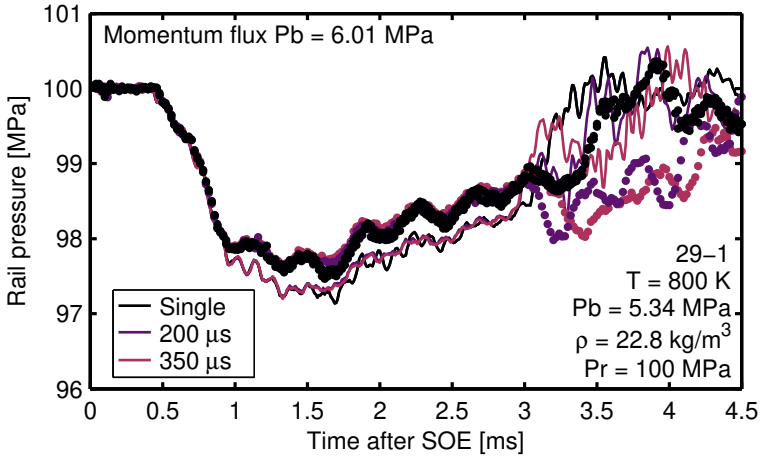

Figure 5.6: Example of the rail pressure signals in a main-post strategy for momentum flux (solid lines) and the spray box (symbols), for boundary conditions where the transition between injections was not depicted for dwell times of 200 µs and 350 µs.

5.4 Spray tip penetration

With the spray segmented, the macroscopic variables were extracted for each of the test points measured. This section presents the spray penetration for both liquid and vapor phase measured in the spray box.

5.4.1 Liquid phase penetration for multiple injection strategies

The effects that traditional boundary conditions have on the spray evaporation of single injection pulses are well-known [19–27], and therefore are not presented in this document. Firstly, liquid length decreases with increasing chamber temperature, as the hotter gases provide more energy reducing the distance required for the fuel to fully vaporize. Secondly, liquid length decreases with increasing density, as more gas is entrained due to a wider spreading angle, and more energy for vaporization is available. Lastly, rail pressure has no apparent role in the liquid length, as the jet velocity increases at higher injection pressures, the higher rate of air entrainment supplies enough energy to maintain the evaporation distance constant.

Examples of the liquid phase penetration results for different dwell times and both pilot quantities are presented in Figures 5.7 and 5.8. Symbols depict

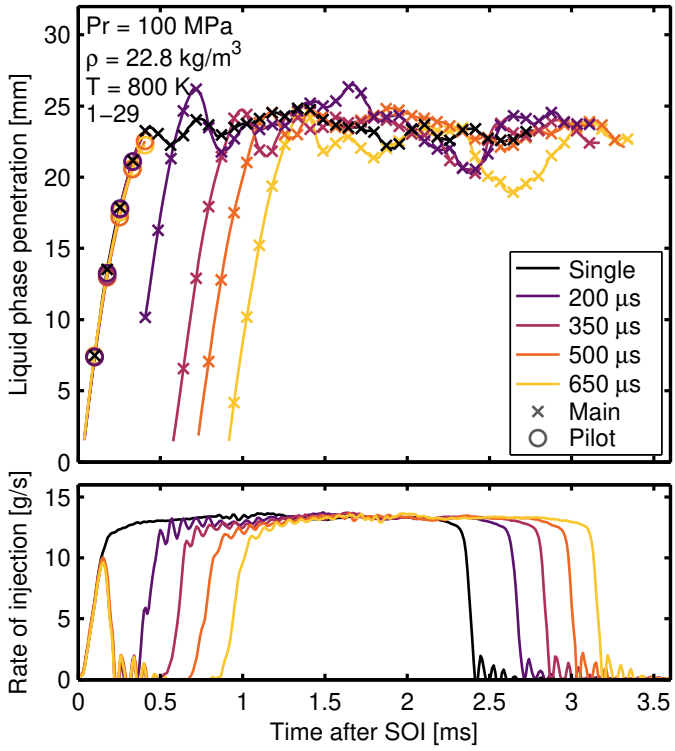

Figure 5.7: Liquid phase penetration for a pilot injected quantity of 1 mg. Symbols depict the spray segmentation of the pilot and main injections.

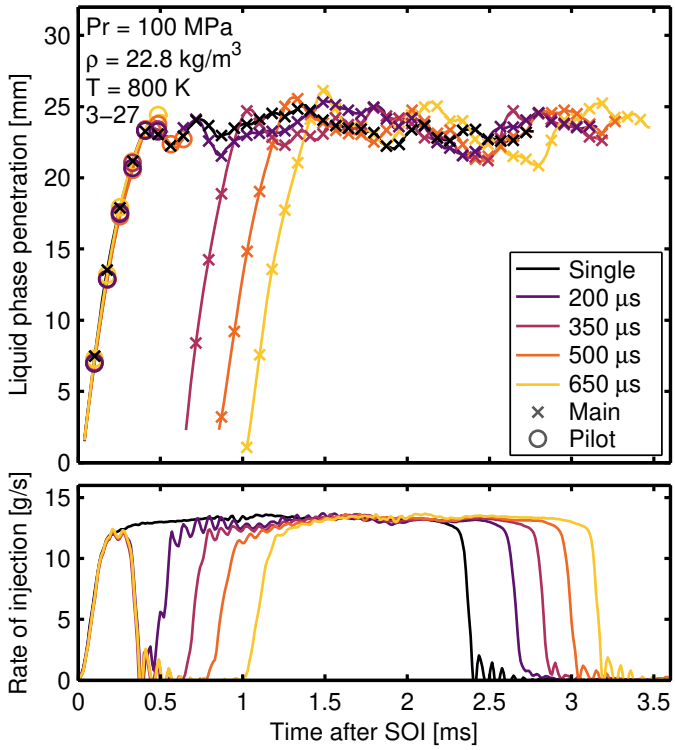

Figure 5.8: Liquid phase penetration for a pilot injected quantity of 3 mg. Symbols depict the spray segmentation of the pilot and main injections. The main event was manually decoupled for a dwell time of 200 µs for visualization purposes.

each of the injection pulses. Nevertheless, when injections were not hydraulically separated in multiple injection cases, pulses were manually decoupled for visualization purposes, using the start of injection of the second event from the rate of injection data.

From the figures, neither the pilot quantity nor its hydraulic separation affected the liquid vaporization length of the main pulse, corresponding to results found in the literature [28, 29]. This trend is somewhat expected in these types of experimental vessels, where the chamber volume is quite large. Therefore, air entrained by the spray provides more or less the same energy (temperature) to the fuel. In test cells with smaller volumes that resemble engine geometries, the liquid length of a second pulse might increase. This strongly depends on the re-entrainment of the vapor structures at the edge of the jet [30, 31], left over by the previous injection. Both pilot masses reach the

same vaporization length than the main injection, but only with 3 mg liquid phase penetration briefly achieved stabilized values. In general, the start of injection values extrapolated from the main injection correlated remarkably well with those from the rate of injection measurements (further analysis is presented in subsection 5.4.2).

Results were summarized by calculating the average value in the stabilized region of the main injection, known as liquid length and presented in Figure 5.9. The x-axis displays the real chamber temperature, not the nominal value, calculated as the average value during the measurement of all the repetitions. No differentiation for rail pressure was done for the plot because it is known it does not affect liquid length. As stated before, both the quantity and dwell time of the pilot injection showed no impact in the stationary vaporization length of the main pulse, at least considering the precision of this experimental diagnostics, as results are grouped mainly by chamber conditions.

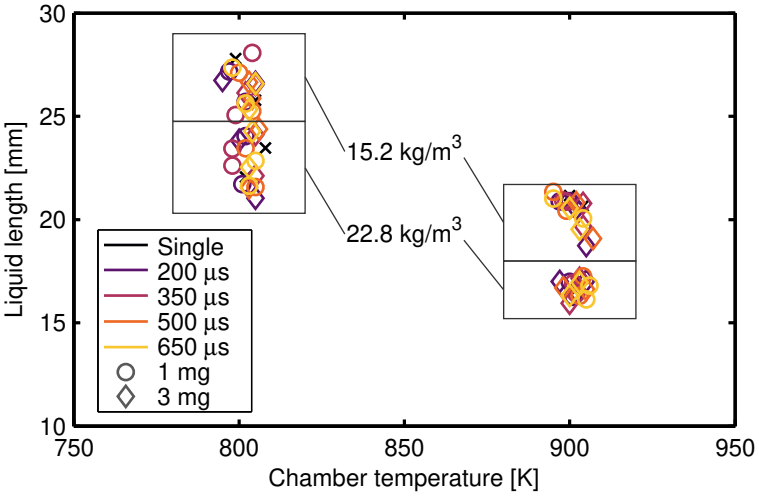

Figure 5.9: Time-averaged liquid length of the main injection for all conditions tested. Single injections are depicted with a cross symbol. Rectangles group conditions with the same chamber density.

An example of the liquid phase penetration results for different dwell times and both post injected quantities is condensed in Figure 5.10. Symbols depict the different injections pulses, and dashed lines represent post mass of 3 mg. Strategies with dwell times of 200 and 350 µs could not be decoupled, as only one more extended injection event was visible. In general, as before, no

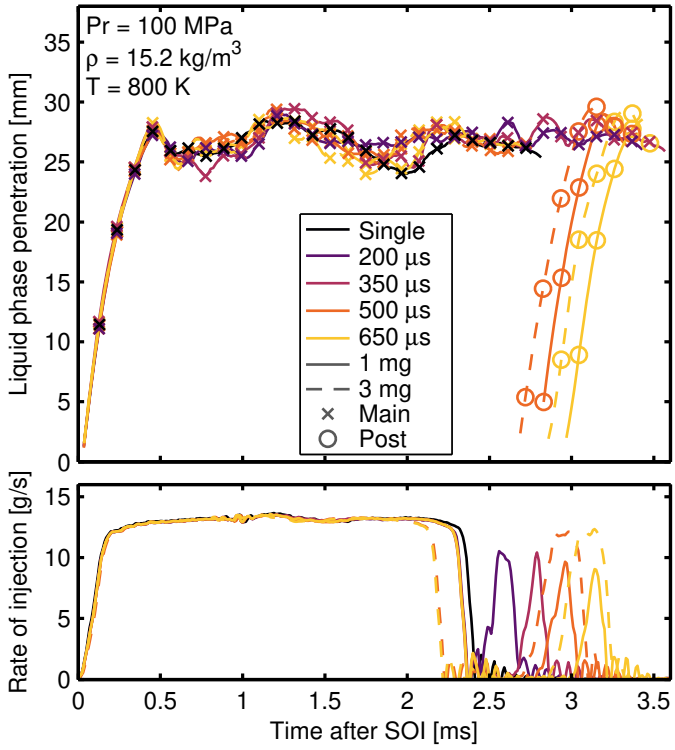

Figure 5.10: Liquid phase penetration for both post injected quantities. Symbols depict the spray segmentation of the main and post injections, and the dashed lines represent the post mass of 3 mg. Strategies with hydraulic dwell times of 200 and 350 µs could not be decoupled.

influence was observed from the main on the post injection liquid vaporization length. Additionally, the start of injection of the second pulse resembles results from the rate of injection measurements reasonably well.

Overall, it was observed that the secondary injection depicted a higher penetration rate than the prior pulse (further analysis is presented in subsection 5.4.2).

5.4.2 Vapor phase penetration for multiple injection strategies

As before, the effects that traditional boundary conditions have on the spray development of single injection pulses are well-documented [22, 24, 26, 27, 32–37], and therefore are not presented in this document. Firstly, vapor spray penetration increases with increasing injection pressure, as an initial higher

kinetic energy is provided to the spray in terms of velocity, as observed from momentum flux measurements. Secondly, spray penetration decreases with increasing chamber density, as the aerodynamic interactions between liquid and gas widen the spray and it loses momentum more rapidly. Lastly, chamber temperature has no apparent role in spray penetration, as is mainly governed by momentum flux and aerodynamic losses.

Examples of the results for different dwell times and both pilots injected quantities are presented in Figures 5.11 and 5.12, and were optically limited by the field of view that was 50 mm. Symbols depict the different injection pulses. As in the previous sections, the SOI of the main injection correlated remarkably well with ROI measurements. Increasing the pilot quantity shifted the transition zone, in which the main injection caught up, downstream of the spray development. The higher momentum flux of the 3 mg pilot enabled it to penetrate farther into the chamber, thus when the main injection started

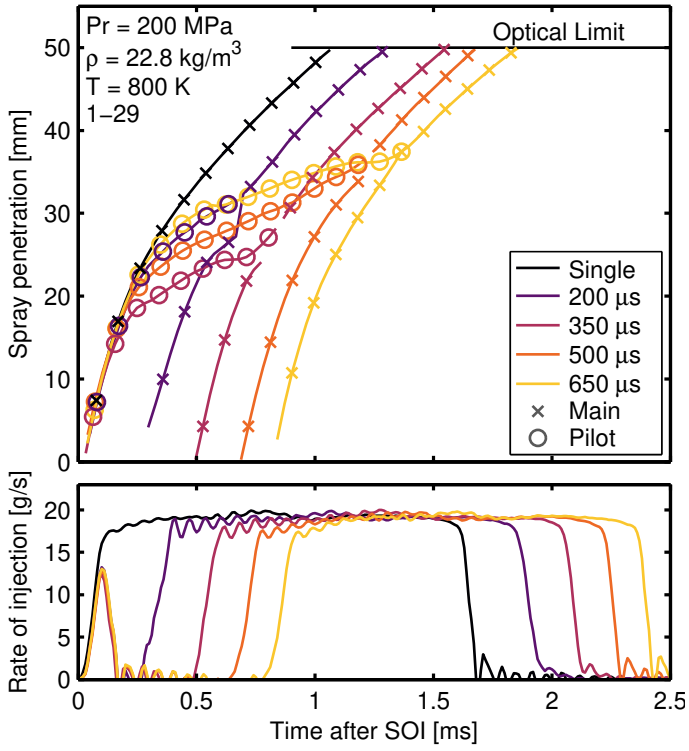

Figure 5.11: Spray penetration for a pilot injected quantity of 1 mg. Symbols depict the spray segmentation of the pilot and main injections.

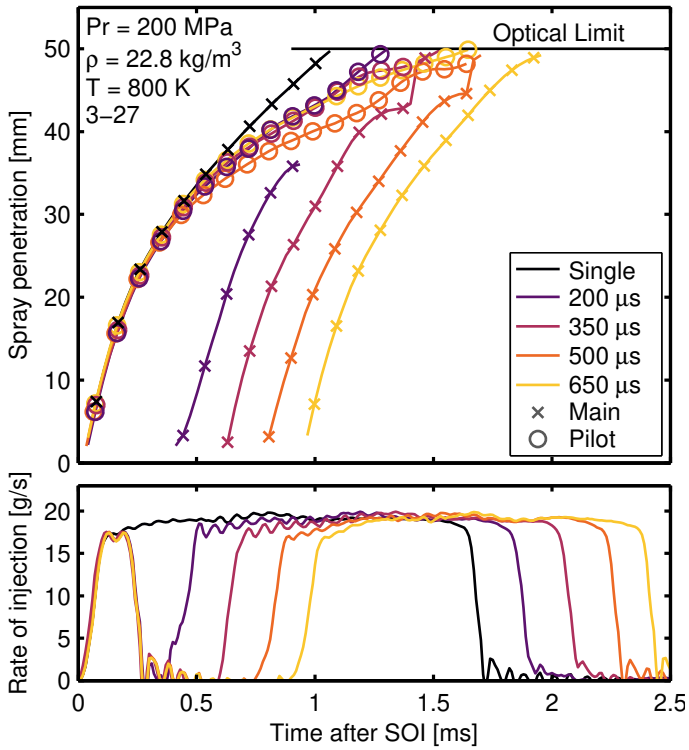

Figure 5.12: Spray penetration for a pilot injected quantity of 3 mg. Symbols depict the spray segmentation of the pilot and main injections.

it was already beyond the optical limit. The spray penetration of the main pulse was somewhat affected by the dwell time. As the pilot injection initially accelerates the stationary gas in the combustion chamber [28, 29, 38–41], the second pulse loses less momentum enabling it to penetrate faster than the reference case, increasing as well the mixing rate at the head of the spray [38]. Wang [40] called this phenomenon induced air driving force, concluding that a shorter dwell time contributes to a stronger induced driving force. Contrarily, a more extended dwell leads to a weaker driving force, as time is provided for the gas to decelerate. In addition, another driving factor that could be added up to this effect was already discussed in the previous chapter, as pressure waves within the injector sac and control volume can accelerate needle lift [8, 10], and they are dependent on the dwell time [10]. However, sac pressure is the driving condition in the early stages of spray [42–44]. Consequently, a higher penetration rate early in the spray development is probably caused by the faster needle lift, as shown in the test condition of 200 µs in Figure 5.7, and

in Figure 4.4 of the previous chapter. But, the effects of higher momentum flux are probably noticeable later in the spray development.

To isolate the effect of the dwell time on the acceleration of the spray development, Figure 5.13 presents the penetration of the main pulse shifted to the same origin as the reference single injection strategy, with the pilot pulses removed for visualization purposes. Only test points with 3 mg presented a somewhat more evident trend, probably due to the difficulty of quantifying such a sensitive variable with the shot-to-shot dispersion of the 1 mg quantity. The figure depicts the trend mentioned before, as the rate of penetration of the main pulse increases with a pilot injection and decreasing dwell time, due to a higher air driving force.

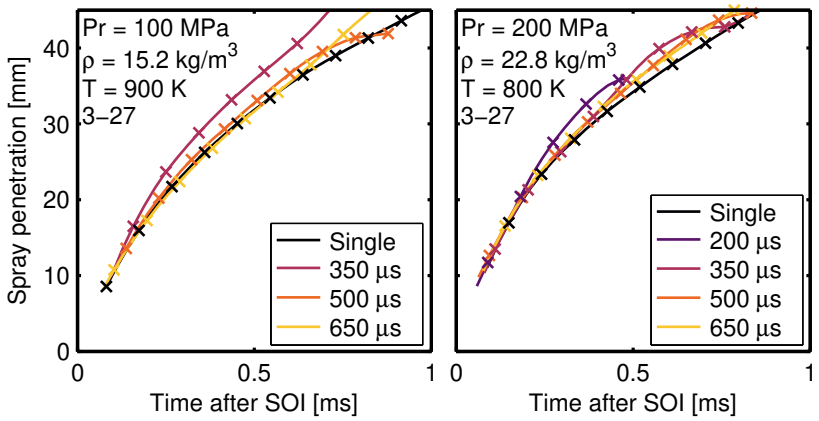

Figure 5.13: Differences of the rate of spray penetration of the main pulse compared to the single injection strategy for different dwell times. The curves were shifted to the same time origin for visualization purposes.

An example of the spray penetration results for different dwell times and both post injected quantities is condensed in Figure 5.14. Symbols depict the different injections pulses, and dashed lines represent post mass of 3 mg. Test points with dwell times of 200 and 350 µs could not be decoupled, as only one more extended injection event was visible. In this strategy, the transition zone was out of the optical limit. As a result, no difference was observed regarding the injected masses. Nevertheless, for the two dwell times of the post injection properly decoupled, the same trend as with the pilot strategy can be depicted, with an increasing spray penetration rate with decreasing dwell time.

The start of injection of the optical measurements was calculated following the methodology presented in section 3.7. Extrapolated values were compared to those from the rate of injection measurements, with results shown in

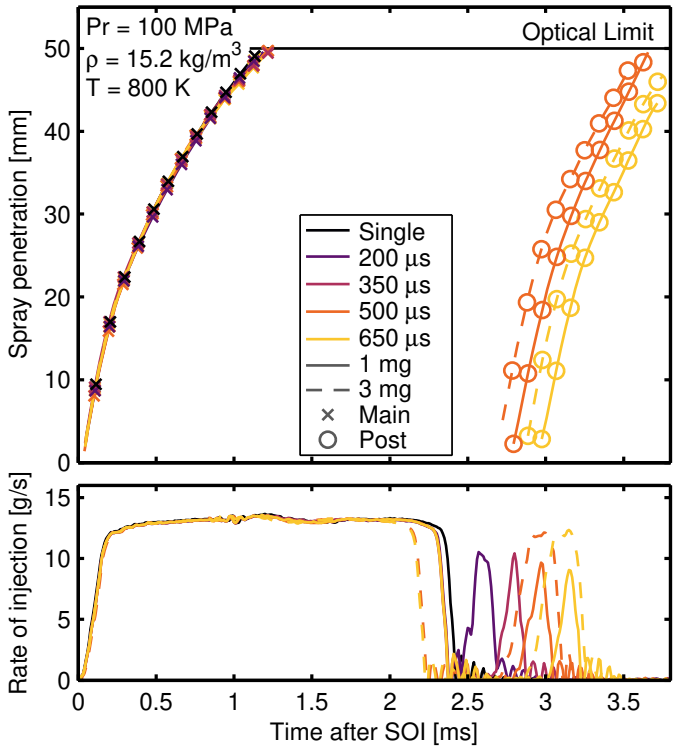

Figure 5.14: Spray penetration for both post injected quantities. Symbols depict the spray segmentation of the main and post injections, and the dashed lines represent the post mass of 3 mg. Strategies with hydraulic dwell times of 200 and 350 µs could not be decoupled.

Figure 5.15. Symbols depict different mass distributions, with filled and non-filled markers respectively representing pilot and post strategies. In the figure, symbols do not differentiate rail pressure, chamber density, and temperature. Therefore, the start of injection from the optical diagnostic is compared to the closest chamber pressure condition found in the rate of injection test plan. The solid line going from edge to edge represents $y = x$, with both dashed lines defining a 5% (dark gray) and 10% (light gray) deviation.

Values of the start of injection from the first injection event (around $0.33ms$) agree remarkably well, as noted in the results previously shown throughout this section. For the second event (the main injection after a pilot, or the post injection after a main) results still concur notably well, generally within a 10% deviation with some outliers. Considering that these deviations can be attributed to the aforementioned shot-to-shot differences

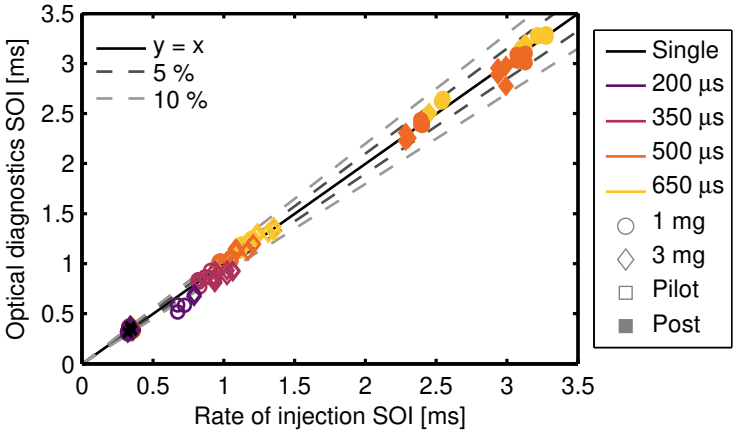

Figure 5.15: Comparison of the start of injection calculated from rate of injection measurements (x-axis) and extrapolated from the optical diagnostics (y-axis). The solid line represents $y = x$, and the dashed lines define a 5% and 10% deviation.

(Figures 4.7 and 4.8) and errors associated with extrapolation process to calculate the start of injection, this is a remarkable result. Moreover, it helps to validate the methodology followed throughout the different experimental vessels. In addition, problems with the performance of the injector for the shorter dwell times can be associated with the transients related to the needle closing process, which points to the presence of external fuel deposits.

5.5 Spray spreading angle

The effects that traditional boundary conditions have on the spray spreading angle are well described in the literature [19, 20, 22, 25, 27, 33, 34, 37, 45, 46], and therefore are not presented in this document. Spreading angle increases with increasing chamber density. No apparent effect from neither rail pressure nor chamber temperature can be noted as it is a complex variable that depends on multiple parameters such as nozzle geometry, cavitation, and fuel properties, among others. This section depicts the results of the spray angle calculated with the definition presented in section 3.7.

5.5.1 Liquid phase spreading angle for pilot-main strategies

The transient liquid phase spreading angle of the main injection was averaged during the stationary stage of the injection, and each test point was compared

to the reference point, to analyze the effect of a pilot pulse. Consequently, results depict the variation in terms of degrees between the conditions with a pilot pulse compared to the single injection case. Values were grouped by rail pressure and are correspondingly presented in Figures 5.16 and 5.17.

From the figures, no trend was observed regarding the influence of the pilot injection in the spreading angle of the main pulse for both rail pressures tested. Interestingly, even though the rate of penetration was higher with decreasing dwell time in the early spray development, liquid phase spreading angle remains more or less constant, as well as the vaporization length. Therefore, this confirms that the rate of air entertainment is directly linked to the spray velocity and that the pilot pulse does not affect the liquid distribution of the main injection within the conditions tested.

5.5.2 Vapor phase spreading angle for pilot-main strategies

The same procedure as in the previous section was carried out to analyze the effect of a pilot pulse on the vapor spray spreading angle of the main injection. Values were grouped by rail pressure and are presented correspondingly in Figures 5.18 and 5.19.

Calculations of the overall spray spreading angle measured through the vapor phase visualization can be significantly affected by the optical sensitivity and the image processing routines [35, 37, 47]. Moreover, even though

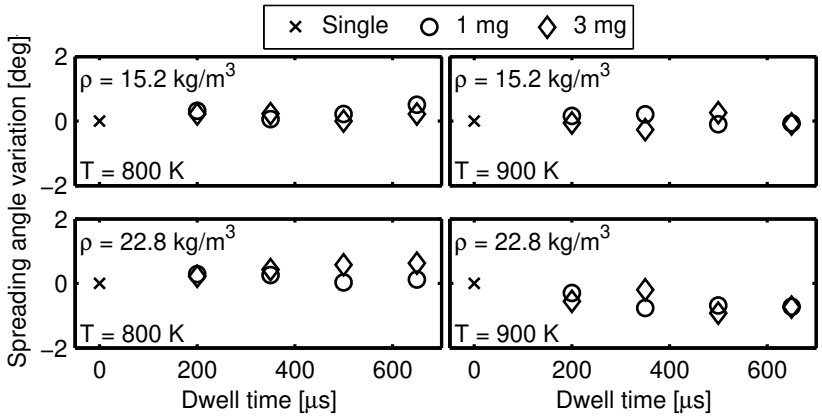

Figure 5.16: Effect of a pilot pulse on the liquid phase spreading angle of the main injection in terms of variation in degrees compared to the single injection case. Symbols depict different pilot quantities and the reference condition. All values depicted are for a rail pressure of 100 MPa.

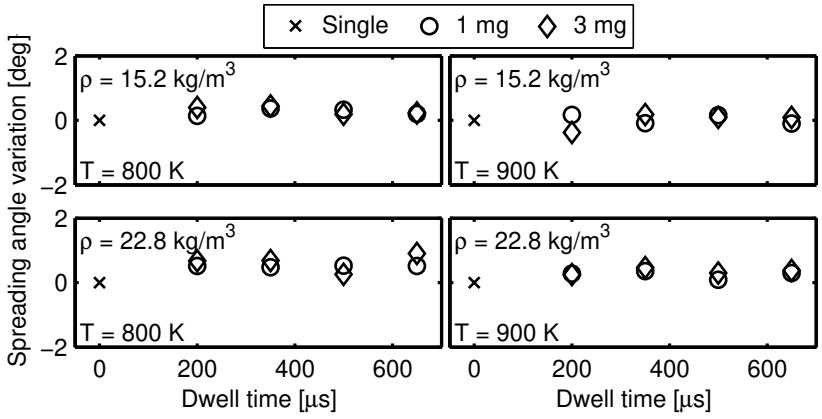

Figure 5.17: Effect of a pilot pulse on the liquid phase spreading angle of the main injection in terms of variation in degrees compared to the single injection case. Symbols depict different pilot quantities and the reference condition. All values depicted are for a rail pressure of 200 MPa.

the spray tip was adequately segmented for the second pulse in the multiple injection cases, the sides of the sprays were difficult to differentiate and properly decouple. Nevertheless, from the figures, a general trend is observed as the spray spreading angle increases with a pilot pulse before the main. The

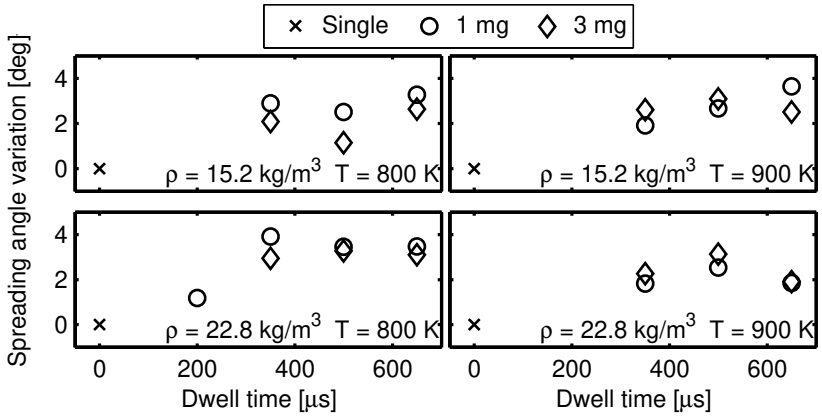

Figure 5.18: Effect of a pilot pulse on the spray spreading angle of the main injection in terms of variation in degrees compared to the single injection case. Symbols depict different pilot quantities and the reference condition. All conditions depicted are for a rail pressure of 100 MPa.

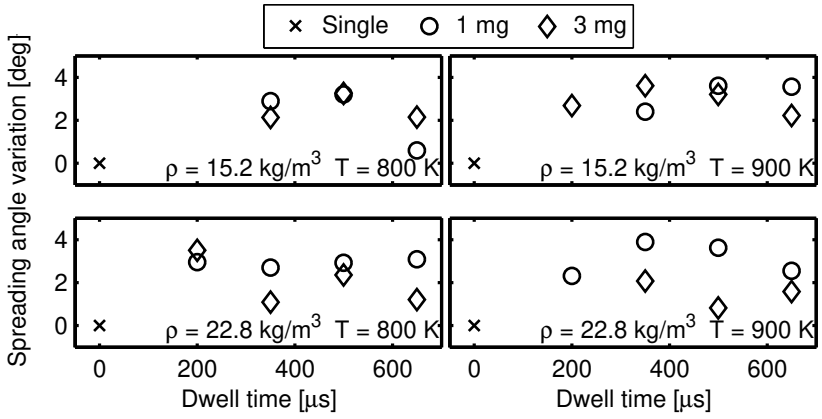

Figure 5.19: Effect of a pilot pulse on the spray spreading angle of the main injection in terms of variation in degrees compared to the single injection case. Symbols depict different pilot quantities and the reference condition. All conditions depicted are for a rail pressure of 200 MPa.

second injection event is introduced into a somewhat stationary medium with a higher density and turbulence, induced by fuel of the first injection, and a higher angle is somewhat expected [48, 49]. However, it is interesting to qualitatively observe that the main injection presents a higher rate of penetration even with a higher spreading angle. Nonetheless, the dependency on either the pilot quantity or dwell time is unclear and might be due to the uncertainties of the angle calculation in vapor contours.

5.6 Summary and conclusions

This chapter collects all the results describing the spray development for multiple injection strategies in non-reactive conditions. Measurements were carried out in an optically-accessible constant pressure and flow vessel, with a diffused back-illumination and a single-pass schlieren to visualize the liquid and vapor phase of the spray, respectively. The field of view allowed for an optical limit of 50 mm. A novel image processing methodology was developed to decouple sprays from multiple injection strategies in the schlieren movies, where the two pulses can coexist in the same frame. In general terms, the difference in performance of the injector affected the correlation between results from the hydraulic characterization and the spray development through optical diagnostics, especially in terms of injected mass and the real dwell time between

multiple injections. Nonetheless, data presented are still valid for qualitative analysis.

From the image processing results:

- Regarding the schlieren images, increasing the pilot quantity introduced more disturbances in the test chamber. Nevertheless, it did not affect the spray segmentation of the second pulse, because the transition zone, where pulses overlapped, was pushed downstream from the nozzle. Consequently, the first pulse was already more diluted, which provided enough contrast in the frames to decouple both contours.

- Dwell time is a critical variable that affects spray segmentation in the optical diagnostics of multiple injection strategies. The closer the injections are, the higher the difficulty is to decouple each event, as the density gradient between pulses is much lower. As a consequence, finer tuning was needed to get acceptable results, but boundaries were remarkably well delimited.

- In general, contour segmentation of the second pulse was a time-consuming task, as the dynamic range between injections is much lower than that between the spray and the background. Nevertheless, with proper tuning, multiple injections of two or more pulses can be properly segmented, and independently analyze, in contrast to only one global spray. The processing methodology was also successfully tested with schlieren images of multiple injections up to 5 pulses.

From the spray development results:

- Neither the pilot mass quantity nor its hydraulic separation affected the liquid vaporization length of the main pulse, which was still mostly governed by chamber density and temperature.

- All the pilot/post injections reached the same vaporization length as the main pulse.

- Overall, increasing the injected mass of the first pulse pushed the transition zone in which the injections overlapped past the optical limit.

- The first pulse accelerated the stationary gas in the combustion chamber, and as a consequence, the second event lost less momentum and penetrated faster than the reference single injection case. This, combined

with the higher start of injection velocity due to internal pressure waves observed in the last chapter, results in a higher rate of penetration with decreasing dwell time. Pilot/post injections with higher mass depicted more evident trends, as they present less shot-to-shot variability.

- The start of injection extrapolated from the optical diagnostics correlated remarkably well with those calculated from the rate of injection measurements. In general, values attained are within 10 % deviation, that can be attributed to shot-to-shot dispersion and the error associated with the extrapolation and camera acquisition speed. The great agreement helps to validate the methodology carried out through the different experimental vessels.

- Pilot injections did not affect liquid phase spreading angle. Contrarily, vapor phase measurements with a pilot pulse showed an increase in the spreading angle compared to the reference case, probably caused by a higher localized density or turbulence from the previous injection. The effect of either the pilot quantity or dwell time was unclear, probably due to the uncertainties of the angle calculation in vapor contours.

References

[1] Engine Combustion Network. *https://ecn.sandia.gov/diesel-spray-combustion/*. Online. 2010.

[2] Sechenyh, V. et al. "Quantification of diesel injector dribble using 3D reconstruction from x-ray and DBI imaging". In: *ILASS Europe 28th Conference on Liquid Atomization and Spray Systems*. Valencia, 2017, pp. 232–239. DOI: 10.4995/ILASS2017.2017.4742.

[3] Kastengren, A. L. et al. "End-of-Injection Behavior of Diesel Sprays Measured With X-Ray Radiography". In: *Journal of Engineering for Gas Turbines and Power* 134.9 (2012). DOI: 10.1115/1.4006981.

[4] Swantek, A. B. et al. "End of Injection, Mass Expulsion Behaviors in Single Hole Diesel Fuel Injectors". In: *ILASS Americas 26th Annual Conference on Liquid Atomization and Spray Systems*. Portland, 2014.

[5] Swantek, A. B. et al. "A further examination of fuel dribble from single hole diesel nozzles". In: *ILASS Europe 26th Annual Conference on Liquid Atomization and Spray Systems*. Bremen, 2014.

[6] Moon, S., Huang, W., Li, Z., and Wang, J. "End-of-injection fuel dribble of multi-hole diesel injector: Comprehensive investigation of phenomenon and discussion on control strategy". In: *Applied Energy* 179 (2016), pp. 7–16. DOI: 10.1016/j.apenergy.2016.06.116.

[7] Stetsyuk, V., Turner, J., Crua, C., Pearson, R., and Gold, M. "Droplet size and morphology characterization for diesel sprays under atmospheric operating conditions". In: *ICLASS 13th International Conference on Liquid Atomization and Spray Systems*. Tainan, 2015.

[8] Manin, J., Pickett, L. M., and Yasutomi, K. "Transient cavitation in transparent diesel injectors". In: *ICLASS 14th Triennial International Conference on Liquid Atomization and Spray Systems*. Chicago, 2018, pp. 1–9.

[9] Kook, S., Pickett, L. M., and Musculus, M. P. B. "Influence of Diesel Injection Parameters on End-of-Injection Liquid Length Recession". In: *SAE International Journal of Engines* 2.1 (2009), pp. 2009–01–1356. DOI: 10.4271/2009-01-1356.

[10] Carreres, M. "Thermal effects influence on the Diesel injector performance through a combined 1D modelling and experimental approach". PhD thesis. Universitat Politècnica de València, 2016. DOI: 10.4995/Thesis/10251/73066.

[11] Ullmann, J., Geduldig, M., Stutzenberger, H., Caprotti, R., and Balfour, G. "Investigation into the Formation and Prevention of Internal Diesel Injector Deposits". In: *SAE Technical Paper 2008-01-0926* (2008). DOI: 10.4271/2008-01-0926.

[12] Lacey, P. et al. "Fuel Quality and Diesel Injector Deposits". In: *SAE International Journal of Fuels and Lubricants* 5.3 (2012), pp. 2012–01–1693. DOI: 10.4271/2012-01-1693.

[13] Leedham, A., Caprotti, R., Graupner, O., and Klaua, T. "Impact of Fuel Additives on Diesel Injector Deposits". In: *SAE Technical Paper 2004-01-2935* (2004). DOI: 10.4271/2004-01-2935.

[14] Caprotti, R., Breakspear, A., Graupner, O., and Klaua, T. "Detergency Requirements of Future Diesel Injection Systems". In: *SAE Technical Paper 2005-01-3901* (2005). DOI: 10.4271/2005-01-3901.

[15] Birgel, A. et al. "Deposit Formation in the Holes of Diesel Injector Nozzles: A Critical Review". In: *SAE Technical Paper 2008-01-2383* (2008). DOI: 10.4271/2008-01-2383.

[16] D'Ambrosio, S. and Ferrari, A. "Diesel Injector Coking: Optical-Chemical Analysis of Deposits and Influence on Injected Flow-Rate, Fuel Spray and Engine Performance". In: *Journal of Engineering for Gas Turbines and Power* 134.6 (2012). DOI: 10.1115/1.4005991.

[17] Argueyrolles, B. et al. "Influence of injector nozzle design and cavitation on coking phenomenon". In: *SAE Technical Paper 2007-01-1896* (2007). DOI: 10.4271/2007-01-1896.

[18] Caprotti, R., Breakspear, A., Graupner, O., Klaua, T., and Kohnen, O. "Diesel injector deposits potential in future fueling systems". In: *SAE Technical Paper 2006-01-3359* (2006). DOI: 10.4271/2006-01-3359.

[19] Siebers, D. L. "Liquid-Phase Fuel Penetration in Diesel Sprays". In: *SAE Technical Paper 980809* (1998). DOI: 10.4271/980809.

[20] Siebers, D. L. "Scaling liquid-phase fuel penetration in diesel sprays based on mixing-limited vaporization". In: *SAE Technical Paper 1999-01-0528* (1999). DOI: 10.4271/1999-01-0528.

[21] Higgins, B. S., Mueller, C. J., and Siebers, D. L. "Measurements of Fuel Effects on Liquid-Phase Penetration in DI Sprays". In: *SAE Technical Paper 1999-01-0519* (1999). DOI: 10.4271/1999-01-0519.

[22] García-Oliver, J. M. "Aportaciones al estudio del proceso de combustión turbulenta de chorros en motores Diesel de inyección directa". PhD thesis. Valencia: Universitat Politècnica de València, 2004. DOI: 10.4995/Thesis/10251/55164.

[23] Manin, J., Bardi, M., and Pickett, L. M. "Evaluation of the liquid length via diffused back-illumination imaging in vaporizing diesel sprays". In: *The Proceedings of the International symposium on diagnostics and modeling of combustion in internal combustion engines*. Vol. 8. Fukuoka, 2012, pp. 665–673. DOI: 10.1299/jmsesdm.2012.8.665.

[24] Montanaro, A. et al. "Schlieren and Mie Scattering Visualization for Single- Hole Diesel Injector under Vaporizing Conditions with Numerical Validation". In: *SAE Technical Paper 2014-01-1406* (2014). DOI: 10.4271/2014-01-1406.

[25] Jung, Y., Manin, J., Skeen, S. A., and Pickett, L. M. "Measurement of Liquid and Vapor Penetration of Diesel Sprays with a Variation in Spreading Angle". In: *SAE Technical Paper 2015-01-0946* (2015). DOI: 10.4271/2015-01-0946.

[26] Maes, N. et al. “Experimental and Numerical Analyses of Liquid and Spray Penetration under Heavy-Duty Diesel Engine Conditions”. In: *SAE International Journal of Fuels and Lubricants* 9.1 (2016), pp. 108–124. DOI: 10.4271/2016-01-0861.

[27] Payri, R., Viera, J. P., Gopalakrishnan, V., and Szymkowicz, P. G. “The effect of nozzle geometry over the evaporative spray formation for three different fuels”. In: *Fuel* 188 (2017), pp. 645–660. DOI: 10.1016/j.fuel.2016.06.041.

[28] Karimi, K. “Characterisation of Multiple-Injection Diesel Sprays at Elevated Pressures and Temperatures”. PhD thesis. University of Brighton, 2007.

[29] Tonini, S., Gavaises, M., Theodorakakos, A., and Cossali, G. E. “Numerical investigation of a multiple injection strategy on the development of high-pressure diesel sprays”. In: *Proceedings of the Institution of Mechanical Engineers, Part D: Journal of Automobile Engineering* 224.1 (2010), pp. 125–141. DOI: 10.1243/09544070JAUTO1083.

[30] Pickett, L. M., Kook, S., and Williams, T. C. “Transient Liquid Penetration of Early-Injection Diesel Sprays”. In: *SAE International Journal of Engines* 2.1 (2009), pp. 2009–01–0839. DOI: 10.4271/2009-01-0839.

[31] Parrish, S. E., Zhang, G., and Zink, R. J. “Liquid and Vapor Envelopes of Sprays from a Multi-Hole Fuel Injector Operating under Closely-Spaced Double-Injection Conditions”. In: *SAE International Journal of Engines* 5.2 (2012), pp. 2012–01–0462. DOI: 10.4271/2012-01-0462.

[32] Su, T. F., Farrell, P. V., and Nagarajan, R. T. “Nozzle effect on high pressure Diesel Injection”. In: *SAE Technical Paper 950083* (1995). DOI: 10.4271/950083.

[33] Naber, J. D. and Siebers, D. L. “Effects of Gas Density and Vaporization on Penetration and Dispersion of Diesel Sprays”. In: *SAE Technical Paper 960034* (1996). DOI: 10.4271/960034.

[34] Frijters, P. J. M., Seykens, X. L. J., Somers, L. M. T., and Klein-Douwel, R. J. H. “Gas Density and Rail Pressure Effects on Diesel Spray Growth from a Heavy-Duty Common Rail Injector”. In: *Energy & Fuels* 23.2 (2009), pp. 1832–1842. DOI: 10.1021/ef8003569.

[35] Pickett, L. M. et al. "Relationship Between Diesel Fuel Spray Vapor Penetration/Dispersion and Local Fuel Mixture Fraction". In: *SAE International Journal of Engines* 4.1 (2011), pp. 2011–01–0686. DOI: 10.4271/2011-01-0686.

[36] Payri, R., Gimeno, J., Bracho, G., and Vaquerizo, D. "Study of liquid and vapor phase behavior on Diesel sprays for heavy duty engine nozzles". In: *Applied Thermal Engineering* 107 (2016), pp. 365–378. DOI: 10.1016/j.applthermaleng.2016.06.159.

[37] Payri, R., Salvador, F. J., Bracho, G., and Viera, A. "Differences between single and double-pass schlieren imaging on diesel vapor spray characteristics". In: *Applied Thermal Engineering* 125 (2017), pp. 220–231. DOI: 10.1016/j.applthermaleng.2017.06.140.

[38] Bruneaux, G. and Maligne, D. "Study of the Mixing and Combustion Processes of Consecutive Short Double Diesel Injections". In: *SAE International Journal of Engines* 2.1 (2009), pp. 2009–01–1352. DOI: 10.4271/2009-01-1352.

[39] Cung, K. et al. "Spray-combustion interaction mechanism of multiple-injection under diesel engine conditions". In: *Proceedings of the Combustion Institute* 35.3 (2015), pp. 3061–3068. DOI: 10.1016/j.proci.2014.07.054.

[40] Wang, Z. "Experimental study on diesel spray with single and multiple injection under room temperature and low temperature". PhD thesis. University of Birmingham, 2015.

[41] Skeen, S. A., Manin, J., and Pickett, L. M. "Visualization of Ignition Processes in High-Pressure Sprays with Multiple Injections of n-Dodecane". In: *SAE International Journal of Engines* 8.2 (2015), pp. 2015–01–0799. DOI: 10.4271/2015-01-0799.

[42] Pastor, J. V., López, J. J., García-Oliver, J. M., and Pastor, J. M. "A 1D model for the description of mixing-controlled inert diesel sprays". In: *Fuel* 87.13-14 (2008), pp. 2871–2885. DOI: 10.1016/j.fuel.2008.04.017.

[43] Manin, J., Bardi, M., Pickett, L. M., Dahms, R. N., and Oefelein, J. C. "Microscopic investigation of the atomization and mixing processes of diesel sprays injected into high pressure and temperature environments". In: *Fuel* 134 (2014), pp. 531–543. DOI: 10.1016/j.fuel.2014.05.060.

[44] Payri, R., Bracho, G., Martí-Aldaraví, P., and Viera, A. "Near field visualization of diesel spray for different nozzle inclination angles in non-vaporizing conditions". In: *Atomization and Sprays* 27.3 (2017), pp. 251–267. DOI: 10.1615/AtomizSpr.2017017949.

[45] Gimeno, J. "Desarrollo y aplicación de la medida del flujo de cantidad de movimiento de un chorro diesel". PhD thesis. Universitat Politècnica de València, 2008. DOI: 10.4995/Thesis/10251/8306.

[46] Pickett, L. M., Genzale, C. L., and Manin, J. "Uncertainty quantification for liquid penetration of evaporating sprays at diesel-like conditions". In: *Atomization and Sprays* 25.5 (2015), pp. 425–452. DOI: 10.1615/AtomizSpr.2015010618.

[47] Bardi, M. et al. "Engine Combustion Network: Comparison of Spray Development, Vaporization, and Combustion in Different Combustion Vessels". In: *Atomization and Sprays* 22.10 (2012), pp. 807–842. DOI: 10.1615/AtomizSpr.2013005837.

[48] Kastengren, A. L. et al. "Correlation of Split-Injection Needle Lift and Spray Structure". In: *SAE Technical Paper 2011-01-0383* (2011). DOI: 10.4271/2011-01-0383.

[49] Borz, M. J., Kim, Y., and O'Connor, J. "The Effects of Injection Timing and Duration on Jet Penetration and Mixing in Multiple-Injection Schedules". In: *SAE Technical Paper 2016-01-0856* (2016). DOI: 10.4271/2016-01-0856.

Chapter 6

Spray ignition and combustion

6.1 Introduction

In this chapter, the results of the second experimental campaign in the optically accessible high-temperature and pressure vessel are presented, carried out in a reactive atmosphere. First, the test plan is shown. Then, results are described in three parts: ignition delay, lift-off length, and soot production. Lastly, the chapter ends with a summary and conclusions.

6.2 Test plan

For the second experimental campaign in the optically accessible vessel, the same boundary conditions as in the previous chapter were selected, but with ambient air instead of pure nitrogen to promote combustion. These include two rail pressures, chamber densities, and temperatures, with the test plan presented in Table 6.1.

The proposed test matrix consists of 72 test points. For DBI and bandpass chemiluminescence, the number of repetitions per test point was increased to twenty to improve the statistical robustness of soot production measurements. The discharge pressure was set to achieve the target density for a given ambient temperature, considering standard air for the calculations. As before,

Table 6.1: Test plan for the reactive spray visualization campaign.

Parameter	**Value**	**Units**
Rail pressure (P_r)	100 - 200	MPa
Chamber density (ρ)	15.2 - 22.8	$\mathrm{kg\,m^{-3}}$
Chamber temperature (T)	800 - 900	K
Oxygen concentration	≈ 21	$\%_{\mathrm{vol}}$
Injector operating temperature	363	K
Pilot/post dwell times	200 - 350 - 500 - 650	µs
Pilot/post injected quantity	1 - 3	mg
Total mass per injection	30	mg
Injection frequency	1	Hz
Repetitions	10 - 20	-

the injection frequency was increased to 1 Hz to retain the same configuration throughout the different experimental campaigns. The reactive atmosphere was achieved using atmospheric air as running gas in the facility, thus the oxygen content was maintained through the measurements. The same high-pressure, injection control unit and driving signals as in the hydraulic characterization were used.

6.3 Ignition delay

The time it takes the fuel to mix, evaporate and reach high-temperature reactions is known in the literature as ignition delay. For single injections, ID is commonly characterized with broadband chemiluminescence [1–4], schlieren imaging [2–6], and high-speed OH chemiluminescence [7–10]. Commercial diesel fuel emits very high-intensity chemiluminescence due to soot, so lowering camera sensitivity to avoid pixel saturation can result in detecting the start of soot incandescence and not the real start of combustion [11]. Besides, no high-speed intensifier was available at the time of the measurement campaign. Consequently, schlieren imaging was thought to characterize ignition delay, as stated in chapter 3.

A schlieren optical setup allows visualizing density gradients that occur in the combustion chamber. Thus for a single injection event, tracing the contour evolution is reasonably straightforward. The second stage ignition is characterized by a premixed combustion with a high-rate of heat release and an increase in chamber pressure. From the optical point of view, this is

visualized as a sudden radial expansion that depends on mixing conditions leading towards the start of combustion [5]. For multiple injection strategies, the secondary injection can ignite in three different scenarios: with a dwell time long enough so is entirely decoupled of the first pulse, with the same ignition as the first pulse, or while the first pulse is still burning.

Nonetheless, the first pulse creates local conditions that could promote a faster start of combustion for the second injection. Thus in some cases, the premixed combustion phase is shortened [12], and the radial expansion is very small or non-existent. An example of the start of combustion for the second pulse in those conditions is presented in Figure 6.1.

This created problems in optically decoupling the start of combustion of the second pulse. Besides, once the chemiluminescence from soot production appeared in the frames, the intensity levels of these pixels resembled the background, creating problems as well in contour depiction. Thus, a different but novel methodology was implemented using movies gathered through DBI, and taking advantage of beam steering effects present due to combining DBI with a single-pass schlieren.

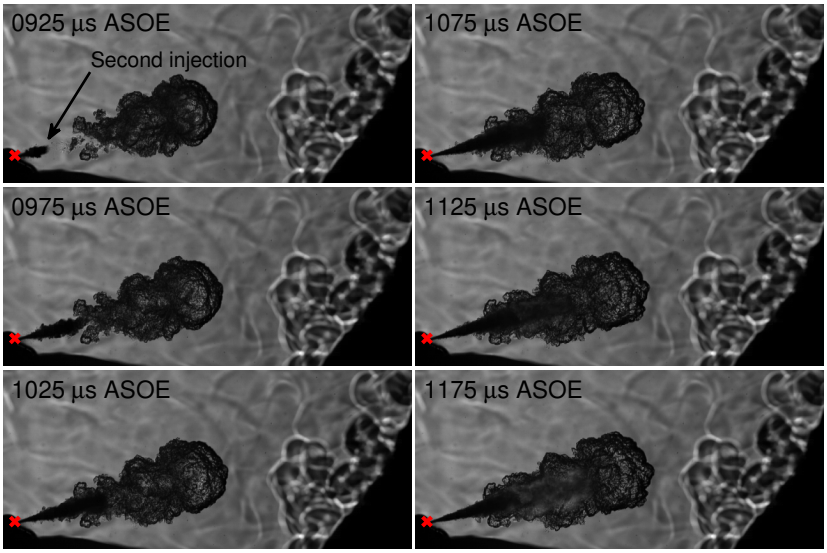

Figure 6.1: Example of the images gathered through schlieren for multiple injection conditions, starting near the SOI of the second pulse. The frames shown are for a 1-29 pilot-main event with a dwell time of 350 µs, a rail pressure of 100 MPa, a chamber density of 22.8 kg m^{-3} and temperature of 900 K.

6.3.1 Calculating the start of combustion for multiple injection events

Images gathered through DBI in reactive conditions presented two very distinctive characteristics. On the one hand, density gradients originated by the combustion caused small but noticeable beam steering that was visible as schlieren structures in the frames. On the other hand, soot production that was also distinguishable due to light extinction by the soot cloud. Therefore, if the combustion of the second pulse had a distinguishable premixed phase, the start of combustion was obtained by tracing the contour evolution as with schlieren. However, if no radial expansion was observed, the SOC was linked to the first traces of soot, as both occurred almost simultaneously.

Hence, DBI images were processed by calculating the total pixel-wise frame-to-frame difference in absolute terms. An example of the results shown in Figure 6.2. Each frame was masked with the steady state liquid length to

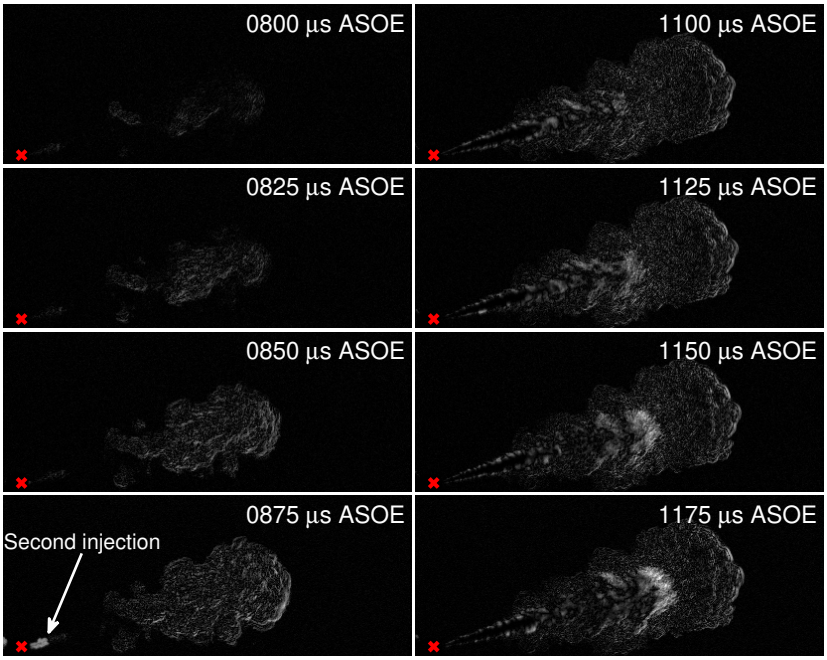

Figure 6.2: Example of absolute pixel-wise frame-to-frame differentiation for multiple injection conditions. The frames shown are for a 1-29 pilot-main event with a dwell time of 350 µs, a rail pressure of 100 MPa, a chamber density of 22.8 kg m^{-3} and temperature of 900 K.

exclude differences induced by the liquid phase penetration. The differentiation was calculated in absolute terms to associate the appearance of soot as a positive contributor to determine the start of combustion.

With the images processed, a similar approach as with schlieren for second stage ignition, presented in chapter 3, is performed. The start of combustion is correlated to the local maximum, after the start of injection, of the total frame-to-frame difference derivative calculated with a 3-point-stencil. An example of the trace obtained with each of the estimated SOC is presented in Figure 6.3, where the derivative (named rate of difference) is plotted for every cycle, with the SOI for each injection also included. In the figure, the SSI of the first injection is noticeable as it represents the maximum rate of difference (ROD), similar to the trace of the schlieren processing for ignition delay. In addition, it can be observed how shortening the dwell time reduces the duration and intensity of the premixed phase of the combustion of the second pulse, as its ROD is more subtle with a decreasing dwell, and comparable, for instance, to the ignition of the pilot injection. In general, this was observed in all the movies when the combustion of the second pulse was decoupled from the first.

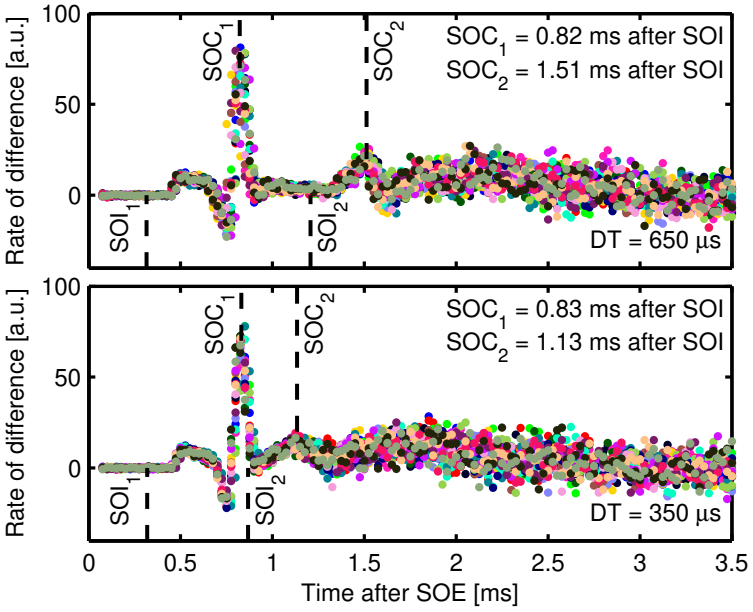

Figure 6.3: Example of the rate of difference represented by a different color for each cycle. Vertical dashed lines represent either SOI or SOC. Results are for a rail pressure of 100 MPa, a chamber density of 22.8 kg m^{-3} and temperature of 900 K.

The rate of difference processing was first validated comparing it with results of ignition delay calculated for the single injection cases from the schlieren movies, with the processing previously explained in chapter 3. A summary of the comparison between methodologies is presented in Figure 6.4. In such cases, the premixed phase of combustion created contour changes that were traced by both processing methodologies almost identically for all boundary conditions.

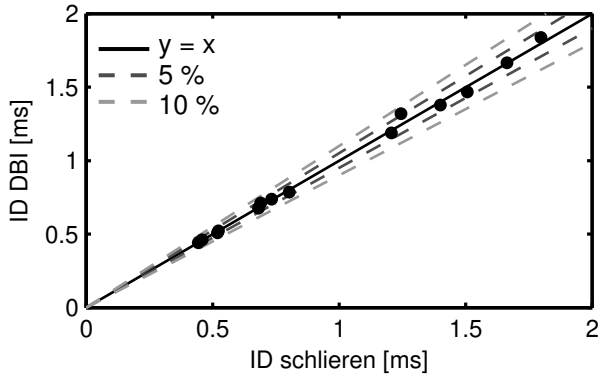

Figure 6.4: Correlation between ignition delays calculated with the traditional schlieren methodology and the rate of difference procedure from DBI movies for single injection cases and all boundary conditions tested.

Additional verification was performed with experimental data from a non-related measurement campaign. In this set of data, the rate of difference methodology was compared with the ignition delay calculated with images from high-speed OH chemiluminescence [7–10]. Both setups visualized the same injection event, for a total of twenty repetitions, using commercial diesel, with a rail pressure of 100 MPa, a chamber density of 19 $kg\,m^{-3}$ and temperature of 900 K. Even though the injected quantities were not measured, the strategy set resembled the pilot-main structure with an approximate dwell time of 350 µs, measured optically from the movies. Results are summarized in Table 6.2, and show that the ROD methodology can be used to accurately measure ignition delays of multiple injection strategies, although validation with more experimental data could further asses the robustness of the new method. The procedure was also tested and can also be applied to schlieren images with multiple injection strategies with acceptable results, but it was used with the DBI movies as a higher number of repetitions were recorded.

Table 6.2: Comparison of the start of combustion calculated with the rate of difference and with high-speed OH chemiluminescence.

Injection	ID ROD	ID OH chem.	Units
Pilot	0.71 ± 0.02	0.68 ± 0.02	ms after SOE
Main	1.24 ± 0.03	1.23 ± 0.08	ms after SOE

6.3.2 Ignition delay for multiple injection strategies

The effects that traditional boundary conditions have on the ignition delay of single injection pulses are well-known [3–6, 13–17], and therefore are not presented in this document. Ignition delay decreases with increasing chamber temperature, as it accelerates oxidation reactions. In addition, it also decreases with increasing chamber density and injection pressure, as both enhance the mixing and evaporation processes. The dependence on the variables is also presented in the Arrhenius function of Equation 2.1. Consequently, in all cases, conditions for ignition are reached in a shorter span.

Ignition delay results for a pilot-main strategy were divided by chamber temperature and are summarized in Figures 6.5 and 6.6. Different symbols and colors depict pilot quantity and the injection number, always compared to the single injection case. Note that the limits of the y-axis change depending on the conditions. The ID values are referenced to the start of injection of either the pilot or the main pulse, respectively organized by columns and stated in each plot. Additionally, each row corresponds to a specific boundary condition. Overall, errors associated with shot-to-shot deviation were under 10 %, decreasing to values under 5 % at higher chamber temperatures and densities.

The results at 800 K referenced to the pilot injection describes how its ignition delay was affected by the main pulse. For most conditions, both injections ignited simultaneously, as symbols overlap each other. In such cases, increasing the dwell time visibly lengthened the ignition delay of the pilot. Even though more time was provided for the first pulse to combust, it was caught up by the main injection in a state where it negatively influenced the ignition process [12], probably cooling down or modifying the local mixture [10, 18, 19]. Meanwhile, decreasing the dwell time changed the interaction between the two injections events and the ID trend to values similar to the single injection.

In the specific cases where the start of combustion of both injections decoupled, the ignition delay of the pilot resembled those to the single injection.

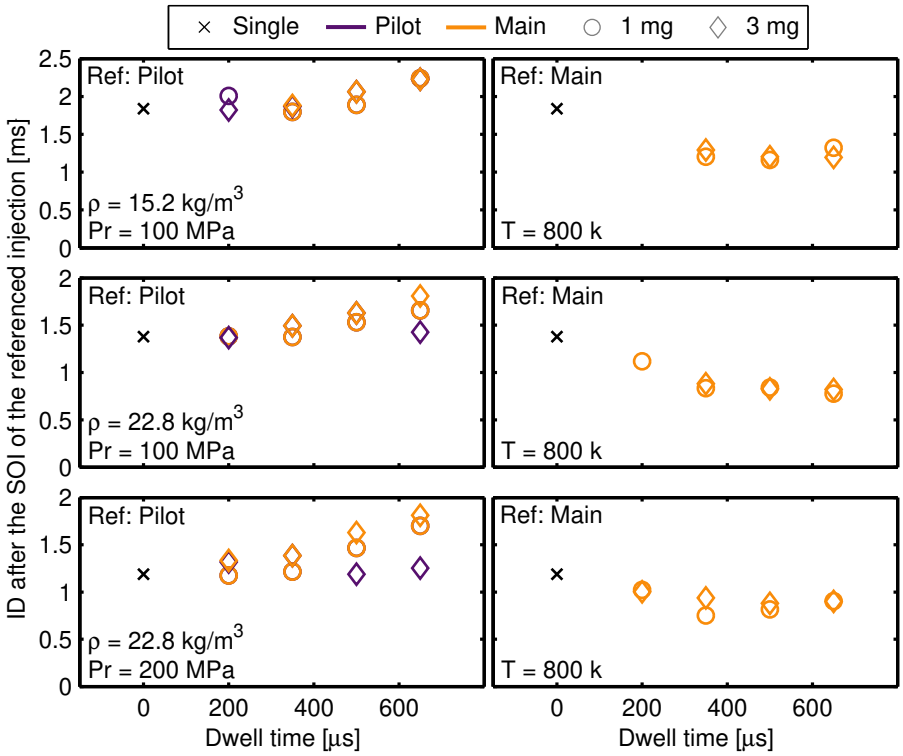

Figure 6.5: Ignition delay results for a pilot-main strategy and a chamber temperature of 800 K. Values are referenced to the start of injection of either the pilot (left column) or main (right column).

Both the dwell time and pilot quantity affected in different ways the main driving parameter: the ignition location. Increasing the pulse separation provided more time for the pilot injection to mix, evaporate and combust before being caught up by the main pulse, consequently moving the ignition location upstream. For example, for a rail pressure of 100 MPa and a chamber density of 22.8 kg m^{-3}, the decoupling of the combustion was observed only for the highest dwell time. Increasing the pilot quantity increased the momentum as noted in the results presented in chapter 4. As a result, the pilot injection ignition kernel penetrated further into the test chamber, away from the main pulse. For instance, for a rail pressure of 200 MPa and a chamber density of 22.8 kg m^{-3}, increasing the pilot quantity enabled the decoupling of the combustion of each injection pulse for dwell times of 500 and 650 µs.

The results at 800 K referenced to the main injection describes how its ignition delay was affected by the pilot. For all conditions, the first pulse

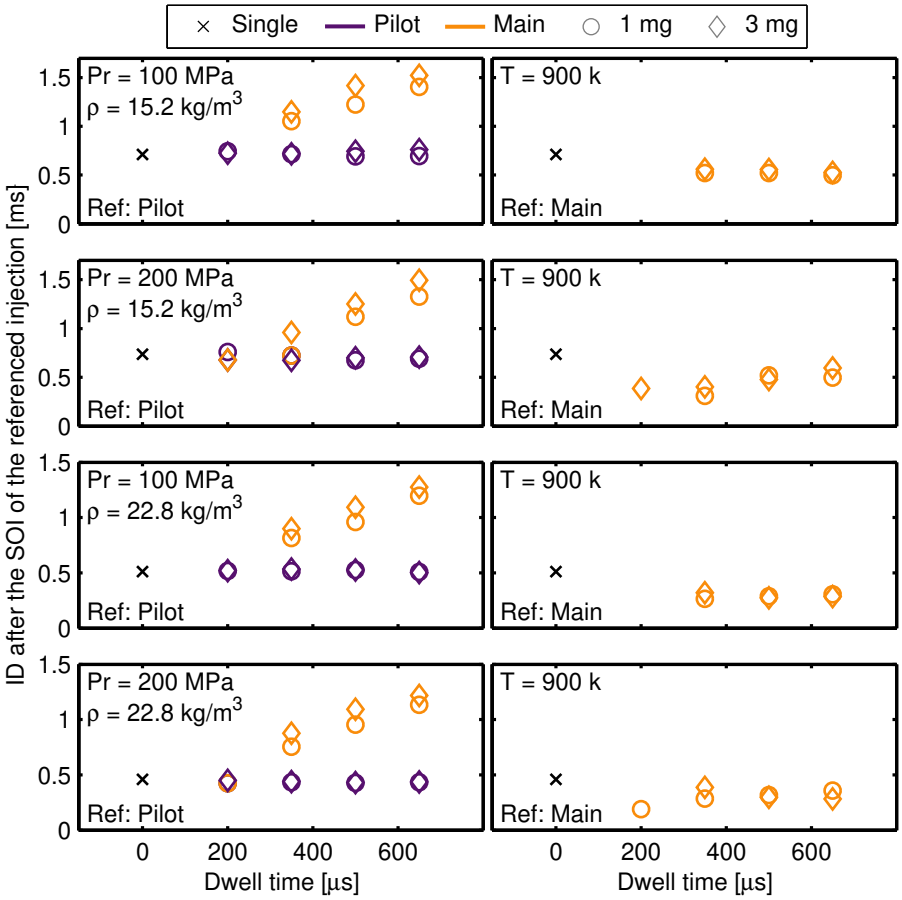

Figure 6.6: Ignition delay results for a pilot-main strategy and a chamber temperature of 900 K. Values are referenced to the start of injection of either the pilot (left column) or main (right column).

promoted a shorter ID of the main injection, either by improving conditions for ignition or by the re-entrainment of hot gases of the pilot combustion [9, 20–23], which speeds up the transition from the newly injected fuel into a reacting state. On average, the ignition delay of the main was shortened from around 30 % to 40 % compared to its reference case. Nevertheless, as the dwell time decreases, the influence seems to diminish, and a trend towards the ignition delay of the single injection is observed [23].

All results at 900 K showed a separate combustion event for each injection. Overall, results referenced to the pilot injection show that its ignition delay is

in accordance to the value obtained for the single injection case, with no effect noted from neither the its quantity nor the main pulse. As before, the results referenced to the main injection depict that its ignition delay is shortened with the inclusion of a pilot pulse. Once again, on average, the ignition delay of the main was shortened from around 30 % to 40 % compared to its reference case. Moreover, the ID of the main injection presented smaller values with decreasing dwell time, probably due to less time available for products of the first combustion to cool down.

Ignition delay results for a main-post strategy are summarized in Figure 6.7. Different symbols and colors depict pilot quantity and the injection

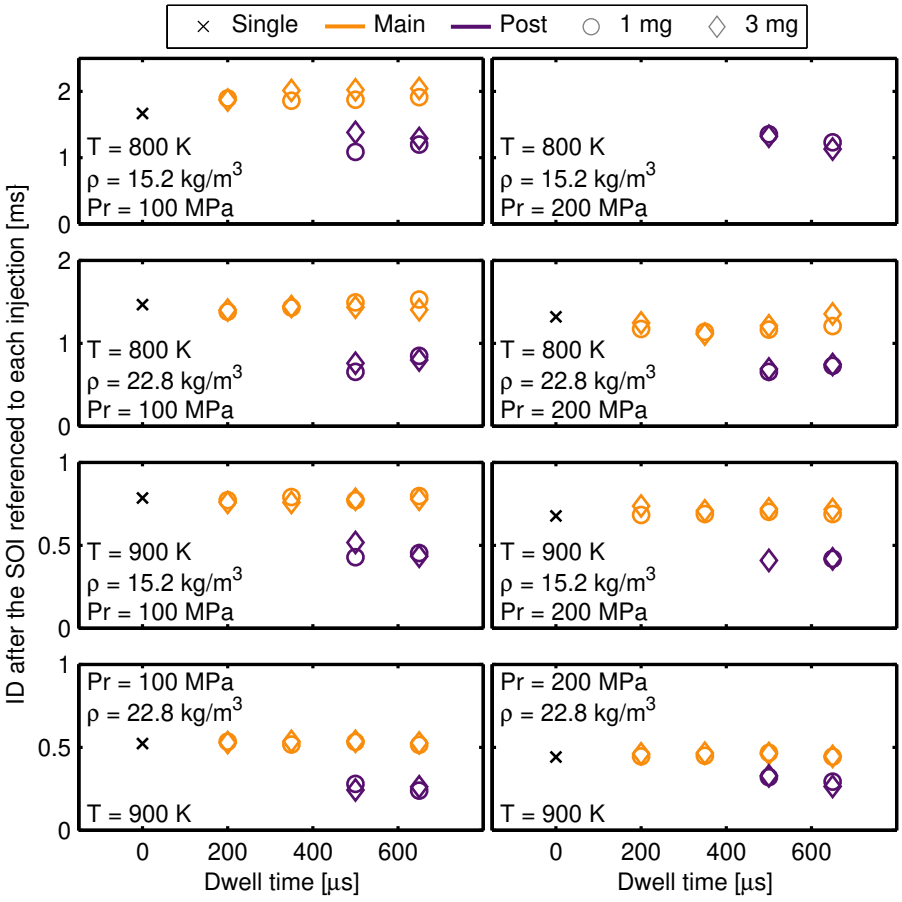

Figure 6.7: Ignition delay results for main-post strategies and all conditions tested. Values are referenced to the start of injection of each pulse.

number, always compared to the single injection case. Note that the limits of the y-axis change depending on the conditions, represented by each subplot. The ID values are referenced to its start of injection. In general, errors associated with shot-to-shot deviation were under 10 %, decreasing to values under 5 % at higher chamber temperatures and densities.

In such a strategy, the main pulse ignites with a delay similar to the single injection. Nonetheless, the second pulse is injected well after the first ignition event took place. Consequently, for the conditions depicted, the start of combustion is always decoupled compared to the previous cases. Overall, the ignition delay of the post injection was shortened by the main pulse, due to the increase in chamber temperature caused by the combustion and re-entrainment of the hot gases [20–23]. No effect is observed either from the post quantity or the dwell time, and probably the driving factor is the local temperature, modified by the main injection. Interestingly, the decrease in the ignition delay in such strategies is notably higher compared to pilot-main combustions, as a longer injection takes place first which increase the local temperature to higher levels, promoting a faster ignition of the second pulse. On average, the ignition delay of the post injection was shortened from around 40 % to 50 % compared to its reference case.

In the pilot-main strategy for a rail pressure of 200 MPa, a chamber density of 15.2 $\mathrm{kg\,m^{-3}}$ and temperature of 800 K, the SOC occurred outside the optical limit. Thus, the values of ignition delay were actually estimated when the combustion entered the field of view. In a main-post strategy, the main injection moves the ignition location of the second pulse closer to the nozzle due to a higher localized temperature, allowing for a proper calculation of its ignition delay.

Jorques Moreno et al. [24] defined in their work different interaction mechanisms to summarize the effects of a pilot injection on the main combustion. These were adapted to analyze the influence of the first pulse on the second event, where four different interactions mechanisms can be described:

- Mixing interaction mode: the second injection takes place during the mixing phase of the first pulse. It was observed only for pilot-main strategies mostly at the lowest chamber density and/or temperature, although also for some intermediate conditions where the pilot did not ignite before the main caught up. As a result, there is only one combustion event that couples both injections, that still presents a defined premixed and mixing controlled phase. The ignition delay of the pilot can be greater than that of a single injection, as the main pulse cools

down and influences the local mixture, with both the dwell time and pilot quantity affecting this interaction. However, the ignition delay of the main combustion is shortened, as is primarily driven by the ignition of the pilot.

- Premixed interaction mode: the second injection takes place during the premixed combustion of the first pulse. It was observed for most of the pilot-main strategies at the highest chamber density and/or temperature, as the pilot mass is not sufficient to reach a diffusive combustion, and also for combinations of either low chamber temperature and high density, or vice versa, with specific dwell times that synchronize both events. As a result, independent combustion events for each injection are visualized. The pilot ignites with the same delay as in a single injection, and the heat released accelerates the vaporization process of the main injection. Consequently, both the ignition delay and the duration of the premixed phase of the main combustion are shortened, because the localized higher temperatures accelerate the reaction rates [25], lengthening the diffusion flame. The extent of the trade-off between the premixed and diffusive combustions is dependent not only on the boundary conditions but on the dwell time and pilot quantity as well, as they determine the temperature of the local gases entrained by the main injection.

- Diffusive interaction mode: the second injection takes place during the diffusive combustion of the first pulse. It was observed for all conditions in main-post strategies due to the time allowed between the SOC of the main injection and the relatively short dwell time to the post-pulse. Additionally, it was also noted for some of the 3 mg pilots at higher chamber temperature and density and low rail pressure, as a diffusive combustion was established and identified with the production of soot (presented in section 6.5). The first pulse ignites with the same delay than the single injection. Equally to the previous interaction mode, the higher localized temperature of the pilot combustion could accelerate the vaporization process, promoting both a shorter ignition delay and a shorter premixed phase. Nevertheless, pilots of 3 mg penetrated further into the combustion chamber, thus reducing their early interaction with the main. Therefore, it is difficult to asses the driving parameter.

- Completed combustion interaction mode: the second injection takes place after the combustion of the first pulse is completed. For the conditions studied, the dwell time was not large enough to achieve this interaction method.

The transition between interaction modes can be controlled by both the injected quantity and the dwell time between pulses. For example in Figure 6.5, a 1-29 pilot-main event with a dwell time of 650 µs, a rail pressure of 100 MPa, and a chamber density of 22.8 $\mathrm{kg\,m^{-3}}$, occurred with a premixed interaction mode. Decreasing the dwell time shifted their interaction to a mixing mode, as the pilot did not have enough time to ignite before being caught up by the main pulse. Contrarily, increasing the pilot quantity by a sufficient amount, and with short dwell time, a diffusive interaction mode might be achieved.

6.4 Lift-off length

The effects that traditional boundary conditions have on the lift-off length of single injection pulses are well-known [3, 4, 6, 8, 15, 26–30], and therefore are not presented in this document. On the one hand, LOL decreases with increasing chamber temperature and density, as it reduces the amount of air required to burn the fuel injected. On the other hand, LOL increases with increasing rail pressure, as a higher injection velocity moves the stabilization region, between the jet and the flame front speed, downstream from the nozzle.

6.4.1 Effect of a pilot injection on the lift-off length of the main pulse

Measurements through OH chemiluminescence were carried out with an ICCD camera, as no high-speed intensifier was available. Consequently, only one average frame can be analyzed per injection cycle, and it was focused on studying how a pilot injection affects the stabilized lift-off length of the main pulse. Using the procedure explained in section 3.7, images from OH chemiluminescence were processed to calculate the stabilized lift-off length of the main injection event. Results are presented in Figure 6.8, where different symbols and colors depict the pilot quantity and injection number, always compared to the single injection case. Note that the limits of the y-axis change depending on the conditions.

The figure shows that, for some cases, a slight reduction in the lift-off length was observed with increasing dwell time. Nevertheless, no clear trend was found regarding the effects of both dwell time and pilot quantity on the LOL of the main injection. The averaged frame taken by the ICCD camera was considering the interval of the stabilized diffusion flame of the main injection. Nevertheless, lift-off length can change from the inception of combustion to an established diffusion flame [9, 21, 31–33], that might not be visible from

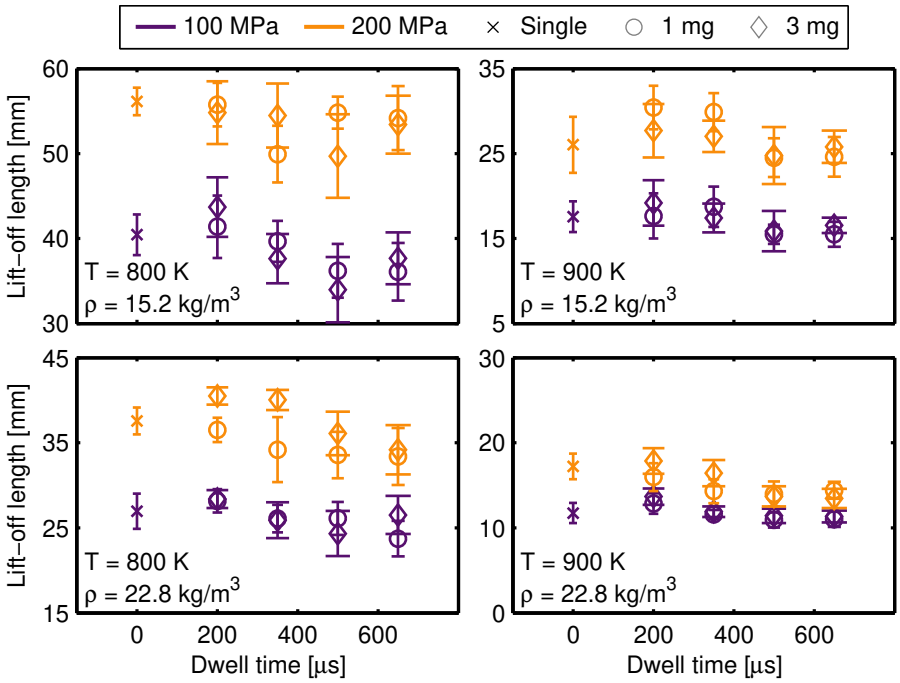

Figure 6.8: Lift-off length of the main injection in a pilot-main strategy for all conditions tested. Error-bars represent shot-to-shot dispersion, depicting a different cap size for the 3 mg (wider) and 1 mg (narrower) pilots.

a time-averaged frame. Reducing the exposure of the camera to focus on the LOL near the start of combustion of the main injection created very irregular contours that were difficult to process, and showed high shot-to-shot variabilities as well.

Nevertheless, the ignition location, related to the ignition delay, is a determinant factor in the lift-off length [34, 35]. Thus, the approximate ignition location was calculated to observe, by means of an indirect way, how a pilot injection might have affected the lift-off length of the main pulse. It was calculated with the centroid of the local maximum rate of difference at the time corresponding to the start of combustion. The term approximate is used because the ignition kernels did not present uniform shapes, but a high shot-to-shot variability. As a result, the values shown are just for qualitative representation.

Results for all conditions tested in which ignition occurred within the field of view are summarized in Figure 6.9. Different symbols and colors depict the

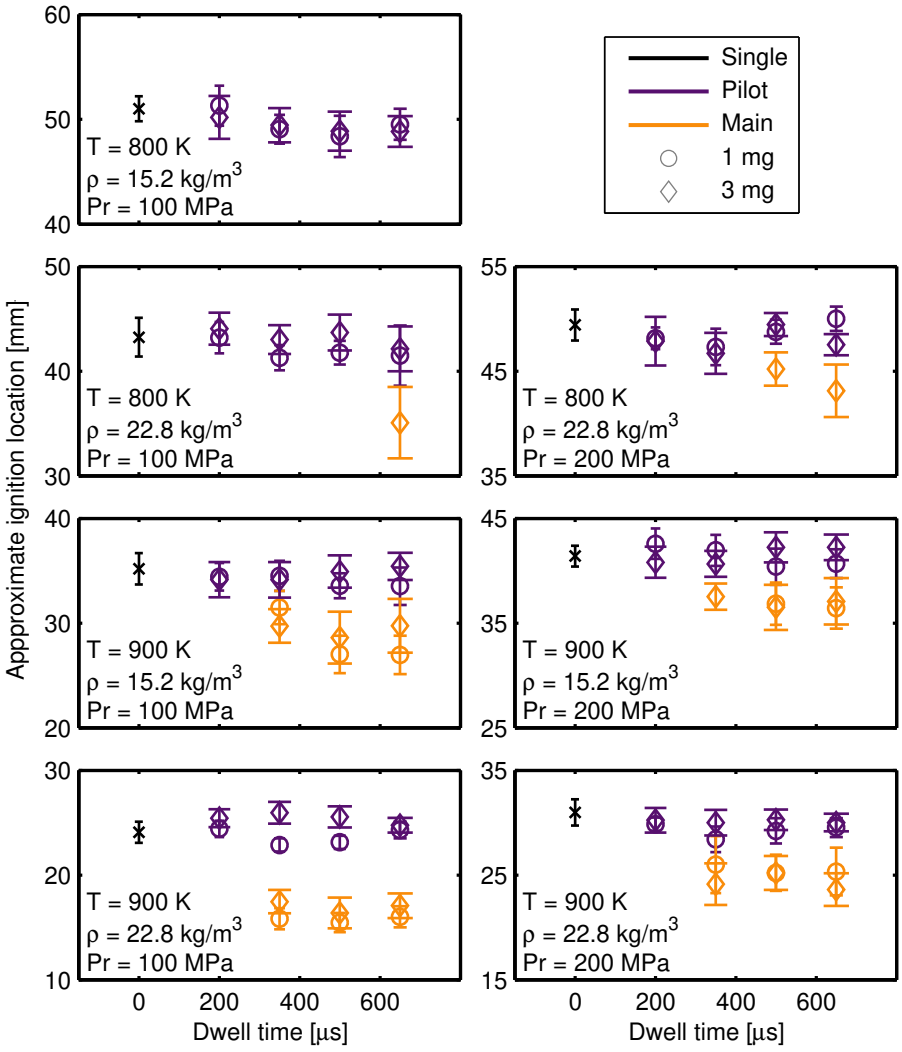

Figure 6.9: Ignition location results for pilot-main strategies and all conditions in which ignition occurred within the field of view. Error-bars represent shot-to-shot dispersion, depicting a different cap size for the 3 mg (wider) and 1 mg (narrower) pilots.

pilot quantity and injection number, always compared to the single injection case. Note that the limits of the y-axis change depending on the conditions.

As expected from the literature [9, 12, 21, 22, 31], the ignition location follows a similar trend as the ignition delay, and is dependent on the interaction

mode between injection pulses: either acting as a single injection in a mixing interaction mode, or as two different combustion events that interact with each other. For a single injection, the first ignition kernels typically occur in richer mixtures near the spray head, propagating on one side towards the spray tip, and on the other towards the nozzle up to the lift-off region. In a pilot-main strategy, the main injection interacts with the hot products of the pilot combustion, accelerating its vaporization process [24] and reaction rate [25], moving the ignition location upstream towards the nozzle, and consequently, presenting a shorter lift-off [9]. Therefore, the trends observed confirm that the lift-off length measured with an ICCD camera mainly recorded the distance once it has recovered its equilibrium location. Thus, to be able to observe the effects of a pilot injection on the temporal evolution of the main pulse lift-off length, it is recommended to use a high-speed intensified camera coupled with the same optical configuration as before.

6.5 Soot measurements through diffused back-illumination

Soot emission in diesel combustion is determined by a competition between its formation and oxidation. With the methodology presented in section 3.7, DBI and chemiluminescence images were processed to calculate the flame soot in terms of the optical thickness (KL). By assuming flame symmetry, soot-maps were constructed to depict its evolution throughout the injection event, by calculating the total KL for each axial distance and time-step. Results are divided into three sections: first, trends of single injection cases varying boundary conditions are compared, while the latter segments account for multiple injection strategies.

6.5.1 Soot distribution for single injection cases

Figures 6.10, 6.11, and 6.12 depict the effect that parametric variations of each of the boundary conditions have on the soot-map distribution for single injections cases. The white dashed line defines the average liquid length for that specific condition. Light extinction below the vaporization length was not considered for representation purposes.

The trends observed in the figures follow those found in the literature [36–38]. From Figure 6.10, it can be observed that increasing the rail pressure drastically reduces the cross-sectional KL. Soot is prone to form in rich reaction zones [27]. Higher rail pressure levels increase the lift-off length while

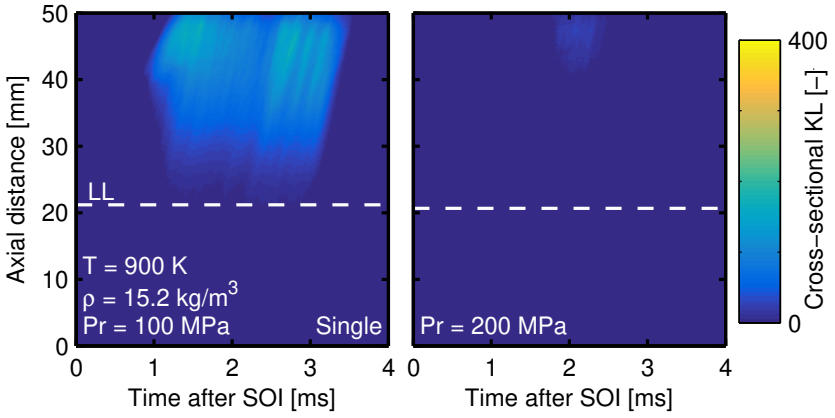

Figure 6.10: Effect of the rail pressure on the evolution of the cross-sectional KL at each axial distance for single injection events. The dashed white line represents the liquid length for each specific condition.

having no impact on the vaporization distance, due to an increase in both the injection velocity [27], and the mixing-rate [39, 40]. In addition, it moves the ignition location downstream of the nozzle, as observed in the previous section. Consequently, fuel vaporization is complete well before reaching the reaction zone, and both the initial combustion and diffusion flame occur in leaner conditions, less ideal for forming soot [11, 22, 27]. Moreover, higher injection velocities also decrease the residence time of the fuel jet in the reacting region [36]. A combination of these factors also shifts the soot formation region downstream from the nozzle.

Figure 6.11 shows how increasing the chamber density increments the cross-sectional KL, and shifts the sooting region closer to the nozzle. Pickett and Siebers [36] and Payri et al. [37] reported a non-linear effect of density on soot. Nevertheless, multiple factors that affect soot production are dependent on the chamber density: mixing rate, liquid length, ignition delay, and lift-off length. Correlations with coefficients calculated from experimental data show that chamber density contributes with a coefficient of $\rho^{-1.35}$ for ignition delay [3, 4], ρ^{-1} for lift-off length [3, 4], and $\rho^{-0.51}$ for liquid length [41–43]. Consequently, the trend is probably described by more complex interactions. However, Pickett and Siebers [36] explained the shift in the soot region as a result of two variables: a decrease in the lift-off length [3, 4, 27], and the increase in the overall air entrained relative to the amount of fuel injected [36].

Figure 6.12 depicts how elevating the chamber temperature increases the cross-sectional KL as well, and also shifts the sooting region close to the

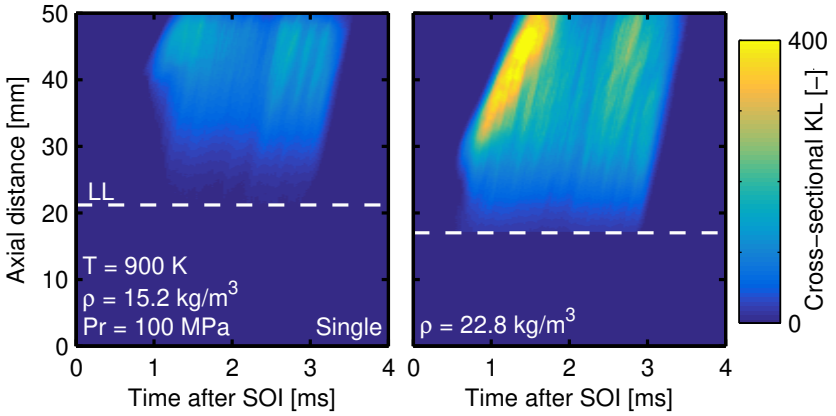

Figure 6.11: Effect of the chamber density on the evolution of the cross-sectional KL at each axial distance for single injection events. The dashed white line represents the liquid length for each specific condition.

nozzle. Both the ignition delay and lift-off length decrease at higher chamber temperature [3, 4, 6, 14], increasing the local equivalence ration at the lift-off location [27, 36]. As a consequence, soot begins forming under generally richer conditions. Note how at 800 K, almost no cross-sectional KL is observed, even at the lowest rail pressure and highest chamber density.

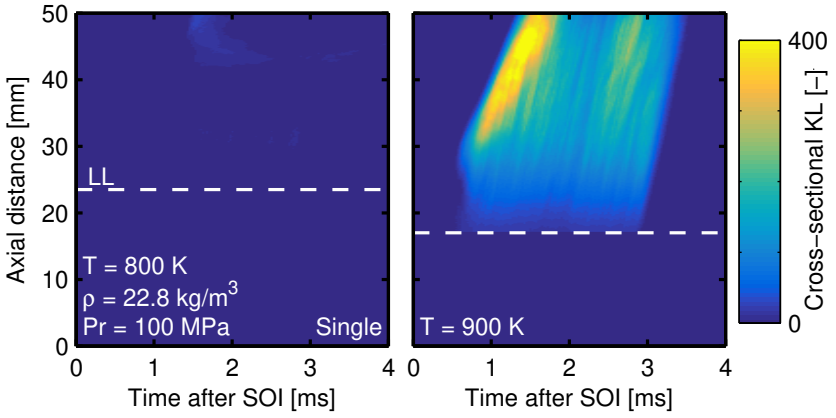

Figure 6.12: Effect of the chamber temperature on the evolution of the cross-sectional KL at each axial distance for single injection events. The dashed white line represents the liquid length for each specific condition.

6.5.2 Soot distribution for pilot-main strategies

Soot-maps for pilot-main strategies are presented on the following pages, from Figures 6.13 to 6.18. Each image shows the cross-sectional KL, organized row-wise by dwell time, and column-wise by pilot quantities. All cases are compared to its reference single injection. Color-bars represent the intensity of the cross-sectional KL, and were divided into two ranges depending on the soot formation: a low-level from 0-100, and a high-level from 0-400. Horizontal and vertical dashed white lines depict the liquid length and start of injection of the main pulse, respectively. Soot-maps for the lowest chamber density and temperature are not presented because no soot formation was observed for both rail pressures.

Overall, it was observed that a pilot-main strategy produces more soot than a single injection event, which is in agreement with trends found in the literature [10, 12, 21, 22, 44–48]. Furthermore, in general, the 1 mg pilots combusted and stagnated closer to the nozzle, promoting a higher soot production from the main injection. This is probably due to the main pulse burning with a higher equivalence ratio, ideal for soot formation, although this observation might be limited to the field of view used. Contrarily, the 3 mg pilot ignition kernel moved farther downstream of the nozzle, because of to the higher momentum flux. Consequently, the main injection reached the kernel probably in leaner conditions producing lower soot quantities. Other authors [12, 46] remarked similar trends.

The increase of soot production, when including a pilot injection, is more noticeable at higher chamber densities and temperatures. As the ignition delay of the main event decreases, as well as the ignition location, its combustion occurs in temperature and mixture conditions that promote the appearance of soot earlier in the injection event [21, 22, 27]. This is also coherent with the shortened premixed combustion of the main pulse. Consequently, a diffusion flame is established early in the temporal evolution of the spray.

In these same figures, it is also possible to recognize how increasing the pilot quantity diminishes the cross-sectional KL to a distribution similar to that of a single injection, at least for the limited field of view. That is, the peak of soot observed near the start of injection of the main pulse for a 1 mg pilot could appear, but out of the optical limit. In addition, pilots of 3 mg for both rail pressures and a chamber density of 22.8 $\mathrm{kg\,m^{-3}}$ and temperature of 900 K presented soot production. In such cases, the pulse was probably long enough allowing chamber conditions to establish a brief diffusion flame, and confirming that the main injection interacts with the pilot in a diffusive mode.

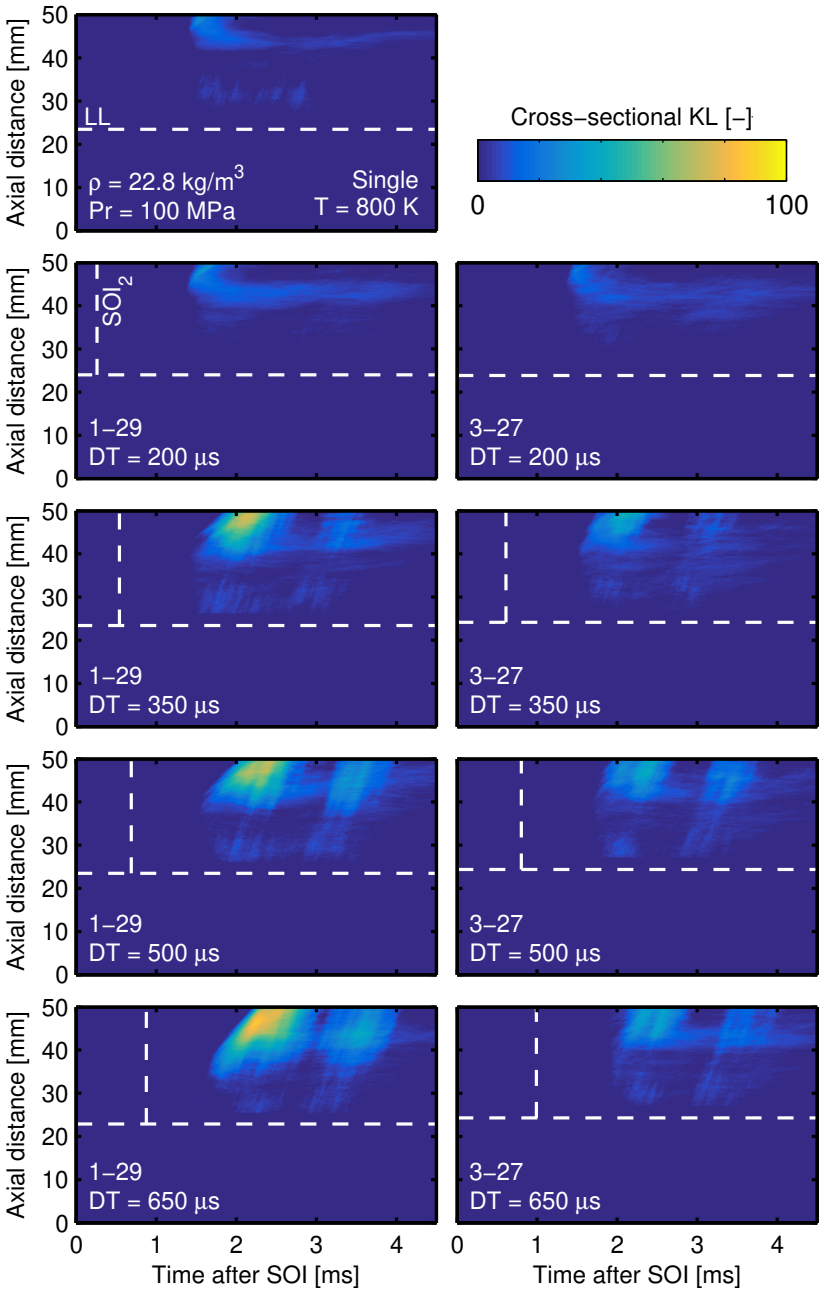

Figure 6.13: Evolution of the cross-sectional KL at each axial distance for pilot-main strategies, for a rail pressure of 100 MPa, a chamber density of 22.8 kg m^{-3} and temperature of 800 K. The dashed white lines depict the liquid length (horizontal) and the start of injection of the main pulse (vertical).

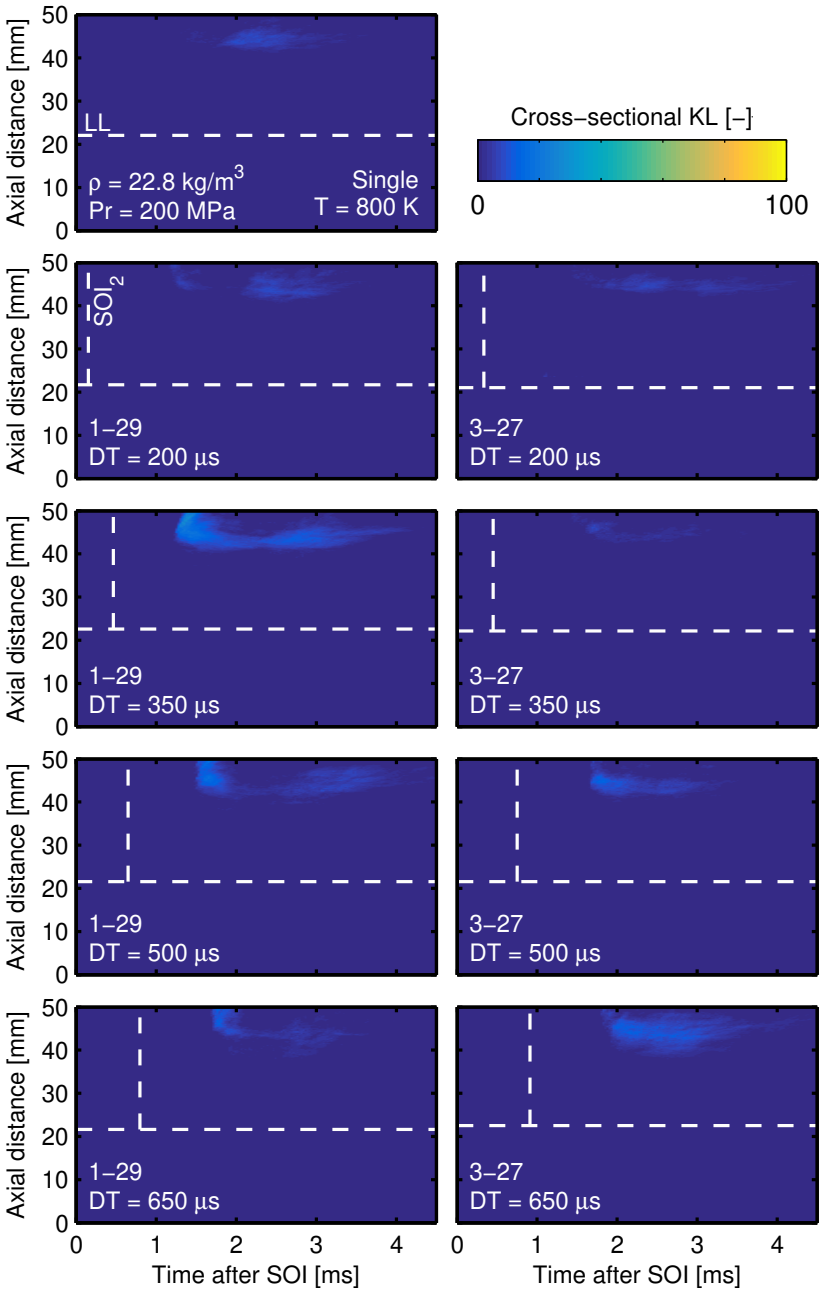

Figure 6.14: Evolution of the cross-sectional KL at each axial distance for pilot-main strategies, for a rail pressure of 200 MPa, a chamber density of 22.8 kg m^{-3} and temperature of 800 K. The dashed white lines depict the liquid length (horizontal) and the start of injection of the main pulse (vertical).

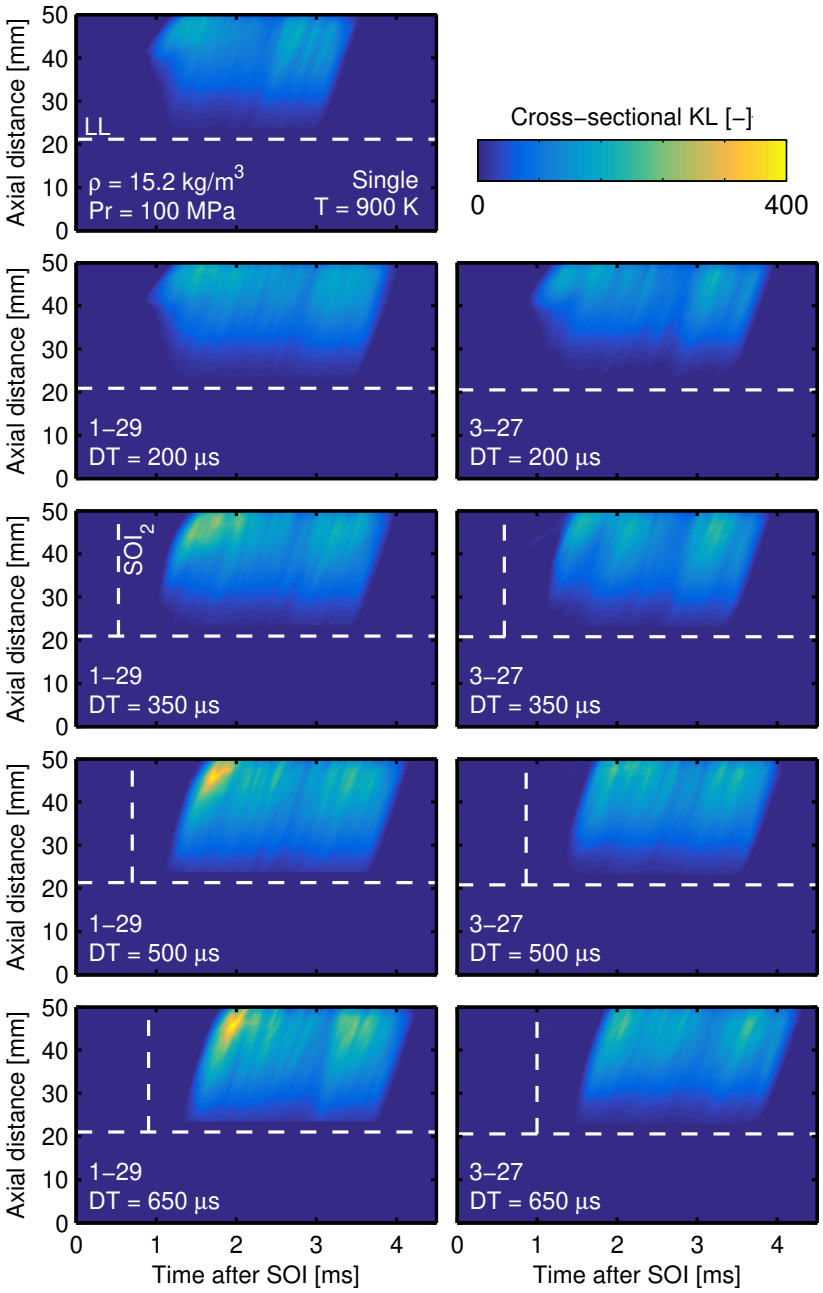

Figure 6.15: Evolution of the cross-sectional KL at each axial distance for pilot-main strategies, for a rail pressure of 100 MPa, a chamber density of 15.2 kg m^{-3} and temperature of 900 K. The dashed white lines depict the liquid length (horizontal) and the start of injection of the main pulse (vertical).

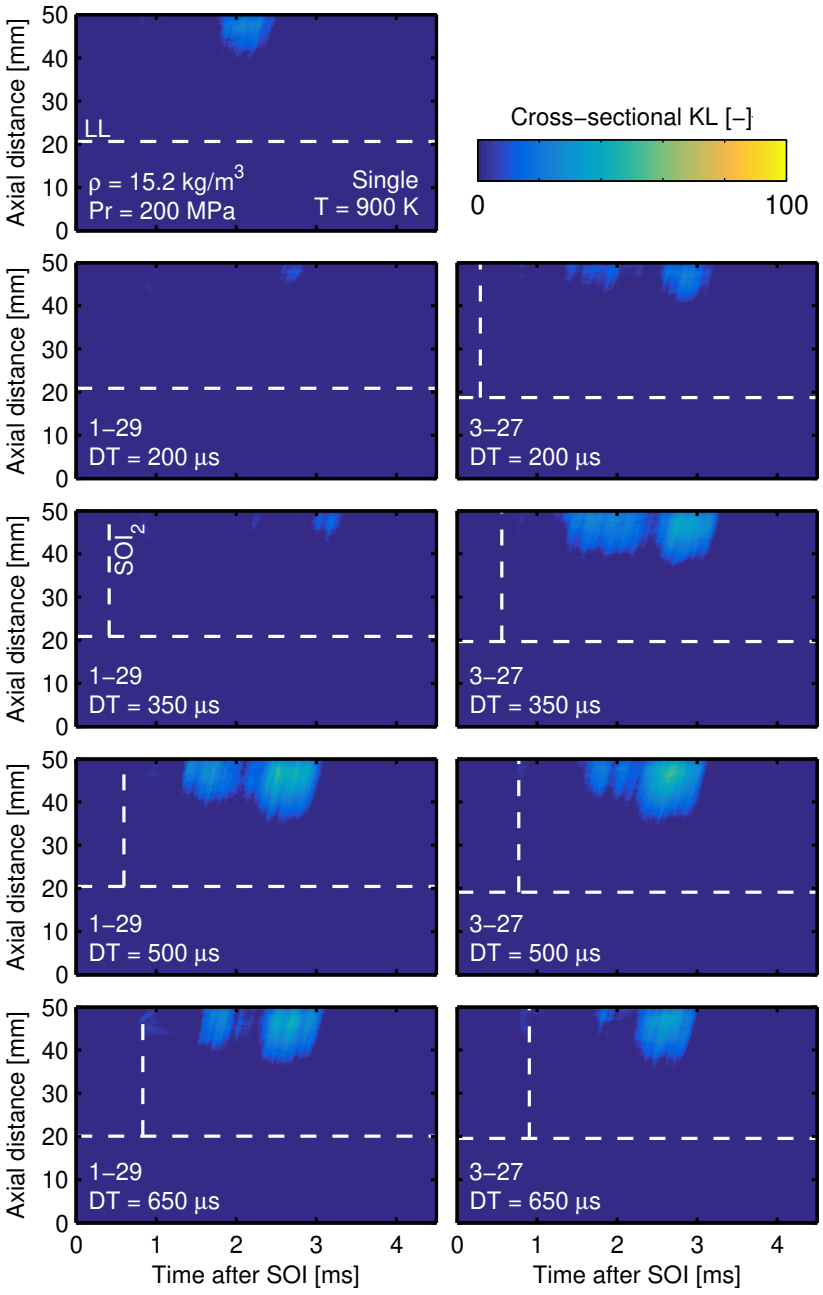

Figure 6.16: Evolution of the cross-sectional KL at each axial distance for pilot-main strategies, for a rail pressure of 200 MPa, a chamber density of 15.2 kg m^{-3} and a temperature of 900 K. The dashed white lines depict the liquid length (horizontal) and the start of injection of the main pulse (vertical).

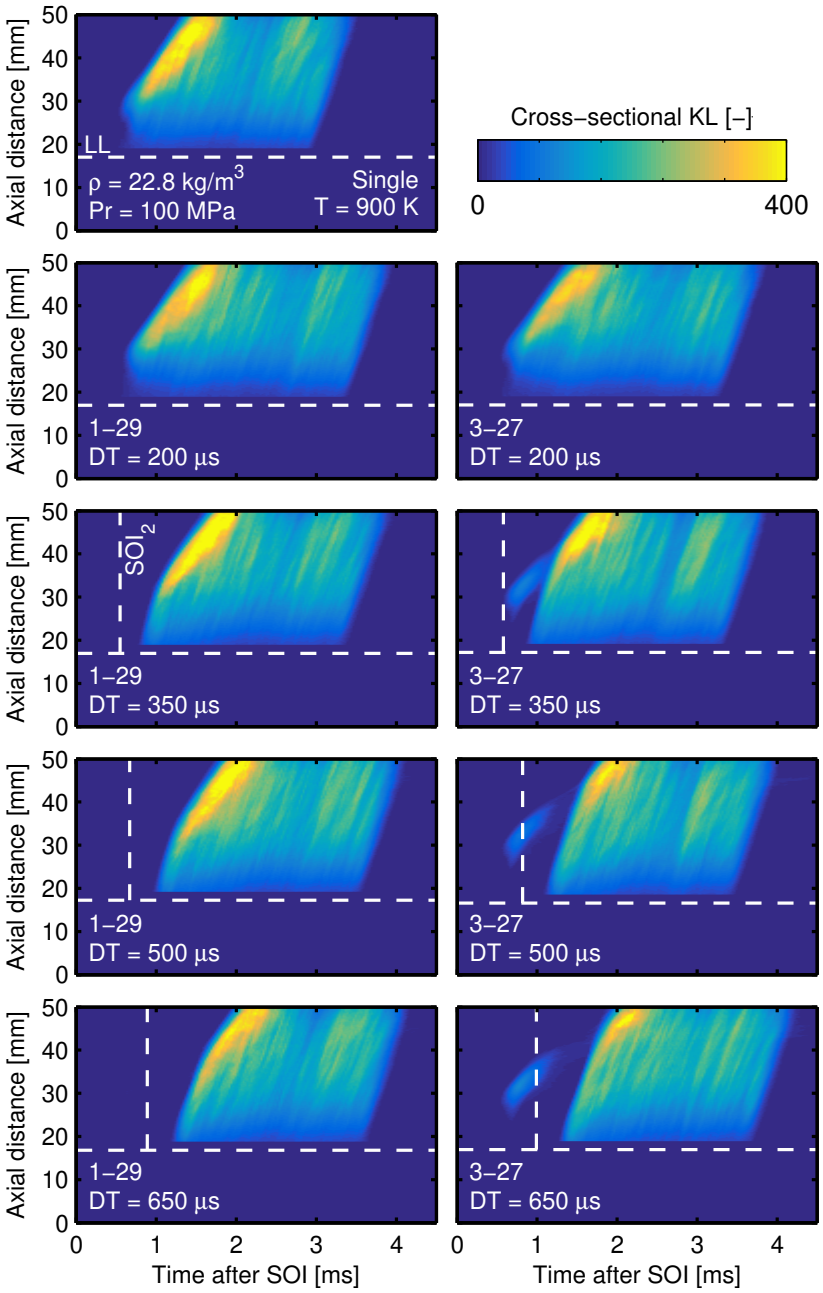

Figure 6.17: Evolution of the cross-sectional KL at each axial distance for pilot-main strategies, for a rail pressure of 100 MPa, a chamber density of 22.8 kg m^{-3} and temperature of 900 K. The dashed white lines depict the liquid length (horizontal) and the start of injection of the main pulse (vertical).

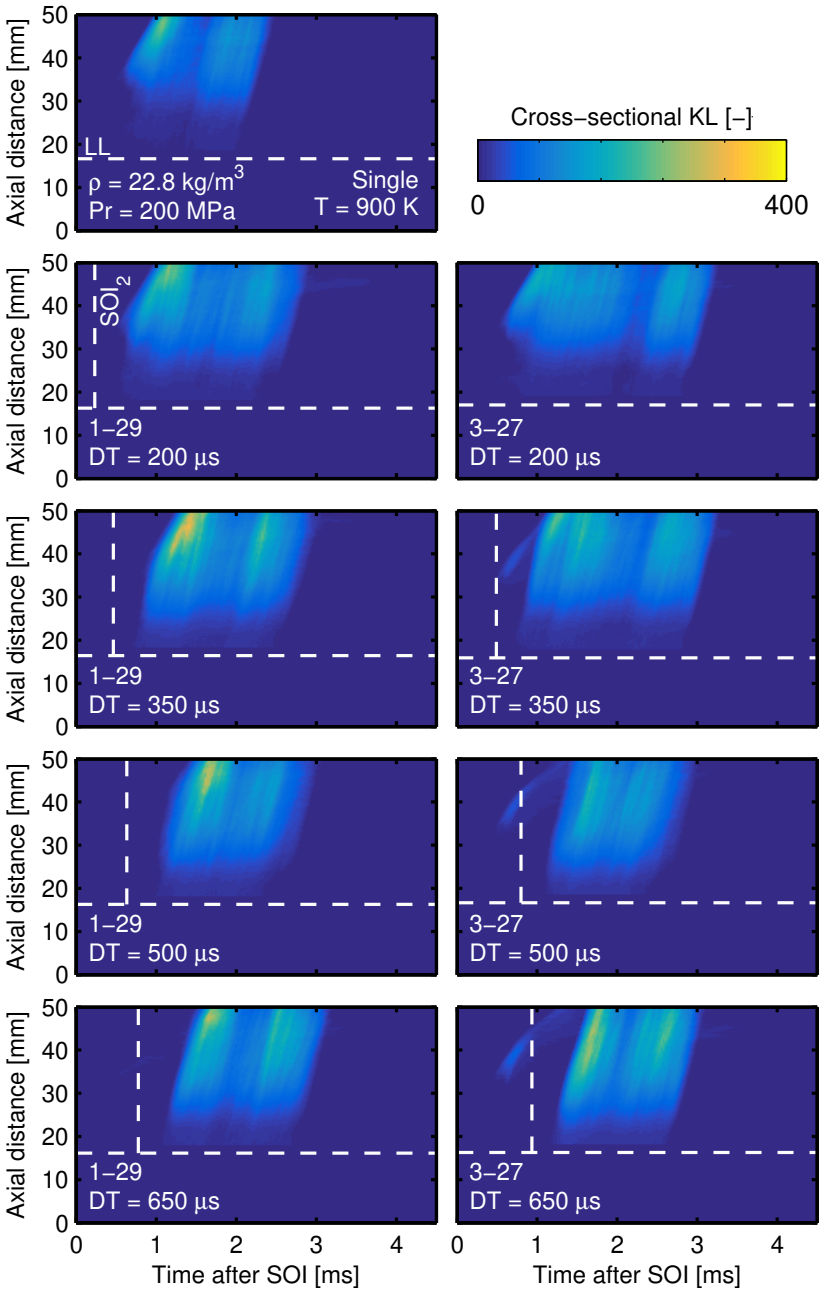

Figure 6.18: Evolution of the cross-sectional KL at each axial distance for pilot-main strategies, for a rail pressure of 200 MPa, a chamber density of 22.8 kg m^{-3} and temperature of 900 K. The dashed white lines depict the liquid length (horizontal) and the start of injection of the main pulse (vertical).

No clear trend of the dependence of soot on the dwell time is seen. However, for a fixed boundary condition and pilot quantity, differences in the cross-sectional KL are depicted in the figures while varying the pulse separation. Multiple factors can affect the interaction mechanism between injection pulses that cause these differences. Siebers and Higgins [27] and Payri et al. [11] remarked the dependence in soot formation when non-vaporized fuel penetrates beyond the flame lift-off length, or ignition kernel. Furthermore, Siebers and Higgins [27] highlighted the strong link between soot and the air entrained upstream of the lift-off length, concluding that higher air entrainment is likely to result in less soot production. Although these studies were performed with a single injection, trends can be extrapolated to the interaction between multiple pulses. A pilot event modifies the conditions in which the main injection develops, and the dwell time provides an extra variable for such conditions to evolve and modify soot formation.

As an additional note, when the pilot and main injection merged for dwell times of 200 µs, the soot-maps depict a nearly identical structure as the reference single injection, but with a longer diffusive flame.

To further assess these statements, equivalence ratios and temperature distributions could be calculated through 1-D modeling [22, 49, 50], using the experimental data presented in this work for validation.

6.5.3 Soot distribution for main-post strategies

Soot-maps for main-post strategies are presented on the following pages, from Figures 6.19 to 6.21. Each image shows the cross-sectional KL, organized row-wise by dwell time and post quantity, and column-wise by rail pressure. All cases are compared to its reference single injection. Color-bars represent the intensity of the cross-sectional KL, and were divided into two ranges depending on the soot formation: a low-level from 0-100, and a high-level from 0-400. Horizontal and vertical dashed white lines depict the liquid length of the main injection, and the SOI of the post pulse, respectively. Soot-maps for dwell times of 200 µs and 350 µs, as well as the lowest chamber density and temperature, are not presented because pulses did not decouple and no soot formation was observed for both rail pressures.

The results show that soot formation increases slightly, or is at least equal, with the inclusion of a post injection compared to the reference case. Moreover, specifically as seen Figures 6.20 and 6.21, decreasing the dwell time and increasing the post quantity notably promoted soot production. In these type of combustion chambers, which provide a large volume for the spray to

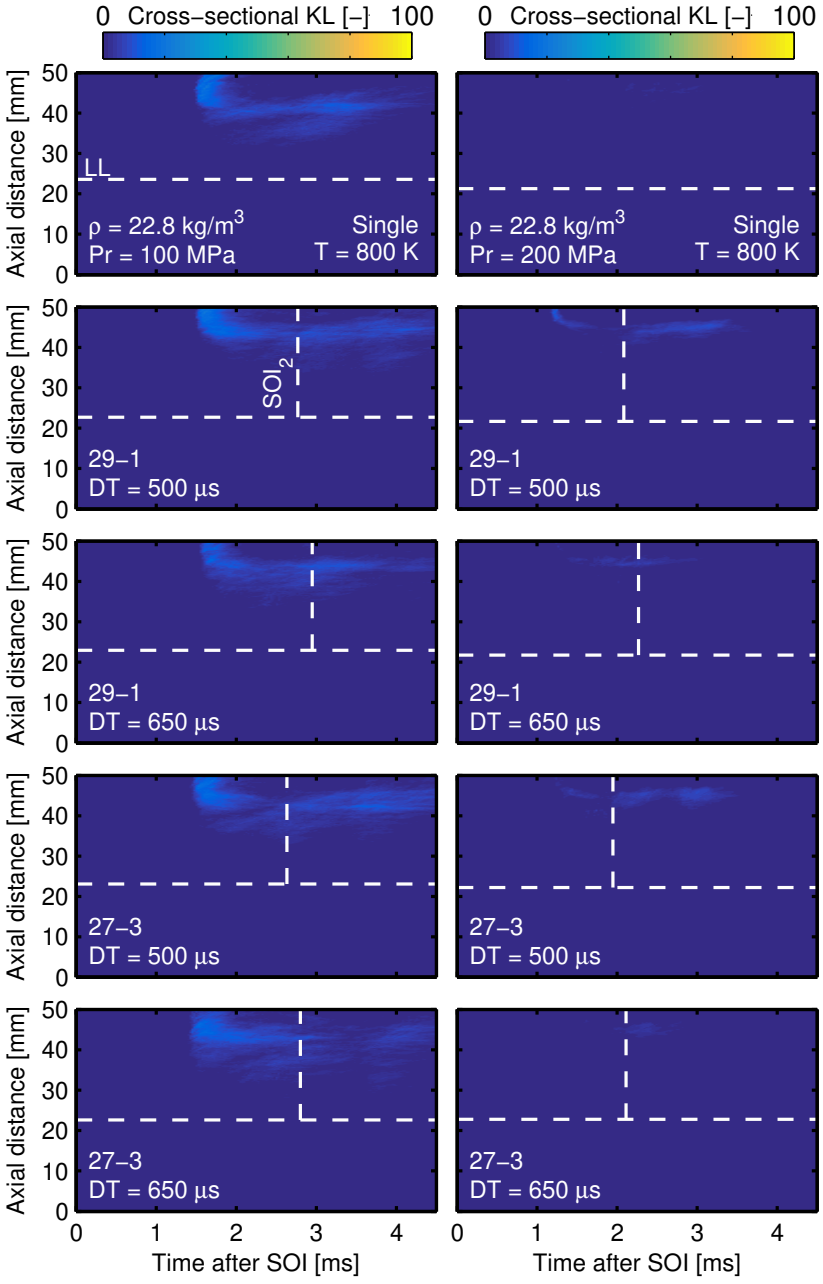

Figure 6.19: Evolution of the cross-sectional KL at each axial distance for main-post strategies, for a rail pressure of 100 MPa (left) and 200 MPa (right), a chamber density of 22.8 kg m^{-3} and temperature of 800 K. The dashed white lines depict the liquid length of the main (horizontal), and start of injection of the post (vertical).

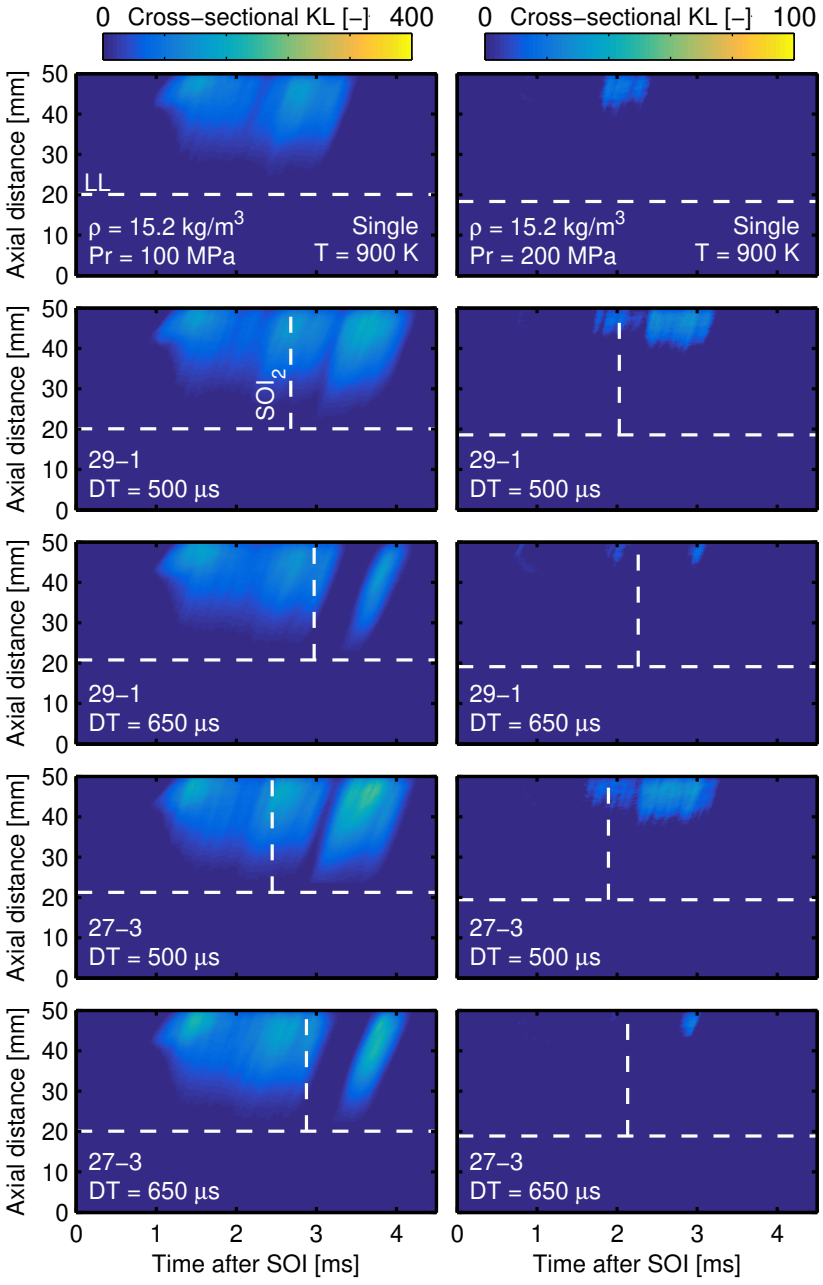

Figure 6.20: Evolution of the cross-sectional KL at each axial distance for main-post strategies, for a rail pressure of 100 MPa (left) and 200 MPa (right), a chamber density of 15.2 kg m^{-3} and temperature of 900 K. The dashed white lines depict the liquid length of the main (horizontal), and start of injection of the post (vertical).

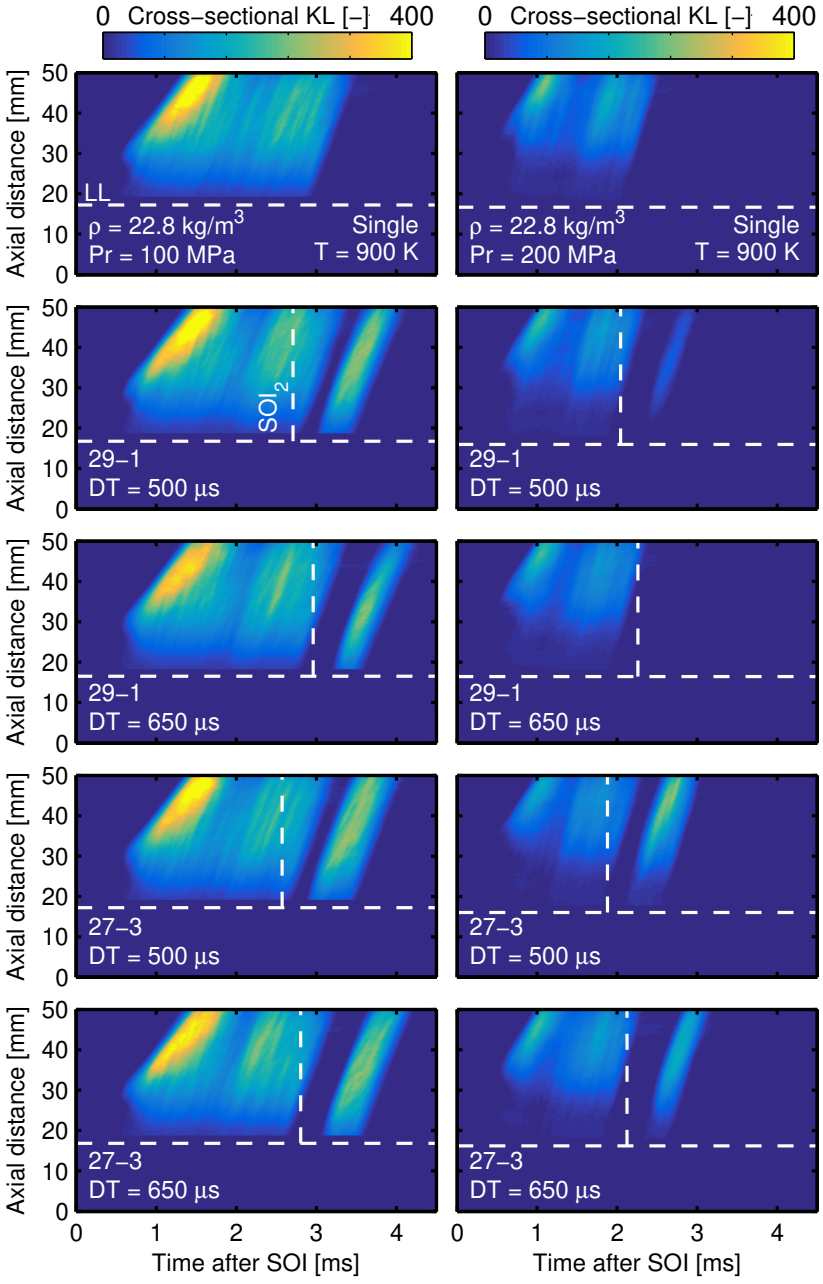

Figure 6.21: Evolution of the cross-sectional KL at each axial distance for main-post strategies, for a rail pressure of 100 MPa (left) and 200 MPa (right), a chamber density of 22.8 kg m^{-3} and temperature of 900 K. The dashed white lines depict the liquid length of the main (horizontal), and start of injection of the post (vertical).

develop, the general problem is that the post injection behaves like a main, and the actual main like a pilot. Therefore, after the combustion recession of the main pulse, local conditions enhance the formation of soot from the post injection, instead of promoting its oxidation.

Researchers have studied the differences in the development between a free jet and with spray-wall interactions under engine-like conditions [51–53]. More notably, specific studies have analyzed soot formation and oxidation between the two configurations [54, 55]. These authors concluded that spray-wall interactions enhanced soot oxidation and reduced its creation due to higher mixing with ambient air caused by wall impingement. Also, the authors found that the heat exchanged with the walls cooled down the jet, slowing the rate of soot formation.

Furthermore, from the literature, it is widely known that post injections are useful for the reduction of soot exhaust emissions [56–66]. O'Connor and Musculus [65] provided a very detailed literature review of the processes involved in soot formation and oxidation with a post injection, with multiple references of both experimental and modeling data from optical and real engines. The authors discussed several mechanisms, some which were previously described in chapter 2. But in general, some of the interactions highlighted the importance of a confined cylinder bowl to increase mixing and enhance the targeting by the post pulse of the main injection residual mixture. Consequently, the effectiveness of the post injection on reducing soot emissions is closely linked to a restrained engine bowl-shaped combustion chamber. Thus, to accurately quantify the effects of post injections on the balance of soot formation/oxidation, similar geometries that emulate these mechanisms must be tested, instead of the large volume high-temperature and pressure vessel used in this thesis.

6.6 Summary and conclusions

This chapter collects and analyses all the results describing the spray development for multiple injection strategies in reactive conditions. Measurements were carried out in an optically-accessible constant pressure and flow vessel. Optical setups included a diffused back-illumination combined with flame chemiluminescence to quantify soot, a single-pass schlieren for ignition delay, and an ICCD camera coupled with a narrow-pass filter to visualize OH chemiluminescence to measure the stabilized lift-off length of the main pulse in pilot-main strategies. The field of view allowed for an optical limit of approximately 50 mm.

From the image processing results:

- In general terms, the inclusion of a pilot injection shortened the premixed phase of the main pulse. Thus, estimations of the ignition delay through schlieren movies proved to be difficult, as the radial expansion, typical of a well-defined premixed combustion phase, was very small or non-existent.
- A novel image processing methodology was developed to decouple the start of combustion of each spray in multiple injection strategies. It is based on the absolute pixel-wise frame-to-frame difference, that quantifies the temporal evolution of pixel structures both in growth and intensity, named rate of difference.
- The rate of difference signal can be processed as the typical data gathered from schlieren imaging to estimate the ignition delay of each injection pulse.
- The processing methodology was successfully used to compare results from a different experimental campaign that included a high-speed intensified camera to measure ignition delay through a temporal discretization of the OH chemiluminescence.

From the ignition delay results:

- For all the test points, the pilot injection enhanced conditions which promoted a faster ignition of the main pulse, as its ignition delay decreased in reference to its start of injection. On average, the ignition delay of the main pulse was reduced around 30 % to 40 % compared to its single injection case.
- At lower chamber temperatures, the pilot and main pulses ignited simultaneously, as the second injection took place during the mixing phase of the first. In such cases, increasing the dwell time lengthened the ignition delay of the pilot, as it negatively influenced the ignition process, probably cooling down or modifying the local mixture. Ignition delay values trended to the reference case when decreasing the dwell time.
- Both the dwell time and pilot quantity affected the interaction mechanisms between injections in different ways. Increasing the dwell time provided more time for the pilot injection to mix and combust before

being caught up by the main pulse. On the contrary, increasing the pilot quantity provided a higher momentum as it penetrates further in the combustion chamber, which increased the distance for the main injection to interact with it.

- At higher chamber temperatures, all conditions presented a separate combustion event for each injection. The pilot pulse showed the same ignition delay as its reference case, with no effect noted from neither its quantity and the dwell time to the main injection. No clear trend was observed regarding specific effects of the pilot quantity on the ignition delay, although it seemed to decrease slightly with decreasing dwell time.
- For main-post strategies, all conditions also showed a separate combustion event for each injection, as the second pulse is injected well after the ignition of the main event. Moreover, as more fuel is burnt in the first injection, higher localized temperature promoted an ever faster ignition of the second pulse compared to pilot-main strategies. On average, for conditions tested, the ignition delay of the post injection was reduced around 40 % to 50 % compared to its reference case.

From the lift-off length results:

- In general, no clear trend was observed regarding the effects of both the dwell time and the pilot quantity on the lift-off length of the main injection. Some cases showed a slight decrease with increasing dwell time.
- The averaged frame taken by the ICCD camera does not consider that the lift-off length can change from the inception of combustion to the established diffusion flame.
- Qualitative measurements of ignition location showed that the lift-off length of the main injection should start closer upstream from the nozzle and slowly shift towards equilibrium in the stabilized diffusion flame.

From soot measurements through DBI:

- Results calculated for the single injection cases follow the trends from the literature. Firstly, soot increased with decreasing injection pressure: as lift-off length decreases with no impact on the vaporization length, combustion occurs in richer conditions that are ideal for soot formation.

Secondly, soot increased with increasing chamber density: as multiple factors are affected by density, it has a non-linear effect on the formation of soot which is probably described by more complex interactions. Thirdly, soot increased with increasing chamber temperature: as both ignition delay and lift-off length decrease, higher local equivalence ratios are present near the lift-off region.

- In general, it was observed that conditions that promote faster premixed combustion enhance soot formation, as most of the fuel is burned in a diffusion flame.

- Overall, pilot-main strategies produced more soot than each of their reference case. A slight decrease in the cross-sectional KL near the start of combustion was observed when increasing the pilot quantity.

- The combustion kernel of 1 mg pilots stagnated closer to the nozzle, promoting a higher soot production from the main injection. Contrarily, the 3 mg pilot moved further downstream of the nozzle once ignited due to its higher momentum. Therefore, the main injection reached the kernel in leaner conditions that diminish soot formation. These observations were limited to the field of view of the experiments.

- No clear trend of the dependence of soot on the dwell time was observed. For fixed boundary conditions differences are noticed, but multiple interaction mechanisms between injections may cause the dissimilarities. A pilot injection modifies the conditions in which the second pulse develops. Thus, the dwell time is an extra variable that alters how the conditions evolve and modify soot formation.

- In contrast to what is reported in the literature, main-post strategies depicted slightly higher (or similar) soot formation than a single injection.

- Different experimental works available in the literature also showed that the soot oxidation processes are very dependent on the interaction between the injections and the confined engine bowl-shaped combustion chamber. Therefore for these type of large volume vessels, the post injection behaved like a main and the actual main like a pilot. As a result, after the combustion recession from the main pulse, local conditions enhanced the formation of soot from the post injection, instead of promoting its oxidation.

6.A Measurements of combustion noise with a pressure transducer

The mass of fuel burned in the premixed combustion is fundamentally dependent on the air-fuel mix rate and the ignition delay [14, 67, 68]. As seen from the results and the literature, a pilot pulse can be used to reduce the ignition delay of the main injection [12, 20–23, 44]. Consequently, less heat is released during the now predominantly mixing-controlled combustion of the main injection, lowering both the duration of the premixed phase and the peak temperature, which is in both cases beneficial for noise [18, 20, 23, 48, 69] and NOx [18, 44, 48, 70] emissions.

Noise related to the spray combustion process is associated with the maximum in-cylinder pressure rise rate of the premixed phase [71–76]. In the constant pressure test vessel, the combustion noise (CN) was qualitatively estimated by calculating the maximum pressure rise rate from the signal measured by a piezoelectric transducer, after applying a low-pass filter to remove resonance and electrical noise [71].

First, to validate the trends of the results, signals from single injection events were compared, and are presented in Figure 6.22. Note that data was not corrected considering the time taken by the pressure wave to reach the sensor, as the primary objective is to compare maximum pressure rise rate between conditions that are not dependent on the speed of sound. Therefore, the time domain has no reference, and curves were phased to the same initial value. Also, the y-axis is displayed in *bar* units as directly captured by the sensor/amplifier system, but is not relevant for qualitative comparisons.

As shown in the figure, results follow the trend expected from the literature [16, 67, 68]. Increasing the injection pressure and chamber density increased air-fuel mix rate [39, 40], and promoted more fuel to burn in the premixed phase of combustion, accelerating the pressure rise, and consequently producing more CN. In contrast, increasing chamber temperature reduces the ignition delay with a minimal impact in the air-fuel mix rate [39, 40, 77], thus less fuel is burned in the premixed combustion.

Results for a pilot-main strategy were processed with the same methodology as before, calculating the maximum pressure rise rate measured with the piezoelectric transducer after applying a low-pass filter. However, trends presented very different results. A constant-pressure vessel with such a large volume as the one utilized is not representative of a real combustion chamber geometry. As a result, the resonance frequencies of the waves are much lower and can interfere with the pressure rise rate. This effect was verified by ana-

lyzing the raw trace in the frequency domain, where the expected resonance peaks showed similar amplitudes to that of the main combustion, at lower frequencies than those for real engine geometries [71, 73, 76]. Consequently, estimations of the combustion noise were not carried out successfully.

Nevertheless, using a piezoelectric transducer shows promise not only for qualitative comparisons of combustion noise of single injection events but also for estimating their relative ignition delay with very high precision. Moreover, to further improve the calculations of the start of combustion, the speed of sound can be determined by correlating the ignition delay measured by multiple proven methods [3, 4, 7, 8, 10] at different chamber conditions.

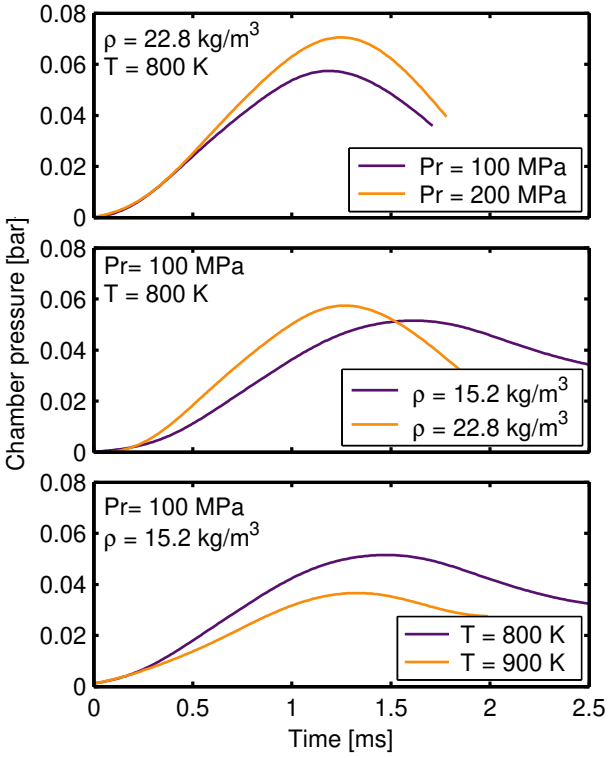

Figure 6.22: Signal from the fast-pressure transducer for the single injection cases at different boundary conditions.

References

[1] Lillo, P. M., Pickett, L. M., Persson, H., Andersson, Ö., and Kook, S. "Diesel Spray Ignition Detection and Spatial/Temporal Correction". In: *SAE International Journal of Engines* 5.3 (2012), pp. 2012–01–1239. DOI: 10.4271/2012-01-1239.

[2] Bardi, M. et al. "Engine Combustion Network: Comparison of Spray Development, Vaporization, and Combustion in Different Combustion Vessels". In: *Atomization and Sprays* 22.10 (2012), pp. 807–842. DOI: 10.1615/AtomizSpr.2013005837.

[3] Benajes, J., Payri, R., Bardi, M., and Martí-Aldaraví, P. "Experimental characterization of diesel ignition and lift-off length using a single-hole ECN injector". In: *Applied Thermal Engineering* 58.1-2 (2013), pp. 554–563. DOI: 10.1016/j.applthermaleng.2013.04.044.

[4] Payri, R., Salvador, F. J., Manin, J., and Viera, A. "Diesel ignition delay and lift-off length through different methodologies using a multi-hole injector". In: *Applied Energy* 162 (2016), pp. 541–550. DOI: 10.1016/j.apenergy.2015.10.118.

[5] Payri, R., García-Oliver, J. M., Xuan, T., and Bardi, M. "A study on diesel spray tip penetration and radial expansion under reacting conditions". In: *Applied Thermal Engineering* 90 (2015), pp. 619–629. DOI: 10.1016/j.applthermaleng.2015.07.042.

[6] Payri, R., Viera, J. P., Gopalakrishnan, V., and Szymkowicz, P. G. "The effect of nozzle geometry over ignition delay and flame lift-off of reacting direct-injection sprays for three different fuels". In: *Fuel* 199 (2017), pp. 76–90. DOI: 10.1016/j.fuel.2017.02.075.

[7] Jakob, M. et al. "Simultaneous high-speed visualization of soot luminosity and OH * chemiluminescence of alternative-fuel combustion in a HSDI diesel engine under realistic operating conditions". In: *Combustion and Flame* 159.7 (2012), pp. 2516–2529. DOI: 10.1016/j.combustflame.2012.03.004.

[8] Zhang, W., Tian, J.-P., and Nishida, K. "Effects of Nozzle Hole Diameter and Injection Pressure on Flame Lift-Off and Soot Formation in D.I. Diesel Combustion". In: *SAE Technical Paper 2011-01-1813* (2011). DOI: 10.4271/2011-01-1813.

[9] Maes, N., Bakker, P. C., Dam, N., and Somers, B. "Transient Flame Development in a Constant-Volume Vessel Using a Split-Scheme Injection Strategy". In: *SAE International Journal of Fuels and Lubricants* 10.2 (2017), pp. 2017–01–0815. DOI: 10.4271/2017-01-0815.

[10] Park, C. and Busch, S. "The influence of pilot injection on high-temperature ignition processes and early flame structure in a high-speed direct injection diesel engine". In: *International Journal of Engine Research* 19.6 (2018), pp. 668–681. DOI: 10.1177/1468087417728630.

[11] Payri, R., Bracho, G., Martí-Aldaraví, P., and Viera, A. "Nozzle Geometry Size Influence on Reactive Spray Development: From Spray B to Heavy Duty Applications". In: *SAE Technical Paper 2017-01-0846* (2017), p. 12. DOI: 10.4271/2017-01-0846.

[12] Mingfa, Y., Hu, W., Zunqing, Z., and Yan, Y. "Experimental Study of Multiple Injections and Coupling Effects of Multi-Injection and EGR in a HD Diesel Engine". In: *SAE Technical Paper 2009-01-2807* (2009). DOI: 10.4271/2009-01-2807.

[13] Dec, J. E. and Espey, C. "Chemiluminescence Imaging of Autoignition in a DI Diesel Engine". In: *SAE Technical Paper 982685* 724 (1998). DOI: 10.4271/982685.

[14] Higgins, B. S., Siebers, D. L., and Aradi, A. "Diesel-Spray Ignition and Premixed-Burn Behavior". In: *SAE Technical Paper 2000-01-0940* (2000). DOI: 10.4271/2000-01-0940.

[15] Pickett, L. M., Siebers, D. L., and Idicheria, C. A. "Relationship Between Ignition Processes and the Lift-Off Length of Diesel Fuel Jets". In: *SAE Technical Paper 2005-01-3843* 724 (2005). DOI: 10.4271/2005-01-3843.

[16] García-Oliver, J. M. "Aportaciones al estudio del proceso de combustión turbulenta de chorros en motores Diesel de inyección directa". PhD thesis. Valencia: Universitat Politècnica de València, 2004. DOI: 10.4995/Thesis/10251/55164.

[17] Lapuerta, M., Sanz-Argent, J., and Raine, R. R. "Ignition Characteristics of Diesel Fuel in a Constant Volume Bomb under Diesel-Like Conditions. Effect of the Operation Parameters". In: *Energy and Fuels* 28.8 (2014), pp. 5445–5454. DOI: 10.1021/ef500535j.

[18] Mendez, S. and Thirouard, B. "Using Multiple Injection Strategies in Diesel Combustion: Potential to Improve Emissions, Noise and Fuel Economy Trade-Off in Low CR Engines". In: *SAE International Journal of Fuels and Lubricants* (2010), pp. 2008–01–1329. DOI: 10.4271/2008-01-1329.

[19] Skeen, S. A. et al. "A Progress Review on Soot Experiments and Modeling in the Engine Combustion Network (ECN)". In: *SAE International Journal of Engines* 9.2 (2016), pp. 2016–01–0734. DOI: 10.4271/2016-01-0734.

[20] Dürnholz, M., Endres, H., and Frisse, P. "Preinjection A Measure to Optimize the Emission Behavior of DI-Diesel Engine". In: *SAE Technical Paper 940674* (1994). DOI: 10.4271/940674.

[21] Bruneaux, G. and Maligne, D. "Study of the Mixing and Combustion Processes of Consecutive Short Double Diesel Injections". In: *SAE International Journal of Engines* 2.1 (2009), pp. 2009–01–1352. DOI: 10.4271/2009-01-1352.

[22] Desantes, J. M., García-Oliver, J. M., García, A., and Xuan, T. "Optical study on characteristics of non-reacting and reacting diesel spray with different strategies of split injection". In: *International Journal of Engine Research* 301 (2018). DOI: 10.1177/1468087418773012.

[23] Busch, S. et al. "Experimental and Numerical Investigations of Close-Coupled Pilot Injections to Reduce Combustion Noise in a Small-Bore Diesel Engine". In: *SAE International Journal of Engines* 8.2 (2015), pp. 2015–01–0796. DOI: 10.4271/2015-01-0796.

[24] Jorques Moreno, C., Stenlaas, O., and Tunestal, P. "Influence of Small Pilot on Main Injection in a Heavy-Duty Diesel Engine". In: *SAE Technical Paper 2017-01-0708* (2017). DOI: 10.4271/2017-01-0708. Copyright.

[25] Connors, K. *Chemical Kinetics:The Study of Reaction Rates in Solution*. Wiley-VCH, 1990.

[26] Peters, N. *Turbulent Combustion*. Vol. 12. Cambridge Monographs on Mechanics 11. Cambridge University Press, 2001, pp. 2022–2022. DOI: 10.1088/0957-0233/12/11/708.

[27] Siebers, D. L. and Higgins, B. S. "Flame Lift-Off on Direct-Injection Diesel Sprays Under Quiescent Conditions". In: *SAE Technical Paper 2001-01-0530* 724 (2001). DOI: 10.4271/2001-01-0530.

[28] Pastor, J. V., Payri, R., García-Oliver, J. M., and Briceño, F. J. "Schlieren Methodology for the Analysis of Transient Diesel Flame Evolution". In: *SAE International Journal of Engines* 6.3 (2013), pp. 2013–24–0041. DOI: 10.4271/2013-24-0041.

[29] Chartier, C., Aronsson, U., Andersson, Ö., Egnell, R., and Johansson, B. "Influence of jet-jet interactions on the lift-off length in an optical heavy-duty DI diesel engine". In: *Fuel* 112 (2013), pp. 311–318. DOI: 10.1016/j.fuel.2013.05.021.

[30] Taskiran, O. O. and Ergeneman, M. "Effect of nozzle dimensions and fuel type on flame lift-off length". In: *Fuel* 115 (2014), pp. 833–840. DOI: 10.1016/j.fuel.2013.03.005.

[31] Skeen, S. A., Manin, J., and Pickett, L. M. "Visualization of Ignition Processes in High-Pressure Sprays with Multiple Injections of n-Dodecane". In: *SAE International Journal of Engines* 8.2 (2015), pp. 2015–01–0799. DOI: 10.4271/2015-01-0799.

[32] Cung, K. et al. "Spray-combustion interaction mechanism of multiple-injection under diesel engine conditions". In: *Proceedings of the Combustion Institute* 35.3 (2015), pp. 3061–3068. DOI: 10.1016/j.proci.2014.07.054.

[33] Pickett, L. M., Kook, S., Persson, H., and Andersson, Ö. "Diesel fuel jet lift-off stabilization in the presence of laser-induced plasma ignition". In: *Proceedings of the Combustion Institute* 32 (2009), pp. 2793–2800. DOI: 10.1016/j.proci.2008.06.082.

[34] Ameen, M. M. and Abraham, J. "RANS and LES Study of Lift-Off Physics in Reacting Diesel Jets". In: *SAE Technical Paper 2014-01-1118* (2014). DOI: 10.4271/2014-01-1118.

[35] Bajaj, C., Ameen, M. M., and Abraham, J. "Evaluation of an unsteady flamelet progress variable model for autoignition and flame lift-off in diesel jets". In: *Combustion Science and Technology* 185.3 (2013), pp. 454–472. DOI: 10.1080/00102202.2012.726667.

[36] Pickett, L. M. and Siebers, D. L. "Soot in diesel fuel jets: effects of ambient temperature, ambient density, and injection pressure". In: *Combustion and Flame* 138.1 (2004), pp. 114–135. DOI: 10.1016/j.combustflame.2004.04.006.

[37] Payri, F., Pastor, J. V., García-Oliver, J. M., and Pastor, J. M. "Contribution to the application of two-colour imaging to diesel combustion". In: *Measurement Science and Technology* 18.8 (2007), pp. 2579–2598. DOI: 10.1088/0957-0233/18/8/034.

[38] Payri, R., Gimeno, J., Cardona, S., and Ayyapureddi, S. "Measurement of Soot Concentration in a Prototype Multi-Hole Diesel Injector by High-Speed Color Diffused Back Illumination Technique". In: *SAE Technical Paper 2017-01-2255*. 2017. DOI: 10.4271/2017-01-2255.

[39] Siebers, D. L. "Liquid-Phase Fuel Penetration in Diesel Sprays". In: *SAE Technical Paper 980809* (1998). DOI: 10.4271/980809.

[40] Siebers, D. L. "Scaling liquid-phase fuel penetration in diesel sprays based on mixing-limited vaporization". In: *SAE Technical Paper 1999-01-0528* (1999). DOI: 10.4271/1999-01-0528.

[41] Desantes, J. M., Pastor, J. V., Payri, R., and Pastor, J. M. "Experimental characterization of internal nozzle flow and diesel spray behavior. Part II: Evaporative conditions". In: *Atomization and Sprays* 15.5 (2005), pp. 489–516. DOI: 10.1615/AtomizSpr.v15.i5.20.

[42] Payri, R., Salvador, F. J., Gimeno, J., and Zapata, L. D. "Diesel nozzle geometry influence on spray liquid-phase fuel penetration in evaporative conditions". In: *Fuel* 87.7 (2008), pp. 1165–1176. DOI: 10.1016/j.fuel.2007.05.058.

[43] Payri, R., Gimeno, J., Bracho, G., and Vaquerizo, D. "Study of liquid and vapor phase behavior on Diesel sprays for heavy duty engine nozzles". In: *Applied Thermal Engineering* 107 (2016), pp. 365–378. DOI: 10.1016/j.applthermaleng.2016.06.159.

[44] Carlucci, P., Ficarella, A., and Laforgia, D. "Effects of pilot injection parameters on combustion for common rail diesel engines". In: *SAE Technical Paper 2003-01-0700* (2003). DOI: 10.4271/2003-01-0700.

[45] Lee, J., Jeon, J., Park, J., and Bae, C. "Effect of Multiple Injection Strategies on Emission and Combustion Characteristics in a Single Cylinder Direct-Injection Optical Engine". In: *SAE Technical Paper 2009-01-1354* (2010). DOI: 10.4271/2009-01-1354.

[46] Torregrosa, A. J., Broatch, A., García, A., and Mónico, L. F. "Sensitivity of combustion noise and NOx and soot emissions to pilot injection in PCCI Diesel engines". In: *Applied Energy* 104 (2013), pp. 149–157. DOI: 10.1016/j.apenergy.2012.11.040.

[47] Herfatmanesh, M. R., Lu, P., Attar, M. A., and Zhao, H. "Experimental investigation into the effects of two-stage injection on fuel injection quantity, combustion and emissions in a high-speed optical common rail diesel engine". In: *Fuel* 109 (2013), pp. 137–147. DOI: 10.1016/j.fuel.2013.01.013.

[48] D'Ambrosio, S. and Ferrari, A. "Potential of double pilot injection strategies optimized with the design of experiments procedure to improve diesel engine emissions and performance". In: *Applied Energy* 155 (2015), pp. 918–932. DOI: 10.1016/j.apenergy.2015.06.050.

[49] Pastor, J. V., López, J. J., García-Oliver, J. M., and Pastor, J. M. "A 1D model for the description of mixing-controlled inert diesel sprays". In: *Fuel* 87.13-14 (2008), pp. 2871–2885. DOI: 10.1016/j.fuel.2008.04.017.

[50] Desantes, J. M., Pastor, J. V., García-Oliver, J. M., and Pastor, J. M. "A 1D model for the description of mixing-controlled reacting diesel sprays". In: *Combustion and Flame* 156.1 (2009), pp. 234–249. DOI: 10.1016/j.combustflame.2008.10.008.

[51] Meingast, U., Staudt, M., Reichelt, L., and Renz, U. "Analysis of Spray / Wall Interaction Under Diesel Engine Conditions". In: *SAE Technical Paper 2000-01-0272* (2000). DOI: 10.4271/2000-01-0272.

[52] Payri, R., Gimeno, J., Peraza, J. E., and Bazyn, T. "Spray / wall interaction analysis on an ECN single-hole injector at diesel-like conditions through Schlieren visualization". In: *ILASS Europe 28th Conference on Liquid Atomization and Spray Systems*. Valencia, 2017, pp. 200–207. DOI: 10.4995/ILASS2017.2017.4709.

[53] Zhao, L. et al. "Evaluation of Diesel Spray-Wall Interaction and Morphology around Impingement Location". In: *SAE Technical Paper 2018-01-0276* (2018). DOI: 10.4271/2018-01-0276.

[54] Pickett, L. M. and Lopez, J. J. "Jet-Wall Interaction Effects on Diesel Combustion and Soot Formation". In: *SAE Technical Paper 2005-01-0921* (2005). DOI: 10.4271/2005-01-0921.

[55] Lopez, J. J. and Pickett, L. M. "Jet/wall interaction effects on soot formation in a diesel fuel jet". In: *International Symposium on Diagnostics and Modeling of Combustion in Internal Combustion Engines (COMODIA)* (2004), pp. 387–394.

[56] Beatrice, C., Belardini, P., Bertoli, C., Lisbona, M. G., and Rossi Sebastiano, G. M. "Diesel Combustion control in common rail engines by new injection strategies". In: *International Journal of Engine Research* 3.1 (2002), pp. 23–36. DOI: 10.1243/1468087021545513.

[57] Hotta, Y., Inayoshi, M., Nakakita, K., Fujiwara, K., and Sakata, I. "Achieving Lower Exhaust Emissions and Better Performance in an HSDI Diesel Engine with Multiple Injection". In: *SAE Technical Paper 2005-01-0928* 1.724 (2005). DOI: 10.4271/2005-01-0928.

[58] Yun, H., Sun, Y., and Reitz, R. D. "An Experimental and Numerical Investigation on the Effect of Post Injection Strategies on Combustion and Emissions in the Low-Temperature Diesel Combustion Regime". In: *ASME Internal Combustion Engine Division Spring Technical Conference*. 2005, pp. 25–35. DOI: 10.1115/ices2005-1043.

[59] Desantes, J. M., Arrègle, J., Lopez, J. J., and García, A. "A Comprehensive Study of Diesel Combustion and Emissions with Post-injection". In: *SAE Technical Paper 2007-01-0915* (2007). DOI: 10.4271/2007-01-0915.

[60] Mancaruso, E., Merola, S. S., and Vaglieco, B. M. "Study of the multi-injection combustion process in a transparent direct injection common rail diesel engine by means of optical techniques". In: *International Journal of Engine Research* 9.6 (2008), pp. 483–498. DOI: 10.1243/14680874JER01308.

[61] Bobba, M., Musculus, M. P. B., and Neel, W. "Effect of Post Injections on In-Cylinder and Exhaust Soot for Low-Temperature Combustion in a Heavy-Duty Diesel Engine". In: *SAE International Journal of Engines* 3.1 (2010), pp. 2010–01–0612. DOI: 10.4271/2010-01-0612.

[62] Molina, S., Desantes, J. M., García, A., and Pastor, J. M. "A Numerical Investigation on Combustion Characteristics with the use of Post Injection in DI Diesel Engines". In: *SAE Technical Paper 2010-01-1260* (2010). DOI: 10.4271/2010-01-1260.

[63] Liu, Y. and Reitz, R. D. "Optimizing HSDI Diesel Combustion and Emissions Using Multiple Injection Strategies". In: *SAE Technical Paper 2005-01-0212* (2010). DOI: 10.4271/2005-01-0212.

[64] Barro, C., Tschanz, F., Obrecht, P., and Boulouchos, K. "Influence of Post-Injection Parameters on Soot Formation and Oxidation in a Common-Rail-Diesel Engine Using Multi-Color-Pyrometry". In: *ASME Internal Combustion Engine Division Fall Technical Conference* (2012), pp. 293–302. DOI: 10.1115/icef2012-92075.

[65] O'Connor, J. and Musculus, M. P. B. "Post Injections for Soot Reduction in Diesel Engines: A Review of Current Understanding". In: *SAE International Journal of Engines* 6.1 (2013), pp. 2013–01–0917. DOI: 10.4271/2013-01-0917.

[66] O'Connor, J. and Musculus, M. P. B. "Effects of exhaust gas recirculation and load on soot in a heavy-duty optical diesel engine with close-coupled post injections for high-efficiency combustion phasing". In: *International Journal of Engine Research* 15.4 (2014), pp. 421–443. DOI: 10.1177/1468087413488767.

[67] Plee, S. L. and Ahmad, T. "Relative Roles of Premixed and Diffusion Burning in Diesel Combustion". In: *SAE Technical Paper 831733* (1983). DOI: 10.4271/831733.

[68] Alkidas, A. C. "On the Premixed Combustion in a Direct-Injection Diesel Engine". In: *Journal of Engineering for Gas Turbines and Power* 109.2 (1987), pp. 187–192. DOI: 10.1115/1.3240023.

[69] Badami, M., Mallamo, F., Millo, F., and Rossi, E. E. "Influence of Multiple Injection Strategies on Emissions, Combustion Noise and BSFC of a DI Common Rail Diesel Engine". In: *SAE Technical Paper 2002-01-0503* (2002). DOI: 10.4271/2002-01-0503.

[70] Badami, M., Millo, F., and D'Amato, D. D. "Experimental investigation on soot and NOx formation in a DI common rail diesel engine with pilot injection". In: *SAE Technical Paper 2001-01-0657* (2001). DOI: 10.4271/2001-01-0657.

[71] Payri, F., Broatch, A., Tormos, B., and Marant, V. "New methodology for in-cylinder pressure analysis in direct injection diesel engines - Application to combustion noise". In: *Measurement Science and Technology* 16.2 (2005), pp. 540–547. DOI: 10.1088/0957-0233/16/2/029.

[72] Austen, A. E. W. and Priede, T. "Origins of diesel engine noise". In: *SAE National Diesel Engine Meeting*. SAE International, 1959. DOI: 10.4271/590127.

[73] Priede, T. "Relation between Form of Cylinder-Pressure Diagram and Noise in Diesel Engines". In: *Proceedings of the Institution of Mechanical Engineers: Automobile Division* 14.1 (1960), pp. 63–97. DOI: 10.1243/pime_auto_1960_000_012_02.

[74] Anderton, D. "Relation Between Combustion System and Engine Noise". In: *SAE Technical Paper 790270* (1979). DOI: 10.4271/790270.

[75] Pischinger, F. F., Schmillen, K. P., and Leipold, F. W. "A New Measuring Method for the Direct Determination of Diesel Engine Combustion Noise". In: *SAE Technical Paper 790267* (1979). DOI: 10.4271/790267.

[76] Gómez, J. "Computational assessment of combustion noise of automotive compression-ignited engines". PhD thesis. Universitat Politècnica de València, 2018. DOI: 10.4995/Thesis/10251/112726.

[77] Naber, J. D. and Siebers, D. L. "Effects of Gas Density and Vaporization on Penetration and Dispersion of Diesel Sprays". In: *SAE Technical Paper 960034* (1996). DOI: 10.4271/960034.

Chapter 7

Summary and future works

This chapter aims at summarizing the work carried out and presented throughout the document. In addition, a list of potential developments, new studies, and multiple improvements to the methodology used in this thesis are listed as well.

7.1 Summary

This thesis sought to contribute to the fundamental understanding of the effect of multiple injection strategies on the spray development, in both a non-reactive and reactive atmosphere, using optical diagnostics. A major effort was put in developing new measurement techniques, data processing tools, and image processing routines for multiple injection strategies.

The work was divided into four experimental campaigns, reported and grouped into three chapters based on their specific target, to thoroughly study different aspects of the injection process with multiple events. These were:

- Rate of injection measurements with a two-scale system.
- Momentum flux measurements with an upstream scale to verify and correct for a target injected mass and its allocation between pulses.
- Spray development in evaporative but non-reactive conditions.
- Spray ignition and combustion.

All experiments were carried out with commercially available diesel, and a piezo-actuated hydraulic common-rail injector, fitted with a custom six-hole-nozzle geometry which has an optically isolated spray. Boundary conditions included two different levels of rail pressure, chamber density, and temperature. Two multiple injection strategies were studied: a pilot followed by a main, and a main followed by a post. Four different hydraulic dwell times and two pilot/post quantities were considered. Measurements were made contemplating a constant injected mass of 30 mg, and all conditions were compared with a simple single injection as a reference case.

As mentioned before, the rate of injection measurements included a two-scale system, instead of one usually downstream of the test rig. A purger device was added to the high-pressure unit that was connected to an upstream scale that acted as the fuel deposit. Mass measured by both scales showed an average deviation of 5 %. Consequently, the upstream device was also used to quantify the injected mass in the momentum flux measurements. Small adjustments to the energizing time were made to correct for differences of liquid-liquid and liquid-gas interfaces in the performance of the injector, to maintain the target injected mass. A new processing algorithm was employed to measure the mass distribution among multiple pulses, for both the rate of injection measurements and more importantly, the momentum flux. On average, both pilot and post target masses were achieved with a deviation of 5 % to 20 %, depending on the quantity. In general, the total target mass was achieved with deviations below 2 %.

From the results, a higher shot-to-shot dispersion was observed for the pilot/post injections that are injected in a fully transitory state, that is, when the needle is throttling flow conditions. Increasing the injected quantity reduced the dispersion, with a slight decrease with decreasing rail pressure as well. The repeatability of the post injections was also affected by internal pressure waves within the injector body, especially for reduced dwell times and injected quantities. The mass allocation was accurately estimated with momentum flux measurements, as curves showed remarkable agreement to those of the rate of injection results. The excellent coherence between the data proves the robustness of the new methodology employed. Also, it ascertains the possibility of measuring the injected mass and its allocation (for multiple injection strategies) in the momentum flux rig.

Measurements of the spray development in non-reactive conditions were carried out in an optically accessible high-temperature and high-pressure test rig, using pure nitrogen. A diffused back-illumination setup coupled with a single-pass schlieren imaging allowed a simultaneous visualization of the liquid

and vapor phases. A novel image processing methodology was used to depict the contour of each injection separately, allowing to study their respective evolution independently.

From the results regarding the liquid phase, no influence of the injected quantity of the pilot and its dwell time to the main pulse was observed in the stabilized liquid length and spreading angle. The vaporization length was driven by the chamber density and temperature, as with the standard single injection strategies. Values of the start of injection, calculated from the optical measurements, agreed remarkably well with those obtained from the rate of injection measurements, thus validating the methodology carried out through the different experimental vessels. In reference to the vapor phase, increasing the injected mass of the first pulse pushed the transition zone, in which the injections overlapped, past the optical limit. As the first injection accelerated the stationary gas in the combustion chamber, the second pulse lost less momentum and penetrated at a faster rate than in the single injection case. Vapor phase spreading angle increased with the inclusion of a pilot injection. No clear trend was observed for different pilot quantities or dwell times.

Measurements of the spray development in reactive conditions were carried out in the same optically accessible high-temperature and high-pressure test rig, using atmospheric air. An intensified CCD camera was added to the previous optical setup, equipped with a narrow band-pass filter to visualize OH chemiluminescence and measure the stabilized lift-off length of the main injection. Additional repetitions were recorded with the DBI arrangement with the light source turned off, to quantify the chemiluminescence of soot for optical thickness measurements. The ignition delay of the main could not be accurately measured with the traditional procedure using schlieren imaging. As the premixed phase of combustion is shortened with the inclusion of a pilot injection, the radial expansion was very small or non-existent. Consequently, a novel image processing methodology was developed to decouple the start of combustion of each spray in multiple injection strategies. It is based on the absolute pixel-wise frame-to-frame variation, that quantifies the temporal evolution of pixel structures both in growth and intensity, named rate of difference. The methodology was successfully verified comparing results from a different experimental campaign, that included a high-speed intensified camera to measure ignition delay through a temporal discretization of the OH chemiluminescence.

From the results related with the start of combustion, for all conditions that included multiple injections, the ignition delay of the second pulse de-

creased referenced to its start of injection. The first injection event enhanced local conditions which promoted a faster ignition of the second pulse. On average, pilot-main strategies showed reductions of 30 % to 40 %, while main-post of 40 % to 50 %. Different interaction mechanism found in the literature were used to describe the synergy between injection pulses. For most conditions of the pilot-main strategy at lower temperatures, pulses ignited simultaneously, as the second injection took place during the mixing phase of the first. In such cases, increasing the dwell time lengthened the ignition delay of the pilot. Both the dwell time and pilot quantity affected the interaction mechanisms between injections in different ways. Increasing the dwell time provided a longer period for the pilot injection to mix and ignite before being caught up by the main pulse. On the contrary, increasing the pilot quantity provided a higher momentum as it penetrated further in the combustion chamber, which increased the distance to the main injection, and the time for their interaction. At higher temperatures, all conditions depicted separate combustion events.

From the results concerning the stabilized lift-off length, no definite trend was observed regarding the effects of both the dwell time and the pilot quantity. Some cases showed a slight decrease with increasing dwell time. The average image taken by the ICCD did not consider that lift-off length may change from the inception of combustion to the established diffusion flame. Qualitative measurements of ignition location showed that lift-off length of the main injection should start closer to the nozzle, and slowly shift towards equilibrium in the stabilized diffusion flame.

About the outcome of the soot measurements through the optical thickness, the formation trends followed the results expected from the literature for single injections: it increased with decreasing injection pressure, increasing chamber density and temperature. In general, it was observed that conditions which promoted a faster premixed combustion enhanced soot formation, as most of the fuel is burned in a diffusion flame. Overall, pilot-main strategies produced more soot than each of their reference cases. A slight decrease in the cross-sectional optical thickness near the start of combustion was noted by increasing the pilot quantity. The combustion kernel of the smaller pilot mass stagnated closer to the nozzle, promoting a higher soot production from the main injection. Contrarily, increasing the pilot quantity moved the reaction zone further downstream of the nozzle once ignited, due to its higher momentum. Therefore, the main injection reached the kernel in leaner conditions, which diminished soot formation. These observations were limited to the field of view of the experiments. No clear dependence of soot on the dwell time was observed, as multiple interaction mechanisms between injections can cause non-linear trends depending on many factors. In contrast to

the literature, main-post strategies depicted a slightly higher (or similar) soot formation than a single injection. In combustion chambers with such a large volume, the post injection behaved like a main and the actual main like a pilot. Thus, local conditions enhanced the formation of soot from the post injection, instead of promoting its oxidation. Consequently, jet-wall interactions are critical for the effectiveness of the post injection on reducing soot emissions.

As observed throughout the document, multiple injection strategies result in different spray dynamics that can improve combustion development and subsequent emissions. Nevertheless, they also bring drawbacks. The injection strategies utilized in this thesis require very accurate control of the fuel delivery process, and dwell requirements also implies a reliable and repeatable system. Even using a state of the art injector, the observed shot-to-shot dispersion could affect the performance of the engine. Moreover, aging or deposits that appeared on the injector unit may drastically change its operating performance in a very short span. Therefore, these problems might increase the difficulty in obtaining a robust engine calibration.

7.2 Future directions

The diesel spray development is very complex, as it is comprised of a large number of phenomena and mechanisms that take place in a very fast event. Optical diagnostics provide an excellent tool for non-intrusive analysis of these processes. As technologies improve, so will the quality and possibilities of the experimental measurements to be carried out. A few examples of the potential developments, additional experiments, or improvements to the current database that could provide fruitful information to assess further the statements of this thesis are:

- Use a single-hole nozzle to expand the optical limit. A few of the interactions between injection events could not be properly traced, due to the short field of view of a multi-hole nozzle coupled with line-of-sight visualization. With the optically accessible hardware available, single-hole nozzles can achieve penetration of up to 80 mm with no additional modifications. On the contrary, small pilot/post quantities such as those presented might be difficult to measure in the rate of injection device. However, mass allocation could be determined with the methodology explained in the momentum flux campaign.

- Equip the injector with a nozzle with a smaller conicity factor, that is less prone to the formation of external fuel deposits that affect its hydraulic performance. Consequently, a complete characterization can be carried out with an exact target mass through experimental vessels.

- Employ a high-speed intensified camera to visualize temporal OH chemiluminescence. This provides an optical diagnostic tool to measure ignition delay, ignition location, and the temporal evolution of lift-off length with a single camera.

- Use the upstream scale system to measure the injected mass in the high-temperature and pressure test cell, with a separate cooling system for the fuel, so it does not affect the mass measurements.

- Quantify NOx formation through laser-induced fluorescence to understand the fundamental implications in the soot-NOx trade-off for multiple injection strategies.

- Carry out studies of different bowl-shaped walls inside the combustion chamber to understand how the post injection targets and oxidizes the soot formed by the main pulse. This can be done either by inserting a bowl-shaped part within the combustion chamber or using a rapid compression-expansion machine.

- Implement simple 1-D models that can estimate the equivalence ratios and temperature distributions along the temporal evolution of the spray. They can be validated using the experimental data presented in this work and could provide essential information to improve the fundamental understanding of the spray mixing in closed-couple multiple injection strategies.

- Measure the rate of injection of the suspected fouled injector to quantify the effect of external deposits in the hydraulic performance for multiple injection strategies.

Global Bibliography

Akkurt, B. "Modelling multi-pulse diesel injection with flamelet generated manifolds". PhD thesis. Technische Universiteit Eindhoven, 2019, p. 232 (cited on page 31).

Alkidas, A. C. "On the Premixed Combustion in a Direct-Injection Diesel Engine". In: *Journal of Engineering for Gas Turbines and Power* 109.2 (1987), pp. 187–192. DOI: 10.1115/1.3240023 (cited on pages 12, 28, 186).

Allocca, L., Lazzaro, M., Meccariello, G., and Montanaro, A. "Schlieren visualization of a GDI spray impacting on a heated wall: Non-vaporizing and vaporizing evolutions". In: *Energy* 108 (2016), pp. 93–98. DOI: 10.1016/j.energy.2015.09.107 (cited on page 66).

Altenschmidt, F., Banzhaf, G., Kraus, E., and Loll, S. "The SI-engine - at the end of its development?" In: *16th Conference The Working Process of the Internal Combustion Engine*. Ed. by H. Eichlseder and A. Wimmer. Graz: Verlag der Technischen Universität Graz, 2017, pp. 35–49 (cited on page 1).

Altieri, L. and Tonoli, A. "Piezoelectric Injectors for Automotive Applications: Modeling and Experimental Validation of Hysteretic Behavior and Temperature Effects". In: *Journal of Dynamic Systems, Measurement, and Control* 135.1 (2012), p. 011005. DOI: 10.1115/1.4006627 (cited on pages 55, 94).

Ameen, M. M. and Abraham, J. "RANS and LES Study of Lift-Off Physics in Reacting Diesel Jets". In: *SAE Technical Paper 2014-01-1118* (2014). DOI: 10.4271/2014-01-1118 (cited on page 166).

Anderton, D. “Relation Between Combustion System and Engine Noise”. In: *SAE Technical Paper 790270* (1979). DOI: 10.4271/790270 (cited on pages 28, 186).

Arcoumanis, C., Gavaises, M., Nouri, J. M., and Abdul-Wahab, E. “Analysis of the flow in the nozzle of a vertical multi-hole Diesel engine injector”. In: *SAE Technical Paper 980811* (1998). DOI: 10.4271/980811 (cited on page 51).

Argueyrolles, B. et al. “Influence of injector nozzle design and cavitation on coking phenomenon”. In: *SAE Technical Paper 2007-01-1896* (2007). DOI: 10.4271/2007-01-1896 (cited on page 130).

Armas, O. “Diagnóstico experimental del proceso de combustión en motores Diesel de inyección directa”. PhD thesis. Universitat Politècnica de València, 1998 (cited on page 11).

Armas, O., Ballesteros, R., and Gómez, A. “The effect of diesel engine operating conditions on exhaust particle size distributions”. In: *Proceedings of the Institution of Mechanical Engineers, Part D: Journal of Automobile Engineering* 222.8 (2008), pp. 1513–1525. DOI: 10.1243/09544070JAUTO747 (cited on page 30).

Armas, O., Mata, C., and Martínez-Martínez, S. “Effect of diesel injection parameters on instantaneous fuel delivery using a solenoid-operated injector with different fuels”. In: *Revista Facultad de Ingeniería Universidad de Antioquia* 64 (2012), pp. 9–21 (cited on page 97).

Arrègle, J. “Análisis de la estructura y dinámica interna de chorros Diesel”. PhD thesis. Valencia: Universitat Politècnica de València, 1997 (cited on page 13).

Austen, A. E. W. and Priede, T. “Origins of diesel engine noise”. In: *SAE National Diesel Engine Meeting*. SAE International, 1959. DOI: 10.4271/590127 (cited on pages 28, 186).

Badami, M., Mallamo, F., Millo, F., and Rossi, E. E. “Influence of Multiple Injection Strategies on Emissions, Combustion Noise and BSFC of a DI Common Rail Diesel Engine”. In: *SAE Technical Paper 2002-01-0503* (2002). DOI: 10.4271/2002-01-0503 (cited on pages 2, 28, 104, 105, 186).

Badami, M., Millo, F., and D’Amato, D. D. “Experimental investigation on soot and NOx formation in a DI common rail diesel engine with pilot injection”. In: *SAE Technical Paper 2001-01-0657* (2001). DOI: 10.4271/2001-01-0657 (cited on pages 2, 28, 29, 186).

Baert, R. S. G. et al. "Design and operation of a high pressure, high temperature cell for HD diesel spray diagnostics: guidelines and results". In: *SAE Technical Paper 2009-01-0649* (2009). DOI: 10.4271/2009-01-0649 (cited on pages 2, 61).

Bajaj, C., Ameen, M. M., and Abraham, J. "Evaluation of an unsteady flamelet progress variable model for autoignition and flame lift-off in diesel jets". In: *Combustion Science and Technology* 185.3 (2013), pp. 454–472. DOI: 10.1080/00102202.2012.726667 (cited on page 166).

Baratta, M., Catania, A. E., and Ferrari, A. "Hydraulic Circuit Design Rules to Remove the Dependence of the Injected Fuel Amount on Dwell Time in Multijet CR Systems". In: *Journal of Fluids Engineering* 130.12 (2008). DOI: 10.1115/1.2969443 (cited on page 98).

Bardi, M. "Partial Needle Lift and Injection Rate Shape Effect on the Formation and Combustion of the Diesel Spray". PhD thesis. Universitat Politècnica de València, 2014. DOI: 10.4995/Thesis/10251/37374 (cited on pages 2, 20, 25, 63, 68).

Bardi, M. et al. "Engine Combustion Network: Comparison of Spray Development, Vaporization, and Combustion in Different Combustion Vessels". In: *Atomization and Sprays* 22.10 (2012), pp. 807–842. DOI: 10.1615/AtomizSpr.2013005837 (cited on pages 14, 51, 63, 64, 68, 73, 76, 77, 79, 142, 154).

Barro, C., Tschanz, F., Obrecht, P., and Boulouchos, K. "Influence of Post-Injection Parameters on Soot Formation and Oxidation in a Common-Rail-Diesel Engine Using Multi-Color-Pyrometry". In: *ASME Internal Combustion Engine Division Fall Technical Conference* (2012), pp. 293–302. DOI: 10.1115/icef2012-92075 (cited on pages 29, 30, 182).

Beatrice, C., Belardini, P., Bertoli, C., Lisbona, M. G., and Rossi Sebastiano, G. M. "Diesel Combustion control in common rail engines by new injection strategies". In: *International Journal of Engine Research* 3.1 (2002), pp. 23–36. DOI: 10.1243/1468087021545513 (cited on pages 29, 30, 182).

Benajes, J., Pastor, J. V., Payri, R., and Plazas, A. H. "Analysis of the influence of Diesel nozzle geometry in the Injection Rate characteristic". In: *Journal of Fluids Engineering* 126.1 (2004), pp. 63–71. DOI: 10.1115/1.1637636 (cited on page 20).

Benajes, J., Payri, R., Bardi, M., and Martí-Aldaraví, P. "Experimental characterization of diesel ignition and lift-off length using a single-hole ECN injector". In: *Applied Thermal Engineering* 58.1-2 (2013), pp. 554–563. DOI: 10.1016/j.applthermaleng.2013.04.044 (cited on pages 15–17, 51, 65, 67, 68, 77, 79, 154, 159, 165, 169, 170, 187).

Bermúdez, V., Payri, R., Salvador, F. J., and Plazas, A. H. "Study of the influence of nozzle seat type on injection rate and spray behavior". In: *Proceedings of the Institution of Mechanical Engineers, Part D: Journal of Automobile Engineering*. Vol. 219. 5. 2005, pp. 677–689. DOI: 10.1243/095440705X28303 (cited on page 20).

Binde, A., Busch, S., Velji, A., and Wagner, U. "Soot and NOx Reduction by Spatially Separated Pilot Injection". In: *SAE International Journal of Engines* Binde, A., (2012), pp. 2012–01–1159. DOI: 10.4271/2012-01-1159 (cited on page 29).

Birgel, A. et al. "Deposit Formation in the Holes of Diesel Injector Nozzles: A Critical Review". In: *SAE Technical Paper 2008-01-2383* (2008). DOI: 10.4271/2008-01-2383 (cited on page 130).

Bobba, M., Musculus, M. P. B., and Neel, W. "Effect of Post Injections on In-Cylinder and Exhaust Soot for Low-Temperature Combustion in a Heavy-Duty Diesel Engine". In: *SAE International Journal of Engines* 3.1 (2010), pp. 2010–01–0612. DOI: 10.4271/2010-01-0612 (cited on pages 29, 30, 182).

Boccardo, G. et al. "Experimental investigation on a 3000 bar fuel injection system for a SCR-free non-road diesel engine". In: *Fuel* 243 (2019), pp. 342–351. DOI: 10.1016/j.fuel.2019.01.122 (cited on page 18).

Boehner, W. and Hummel, K. "Common Rail Injection System for Commercial Diesel Vehicles". In: *SAE Technical Paper 970345* (1997). DOI: 10.4271/970345 (cited on pages 17, 18).

Borz, M. J., Kim, Y., and O'Connor, J. "The Effects of Injection Timing and Duration on Jet Penetration and Mixing in Multiple-Injection Schedules". In: *SAE Technical Paper 2016-01-0856* (2016). DOI: 10.4271/2016-01-0856 (cited on page 144).

Bosch, W. "The Fuel Rate Indicator: A New Measuring Instrument For Display of the Characteristics of Individual Injection". In: *SAE Technical Paper 660749* (1966). DOI: 10.4271/660749 (cited on page 52).

Bruneaux, G. "Development of optical diagnostics techniques to correlate mixing and auto-ignition processes in high pressure diesel jets". In: *Oil & Gas Science and Technology* 63.4 (2008), pp. 461–477. DOI: 10.2516/ogst:2008031 (cited on page 15).

Bruneaux, G. and Maligne, D. "Study of the Mixing and Combustion Processes of Consecutive Short Double Diesel Injections". In: *SAE International Journal of Engines* 2.1 (2009), pp. 2009–01–1352. DOI: 10.4271/2009-01-1352 (cited on pages 2, 22, 28, 31, 138, 161, 163, 165, 167, 171, 186).

Busch, S. et al. "Experimental and Numerical Investigations of Close-Coupled Pilot Injections to Reduce Combustion Noise in a Small-Bore Diesel Engine". In: *SAE International Journal of Engines* 8.2 (2015), pp. 2015–01–0796. DOI: 10.4271/2015-01-0796 (cited on pages 28, 161, 163, 186).

Caprotti, R., Breakspear, A., Graupner, O., and Klaua, T. "Detergency Requirements of Future Diesel Injection Systems". In: *SAE Technical Paper 2005-01-3901* (2005). DOI: 10.4271/2005-01-3901 (cited on page 130).

Caprotti, R., Breakspear, A., Graupner, O., Klaua, T., and Kohnen, O. "Diesel injector deposits potential in future fueling systems". In: *SAE Technical Paper 2006-01-3359* (2006). DOI: 10.4271/2006-01-3359 (cited on page 130).

Carlucci, P., Ficarella, A., and Laforgia, D. "Effects of pilot injection parameters on combustion for common rail diesel engines". In: *SAE Technical Paper 2003-01-0700* (2003). DOI: 10.4271/2003-01-0700 (cited on pages 28, 29, 171, 186).

Carlucci, P., Ficarella, A., and Laforgia, D. "Effects on combustion and emissions of early and pilot fuel injections in diesel engines". In: *International Journal of Engine Research* 6.1 (2005), pp. 43–60. DOI: 10.1243/146808705X7301 (cited on pages 27, 29).

Carreres, M. "Thermal effects influence on the Diesel injector performance through a combined 1D modelling and experimental approach". PhD thesis. Universitat Politècnica de València, 2016. DOI: 10.4995/Thesis/10251/73066 (cited on pages 20, 97–99, 104, 105, 109, 130, 138).

Chaplya, P. M., Mitrovic, M., Carman, G. P., and Straub, F. K. "Durability properties of piezoelectric stack actuators under combined electromechanical loading". In: *Journal of Applied Physics* 100.12 (2006), p. 124111. DOI: 10.1063/1.2407269 (cited on page 20).

Chartier, C., Aronsson, U., Andersson, Ö., Egnell, R., and Johansson, B. "Influence of jet-jet interactions on the lift-off length in an optical heavy-duty DI diesel engine". In: *Fuel* 112 (2013), pp. 311–318. DOI: 10.1016/j.fuel.2013.05.021 (cited on page 165).

Chaves, H., Kirmse, C., and Obermeier, F. "Velocity measurements of dense diesel fuel sprays in dense air". In: *Atomization and Sprays* 14.6 (2004), pp. 589–609. DOI: 10.1615/AtomizSpr.v14.i6.60 (cited on page 22).

Connors, K. *Chemical Kinetics:The Study of Reaction Rates in Solution.* Wiley-VCH, 1990 (cited on pages 164, 168).

Correas, D. "Estudio teórico-experimental del chorro libre Diesel isotermo". PhD thesis. Valencia: Universitat Politècnica de València, 1998 (cited on pages 11, 13, 22).

Cung, K. et al. "Spray-combustion interaction mechanism of multiple-injection under diesel engine conditions". In: *Proceedings of the Combustion Institute* 35.3 (2015), pp. 3061–3068. DOI: 10.1016/j.proci.2014.07.054 (cited on pages 138, 165).

D'Ambrosio, S. and Ferrari, A. "Diesel Injector Coking: Optical-Chemical Analysis of Deposits and Influence on Injected Flow-Rate, Fuel Spray and Engine Performance". In: *Journal of Engineering for Gas Turbines and Power* 134.6 (2012). DOI: 10.1115/1.4005991 (cited on page 130).

D'Ambrosio, S. and Ferrari, A. "Potential of double pilot injection strategies optimized with the design of experiments procedure to improve diesel engine emissions and performance". In: *Applied Energy* 155 (2015), pp. 918–932. DOI: 10.1016/j.apenergy.2015.06.050 (cited on pages 28, 171, 186).

De Lima Moradell, D. "Analysis of combustion concepts in a poppet valve two-stroke downsized compression ignition engine designed for passenger car applications". PhD thesis. Universitat Politècnica de València, 2016. DOI: 10.4995/Thesis/10251/68502 (cited on pages 25, 26).

Dec, J. E. "A Conceptual Model of DI Diesel Combustion Based on Laser-Sheet Imaging". In: *SAE Technical Paper 970873* (1997) (cited on page 16).

Dec, J. E. and Canaan, R. E. "PLIF Imaging of NO Formation in a DI Diesel Engine". In: *SAE Technical Paper 980147* (1998). DOI: 10.4271/980147 (cited on page 17).

Dec, J. E. and Coy, E. B. "OH Radical Imaging in a DI Diesel Engine and the Structure of the Early Diffusion Flame". In: *SAE Technical Paper 960831* (1996). DOI: 10.4271/960831 (cited on pages 16, 67).

Dec, J. E. and Espey, C. "Chemiluminescence Imaging of Autoignition in a DI Diesel Engine". In: *SAE Technical Paper 982685* 724 (1998). DOI: 10.4271/982685 (cited on pages 68, 159).

Delacourt, E., Desmet, B., and Besson, B. "Characterisation of very high pressure Diesel sprays using digital imaging techniques". In: *Fuel* 84.7-8 (2005), pp. 859–867. DOI: 10.1016/j.fuel.2004.12.003 (cited on page 24).

Desantes, J. M., Arrègle, J., Lopez, J. J., and García, A. "A Comprehensive Study of Diesel Combustion and Emissions with Post-injection". In: *SAE Technical Paper 2007-01-0915* (2007). DOI: 10.4271/2007-01-0915 (cited on pages 29–31, 182).

Desantes, J. M., García-Oliver, J. M., García, A., and Xuan, T. "Optical study on characteristics of non-reacting and reacting diesel spray with different strategies of split injection". In: *International Journal of Engine Research* 301 (2018). DOI: 10.1177/1468087418773012 (cited on pages 2, 28, 31, 81, 161, 163, 167, 169, 171, 178, 186).

Desantes, J. M., García-Oliver, J. M., Pastor, J. M., and Pandal, A. "A Comparison of Diesel Sprays CFD Modeling Approaches: Ddm Versus E-Y Eulerian Atomization Model". In: *Atomization and Sprays* 26.7 (2016), pp. 713–737. DOI: 10.1615/AtomizSpr.2015013285 (cited on page 51).

Desantes, J. M., Pastor, J. V., García-Oliver, J. M., and Pastor, J. M. "A 1D model for the description of mixing-controlled reacting diesel sprays". In: *Combustion and Flame* 156.1 (2009), pp. 234–249. DOI: 10.1016/j.combustflame.2008.10.008 (cited on pages 3, 22, 178).

Desantes, J. M., Pastor, J. V., Payri, R., and Pastor, J. M. "Experimental characterization of internal nozzle flow and diesel spray behavior. Part II: Evaporative conditions". In: *Atomization and Sprays* 15.5 (2005), pp. 489–516. DOI: 10.1615/AtomizSpr.v15.i5.20 (cited on pages 24, 169).

Desantes, J. M., Payri, R., Gimeno, J., and Martí-Aldaraví, P. "Simulation of the First Millimeters of the Diesel Spray by an Eulerian Spray Atomization Model Applied on ECN Spray A Injector". In: *SAE Technical Paper 2014-01-1418*. 2014. DOI: 10.4271/2014-01-1418 (cited on page 51).

Desantes, J. M., Payri, R., Salvador, F. J., and Gil, A. "Development and validation of a theoretical model for diesel spray penetration". In: *Fuel* 85.7-8 (2006), pp. 910–917 (cited on page 22).

Desantes, J. M., Payri, R., Salvador, F. J., and Gimeno, J. "Measurements of spray momentum for the study of cavitation in diesel injection nozzles". In: *SAE Technical Paper 2003-01-0703* (2003). DOI: 10.4271/2003-01-0703 (cited on page 109).

Desantes, J. M., Salvador, F. J., Carreres, M., and Martínez-López, J. "Large-eddy simulation analysis of the influence of the needle lift on the cavitation in diesel injector nozzles". In: *Proceedings of the Institution of Mechanical Engineers, Part D: Journal of Automobile Engineering* 229.4 (2014), pp. 407–423. DOI: 10.1177/0954407014542627 (cited on page 21).

Dronniou, N., Lejeune, M., Balloul, I., and Higelin, P. "Combination of High EGR Rates and Multiple Injection Strategies to Reduce Pollutant Emissions". In: *SAE Technical Paper 2005-01-3726* (2005). DOI: 10.4271/2005-01-3726 (cited on page 30).

Duke, D. J. et al. "Internal and near nozzle measurements of Engine Combustion Network Spray G gasoline direct injectors". In: *Experimental Thermal and Fluid Science* 88 (2017), pp. 608–621. DOI: 10.1016/j.expthermflusci.2017.07.015 (cited on page 63).

Dürnholz, M., Endres, H., and Frisse, P. "Preinjection A Measure to Optimize the Emission Behavior of DI-Diesel Engine". In: *SAE Technical Paper 940674* (1994). DOI: 10.4271/940674 (cited on pages 28, 161, 163, 186).

Engine Combustion Network. *https://ecn.sandia.gov/diesel-spray-combustion/*. Online. 2010 (cited on pages 3, 51, 54, 79, 93, 123).

Espey, C. and Dec, J. E. "The effect of TDC temperature and density on the liquid-phase fuel penetration in a D.I. Diesel engine". In: *SAE Technical Paper 952456* (1995). DOI: 10.4271/952456 (cited on pages 14, 23).

Estepa Ruiz, D. "Study of different fuel injection and air management strategies as a tool for emissions control in a compression ignition engine (Diesel engine)." PhD thesis. Universitat Politècnica de València, 2018. DOI: 10.4995/Thesis/10251/113076 (cited on pages 25, 26).

European Parliament. "Regulation (EC) No 715". In: *The Council Of The European Union - Official journal of the European Union*. Vol. L171. 2007 (cited on page 1).

Fansler, T. D. and Parrish, S. E. "Spray measurement technology: a review". In: *Measurement Science and Technology* 26.1 (2015), p. 012002. DOI: 10.1088/0957-0233/26/1/012002 (cited on pages 1, 2).

Fitzgerald, R. P., Svensson, K., Martin, G., Qi, Y., and Koci, C. "Early Investigation of Ducted Fuel Injection for Reducing Soot in Mixing-Controlled Diesel Flames". In: *SAE Technical Paper 2018-01-0238* (2018), pp. 1–17. DOI: 10.4271/2018-01-0238 (cited on page 62).

Flaig, U., Polach, W., and Ziegler, G. "Common Rail System (CR-System) for Passenger Car DI Diesel Engines ; Experiences with Applications for Series Production Projects". In: *SAE Technical Paper 1999-01-0191* (1999). DOI: 10.4271/1999-01-0191 (cited on page 17).

Flynn, P. et al. "Diesel combustion: an integrated view combining laser diagnostics, chemical kinetics, and empirical validation". In: *SAE Technical Paper 1999-01-0509* 724 (1999) (cited on page 16).

Fox, T. A. and Stark, J. "Discharge coefficients for miniature fuel injectors". In: *Aerospace Engineering* 203.1 (1989), pp. 75–78. DOI: 10.1243/PIME_PROC_1989_203_056_01 (cited on page 21).

Frijters, P. J. M., Seykens, X. L. J., Somers, L. M. T., and Klein-Douwel, R. J. H. "Gas Density and Rail Pressure Effects on Diesel Spray Growth from a Heavy-Duty Common Rail Injector". In: *Energy & Fuels* 23.2 (2009), pp. 1832–1842. DOI: 10.1021/ef8003569 (cited on pages 136, 141).

Fujimoto, H., Arai, M., Senda, J., Suzuki, H., and Myong, K. "Vaporization Characteristics and Liquid-Phase Penetration for Multi-Component Fuels". In: *SAE Technical Paper 2004-01-0529* (2004). DOI: 10.4271/2004-01-0529 (cited on page 23).

García-Oliver, J. M. "Aportaciones al estudio del proceso de combustión turbulenta de chorros en motores Diesel de inyección directa". PhD thesis. Valencia: Universitat Politècnica de València, 2004. DOI: 10.4995/Thesis/10251/55164 (cited on pages 11–13, 133, 136, 141, 159, 186).

Gaydon, A. G. *The Spectroscopy of Flames*. Springer, 1974. DOI: 10.1007/978-94-009-5720-6 (cited on pages 67, 68).

Ghandhi, J. B. and Heim, D. M. "An optimized optical system for backlit imaging". In: *Review of Scientific Instruments* 80.5 (2009). DOI: 10.1063/1.3128728 (cited on page 64).

Gimeno, J. "Desarrollo y aplicación de la medida del flujo de cantidad de movimiento de un chorro diesel". PhD thesis. Universitat Politècnica de València, 2008. DOI: 10.4995/Thesis/10251/8306 (cited on pages 13, 19–22, 24, 57, 59, 97, 109, 115, 141).

Giraldo Valderrama, J. S. "Macroscopic and microscopic characterization of non-reacting diesel sprays at low and very high injection pressures". PhD thesis. Universitat Politècnica de València, 2018. DOI: 10.4995/Thesis/10251/113643 (cited on pages 2, 18, 22).

Gladstone, J. H. and Dale, T. P. "Researches on the Refraction, Dispersion, and Sensitiveness of Liquids". In: *Proceedings of the Royal Society of London* 12 (1862), pp. 448–453. DOI: 10.1098/rstl.1863.0014 (cited on page 65).

Gómez, J. "Computational assessment of combustion noise of automotive compression-ignited engines". PhD thesis. Universitat Politècnica de València, 2018. DOI: 10.4995/Thesis/10251/112726 (cited on pages 28, 186, 187).

Han, J.-S. et al. "Dynamics of Multiple-Injection Fuel Sprays in a Small-bore HSDI Diesel Engine". In: *SAE Technical Paper 2000-01-1256* (2000). DOI: 10.4271/2000-01-1256 (cited on page 98).

Han, M., Assanis, D. N., and Bohac, S. V. "Sources of hydrocarbon emissions from low-temperature premixed compression ignition combustion from a common rail direct injection diesel engine". In: *Combustion Science and Technology* 181.3 (2009), pp. 496–517. DOI: 10.1080/00102200802530066 (cited on page 30).

Han, S., Kim, J., and Bae, C. "Effect of air-fuel mixing quality on characteristics of conventional and low temperature diesel combustion". In: *Applied Energy* 119 (2014), pp. 454–466. DOI: 10.1016/j.apenergy.2013.12.045 (cited on page 1).

Han, Z., Uludogan, A., Hampson, G. J., and Reitz, R. D. "Mechanism of Soot and NOx Emission Reduction Using Multiple-injection in a Diesel Engine". In: *SAE Technical Paper 960633* (1996). DOI: 10.4271/960633 (cited on pages 2, 28).

El-hannouny, E. M. et al. "Near-Nozzle Spray Characteristics of Heavy-Duty Diesel Injectors". In: *SAE Technical Paper 2003-01-3150* 724 (2013). DOI: 10.1016/B978-0-444-88351-3.50017-9 (cited on page 63).

Herfatmanesh, M. R., Lu, P., Attar, M. A., and Zhao, H. "Experimental investigation into the effects of two-stage injection on fuel injection quantity, combustion and emissions in a high-speed optical common rail diesel engine". In: *Fuel* 109 (2013), pp. 137–147. DOI: 10.1016/j.fuel.2013.01.013 (cited on pages 31, 171).

Heywood, J. B. *Internal Combustion Engine Fundamentals*. McGraw-Hill, 1988 (cited on pages 11, 12, 15).

Higgins, B. S., Mueller, C. J., and Siebers, D. L. "Measurements of Fuel Effects on Liquid-Phase Penetration in DI Sprays". In: *SAE Technical Paper 1999-01-0519* (1999). DOI: 10.4271/1999-01-0519 (cited on pages 14, 23, 133).

Higgins, B. S. and Siebers, D. L. "Measurement of the Flame Lift-Off Location on DI Diesel Sprays Using OH Chemiluminescence". In: *SAE Technical Paper 2001-01-0918* (2001). DOI: 10.4271/2001-01-0918 (cited on pages 16, 17, 67, 68).

Higgins, B. S., Siebers, D. L., and Aradi, A. "Diesel-Spray Ignition and Premixed-Burn Behavior". In: *SAE Technical Paper 2000-01-0940* (2000). DOI: 10.4271/2000-01-0940 (cited on pages 14, 28, 159, 170, 186).

Hiroyasu, H. and Arai, M. "Structures of Fuel Sprays in Diesel Engines". In: *SAE Technical Paper 900475*. 1990. DOI: 10.4271/900475 (cited on pages 22–24).

Hiroyasu, H., Arai, M., and Tabata, M. "Empirical equations for the Sauter mean diameter of Diesel spray". In: *SAE Technical Paper 890464* (1989). DOI: 10.4271/890464 (cited on page 22).

Hotta, Y., Inayoshi, M., Nakakita, K., Fujiwara, K., and Sakata, I. "Achieving Lower Exhaust Emissions and Better Performance in an HSDI Diesel Engine with Multiple Injection". In: *SAE Technical Paper 2005-01-0928* 1.724 (2005). DOI: 10.4271/2005-01-0928 (cited on pages 29, 30, 182).

Hulkkonen, T., Sarjovaara, T., Kaario, O., Hamalainen, I., and Larmi, M. "Experimental Study of Conical Diesel Nozzle Orifice Geometry". In: *Atomization and Sprays* 25.6 (2015), pp. 519–538. DOI: 10.1615/AtomizSpr.2015010383 (cited on page 63).

Ishida, M., Chen, Z.-L., Luo, G.-F., and Ueki, H. "The Effect of Pilot Injection on Combustion in a Turbocharged D. I. Diesel Engine". In: *SAE Technical Paper 941692* (1996). DOI: 10.4271/941692 (cited on page 28).

Jafer, D. "Pilot Injection". In: *Engineering* (1937) (cited on page 28).

Jakob, M. et al. "Simultaneous high-speed visualization of soot luminosity and OH * chemiluminescence of alternative-fuel combustion in a HSDI diesel engine under realistic operating conditions". In: *Combustion and Flame* 159.7 (2012), pp. 2516–2529. DOI: 10.1016/j.combustflame.2012.03.004 (cited on pages 154, 158, 187).

Johnson, J. E. et al. "Characteristics of 3000 bar Diesel Spray Injection under Non-Vaporizing and Vaporizing Conditions". In: *ICLASS 12th Triennial International Conference on Liquid Atomization and Spray Systems*. Heidelberg, 2012 (cited on page 18).

Johnson, J. E. et al. “Correlations of Non-Vaporizing Spray Penetration for 3000 Bar Diesel Spray Injection”. In: *SAE Technical Paper 2013-24-0033* (2013). DOI: 10.4271/2013-24-0033 (cited on page 18).

Johnson, T. V. “Diesel engine emissions and their control”. In: *Platinum Metals Review* 52.1 (2008), pp. 23–37. DOI: 10.1595/147106708X248750 (cited on page 1).

Johnson, T. V. “Diesel Emission in Review”. In: *SAE Technical Paper 2011-01-0304* (2011). DOI: 10.4271/2011-01-0304 (cited on page 1).

Jorques Moreno, C., Stenlaas, O., and Tunestal, P. “Influence of Small Pilot on Main Injection in a Heavy-Duty Diesel Engine”. In: *SAE Technical Paper 2017-01-0708* (2017). DOI: 10.4271/2017-01-0708.Copyright (cited on pages 163, 168).

Jung, Y., Manin, J., Skeen, S. A., and Pickett, L. M. “Measurement of Liquid and Vapor Penetration of Diesel Sprays with a Variation in Spreading Angle”. In: *SAE Technical Paper 2015-01-0946* (2015). DOI: 10.4271/2015-01-0946 (cited on pages 2, 24, 51, 64, 76, 133, 141).

Kamimoto, T. and Bae, M.-h. “High Combustion Temperature for the Reduction of Particulate in Diesel Engines”. In: *SAE Technical Paper 880423* (1988). DOI: 10.4271/880423 (cited on page 26).

Karimi, K. “Characterisation of Multiple-Injection Diesel Sprays at Elevated Pressures and Temperatures”. PhD thesis. University of Brighton, 2007 (cited on pages 134, 138).

Kastengren, A. L. et al. “Correlation of Split-Injection Needle Lift and Spray Structure”. In: *SAE Technical Paper 2011-01-0383* (2011). DOI: 10.4271/2011-01-0383 (cited on pages 31, 144).

Kastengren, A. L. et al. “End-of-Injection Behavior of Diesel Sprays Measured With X-Ray Radiography”. In: *Journal of Engineering for Gas Turbines and Power* 134.9 (2012). DOI: 10.1115/1.4006981 (cited on page 130).

Kastengren, A. L. et al. “Engine Combustion Network (ECN): Measurements of Nozzle Geometry and Hydraulic Behavior”. In: *Atomization and Sprays* 22.12 (2012), pp. 1011–1052. DOI: 10.1615/AtomizSpr.2013006309 (cited on pages 20, 51).

Kastengren, A. L. et al. “Measurements of droplet size in shear-driven atomization using ultra-small angle x-ray scattering”. In: *International Journal of Multiphase Flow* 92 (2017), pp. 131–139. DOI: 10.1016/j.ijmultiphaseflow.2017.03.005 (cited on pages 22, 63).

Knox, B. and Genzale, C. L. "Effects of End-of-Injection Transients on Combustion Recession in Diesel Sprays". In: *SAE International Journal of Engines* 9.2 (2016), pp. 2016–01–0745. DOI: 10.4271/2016-01-0745 (cited on page 66).

Kobori, S., Kamimoto, T., and Aradi, A. "A study of ignition delay of diesel fuel sprays". In: *International Journal of Engine Research* 1.29 (2000), pp. 29–39. DOI: 10.1243/1468087001545245 (cited on page 15).

Kook, S. and Pickett, L. M. "Liquid length and vapor penetration of conventional, Fischer-Tropsch, coal-derived, and surrogate fuel sprays at high-temperature and high-pressure ambient conditions". In: *Fuel* 93 (2012), pp. 539–548. DOI: 10.1016/j.fuel.2011.10.004 (cited on page 66).

Kook, S., Pickett, L. M., and Musculus, M. P. B. "Influence of Diesel Injection Parameters on End-of-Injection Liquid Length Recession". In: *SAE International Journal of Engines* 2.1 (2009), pp. 2009–01–1356. DOI: 10.4271/2009-01-1356 (cited on page 130).

Lacey, P. et al. "Fuel Quality and Diesel Injector Deposits". In: *SAE International Journal of Fuels and Lubricants* 5.3 (2012), pp. 2012–01–1693. DOI: 10.4271/2012-01-1693 (cited on page 130).

Lahaye, J. "Mechanisms of soot formation". In: *Polymer Degradation and Stability* 30.1 (1990), pp. 111–121. DOI: 10.1016/0141-3910(90)90121-M (cited on pages 17, 29).

Lapuerta, M., Sanz-Argent, J., and Raine, R. R. "Ignition Characteristics of Diesel Fuel in a Constant Volume Bomb under Diesel-Like Conditions. Effect of the Operation Parameters". In: *Energy and Fuels* 28.8 (2014), pp. 5445–5454. DOI: 10.1021/ef500535j (cited on page 159).

Lee, J., Jeon, J., Park, J., and Bae, C. "Effect of Multiple Injection Strategies on Emission and Combustion Characteristics in a Single Cylinder Direct-Injection Optical Engine". In: *SAE Technical Paper 2009-01-1354* (2010). DOI: 10.4271/2009-01-1354 (cited on pages 2, 26, 28, 171).

Lee, J. et al. "Effect of piezo-driven and solenoid-driven needle opening of common-rail diesel injectors on internal nozzle flow and spray development". In: *International Journal of Engine Research* 7.6 (2006), pp. 489–502. DOI: 10.1243/14680874JER00806 (cited on page 20).

Leedham, A., Caprotti, R., Graupner, O., and Klaua, T. "Impact of Fuel Additives on Diesel Injector Deposits". In: *SAE Technical Paper 2004-01-2935* (2004). DOI: 10.4271/2004-01-2935 (cited on page 130).

Levy, N., Amara, S., Champoussin, J. C., and Guerrassi, N. "Non-Reactive Diesel Spray Computations Supported by PDA Measurements". In: *SAE Technical Paper 970049* (1997). DOI: 10.4271/970049 (cited on page 13).

Li, T. and Ogawa, H. "Analysis of the Trade-off between Soot and Nitrogen Oxides in Diesel-Like Combustion by Chemical Kinetic Calculation". In: *SAE International Journal of Engines* (2011), pp. 2011–01–1847. DOI: 10.4271/2011-01-1847 (cited on pages 25, 26, 29).

Li, T., Suzuki, M., and Ogawa, H. "Characteristics of Smokeless Low Temperature Diesel Combustion in Various Fuel-Air Mixing and Expansion of Operating Load Range". In: *SAE Technical Paper 2009-01-1449* (2009). DOI: 10.4271/2009-01-1449 (cited on page 26).

Lillo, P. M., Pickett, L. M., Persson, H., Andersson, Ö., and Kook, S. "Diesel Spray Ignition Detection and Spatial/Temporal Correction". In: *SAE International Journal of Engines* 5.3 (2012), pp. 2012–01–1239. DOI: 10.4271/2012-01-1239 (cited on pages 15, 63, 65, 66, 154).

Liu, Y. and Reitz, R. D. "Optimizing HSDI Diesel Combustion and Emissions Using Multiple Injection Strategies". In: *SAE Technical Paper 2005-01-0212* (2010). DOI: 10.4271/2005-01-0212 (cited on pages 27–30, 182).

Lopez, J. J. and Pickett, L. M. "Jet/wall interaction effects on soot formation in a diesel fuel jet". In: *International Symposium on Diagnostics and Modeling of Combustion in Internal Combustion Engines (COMODIA)* (2004), pp. 387–394 (cited on pages 30, 182).

Macian, V., Payri, R., García, A., and Bardi, M. "Experimental Evaluation of the Best Approach for Diesel Spray Images Segmentation". In: *Experimental Techniques* 36.6 (2012), pp. 26–34. DOI: 10.1111/j.1747-1567.2011.00730.x (cited on page 24).

Macian, V., Payri, R., Ruiz, S., Bardi, M., and Plazas, A. H. "Experimental study of the relationship between injection rate shape and Diesel ignition using a novel piezo-actuated direct-acting injector". In: *Applied Energy* 118 (2014), pp. 100–113. DOI: 10.1016/j.apenergy.2013.12.025 (cited on page 20).

Maes, N., Bakker, P. C., Dam, N., and Somers, B. "Transient Flame Development in a Constant-Volume Vessel Using a Split-Scheme Injection Strategy". In: *SAE International Journal of Fuels and Lubricants* 10.2 (2017), pp. 2017–01–0815. DOI: 10.4271/2017-01-0815 (cited on pages 31, 154, 158, 161, 165, 167, 168).

Maes, N. et al. “Experimental and Numerical Analyses of Liquid and Spray Penetration under Heavy-Duty Diesel Engine Conditions”. In: *SAE International Journal of Fuels and Lubricants* 9.1 (2016), pp. 108–124. DOI: 10.4271/2016-01-0861 (cited on pages 133, 136).

Mancaruso, E., Merola, S. S., and Vaglieco, B. M. “Study of the multi-injection combustion process in a transparent direct injection common rail diesel engine by means of optical techniques”. In: *International Journal of Engine Research* 9.6 (2008), pp. 483–498. DOI: 10.1243/14680874JER01308 (cited on pages 29, 182).

Manin, J., Bardi, M., and Pickett, L. M. “Evaluation of the liquid length via diffused back-illumination imaging in vaporizing diesel sprays”. In: *The Proceedings of the International symposium on diagnostics and modeling of combustion in internal combustion engines*. Vol. 8. Fukuoka, 2012, pp. 665–673. DOI: 10.1299/jmsesdm.2012.8.665 (cited on pages 64, 65, 74, 133).

Manin, J., Bardi, M., Pickett, L. M., Dahms, R. N., and Oefelein, J. C. “Microscopic investigation of the atomization and mixing processes of diesel sprays injected into high pressure and temperature environments”. In: *Fuel* 134 (2014), pp. 531–543. DOI: 10.1016/j.fuel.2014.05.060 (cited on pages 2, 23, 63, 64, 138).

Manin, J., Bardi, M., Pickett, L. M., and Payri, R. “Boundary condition and fuel composition effects on injection processes of high-pressure sprays at the microscopic level”. In: *International Journal of Multiphase Flow* 83 (2016), pp. 267–278. DOI: 10.1016/j.ijmultiphaseflow.2015.12.001 (cited on pages 23, 78).

Manin, J., Kastengren, A. L., and Payri, R. “Understanding the Acoustic Oscillations Observed in the Injection Rate of a Common-Rail Direct Injection Diesel Injector”. In: *Journal of Engineering for Gas Turbines and Power* 134.12 (2012). DOI: 10.1115/1.4007276 (cited on page 107).

Manin, J., Pickett, L. M., and Skeen, S. A. “Two-Color Diffused Back-Illumination Imaging as a Diagnostic for Time-Resolved Soot Measurements in Reacting Sprays”. In: *SAE International Journal of Engines* 6.4 (2013), pp. 2013–01–2548. DOI: 10.4271/2013-01-2548 (cited on pages 2, 64, 80).

Manin, J., Pickett, L. M., and Yasutomi, K. “Transient cavitation in transparent diesel injectors”. In: *ICLASS 14th Triennial International Conference on Liquid Atomization and Spray Systems*. Chicago, 2018, pp. 1–9 (cited on pages 2, 97, 98, 104, 107, 130, 138).

Martínez-López, J. "Estudio computacional de la influencia del levantamiento de aguja sobre el flujo interno y el fenómeno de la cavitación en toberas de inyección Diesel". PhD thesis. Valencia: Universitat Politecnica de Valencia, 2013 (cited on page 21).

Martínez-Martínez, S. "Desarrollo de una instalación experimental para el estudio de chorros diesel evaporados en atmósfera inerte y reactiva". PhD thesis. Universitat Politècnica de València, 2003 (cited on pages 14, 23).

Meijer, M., Malbec, L. M., Bruneaux, G., and Somers, B. "Engine Combustion Network: Spray A Basic Measurements and Advanced Diagnostics". In: *ICLASS 12th Triennial International Conference on Liquid Atomization and Spray Systems*. 2012 (cited on page 51).

Meijer, M. et al. "Engine Combustion Network (ECN): Characterization and Comparison of Boundary Conditions for Different Combustion Vessels". In: *Atomization and Sprays* 22.9 (2012), pp. 777–806. DOI: 10.1615/AtomizSpr.2012006083 (cited on pages 51, 61, 62).

Meingast, U., Staudt, M., Reichelt, L., and Renz, U. "Analysis of Spray / Wall Interaction Under Diesel Engine Conditions". In: *SAE Technical Paper 2000-01-0272* (2000). DOI: 10.4271/2000-01-0272 (cited on page 182).

Mendez, S. and Thirouard, B. "Using Multiple Injection Strategies in Diesel Combustion: Potential to Improve Emissions, Noise and Fuel Economy Trade-Off in Low CR Engines". In: *SAE International Journal of Fuels and Lubricants* (2010), pp. 2008–01–1329. DOI: 10.4271/2008-01-1329 (cited on pages 26, 28, 31, 159, 186).

Miles, R. B. "Optical diagnostics for high-speed flows". In: *Progress in Aerospace Sciences* 72 (2015), pp. 30–36. DOI: 10.1016/j.paerosci.2014.09.007 (cited on page 63).

Mingfa, Y., Hu, W., Zunqing, Z., and Yan, Y. "Experimental Study of Multiple Injections and Coupling Effects of Multi-Injection and EGR in a HD Diesel Engine". In: *SAE Technical Paper 2009-01-2807* (2009). DOI: 10.4271/2009-01-2807 (cited on pages 2, 26, 28, 29, 155, 159, 167, 171, 186).

Mohan, B., Yang, W., and Chou, S. K. "Fuel injection strategies for performance improvement and emissions reduction in compression ignition engines: a review". In: *Renewable and Sustainable Energy Reviews* 28 (2013), pp. 664–676. DOI: 10.1016/j.rser.2013.08.051 (cited on pages 28, 31).

Molina, S. *Influencia de los parámetros de inyección y la recirculación de gases de escape sobre el proceso de combustión en un motor diesel*. Ed. by F. Payri and J. M. Desantes. Barcelona, 2005 (cited on pages 12, 16).

Molina, S., Desantes, J. M., García, A., and Pastor, J. M. "A Numerical Investigation on Combustion Characteristics with the use of Post Injection in DI Diesel Engines". In: *SAE Technical Paper 2010-01-1260* (2010). DOI: 10.4271/2010-01-1260 (cited on pages 29–31, 182).

Montanaro, A. et al. "Schlieren and Mie Scattering Visualization for Single-Hole Diesel Injector under Vaporizing Conditions with Numerical Validation". In: *SAE Technical Paper 2014-01-1406* (2014). DOI: 10.4271/2014-01-1406 (cited on pages 66, 133, 136).

Moon, S., Huang, W., Li, Z., and Wang, J. "End-of-injection fuel dribble of multi-hole diesel injector: Comprehensive investigation of phenomenon and discussion on control strategy". In: *Applied Energy* 179 (2016), pp. 7–16. DOI: 10.1016/j.apenergy.2016.06.116 (cited on page 130).

Musculus, M. P. B., Lachaux, T., Pickett, L. M., and Idicheria, C. A. "End-of-Injection Over-Mixing and Unburned Hydrocarbon Emissions in Low-Temperature-Combustion Diesel Engines". In: *SAE Technical Paper 2007-01-0907* (2007). DOI: 10.4271/2007-01-0907 (cited on page 30).

Musculus, M. P. B., Miles, P. C., and Pickett, L. M. "Conceptual models for partially premixed low-temperature diesel combustion". In: *Progress in Energy and Combustion Science* 39.2-3 (2013), pp. 246–283. DOI: 10.1016/j.pecs.2012.09.001 (cited on page 1).

Naber, J. D. and Siebers, D. L. "Effects of Gas Density and Vaporization on Penetration and Dispersion of Diesel Sprays". In: *SAE Technical Paper 960034* (1996). DOI: 10.4271/960034 (cited on pages 22–24, 65, 66, 74, 136, 141, 186).

Neely, G. D., Sasaki, S., Huang, Y., Leet, J. A., and Stewart, D. W. "New Diesel Emission Control Strategy to Meet US Tier 2 Emissions Regulations". In: *SAE Technical Paper 2005-01-1091* (2005). DOI: 10.4271/2005-01-1091 (cited on page 26).

Nerva, J.-G., Genzale, C. L., Kook, S., García-Oliver, J. M., and Pickett, L. M. "Fundamental spray and combustion measurements of soy methyl-ester biodiesel". In: *International Journal of Engine Research* 14.4 (2013), pp. 373–390. DOI: 10.1177/1468087412456688 (cited on page 66).

O'Connor, J. and Musculus, M. P. B. "Post Injections for Soot Reduction in Diesel Engines: A Review of Current Understanding". In: *SAE International Journal of Engines* 6.1 (2013), pp. 2013–01–0917. DOI: 10.4271/2013-01-0917 (cited on pages 29, 182).

O'Connor, J. and Musculus, M. P. B. "Effects of exhaust gas recirculation and load on soot in a heavy-duty optical diesel engine with close-coupled post injections for high-efficiency combustion phasing". In: *International Journal of Engine Research* 15.4 (2014), pp. 421–443. DOI: 10.1177/1468087413488767 (cited on pages 30, 182).

O'Connor, J., Musculus, M. P. B., and Pickett, L. M. "Effect of post injections on mixture preparation and unburned hydrocarbon emissions in a heavy-duty diesel engine". In: *Combustion and Flame* 170 (2016), pp. 111–123. DOI: 10.1016/j.combustflame.2016.03.031 (cited on pages 2, 28).

Park, C. and Busch, S. "The influence of pilot injection on high-temperature ignition processes and early flame structure in a high-speed direct injection diesel engine". In: *International Journal of Engine Research* 19.6 (2018), pp. 668–681. DOI: 10.1177/1468087417728630 (cited on pages 154, 158, 159, 171, 187).

Parrish, S. E., Zhang, G., and Zink, R. J. "Liquid and Vapor Envelopes of Sprays from a Multi-Hole Fuel Injector Operating under Closely-Spaced Double-Injection Conditions". In: *SAE International Journal of Engines* 5.2 (2012), pp. 2012–01–0462. DOI: 10.4271/2012-01-0462 (cited on pages 31, 134).

Pastor, J. V., García-Oliver, J. M., Novella, R., and Xuan, T. "Soot Quantification of Single-Hole Diesel Sprays by Means of Extinction Imaging". In: *SAE International Journal of Engines* 8.5 (2015), pp. 2068–2077. DOI: 10.4271/2015-24-2417 (cited on page 64).

Pastor, J. V., García-Oliver, J. M., Pastor, J. M., and Zapata, L. D. "Evaporating Diesel Spray Visualization using a Double-pass Shadowgraphy/Schlieren imaging". In: *SAE Technical Paper 2007-24-0026* (2007). DOI: 10.4271/2007-24-0026 (cited on page 66).

Pastor, J. V., López, J. J., García-Oliver, J. M., and Pastor, J. M. "A 1D model for the description of mixing-controlled inert diesel sprays". In: *Fuel* 87.13-14 (2008), pp. 2871–2885. DOI: 10.1016/j.fuel.2008.04.017 (cited on pages 3, 22, 23, 138, 178).

Pastor, J. V., Payri, R., García-Oliver, J. M., and Briceño, F. J. "Schlieren Methodology for the Analysis of Transient Diesel Flame Evolution". In: *SAE International Journal of Engines* 6.3 (2013), pp. 2013–24–0041. DOI: 10.4271/2013-24-0041 (cited on pages 65, 66, 165).

Pastor, J. V., Payri, R., García-Oliver, J. M., and Nerva, J.-G. "Schlieren Measurements of the ECN-Spray A Penetration under Inert and Reacting Conditions". In: *SAE Technical Paper 2012-01-0456* (2012). DOI: 10.4271/2012-01-0456 (cited on pages 66, 67, 73).

Payri, F., Benajes, J., Pastor, J. V., and Molina, S. "Influence of the Post-Injection Pattern on Performance, Soot and NOx Emissions in a HD Diesel Engine". In: *SAE Technical Paper 2002-01-0502* (2002). DOI: 10.4271/2002-01-0502 (cited on pages 2, 28).

Payri, F., Bermúdez, V., Payri, R., and Salvador, F. J. "The influence of cavitation on the internal flow and the spray characteristics in diesel injection nozzles". In: *Fuel* 83.4-5 (2004), pp. 419–431. DOI: 10.1016/j.fuel.2003.09.010 (cited on pages 22, 24).

Payri, F., Broatch, A., Tormos, B., and Marant, V. "New methodology for in-cylinder pressure analysis in direct injection diesel engines - Application to combustion noise". In: *Measurement Science and Technology* 16.2 (2005), pp. 540–547. DOI: 10.1088/0957-0233/16/2/029 (cited on pages 28, 186, 187).

Payri, F. and Desantes, J. M. *Motores de combustion interna alternativos*. Editorial Universitat Politecnica de Valencia, 2011 (cited on pages 11, 12).

Payri, F., Pastor, J. V., García-Oliver, J. M., and Pastor, J. M. "Contribution to the application of two-colour imaging to diesel combustion". In: *Measurement Science and Technology* 18.8 (2007), pp. 2579–2598. DOI: 10.1088/0957-0233/18/8/034 (cited on pages 168, 169).

Payri, F., Payri, R., Salvador, F. J., and Gimeno, J. "Influence of Nozzle Geometry on Spray Characteristics in Non-Evaporative and evaporative conditions". In: *SAE Technical Paper 2007-24-0023* (2007). DOI: 10.4271/2007-24-0023 (cited on page 20).

Payri, R., Araneo, L., Shakal, J. S., and Soare, V. "Phase doppler measurements: System set-up optimization for characterization of a diesel nozzle". In: *Journal of Mechanical Science and Technology* 22.8 (2008), pp. 1620–1632. DOI: 10.1007/s12206-008-0432-7 (cited on page 22).

Payri, R., Bracho, G., Martí-Aldaraví, P., and Viera, A. "Near field visualization of diesel spray for different nozzle inclination angles in non-vaporizing conditions". In: *Atomization and Sprays* 27.3 (2017), pp. 251–267. DOI: 10.1615/AtomizSpr.2017017949 (cited on pages 2, 13, 23, 24, 51, 63, 64, 76, 78, 138).

Payri, R., Bracho, G., Martí-Aldaraví, P., and Viera, A. "Nozzle Geometry Size Influence on Reactive Spray Development: From Spray B to Heavy Duty Applications". In: *SAE Technical Paper 2017-01-0846* (2017), p. 12. DOI: 10.4271/2017-01-0846 (cited on pages 17, 20, 61, 63, 68, 79, 80, 154, 169, 178).

Payri, R., García-Oliver, J. M., Bardi, M., and Manin, J. "Fuel temperature influence on diesel sprays in inert and reacting conditions". In: *Applied Thermal Engineering* 35.1 (2012), pp. 185–195. DOI: 10.1016/j.applthermaleng.2011.10.027 (cited on pages 14, 23, 24, 62, 63).

Payri, R., García-Oliver, J. M., Salvador, F. J., and Gimeno, J. "Using spray momentum flux measurements to understand the influence of diesel nozzle geometry on spray characteristics". In: *Fuel* 84.5 (2005), pp. 551–561. DOI: 10.1016/j.fuel.2004.10.009 (cited on pages 20–22, 24, 57, 109).

Payri, R., García-Oliver, J. M., Xuan, T., and Bardi, M. "A study on diesel spray tip penetration and radial expansion under reacting conditions". In: *Applied Thermal Engineering* 90 (2015), pp. 619–629. DOI: 10.1016/j.applthermaleng.2015.07.042 (cited on pages 66, 77, 154, 155, 159).

Payri, R., Gimeno, J., Bardi, M., and Plazas, A. H. "Effect of Injection Rate Shaping Over Diesel Spray Development in Non Reacting Evaporative Conditions". In: *ASME 2012 Internal Combustion Engine Division Spring Technical Conference*. 2012, p. 347. DOI: 10.1115/ICES2012-81206 (cited on pages 2, 75).

Payri, R., Gimeno, J., Bardi, M., and Plazas, A. H. "Study liquid length penetration results obtained with a direct acting piezo electric injector". In: *Applied Energy* 106 (2013), pp. 152–162. DOI: 10.1016/j.apenergy.2013.01.027 (cited on pages 2, 14, 20, 23, 78).

Payri, R., Gimeno, J., Bracho, G., and Vaquerizo, D. "Study of liquid and vapor phase behavior on Diesel sprays for heavy duty engine nozzles". In: *Applied Thermal Engineering* 107 (2016), pp. 365–378. DOI: 10.1016/j.applthermaleng.2016.06.159 (cited on pages 14, 23, 24, 65, 72, 74–76, 136, 169).

Payri, R., Gimeno, J., Cardona, S., and Ayyapureddi, S. "Measurement of Soot Concentration in a Prototype Multi-Hole Diesel Injector by High-Speed Color Diffused Back Illumination Technique". In: *SAE Technical Paper 2017-01-2255*. 2017. DOI: 10.4271/2017-01-2255 (cited on pages 61, 63, 64, 80, 168).

Payri, R., Gimeno, J., Cuisano, J., and Arco, J. "Hydraulic characterization of diesel engine single-hole injectors". In: *Fuel* 180 (2016), pp. 357–366. DOI: 10.1016/j.fuel.2016.03.083 (cited on page 21).

Payri, R., Gimeno, J., Mata, C., and Viera, A. "Rate of injection measurements of a direct-acting piezoelectric injector for different operating temperatures". In: *Energy Conversion and Management* 154 (2017), pp. 387–393. DOI: 10.1016/j.enconman.2017.11.029 (cited on pages 20, 21, 55, 57, 94, 106).

Payri, R., Gimeno, J., Novella, R., and Bracho, G. "On the rate of injection modeling applied to direct injection compression ignition engines". In: *International Journal of Engine Research* 17.10 (2016), pp. 1015–1030. DOI: 10.1177/1468087416636281 (cited on page 100).

Payri, R., Gimeno, J., Peraza, J. E., and Bazyn, T. "Spray / wall interaction analysis on an ECN single-hole injector at diesel-like conditions through Schlieren visualization". In: *ILASS Europe 28th Conference on Liquid Atomization and Spray Systems*. Valencia, 2017, pp. 200–207. DOI: 10.4995/ILASS2017.2017.4709 (cited on page 182).

Payri, R., Gimeno, J., Viera, J. P., and Plazas, A. H. "Needle lift profile influence on the vapor phase penetration for a prototype diesel direct acting piezoelectric injector". In: *Fuel* 113 (2013), pp. 257–265. DOI: 10.1016/j.fuel.2013.05.057 (cited on pages 2, 20, 66, 67, 75, 78).

Payri, R., Molina, S., Salvador, F. J., and Gimeno, J. "A study of the relation between nozzle geometry, internal flow and sprays characteristics in diesel fuel injection systems". In: *KSME International Journal* 18.7 (2004), pp. 1222–1235. DOI: 10.1007/BF02983297 (cited on pages 21, 24).

Payri, R., Salvador, F. J., Bracho, G., and Viera, A. "Differences between single and double-pass schlieren imaging on diesel vapor spray characteristics". In: *Applied Thermal Engineering* 125 (2017), pp. 220–231. DOI: 10.1016/j.applthermaleng.2017.06.140 (cited on pages 51, 67, 72–77, 136, 141, 142).

Payri, R., Salvador, F. J., Carreres, M., and De la Morena, J. "Fuel temperature influence on the performance of a last generation common-rail diesel ballistic injector. Part II: 1D model development, validation and analysis". In: *Energy Conversion and Management* 114 (2016), pp. 376–391. DOI: 10.1016/j.enconman.2016.02.043 (cited on pages 97, 98).

Payri, R., Salvador, F. J., García, A., and Gil, A. "Combination of visualization techniques for the analysis of evaporating diesel sprays". In: *Energy and Fuels* 26.9 (2012), pp. 5481–5490. DOI: 10.1021/ef3008823 (cited on page 66).

Payri, R., Salvador, F. J., Gimeno, J., and Bracho, G. "A new methodology for correcting the signal cumulative phenomenon on injection rate measurements". In: *Experimental Techniques* 32.1 (2008), pp. 46–49. DOI: 10.1111/j.1747-1567.2007.00188.x (cited on pages 56, 57, 106).

Payri, R., Salvador, F. J., Gimeno, J., and Bracho, G. "The effect of temperature and pressure on thermodynamic properties of diesel and biodiesel fuels". In: *Fuel* 90.3 (2011), pp. 1172–1180. DOI: 10.1016/j.fuel.2010.11.015 (cited on pages 53, 115).

Payri, R., Salvador, F. J., Gimeno, J., and Viera, A. "Effect of Injection Rate Shaping over Diesel Spray Development in Non-Reacting Evaporative Conditions". In: *10. Tagung Diesel- und Benzindirekteinspritzung 2016*. Ed. by H. Tschöke and R. Marohn. 1. Springer, 2017, pp. 133–152. DOI: 10.1007/978-3-658-15327-4 (cited on pages 61, 63, 65, 66, 72).

Payri, R., Salvador, F. J., Gimeno, J., and Zapata, L. D. "Diesel nozzle geometry influence on spray liquid-phase fuel penetration in evaporative conditions". In: *Fuel* 87.7 (2008), pp. 1165–1176. DOI: 10.1016/j.fuel.2007.05.058 (cited on page 169).

Payri, R., Salvador, F. J., Manin, J., and Viera, A. "Diesel ignition delay and lift-off length through different methodologies using a multi-hole injector". In: *Applied Energy* 162 (2016), pp. 541–550. DOI: 10.1016/j.apenergy.2015.10.118 (cited on pages 15–17, 51, 63, 65–68, 77, 79, 154, 159, 165, 169, 170, 187).

Payri, R., Salvador, F. J., Martí-Aldaraví, P., and Vaquerizo, D. "ECN Spray G external spray visualization and spray collapse description through penetration and morphology analysis". In: *Applied Thermal Engineering* 112 (2017), pp. 304–316. DOI: 10.1016/j.applthermaleng.2016.10.023 (cited on page 66).

Payri, R., Tormos, B., Salvador, F. J., and Araneo, L. "Spray droplet velocity characterization for convergent nozzles with three different diameters". In: *Fuel* 87.15-16 (2008), pp. 3176–3182. DOI: 10.1016/j.fuel.2008.05.028 (cited on page 22).

Payri, R., Tormos, B., Salvador, F. J., and Plazas, A. H. "Using one-dimensional modelling codes to analyse the influence of diesel nozzle geometry on injection rate characteristics". In: *International Journal of Vehicle Design* 38.1 (2005), pp. 58–78. DOI: 10.1504/IJVD.2005.006605 (cited on page 18).

Payri, R., Viera, J. P., Gopalakrishnan, V., and Szymkowicz, P. G. "The effect of nozzle geometry over ignition delay and flame lift-off of reacting direct-injection sprays for three different fuels". In: *Fuel* 199 (2017), pp. 76–90. DOI: 10.1016/j.fuel.2017.02.075 (cited on pages 2, 15, 51, 63, 65, 66, 77, 79, 154, 159, 165, 170).

Payri, R., Viera, J. P., Gopalakrishnan, V., and Szymkowicz, P. G. "The effect of nozzle geometry over the evaporative spray formation for three different fuels". In: *Fuel* 188 (2017), pp. 645–660. DOI: 10.1016/j.fuel.2016.06.041 (cited on pages 2, 14, 23, 24, 51, 73, 76, 78, 133, 136, 141).

Payri, R., Viera, J. P., Pei, Y., and Som, S. "Experimental and numerical study of lift-off length and ignition delay of a two-component diesel surrogate". In: *Fuel* 158 (2015), pp. 957–967. DOI: 10.1016/j.fuel.2014.11.072 (cited on pages 15, 65, 68, 73, 77, 79).

Payri, R., Viera, J. P., Wang, H., and Malbec, L. M. "Velocity field analysis of the high density, high pressure diesel spray". In: *International Journal of Multiphase Flow* 80 (2016), pp. 69–78. DOI: 10.1016/j.ijmultiphaseflow.2015.10.012 (cited on page 22).

Payri, R. et al. "One-dimensional modeling of the interaction between close-coupled injection events for a ballistic solenoid injector". In: *International Journal of Engine Research* 20.4 (2019), pp. 452–469. DOI: 10.1177/1468087418760973 (cited on pages 98, 104).

Peters, N. *Turbulent Combustion*. Vol. 12. Cambridge Monographs on Mechanics 11. Cambridge University Press, 2001, pp. 2022–2022. DOI: 10.1088/0957-0233/12/11/708 (cited on pages 67, 165).

Pickett, L. M., Genzale, C. L., and Manin, J. "Uncertainty quantification for liquid penetration of evaporating sprays at diesel-like conditions". In: *Atomization and Sprays* 25.5 (2015), pp. 425–452. DOI: 10.1615/AtomizSpr.2015010618 (cited on pages 51, 141).

Pickett, L. M., Kook, S., Persson, H., and Andersson, Ö. "Diesel fuel jet lift-off stabilization in the presence of laser-induced plasma ignition". In: *Proceedings of the Combustion Institute* 32 (2009), pp. 2793–2800. DOI: 10.1016/j.proci.2008.06.082 (cited on pages 16, 17, 165).

Pickett, L. M., Kook, S., and Williams, T. C. "Transient Liquid Penetration of Early-Injection Diesel Sprays". In: *SAE International Journal of Engines* 2.1 (2009), pp. 2009–01–0839. DOI: 10.4271/2009-01-0839 (cited on page 134).

Pickett, L. M., Kook, S., and Williams, T. C. "Visualization of Diesel Spray Penetration, Cool-Flame, Ignition, High-Temperature Combustion, and Soot Formation Using High-Speed Imaging". In: *SAE International Journal of Engines* 2.1 (2009), pp. 2009–01–0658. DOI: 10.4271/2009-01-0658 (cited on pages 51, 65, 77).

Pickett, L. M. and Lopez, J. J. "Jet-Wall Interaction Effects on Diesel Combustion and Soot Formation". In: *SAE Technical Paper 2005-01-0921* (2005). DOI: 10.4271/2005-01-0921 (cited on pages 30, 182).

Pickett, L. M., Manin, J., Payri, R., Bardi, M., and Gimeno, J. "Transient Rate of Injection Effects on Spray Development". In: *SAE Technical Paper 2013-24-0001* (2013). DOI: 10.4271/2013-24-0001 (cited on page 107).

Pickett, L. M. and Siebers, D. L. "Soot in diesel fuel jets: effects of ambient temperature, ambient density, and injection pressure". In: *Combustion and Flame* 138.1 (2004), pp. 114–135. DOI: 10.1016/j.combustflame.2004.04.006 (cited on pages 168–170).

Pickett, L. M. and Siebers, D. L. "Soot formation in diesel fuel jets near the lift-off length". In: *International Journal of Engine Research* 7.2 (2006), pp. 103–130. DOI: 10.1243/146808705X57793 (cited on page 30).

Pickett, L. M., Siebers, D. L., and Idicheria, C. A. "Relationship Between Ignition Processes and the Lift-Off Length of Diesel Fuel Jets". In: *SAE Technical Paper 2005-01-3843* 724 (2005). DOI: 10.4271/2005-01-3843 (cited on pages 15, 159, 165).

Pickett, L. M. et al. "Relationship Between Diesel Fuel Spray Vapor Penetration/Dispersion and Local Fuel Mixture Fraction". In: *SAE International Journal of Engines* 4.1 (2011), pp. 2011–01–0686. DOI: 10.4271/2011-01-0686 (cited on pages 66, 136, 142).

Pierpont, D. A., Montgomery, D. T., and Reitz, R. D. "Reducing Particulate and NOx Using Multiple Injections and EGR in a D.I. Diesel". In: *SAE Technical Paper 950217* (1995). DOI: 10.4271/950217 (cited on pages 2, 26, 28, 31).

Pischinger, F. F., Schmillen, K. P., and Leipold, F. W. "A New Measuring Method for the Direct Determination of Diesel Engine Combustion Noise". In: *SAE Technical Paper 790267* (1979). DOI: 10.4271/790267 (cited on pages 28, 186).

Pittermann, R. "Spectroscopic Analysis of the Combustion in Diesel and Gas Engines". In: *MTZ worldwide* 69 (2008), pp. 66–73. DOI: doi.org/10.1007/BF03227907 (cited on page 68).

Plee, S. L. and Ahmad, T. "Relative Roles of Premixed and Diffusion Burning in Diesel Combustion". In: *SAE Technical Paper 831733* (1983). DOI: 10.4271/831733 (cited on pages 28, 186).

Postrioti, L., Mariani, F., Battistoni, M., and Mariani, A. "Experimental and Numerical Evaluation of Diesel Spray Momentum Flux". In: *SAE International Journal of Engines* 4970.2 (2009). DOI: doi.org/10.4271/2009-01-2772 (cited on page 109).

Potter, M. and Durrett, R. P. "High-Efficiency Clean Combustion Design for Compression Ignition Engines". In: *Diesel Engine-Efficiency and Emissions Research*. Detroit, 2006 (cited on page 26).

Priede, T. "Relation between Form of Cylinder-Pressure Diagram and Noise in Diesel Engines". In: *Proceedings of the Institution of Mechanical Engineers: Automobile Division* 14.1 (1960), pp. 63–97. DOI: 10.1243/pime_auto_1960_000_012_02 (cited on pages 28, 186, 187).

Ramos, Á., Muñoz, J., Andrés, F., and Armas, O. "NOx emissions from diesel light duty vehicle tested under NEDC and real-word driving conditions". In: *Transportation Research Part D: Transport and Environment* 63 (2018), pp. 37–48. DOI: 10.1016/j.trd.2018.04.018 (cited on page 30).

Reitz, R. D. "Atomisation and other breakup regimes of a liquid jet". PhD thesis. Princeton University, 1978 (cited on page 13).

Reitz, R. D. and Bracco, F. V. *Mechanism of breakup of round liquid jets*. Ed. by N. Cheremisnoff. Vol. 3. Houston: Gulf Publishing, 1984, pp. 233–249 (cited on page 13).

Salvador, F. J. "Estudio teórico experimental de la influencia de la geometría de toberas de inyección Diésel sobre las características del flujo interno y del chorro". PhD thesis. Valencia: Universitat Politècnica de València, 2003 (cited on page 21).

Salvador, F. J., De la Morena, J., Crialesi-Esposito, M., and Martínez-López, J. "Comparative study of the internal flow in diesel injection nozzles at cavitating conditions at different needle lifts with steady and transient simulations approaches". In: *Proceedings of the Institution of Mechanical Engineers, Part D: Journal of Automobile Engineering* 232.8 (2018), pp. 1060–1078. DOI: 10.1177/0954407017725672 (cited on page 21).

Salvador, F. J., Gimeno, J., Carreres, M., and Crialesi-Esposito, M. "Fuel temperature influence on the performance of a last generation common-rail diesel ballistic injector. Part I: Experimental mass flow rate measurements and discussion". In: *Energy Conversion and Management* 114 (2016), pp. 364–375. DOI: 10.1016/j.enconman.2016.02.042 (cited on pages 57, 97).

Salvador, F. J., Martínez-López, J., Caballer, M., and De Alfonso, C. "Study of the influence of the needle lift on the internal flow and cavitation phenomenon in diesel injector nozzles by CFD using RANS methods". In: *Energy Conversion and Management* 66 (2013), pp. 246–256. DOI: 10.1016/j.enconman.2012.10.011 (cited on page 21).

Schöppe, D., Stahl, C., Krüger, G., and Dian, V. "Servo-Driven Piezo Common Rail Diesel Injection System". In: *ATZ Autotechnology* 12.2 (2012), pp. 42–47. DOI: 10.1365/s35595-012-0107-y (cited on pages 2, 11, 17, 20, 27, 50).

Sechenyh, V. et al. "Quantification of diesel injector dribble using 3D reconstruction from x-ray and DBI imaging". In: *ILASS Europe 28th Conference on Liquid Atomization and Spray Systems*. Valencia, 2017, pp. 232–239. DOI: 10.4995/ILASS2017.2017.4742 (cited on pages 2, 130).

Settles, G. S. *Shadowgraph and Schlieren Techniques*. Springer Berlin Heidelberg, 2001. DOI: 10.1007/978-3-642-56640-0 (cited on pages 65, 66).

Siebers, D. L. "Liquid-Phase Fuel Penetration in Diesel Sprays". In: *SAE Technical Paper 980809* (1998). DOI: 10.4271/980809 (cited on pages 2, 13, 14, 23, 63, 74, 76, 79, 111, 133, 141, 169, 186).

Siebers, D. L. "Scaling liquid-phase fuel penetration in diesel sprays based on mixing-limited vaporization". In: *SAE Technical Paper 1999-01-0528* (1999). DOI: 10.4271/1999-01-0528 (cited on pages 13, 14, 23, 133, 141, 169, 186).

Siebers, D. L. and Higgins, B. S. "Flame Lift-Off on Direct-Injection Diesel Sprays Under Quiescent Conditions". In: *SAE Technical Paper 2001-01-0530* 724 (2001). DOI: 10.4271/2001-01-0530 (cited on pages 16, 17, 67, 165, 168–171, 178).

Singh, N., Rutland, C. J., Foster, D. E., Narayanaswamy, K., and He, Y. "Investigation into Different DPF Regeneration Strategies Based on Fuel Economy Using Integrated System Simulation". In: *SAE Technical Paper 2009-01-1275* 1 (2009). DOI: 10.4271/2009-01-1275 (cited on page 30).

Skeen, S. A., Manin, J., Dalen, K., and Pickett, L. M. "Extinction-based Imaging of Soot Processes over a Range of Diesel Operating Conditions". In: *8th US National Combustion Meeting*. Utah, USA, 2013, pp. 070IC–0355. DOI: 10.1016/j.coal.2015.03.006 (cited on pages 64, 80).

Skeen, S. A., Manin, J., and Pickett, L. M. "Visualization of Ignition Processes in High-Pressure Sprays with Multiple Injections of n-Dodecane". In: *SAE International Journal of Engines* 8.2 (2015), pp. 2015–01–0799. DOI: 10.4271/2015-01-0799 (cited on pages 31, 138, 165, 167).

Skeen, S. A. et al. "A Progress Review on Soot Experiments and Modeling in the Engine Combustion Network (ECN)". In: *SAE International Journal of Engines* 9.2 (2016), pp. 2016–01–0734. DOI: 10.4271/2016-01-0734 (cited on pages 63, 80, 159).

Soriano, J. A., Mata, C., Armas, O., and Ávila, C. "A zero-dimensional model to simulate injection rate from first generation common rail diesel injectors under thermodynamic diagnosis". In: *Energy* 158 (2018), pp. 845–858. DOI: 10.1016/j.energy.2018.06.054 (cited on page 100).

Steinparzer, F., Stütz, W., and Brüne, H.-j. "Reliable, efficient and environmentally friendly: The new BMW Diesel engines with RDE technology". In: *16th Conference The Working Process of the Internal Combustion Engine*. Ed. by H. Eichlseder and A. Wimmer. Graz: Verlag der Technischen Universität Graz, 2017, pp. 15–22 (cited on page 1).

Stetsyuk, V., Turner, J., Crua, C., Pearson, R., and Gold, M. "Droplet size and morphology characterization for diesel sprays under atmospheric operating conditions". In: *ICLASS 13th International Conference on Liquid Atomization and Spray Systems*. Tainan, 2015 (cited on page 130).

Su, T. F., Farrell, P. V., and Nagarajan, R. T. "Nozzle effect on high pressure Diesel Injection". In: *SAE Technical Paper 950083* (1995). DOI: 10.4271/950083 (cited on page 136).

Suh, H. K., Park, S. W., and Lee, C. S. "Effect of piezo-driven injection system on the macroscopic and microscopic atomization characteristics of diesel fuel spray". In: *Fuel* 86.17-18 (2007), pp. 2833–2845. DOI: 10.1016/j.fuel.2007.03.015 (cited on page 20).

Swantek, A. B. et al. "A further examination of fuel dribble from single hole diesel nozzles". In: *ILASS Europe 26th Annual Conference on Liquid Atomization and Spray Systems*. Bremen, 2014 (cited on page 130).

Swantek, A. B. et al. “End of Injection, Mass Expulsion Behaviors in Single Hole Diesel Fuel Injectors”. In: *ILASS Americas 26th Annual Conference on Liquid Atomization and Spray Systems*. Portland, 2014 (cited on page 130).

Taskiran, O. O. and Ergeneman, M. “Effect of nozzle dimensions and fuel type on flame lift-off length”. In: *Fuel* 115 (2014), pp. 833–840. DOI: 10.1016/j.fuel.2013.03.005 (cited on pages 16, 17, 165).

Taylor, C. F. *The internal-combustion engine in theory and practice*. 2nd ed. Cambridge: MIT Press, 1989 (cited on pages 11, 12).

Tonini, S., Gavaises, M., Theodorakakos, A., and Cossali, G. E. “Numerical investigation of a multiple injection strategy on the development of high-pressure diesel sprays”. In: *Proceedings of the Institution of Mechanical Engineers, Part D: Journal of Automobile Engineering* 224.1 (2010), pp. 125–141. DOI: 10.1243/09544070JAUTO1083 (cited on pages 134, 138).

Torregrosa, A. J., Broatch, A., García, A., and Mónico, L. F. “Sensitivity of combustion noise and NOx and soot emissions to pilot injection in PCCI Diesel engines”. In: *Applied Energy* 104 (2013), pp. 149–157. DOI: 10.1016/j.apenergy.2012.11.040 (cited on page 171).

Tree, D. R. and Svensson, K. “Soot processes in compression ignition engines”. In: *Progress in Energy and Combustion Science* 33.3 (2007), pp. 272–309. DOI: 10.1016/j.pecs.2006.03.002 (cited on page 30).

Ullmann, J., Geduldig, M., Stutzenberger, H., Caprotti, R., and Balfour, G. “Investigation into the Formation and Prevention of Internal Diesel Injector Deposits”. In: *SAE Technical Paper 2008-01-0926* (2008). DOI: 10.4271/2008-01-0926 (cited on page 130).

Venegas, O. “Estudio del fenómeno de la cavitación en la inyección Diesel mediante la visualización del flujo interno en orificios transparentes.” PhD thesis. Universitat Politècnica de València, 2014. DOI: 10.4995/Thesis/10251/37375 (cited on pages 20, 24, 57, 97, 109).

Viera, J. P. “Experimental study of the effect of nozzle geometry on the performance of direct-injection diesel sprays for three different fuels”. PhD thesis. Universitat Politècnica de València, 2017. DOI: 10.4995/Thesis/10251/81857 (cited on pages 2, 20, 97, 109).

Viera, J. P. et al. “Linking instantaneous rate of injection to X-ray needle lift measurements for a direct-acting piezoelectric injector”. In: *Energy Conversion and Management* 112 (2016), pp. 350–358. DOI: 10.1016/j.enconman.2016.01.038 (cited on pages 20, 63).

Wan, Y. and Peters, N. "Scaling of spray penetration with evaporation". In: *Atomization and Sprays* 9.2 (1999), pp. 111–132. DOI: 10.1615/AtomizSpr.v9.i2.10 (cited on page 22).

Wang, Z. "Experimental study on diesel spray with single and multiple injection under room temperature and low temperature". PhD thesis. University of Birmingham, 2015 (cited on page 138).

Westbrook, C. K. et al. "The effects of pressure, temperature, and concentration on the reactivity of alkanes: Experiments and modeling in a rapid compression machine". In: *International Symposium on Combustion* 27.1 (1998), pp. 371–378. DOI: 10.1016/S0082-0784(98)80425-6 (cited on pages 14, 15).

Westlye, F. R. et al. "Penetration and combustion characterization of cavitating and non-cavitating fuel injectors under diesel engine conditions". In: *SAE Technical Paper 2016-01-0860* (2016), p. 15. DOI: 10.4271/2016-01-0860 (cited on page 79).

Westlye, F. R. et al. "Diffuse back-illumination setup for high temporally resolved extinction imaging". In: *Applied Optics* 56.17 (2017), p. 5028. DOI: 10.1364/AO.56.005028 (cited on pages 2, 63, 74).

Wu, K. J., Su, C. C., Steinberger, R. L., Santavicca, D. A., and Bracco, F. V. "Measurements of the spray angle of atomizing jets". In: *Journal of fluids Engineering* 105.4 (1983), pp. 406–410. DOI: 10.1115/1.3241019 (cited on page 24).

Xi, J. and Zhong, B. J. "Soot in diesel combustion systems". In: *Chemical Engineering and Technology* 29.6 (2006), pp. 665–673. DOI: 10.1002/ceat.200600016 (cited on pages 17, 29).

Xue, Q. et al. "Three-dimensional Simulations of the Transient Internal Flow in a Diesel Injector: Effects of Needle Movement". In: *ILASS Americas 25th Annual Conference on Liquid Atomization and Spray Systems*. Pittsburgh, 2013 (cited on page 51).

Xue, Q. et al. "Eulerian CFD Modeling of Coupled Nozzle Flow and Spray with Validation Against X-Ray Radiography Data". In: *SAE International Journal of Engines* 7.2 (2014), pp. 2014–01–1425. DOI: 10.4271/2014-01-1425 (cited on page 51).

Xue, Q. et al. "An Eulerian CFD model and X-ray radiography for coupled nozzle flow and spray in internal combustion engines". In: *International Journal of Multiphase Flow* 70 (2015), pp. 77–88. DOI: 10.1016/j.ijmultiphaseflow.2014.11.012 (cited on page 51).

Yehliu, K., Boehman, A. L., and Armas, O. “Emissions from different alternative diesel fuels operating with single and split fuel injection”. In: *Fuel* 89.2 (2010), pp. 423–437. DOI: 10.1016/j.fuel.2009.08.025 (cited on page 31).

Yoon, S., Kim, H., Kim, D., and Park, S. “Effect of Fuel Injection Strategy on DPF Regeneration in Single Cylinder Diesel Engine”. In: *ASME Internal Combustion Engine Division Fall Technical Conference*. Houston, 2015. DOI: 10.1115/icef2015-1140 (cited on page 30).

Yun, H., Sun, Y., and Reitz, R. D. “An Experimental and Numerical Investigation on the Effect of Post Injection Strategies on Combustion and Emissions in the Low-Temperature Diesel Combustion Regime”. In: *ASME Internal Combustion Engine Division Spring Technical Conference*. 2005, pp. 25–35. DOI: 10.1115/ices2005-1043 (cited on pages 29, 30, 182).

Zama, Y., Ochiai, W., Furuhata, T., and Arai, M. “Velocity measurement inside a diesel spray by using time-resolved PIV under high ambient density condition”. In: *ICLASS 12th Triennial International Conference on Liquid Atomization and Spray Systems*. Heidelberg, 2012 (cited on page 22).

Zhang, W., Tian, J.-P., and Nishida, K. “Effects of Nozzle Hole Diameter and Injection Pressure on Flame Lift-Off and Soot Formation in D.I. Diesel Combustion”. In: *SAE Technical Paper 2011-01-1813* (2011). DOI: 10.4271/2011-01-1813 (cited on pages 154, 158, 165, 187).

Zhao, L. et al. “Evaluation of Diesel Spray-Wall Interaction and Morphology around Impingement Location”. In: *SAE Technical Paper 2018-01-0276* (2018). DOI: 10.4271/2018-01-0276 (cited on page 182).